Surface modified cubosomes for drug delivery across the blood-brain barrier

Hanisah Azhari

A thesis submitted for the degree of

Doctor of Philosophy

at the University of Otago

Dunedin

New Zealand

October 2018

Abstract

The bottleneck in delivering drugs to the brain for treatment of diseases related to central nervous system (CNS), lies behind the presence of blood-brain barrier (BBB). This barrier prevents most of the large and a number of small molecules from entering the brain, thus posing a considerable challenge in administration of drugs. The present treatment for CNS diseases involves oral drug delivery that seems to result in limited efficacy of drug therapy and undesired peripheral side effects. While invasive strategies have been proved to increase drug loading into the brain, the procedures can be risky with debilitating side effects, thus unsuitable for long-term treatment. Nevertheless, the use of particulate drug carriers, such as nanoparticles, can be a promising non-invasive strategy to increase drug loading into the brain by masking drug properties, to ascertain higher encapsulation efficacy and to enhance the stability of the drugs. One type of lipid-based nanoparticles, cubosomes, had been investigated in this study to determine its suitability as a drug carrier. By decorating and modifying the surface of cubosomes with specific moieties, several pathways can serve as targets at the BBB. With that, this thesis looked into intraveneous formulation of cubosomes as a drug carrier to cross the BBB, primarily due to several advantages it has to offer. The overarching aim of this thesis, hence, is to assess the hypothesis that the surface of cubosomes can be modified with specific moieties so as to serve as effective drug carriers to enter the brain.

In order to target low-density lipoprotein (LDL) receptors at the BBB, **Chapter 3** presents the investigation of phytantriol cubosomes stabilised with BBB-targeting moieties; Tween 80 and Poloxamer 188. These stabilisers serve as cubosome stabilisers and also to target the BBB. Optimum concentrations of Tween 80 and Poloxamer 188 had been determined at 15% w/w (of phytantriol), where the cubosomes formed *Im3m* and *Pn3m* internal structures, respectively. The homogeneous cubosomes were formed

and no vesicles had been observed with cubosomes stabilised using Tween 80. Nevertheless, *in vitro* cellular uptake displayed lack of uptake proposed to be from lack of ApoE in the cell culture media, which appeared to prevent the interaction of the cubosomes with LDL-receptors. This indicates the significance of ApoE in the plasma which initially binds to the cubosomes surface decorated with Tween 80 and Poloxamer 188, followed by the interaction with LDL-receptor and internalisation into the brain endothelial cells.

In **Chapter 4**, cationic cubosomes were investigated as an alternative potential drug carrier to enter the brain. In order to investigate the effects of using single and double chain cationic lipids; cetyltrimethylammonium bromide, CTAB (single chain), 1,2-Dioleoyl-3-trimethylammonium-propane, DOTAP and 1,2-di-O-octadecenyl-3-trimethylammonium propane, DOTMA (double chain) were added into the standard cubosome formulation which were stabilised by Pluronic F127. The concentration of cationic lipids in the cubosome formulation was optimised to avoid instability and to hinder any changes from occurring in the internal structure. The addition of 1.4 mol% cationic lipids maintained the internal structure as *Pn3m* structure and formed homogenous dispersion. In addition, observation under electron microscopy displayed the presence of vesicles which is believed to be the precursors to cubosome formation. Despite of the associated cellular toxicity risks of using cationic lipids, *in vitro* study exhibited that the addition of cationic lipids was not toxic at the studied concentration. Incorporation of cationic lipids increased the cellular uptake of the cubosomes, which was due to the electrostatic interaction with the cell membrane, followed by uptake via adsorptive endocytosis pathway.

In order to further determine the potential of using surface modified cubosomes to target the BBB, all the formulations were administered intraveneously into zebrafish

larvae *in vivo* in **Chapter 5**, where the uptake and the toxicity of cubosomes in the midbrain region had been assessed. There was a significant two-fold uptake of cubosomes from larvae treated with Tween 80 and CTAB cubosomes, while lack of uptake observed in other formulations. The uptake of CTAB cubosomes into the midbrain could be related to the local toxicity effect, as visualised in toxicity studies. Other formulations, nonetheless, did not cause toxicity to the brain and no significant uptake. The uptake of Tween 80 cubosomes was not related to local toxicity and observation under electron microscopy revealed that gold-labelled Tween 80 cubosomes ended up in the brain parenchyma of the larvae. This observation highlights the potential of Tween 80 cubosomes as a drug carrier to target the brain.

In summary, this thesis supported the hypothesis that cubosomes can act as a drug carrier and be surface modified to cross the blood-brain barrier through selected pathways. Despite the lack of uptake in other cubosome formulations, Tween 80 stabilised cubosomes represent a promising approach as a drug carrier to cross the BBB.

Acknowledgements

First of all, I would like to express my biggest gratitude to my beloved husband for embarking this PhD journey together with me. Without his continuous support and inspiration, I might not be able to finish this thesis in one piece. Thank you for your encouragement to make the decision that both of us did PhD at the same time and the same place. Not to forget, our beautiful twins, Nuha and Furqan who had sacrificed their 5 years of life watching mum and dad trying to follow our dreams and future. Sorry for not being able to spend more time with you both. But I hope that one day, once both of you are big enough, you will understand what PhD really mean to us.

I owe my deepest gratitude to Dr. Shakila Rizwan for taking me as her first PhD student and guide me throughout the journey. Your support was precious and endless. The opportunity that was given is beyond words. And thank you to Prof Sarah Hook and Prof Ben Boyd for your invaluable guidance throughout the years. I am most grateful to School of Pharmacy (University of Otago) for providing me the PhD scholarship to support my study for the past few years. It is a pleasure to receive this generous scholarship to allow me to complete my journey.

Not to forget, my sincere gratitude to the staffs at Otago Zebrafish facility and Otago Centre of Electron Microscope (OCEM) for their continuous support in using zebrafish and microscopy techniques throughout my study. I am honored to receive the Electron Microscopy Award by OCEM and Travel Award by Brain Health Research Centre which have provided the opportunity to me to use exceptional techniques for my experiments and present it to the world.

Thank you to all my friends and lab mates at School of Pharmacy (Sasi, Younus and Richard), and not to forget all the supporting staffs that help me to make sure everything works well. The help, guidance and support from all of you are beyond words.

Last but not least, thank you to National University of Malaysia and Ministry of Higher Education for sending me over to University of Otago and provide me with the opportunity to further my studies and achieve my dream. Not to forget, my parents and family members for their continuous support; physically and mentally throughout my journey. Only God knows how many people have involved in this journey, and only God can reward everyone accordingly for their help and support. Thank you, thank you and thank you.

"Sarang tempua di daun palas
Alas pelitup puteri kayangan
Jasamu semua tidak terbalas
Seumur hidup jadi ingatan"

Publication arising from thesis

1. Azhari, H., Strauss, M., Hook, S., Boyd, B. J., & Rizwan, S. B. (2016). Stabilising cubosomes with Tween 80 as a step towards targeting lipid nanocarriers to the blood–brain barrier. *European Journal of Pharmaceutics and Biopharmaceutics*, *104*, 148-155.

2. Azhari, H., Hook, S., Boyd, B. J., & Rizwan, S. B. (2018). Formulation and uptake of Tween 80 cubosomes in the zebrafish brain. *Zebrafish*. Manuscript in preparation.

3. Azhari, H., Hook, S., Boyd, B. J., & Rizwan, S. B. (2018). Cationic cubosomes as drug carriers to target the blood-brain barrier. *International Journal of Pharmaceutics*. Manuscript in preparation.

4. Azhari, H., Hook, S., Boyd, B. J., & Rizwan, S. B. (2018). Characterisation and visualisation of Tween 80 cubosomes using cryo transmission electron microscopy (cryo TEM). *Journal of Microscopy*. Manuscript in preparation.

Conference presentations

1. Azhari, H., Hook, S., Boyd, B. J., & Rizwan, S. B. (2013). Liquid crystalline nanoparticles of phytantriol sterically stabilised with different surfactants: formulation, characterization and permeability studies in an *in vitro* model of the blood-brain barrier. *Australasian Pharmaceutical Science Association (APSA)*, Dunedin, New Zealand (2013)

2. Azhari, H., Hook, S., Boyd, B. J., & Rizwan, S. B. (2014). Influence of the surfactant Tween 80 on aqueous self-assembly of phytantriol. *The International Pharmaceutical Federation (FIP),* Melbourne, Australia.

3. Azhari, H., Hook, S., Boyd, B. J., & Rizwan, S. B. (2014). Investigating the influence of cationic lipids on phytantriol dispersions. *Formulation and Delivery of Bioactives (FDB),* Dunedin, New Zealand.

4. Azhari, H., Strauss, M., Hook, S., Boyd, B. J., & Rizwan, S. B. (2014). Influence of the surfactant Tween 80 on aqueous self-assembly of and dispersions of phytantriol. *Health Science Research Forum*, Dunedin, New Zealand.

5. Azhari, H., Strauss, M., Hook, S., Boyd, B. J., & Rizwan, S. B. (2015). Utilising electron microscopy to investigate the nanostructure of nanoparticles. *Microscopy New Zealand Conference*, Dunedin, New Zealand.

6. Azhari, H., Hook, S., Boyd, B. J., & Rizwan, S. B. (2015). Enhanced uptake of drug into the brain when delivered in BBB-targeted cubosomes. *Australasian Winter Conference on Brain Research*, Queenstown, New Zealand.

7. Azhari, H., Hook, S., Boyd, B. J., & Rizwan, S. B. (2015). Interaction of cationic cubosomes with immortalized human brain endothelial cells. *Diagnosis, Drugs, Devices and Discovery Conference (D4)*, Dunedin, New Zealand (2015)

8. Azhari, H., Strauss, M., Hook, S., Boyd, B. J., & Rizwan, S. B. (2015). Zebrafish can be used to determine permeability of nanoparticles across the blood-brain barrier *in vivo*. *11th International Conference on Cerebral Vascular Biology (CVB)*, Paris, France.

9. Azhari, H., Hook, S., Boyd, B. J., & Rizwan, S. B. (2016). Formulation and uptake of cationic cubosomes in the zebrafish brain. *Drug Delivery Australia Conference (DDA)*, Sydney, Australia.

Awards

1. Best poster presentation, Health Science Research Forum, University of Otago, Dunedin, New Zealand (2014).

2. Electron microscopy student award, University of Otago, Dunedin, New Zealand (2014).

3. Best paper award, Green Cross Health Pharmacy Awards, University of Otago, Dunedin, New Zealand (2017).

Table of contents

List of figures

List of tables

List of equations

List of abbreviations

AJ	adherens junction
AOT	sodium bis(2-ethylhexyl) sulfosuccinate
Apo	apolipoproteins
AUC	area under curve
ABC	adenosine triphosphate-binding cassette
BBB	blood-brain barrier
BCRP	breast cancer resistance protein
CNS	central nervous system
CPP	cell penetrating peptide
CTAB	cetyltrimethylammonium bromide
Cryo-TEM	cryo-transmission electron microscopy
CSPGs	chondroitin sulfate proteoglycans
DLS	dynamic light scattering
DMPG	1,2-dimyristoyl-*sn*-glycero-3-phospho 1'-*rac* glycerol
DOTAP	1,2-Dioleoyl-3-trimethylammonium-propane
DOTMA	1,2-di-O-octadecenyl-3-trimethylammonium propane
d.p.f	days post fertilisation
EEG	electroencephalogram
EM	electron microscopy
GABA	gamma-aminobutyric acid
GMO	glyceryl monooleate
HBMEC	human brain-microvascular endothelial cells
hCMEC/D3	immortalised human brain capillary endothelial cells

h.p.f	hours post fertilisation
HSPG	heparan sulfate proteoglycans
LDL	low density lipoprotein
LR	lissamine rhodamine B sulfonyl
MDR	multidrug resistant
MRP	multidrug-resistance protein family
NBD	1,2-dipalmitoyl-*sn*-glycero-3-phosphoethanolamine-N-(7-nitro-2-1,3-benzoxadiazol-4-yl)
NVU	neurovascular unit
PBCA	poly(butyl cyanoacrylate)
PDI	polydispersity index
PEO	polyethylene oxide
PEG	pegylated
P-gp	P-glycoprotein
PI	propidium iodide
PIHCA	poly(isohexyl cyanoacrylate)
PLGA	polyacrylamide-chitosan-poly(lactide-co-glycolide)
PPO	polypropylene oxide
SAXS	small angle X-ray scattering
SEM	scanning electron microscope
SLN	solid lipid nanoparticle
TEM	transmission electron microscope
TJ	tight junctions
TfR	transferrin receptor
ZO	zonular occludens

Chapter 1

General introduction

1 General introduction

1.1 Problem statement

In the past few decades, there has been a steady increase in the incidence of central nervous system (CNS) diseases worldwide such as Alzheimer's disease, Parkinson's disease, epilepsy, brain tumour, migraine and spectrum disorders [1]. The projection of patients diagnosed with Alzheimer's disease is expected to be 13.2 million people in the United States by the year 2050 [2], with Parkinson's disease showing a similar trend. In 2005, about 4.6 million people in Western Europe were diagnosed with Parkinson's disease and this number is expected to rise up to 9.3 million in 2030 [3]. CNS disorders not only impact the aging population, but also extend to the younger population [4]. The increase in the incidence of spectrum disorders like autism has also sparked a worldwide concern and the need for better therapies, adding a significant pressure to the health authorities [5]. CNS diseases not only contribute to the economic burden of a country, but also affect people's quality of lives [4]. There is a need to develop better treatment options to stop or slow down the disease progression of these aforementioned debilitating CNS diseases.

Even though there are a large number of CNS drugs being used clinically, achieving therapeutic levels of drug in the brain, particularly for new therapeutic compounds remains a significant challenge due to the presence of physical and chemical barriers at the brain that limits the type and amount of CNS drugs to enter the brain [6-8]. One of the major barriers to achieve therapeutic levels of drug in the brain to treat CNS disorders lies behind the presence of the blood-brain barrier (BBB) that selectively prevents drug molecules from entering the brain parenchyma [9]. Large molecules such as monoclonal antibodies, antisense drugs and recombinant proteins show potential benefits

in treating CNS diseases, however, due to the size and the physical properties of these molecules, their uptake is limited [10-13]. Furthermore, small or water-soluble drug molecules with therapeutic CNS effects are also prohibited from entering the brain because of the selectivity at the BBB. If these selectivity issues at the BBB can be resolved by masking the properties of the drug molecules, there is a high chance that a variety of drugs can be utilised to treat CNS diseases, reach therapeutic levels in the brain and at the same time reduce any peripheral side effects [14].

Nanoparticles can be used as drug carriers to improve drug delivery to the brain. Various nanoparticles synthesised from polymers and lipid such as polymeric nanoparticles and liposomes have been developed to increase delivery of drugs into the brain. Surface decorations or modification on the surface of the nanoparticles have been developed to target specific pathways at the BBB and to allow uptake of drug molecules into the brain [7, 15-21].

Lipid-based nanoparticles have been investigated as drug carriers, including liposomes and solid lipid nanoparticles [22, 23]. For example, liposomes were surface modified with the addition of transferrin to target the transferrin receptor at the BBB [22, 24, 25] where docetaxel encapsulated in the transferrin conjugated liposomes was delivered into the brain (rats) as compared to non-targeted liposomes [25]. A number of studies on transferrin-conjugated liposomes were studied and reviewed [22] to show that transferrin conjugated liposomes can be a potential carrier to target the BBB. Meanwhile, solid lipid nanoparticles are also widely studied as drug carriers to target the brain. The studies on solid lipid nanoparticles were compiled and reviewed previously [23, 26]. To target the BBB, the surface of solid lipid nanoparticles was coated with apolipoprotein E and Tween 80 [27] for uptake through LDL-receptors, while melanotransferrin antibody was conjugated on the surface to utilise the transferrin receptors [28]. Even though these studies were

showing the potential of liposomes and solid lipid nanoparticles as drug carrier to target the brain, this thesis will explore a different type of a more versatile platform of drug carriers with ease of preparation and a higher drug loading potential to maximise the uptake of drugs into the brain.

The use of lipid-based nanoparticles, cubosomes as drug carrier to the brain is yet to be discovered. This thesis will explore a novel lipid-based delivery system, cubosomes to target different endogenous molecular trafficking pathways at the BBB with the aim of increasing drug delivery to the brain. Suitable *in vitro* and *in vivo* models will be used to investigate the potential of cubosomes for cellular uptake and toxicity at the BBB.

1.2 The role of blood-brain barrier (BBB) in drug delivery to the brain

The anatomy and the transport systems at the BBB play an important role in developing a suitable strategy for delivering drugs into the brain.

1.2.1 Anatomy of the BBB

The discovery of the BBB was documented back in the 1880s where Paul Ehrlich showed that when an aniline dye was administered intravenously into a rat, all the organs were stained except for the brain and the spinal cord (reviewed by [29-31]). This observation formed the basis of the presence of a barrier at the brain, which selectively allows molecules to pass. The biological reason for this barrier is now well established and is to protect the brain from toxins and cells of the immune system by regulating the entry of compounds into and out of the brain, while only allowing the entry of molecules that are crucial for brain homeostasis [32-34]. The BBB is made of the cellular complex known as

the neurovascular unit (NVU), which collectively forms the physical, transport and metabolic barrier at the BBB [35, 36].

The NVU consists of endothelial cells, astrocytes, pericytes, neurons and surrounded by basal lamina (**Figure 1.1**). The network of constant "communication" within the NVU forms a functional BBB and maintains the integrity of the barrier. The presence of NVU limits the uptake of drug molecules into the brain as the cells are "cemented" together by the presence of tight junctions (TJ) and adherens junctions (AJ) [37]. TJ are the predominant barrier for paracellular diffusion of molecules across BBB. They appear as a parallel series of interconnected strands or fibrils and are comprised of integral membrane proteins; occludin, claudin and junctional adhesion molecules [36, 38-40]. Signalling and regulatory proteins like ZO-1-associated nucleic acid binding protein, multi-PDZ-protein 1, afadin (AF6) and membrane-associated guanylate kinase tightly regulate the paracellular pathway, hindering the free diffusion of polar solutes and drugs across the BBB.

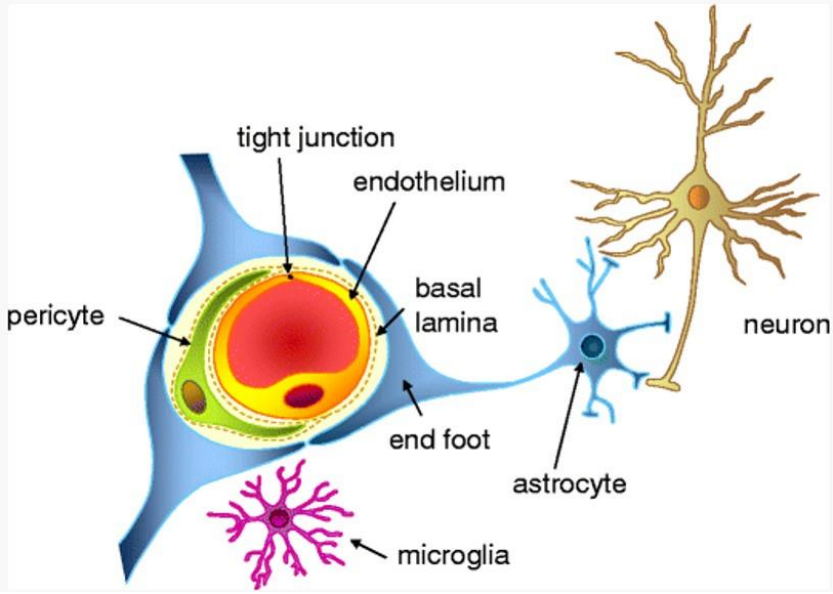

Figure 1.1 The neurovascular unit (Adapted from [9] and reproduced with permission).

Astrocytes and pericytes are located in close proximity within the NVU and together they modulate the maturation of brain endothelial cells. Pericytes are often found in between endothelial cells whilst astrocytes are located at the capillary basement membrane. Pericytes are involved in the angiogenesis of micro-capillaries at the BBB and provide structural integrity to the blood vessels through their close contact with endothelial cells [29, 30, 38, 41-43]. Astrocytes are involved in phenotypic changes of the endothelial cells at BBB and contribute to the BBB development [38, 44-46]. Soluble factors secreted by astrocytes (for example zonular occludin, ZO) have been shown to promote the TJ formation by increasing the length, width and number of TJ [47, 48].

1.2.2 The transport of drug molecules across the BBB

In contrast to peripheral capillaries, brain endothelial cells lack fenestrations, have lower pinocytic activity, higher mitochondrial content and presence of tight junctions [30]. As a result, the transport of molecules across the brain endothelial cells is strictly limited as compared to peripheral endothelial, as illustrated in **Figure 1.2**.

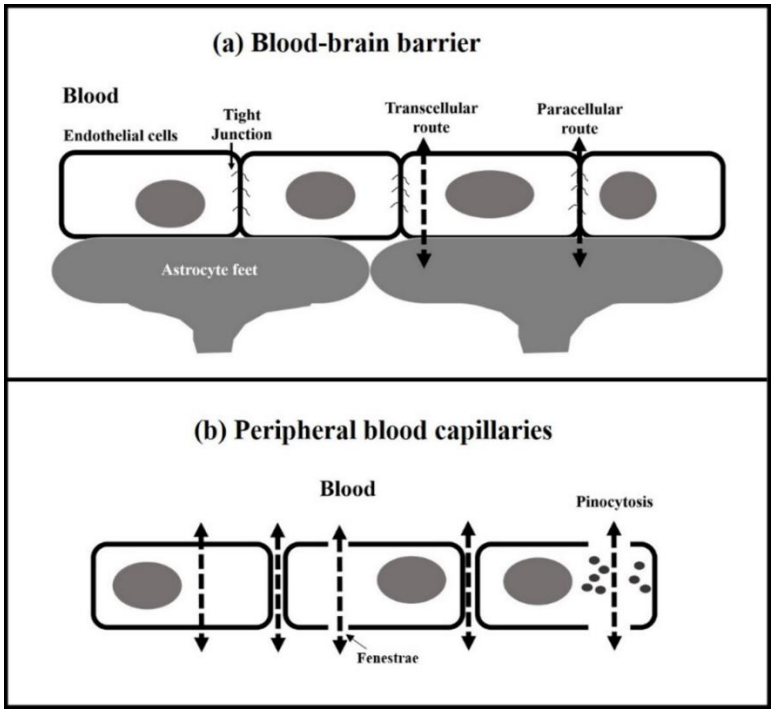

Figure 1.2 Schematic diagrams of (a) the BBB which shows the tight junction that limits the permeability of molecules through paracellular route. Peripheral blood capillaries (b) have loose tight junctions, presence of fenestrae and high pinocytic activities that allow more molecules to pass through.

Despite the strict regulation at BBB, selected drug molecules are still able to enter the brain through similar pathways to that used by endogenous molecules such as glucose, hormones, proteins and ions, to maintain homeostasis [49, 50]. Small hydrophilic molecules can enter the brain through the paracellular pathway whilst lipid molecules enter predominantly through the transcellular pathway as shown in **Figure 1.3**. Large molecules utilise carrier-mediated, receptor-mediated and adsorptive endocytosis transport pathways. Molecules that are substrates to efflux pumps are pumped out of the cells by active efflux transporters [37, 51, 52]. In addition, molecules are also subjected to metabolism by intracellular and extracellular enzymes such as monoamine oxidase, peptidases, nucleotidases and cytochrome P450 enzymes [53]. The transport pathways at BBB is summarised in **Figure 1.3** and discussed in more details in subsequent sections.

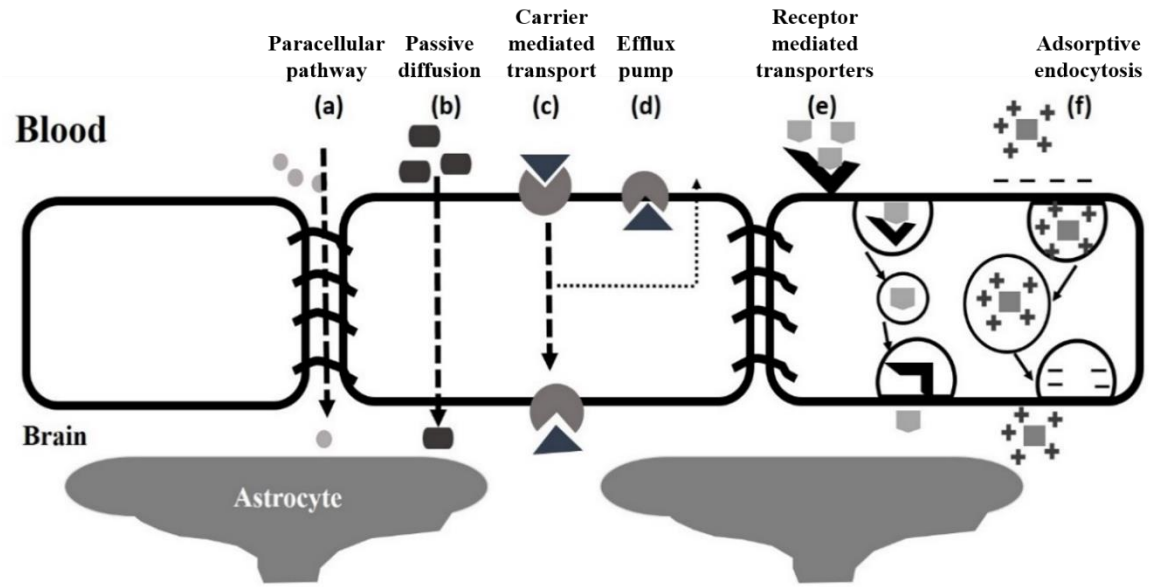

Figure 1.3 Schematic illustration of the different routes of molecular transport across BBB.

1.2.2.1 Passive transport system

Passive transport of molecules across the BBB can be through the paracellular pathway (**Figure 1.3a**) where the transport is often restricted to small polar molecules and ions of less than 500 Da due to the presence of TJs [54-56]. The transient opening of TJs has been explored as a mean to allow drug molecules to pass through the paracellular pathway [57-59]. Administration of bradykinin and its analogues in patients with malignant glioma has been shown to transiently increase the permeability of drugs such as the chemotherapeutic carboplatin across BBB through paracellular transport in pre-clinical studies [60]. These molecules initially bind to the B_2 bradykinin receptor and trigger an increase in intracellular Ca^{2+} that causes contraction of brain endothelial cells and malformation of TJs and an increase in drug permeability at the BBB [61-63]. This technique was tested on small polar molecule, inulin (400 Da) where the opening of TJs by Cereport (bradykinin agonist) allowed the diffusion of inulin across the HBMEC cell [62]. However, the permeability across the TJs from Cereport administration was restricted to small polar molecules only.

Several peptides have also been investigated as potential TJ modulators. PN-159 (permeabilising peptide) was found to increase the uptake of larger polar molecules such as albumin (65 kDa) across the tight junction. The exact mechanism of action of the peptide remains to be fully elucidated, but "leakiness" of the TJs due to the inhibition of ZO-1 cytoplasmic TJ linker protein, which decreases the tightness in between endothelial cells has been proposed as a potential mechanism of action [64]. Other peptides such as 7-mer and AT-1002 have also been shown to induce transient TJ opening at the BBB [65-68]. However, chronic administration of TJ modulators have not been fully explored and there are concerns that it may lead to the damage at BBB and disrupt its protective role [59, 65].

Another passive pathway at the BBB is through transcellular pathway, where small lipophilic and amphiphilic molecules (< 700 Da) have been reported to passively diffuse across the endothelial plasma membrane [9, 69, 70]. Transcellular transport of small molecules and drugs with high lipophilicity is favoured across the BBB, as the cell membrane is made of lipid bilayers which impart a large surface area to the cell membrane and allows high rates of diffusion into cells [71]. However, the amount of cholesterol in endothelial cells increases lipid-packing density in the endothelial cell membrane, and limits the movement of large lipid molecules across the cell [72, 73]. The permeability of the BBB to lipophilic drugs can be predicted from the octanol/water partition coefficient at pH 7.4 (log P) for non-ionised and ionised molecules. In general, drug molecules with $-1 \leq \log P \leq 4$ show increased permeability across the BBB [74]. Increasing lipophilicity of drugs has been used as a strategy to increase their permeability across BBB, however this does not always improve transcellular diffusion. Increasing lipophilicity of drugs favours binding to efflux transporters, thus prohibiting their entry into the brain [75].

Active efflux transporters (**Figure 1.3d**) are important in regulating brain homeostasis by preventing certain xenobiotic, hydrophilic and hydrophobic molecules from entering the brain, thus protecting the brain from potential damage [43, 76]. The adenosine triphosphate-binding cassette (ABC) transporters, which include the P-glycoprotein (P-gp) transporter, multidrug-resistance protein family (MRP) and breast cancer resistance protein (BCRP) are the main efflux transporters at the BBB.

P-gp is an efficient gatekeeper, as it actively transports molecules out of the brain with high efficiency and it is highly expressed at the BBB [77]. A large number of lipophilic drugs are pumped out by P-gp [75]. For example, cyclosporine A, which is lipid soluble, does not show high therapeutic accumulation as expected due to the presence of efflux

transporters [37]. The drug molecules are actively being pumped out of the cells by the efflux transporters. Co-administration of cyclosporine A with a P-gp inhibitor was shown to increase its uptake [78]. In addition, successful seizure treatment has been reported with co-administration of phenytoin drug (P-gp substrate) with verapamil, a P-gp inhibitor [79, 80].

Regadenoson®, an A2 adenosine receptor agonist is a coronary vasodilator commonly used in cardio stress test and known to inhibit the efflux transporter P-gp. In a clinical trial, co-administration of Regadenoson® with temozolamide in patients with malignant glioma and resectable brain tumours showed a positive impact on the survival of the patient (life expectancy). Increased uptake of temozolamide into the brain was observed and associated with the inhibition of P-gp transport by Regadenoson® [81-85]. Moreover, the short half-life of Regadenoson® (2 to 3 min) can induce transient increase in the permeability of the BBB to allow higher drug accumulation in the brain [86]. However, chronic administration of efflux pumps inhibitors can lead to neurotoxicity [87, 88]. Defects in efflux transporter have been implicated in neurological conditions such as Alzheimer's disease where amyloids accumulate in the brain without being cleared [88].

1.2.2.3 Carrier-mediated transporters

To maintain brain homeostasis, important nutrients such as glucose, amino acids, nucleosides and organic ions move from the blood into the brain (influx transport system), while to prevent the accumulation of toxins, neurotoxic compounds and metabolites are transported out (efflux transport system). Selected polar macromolecules enter the brain through carrier-mediated transporters (**Figure 1.3c**), which are located at the luminal or abluminal side of the cells, making this a form of molecular transport unidirectional. The type of transporter determines the direction of molecular transport; either into or out of the brain [89]. Sodium-independent neutral amino acid transporter (system L) transports L-tyrosine, L-tryptophan and L-histidine into the brain as neurotransmitter precursors [90, 91]. Other amino acids including L-leucine, L-isoleucine, L-methionine, L-phenylalanine, L-valine and L-threonine are transported through system L and involved in protein synthesis in the brain.

In order to use the carrier-mediated pathway for drug delivery, the drug molecules need to mimic the structure of endogeneous substrates. Only two transporters will be discussed here as examples of carrier-mediated transporters used for drug delivery; LAT1 and GLUT1. System L has LAT1 (SLC7A6), to transport amino acid-mimetic drugs such as L-Dopa into the brain. L-Dopa is converted into dopamine and used as a treatment for schizophrenia and Parkinson's disease [92-95].

GLUT1 is located at luminal and abluminal sites of the BBB but allows only unidirectional transport of D-glucose from the blood into cell and into the brain parenchyma. Initially D-glucose enters the endothelial cells through GLUT1 at the luminal site and then transported out of the cell into the brain parenchyma using GLUT1 on the abluminal site. GLUT1 is also able to transport L-dehydroascorbic acid into the brain which is converted to L-ascorbic acid. L-ascorbic acid is not a substrate of GLUT1

which means that it will retain in the brain without being transported out and leads to a higher concentration of L-ascorbic acid in the brain [96, 97]. Based on the knowledge of D-glucose transport, drug molecules have been conjugated with glucose molecule to improve their delivery into the brain. For example, glucose conjugated to chlorambucil was shown to bind to the GLUT1 receptor and inhibit the binding of other glucose molecules from the blood. The binding of glucose conjugated chlorambucil to GLUT1 was in a concentration dependent manner which shows that the transport of chlorambucil into the cells can be increased from the conjugation with glucose [98].

Nanoparticles have also been coated with glucose to target the GLUT-1 glucose transporters at the BBB. For example, intranasal administration of exosomes which are a type of nanoparticle, coated with glucose led to increased uptake and localisation of the exosomes at the lesion site in the mouse model of brain ischaemia within 24 hours after intranasal administration. As compared to intravenous administration of glucose coated exosomes, the exosomes retained in the brain after intranasal administration. This showed that while both routes demonstrate significant uptake of exosomes in the brain, but the administration through IV route was subjected to rapid clearance from the brain. However, in both routes, from the receptor inhibition study using cytochalasin B (glucose transport inhibitor) and receptor saturation using D-glucose, the uptake of glucose coated exosomes into the cell were proposed to be via GLUT-1 transporters at BBB. In addition, dual labelling with fluorescence molecule allows the tracking of nanoparticle's fate after the administration [99]. A detailed review on developing nanoparticles conjugated to glucose transporter substrates in order to utilise GLUT receptors at the BBB was previously published [100]. In addition, there are other carrier-mediated transporters such as nucleoside transport system, organic anion transport system and neurotransmitter transport system available which will not be discussed in any further detail in this thesis.

Despite the potential, there are some major drawbacks in developing drug molecules to target carrier-mediated transporters. The drug molecule has to be designed to structurally mimic the endogenous substrates or conjugated to the substrates for successful binding and uptake by the transporters. This can lead to competitive binding with endogenous substrates. Furthermore, chronic administration of the drug molecules can lead to receptor saturation and disrupt normal homeostasis at the BBB [101]. Nevertheless, this pathway is promising, and drug molecules are being developed to utilise the transporters to deliver drug to the brain.

1.2.2.4 Receptor-mediated transcytosis

Macromolecules like peptide and proteins bind to specific receptors on the surface of the endothelial cells and are endocytosed (**Figure 1.3e**) [102]. The uptake process starts with ligand binding to a receptor, which triggers a cascade of reactions. Firstly, the receptor-ligand complex is internalised by clathrin-coated pits into the cell, and forms an early endosome [103]. Then the contents of the endosome are released into the cell upon the enzymatic activity by the lysosome, and the receptors are recycled back to the plasma membrane. The content will either stay in the cytosol or is translocated to the cell basement membrane and enters the brain parenchyma [104]. This process is energy dependent [105].

Certain receptor-mediated pathways are currently being explored as potential target to design "Trojan horse" molecules which are endocytosed by the endothelial cells [106, 107]. For example, the transferrin receptor (TfR) expressed at the luminal and abluminal side of endothelial cells allows bidirectional transport of transferrin molecules [107]. TfR is expressed at the luminal and abluminal side of endothelial cell to allow the transport of TfR substrate in both ways [108, 109, 110]. Chitosan nanoparticles functionalised with transferrin molecules and loaded with fibroblast growth factor had increased uptake into the brain as compared to non-functionalised chitosan nanoparticles. The inhibition of uptake by imatinib suggested that the uptake of transferrin functionalised chitosan nanoparticles was from the binding with TfR at the BBB [111]. Insulin receptors and low density lipoprotein (LDL) receptors are also expressed on endothelial cells at relatively high levels [112-114] and have been explored for drug and nanoparticle delivery into the brain [37]. This pathway will be explored in this thesis by developing cubosomes nanoparticles surface decorated with specific moiety to target the LDL-receptor at the brain. Further discussion will be outlined in detail in **Chapter 3**.

1.2.2.5 Adsorptive endocytosis

Macromolecules such as albumin can enter the brain through adsorptive endocytosis pathway (**Figure 1.3f**). Uptake of molecules via this pathway depends on the electrostatic interactions between positively charged molecules or ligands and the negatively charged cell membrane (endothelial glycocalyx) [37]. An endocytic cascade follows, and the molecules are translocated from the blood to the brain. The whole process is energy and temperature dependent [37, 115-118]. The uptake is low affinity, high capacity and less specific than receptor-mediated transcytosis, as electrostatic interactions can occur on cells from other tissues in the body [119]. Ebiratide, a drug used for treating Alzheimer's disease has a positive charge and in *in vitro* studies with primary cultured bovine brain capillary endothelial cells showed that the uptake of Ebiratide into the cells was via adsorptive endocytosis [120, 121]. This pathway will be explored by developing cationic cubosomes to target the negatively charged membrane of the brain endothelial cells for further uptake by the brain. A more detailed discussion on this pathway will be outlined in **Chapter 4**.

1.3 Strategies for drug delivery to the brain

1.3.1 Invasive strategies

Although advanced drug development has led to various drug formulations and techniques to improve drug delivery to the brain, several potent drug molecules are still not able to cross the BBB and reach the desired therapeutic level. One strategy to overcome this problem is to use invasive methods often involving surgery to breach the BBB and directly deliver the drug into the brain parenchyma. These approaches are discussed in more detail below.

1.3.1.1 Intracerebroventricular injection

Intracerebroventricular injection involves the direct delivery of drug molecules that have limited permeability across the BBB, by administering into specific sites within the brain parenchyma [122-124]. This pathway is preferred when a high dose of drug loading in the brain is desired. It has been studied for treating Alzheimer's disease, autism, seizure and in cerebral ischemia-reperfusion injury [125-127]. It provides a faster effect as compared to intravenous and oral administration. For example, intracerebroventricular injection of fibroblast growth factor reached a higher concentration in the brain as compared to intravenous injection [128, 129]. However, due to the invasive technique involved in this method, it is not suitable for chronic administration [130-132].

1.3.1.2 Intracerebral administration

Intracerebral administration involves administration of drugs directly into the brain parenchyma. In convection enhanced delivery, a catheter is implanted directly in

the brain and the application of hydrostatic pressure allows the drugs to diffuse directly for further penetration into the brain. Another way is to implant degradable or non-degradable polymers directly into the brain to release the drug slowly over time. In phase I/II clinical trial, the cancer drug, D2C7-IT was studied as immunotoxin for glioblastoma treatment and delivered through intracerebral convection-enhanced delivery using osmotic pumps. D2C7-IT was shown to have strong anti-tumour effect by inhibiting the protein synthesis and kills the epidermal growth factor receptors expressed on the glioblastoma cells [133]. The continuous release of drugs from this method can reduce the frequency of drug administration and costs. The result from this study is promising and the study is on its way for Phase I/II clinical trials for adults with recurrent malignant glioma.

Gliadel® wafer which contains carmustine (alkylating agent) was released into the market to treat high-grade glioma. This wafer is implanted at the tumour site, during tumour removal surgery in the brain. The degradation of the wafers leads to the release of carmustine and kills the tumour tissues. Even though the prognosis after using Gliadel® is still poor (increased survival by 2 months), this treatment still offers an improvement in survival for glioma patients [134].

Another CNS drug, vigabatrin, an epilepsy drug that is commonly administered orally; was delivered via intracerebral administration in rat models with refractory epilepsy and showed that there was a small increase ($p<0.05$) in seizure threshold, which comes from the increase in local GABA concentration [135]. It is used as an adjuvant treatment for epilepsy and seizure. This drug is commonly used orally; however, delivering this drug through intracerebral administration has shown potential in treating refractory epilepsy. Unfortunately, chronic intracerebral administration of vigabatrin in the brain was associated with encephalopathy and extrapyramidal symptoms [136].

Despite the advantages offered from intracerebral administration of drugs, the other limitations behind this technique are (1) the risk of developing astrogliosis (abnormal increase of astrocytes due to trauma) because of the hydrostatic pressure from the infusion, and (2) the need to replace the implant in the brain which necessitates expensive and invasive procedures [35, 137].

1.3.1.3 Osmotic disruption

Reversible osmotic disruption at the BBB can temporarily open the cerebral vessel TJs to deliver drug molecules into the brain. To induce disruption, a hypertonic solution such as mannitol (around 1.4 M) is administered via carotid artery as a short (often 30 min) infusion. The changes in osmolarity lead to a transient increase in intracellular Ca^{2+} concentrations and alter intracellular signal transduction. The change in Ca^{2+} concentration leads to calcium-mediated oxidative stress and causes the opening of TJs between the endothelial cells [138, 139]. During this period, BBB becomes "leaky" and significantly more administered drugs can cross the BBB [140, 141]. However, after removal of the mannitol, the BBB does not fully recover as the osmotic disruption causes damage to the cells. Repeated application of this procedure can lead to a long-term damage to BBB and compromising the BBB integrity. Risks of stroke and epileptic seizures are associated with this method of drug delivery [142]. However, it can be used in later stage of neurological disease when aggressive drug loading is desired to reduce the severity of the disease, improve prognosis and the risk of death outweigh the risk of associated side effects [143-146].

1.3.1.4 Focused ultrasound

Ultrasound energy has been studied as a less invasive method to deliver drug molecules to targeted areas within the brain. Focused ultrasound allows transcranial delivery of drug into a specific area in the brain with higher drug penetration and longer drug retention at the target site [147]. Microbubbles are used in focused ultrasound therapy where they function as a catalyst to amplify the local cavitation in the capillary of the brain. Conventional microbubbles are made of perflutren (Definity® and Optison™) or sulphur hexafluoride (Sonovue) [148]. Initially, microbubbles are injected intravenously as a contrast agent followed by administration of the drug molecule, or the drug can be incorporated into the core shell of the microbubble and the ultrasound is applied (0.1 to 1.5 MHz) to the brain region of interest. Ultrasound causes an oscillation in the blood vessel and increases permeability of the endothelial cells by opening the TJs [149]. The permeability at the BBB can last anywhere from six to eight hours after the procedure [150-152]. The core shell is stabilised using phospholipids, proteins or polymers [153, 154]. Adding ligands on the surface of microbubbles can further promote specific tissue targeting for localised drug delivery [155]. Polyethylene glycol (PEG)ylated liposomes containing glial cell line-derived neurotrophic factor and nuclear receptor-related factor 1 was conjugated to microbubbles and was found to increase dopaminergic neurons in the rat model of Parkinson's disease [156]. The opening of endothelial cells at the BBB by microbubbles and ultrasound is illustrated in **Figure 1.4**.

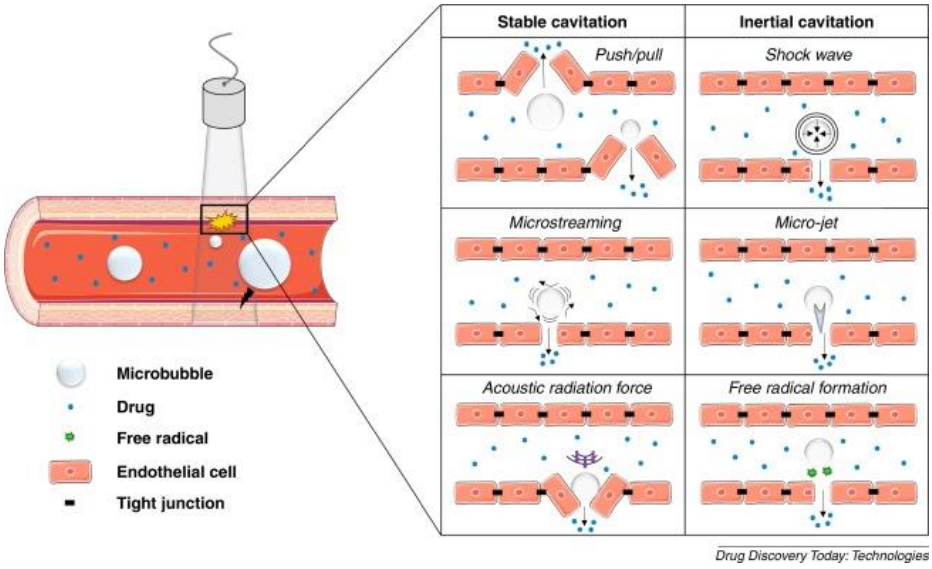

Figure 1.4 Schematic illustration of the effects from microbubbles during ultrasound application. Ultrasound causes microbubbles to oscillate (stable cavitation) or implode (inertial cavitation). In stable cavitation, the tight junctions on the endothelial cells can temporarily open from push-pull mechanisms while microstream is a fluid-flow that occurs from the rapid expansion and contraction of microbubbles which affect the integrity of the endothelial lining. In addition, acoustic radiation force occurs due to the pressure gradients that lead to a reduction in vascular permeability. Meanwhile, in "inertial cavitation", the fragmentation of microbubbles causes an increase in temperature and pressure, which lead to formation of "shock waves" and "micro jet". These effects will increase vascular permeability. Lastly, "free radical" can also be formed and permeabilise the endothelial cells. Drug molecules in the blood or in the microbubbles core shell can cross the BBB from one of the mechanism shown (Reproduced with permission from [157]).

The degree of permeability from BBB disruption can be controlled by the concentration and size of the microbubbles [158-160]. The leakiness at the BBB allows the movement of small and large molecules into the brain. Doxorubicin (580 Da), paclitaxel (854 Da), and herceptin (148 kDa) were shown to have increased permeability into the brain using the focused ultrasound method [6, 161]. Temozolamide delivery using ultrasound is in clinical trials for the treatment of glioblastoma [162]. Moreover, a leaky BBB was shown to contribute to the clearance of amyloid from the brain in Alzheimer's patient.

This technology is still in the pre-clinical stage but shows great promise in treating Alzheimer's disease [163]. The limitation in using focused ultrasound comes from the unpredictable disturbance in the brain from the ultrasound with unknown long-term damage from the repeated opening of the BBB. More studies are underway in utilising magnetic resonance imaging as a guide to target ultrasound precisely and to evaluate any damage at BBB from the ultrasound [164].

1.3.2 Non-invasive strategies

Even though invasive strategies can provide a higher drug loading in the brain parenchyma, risks associated with the techniques can be high with expensive costs and require specialist expertise [165-167]. Invasive strategies are also not often suitable for chronic drug administration. Hence, non-invasive strategies are more favourable for long-term treatment of neurological diseases. Non-invasive strategies currently being investigated include chemical modification of drug molecules, intranasal drug delivery and formulation approaches to manipulate the BBB pathways [70, 168-170]. These are discussed in more detail below.

1.3.2.1 Chemical modification of drug molecules

Since the majority of drug molecules lack properties for entry into endothelial cells (such as being lipophilic and having a molecular weight <400 Da), the development of prodrugs has been investigated [171, 172]. Prodrugs are inactive molecules that require a chemical or enzymatic reaction to convert them into active drug molecule such as L-dopa as discussed in **Section 1.2.2.3**.

Recently, paliperidone prodrug dimer (Pal-8SSme) was synthesised where the original drug, paliperidone (anti-psychotic) is a substrate to P-gp and ABC transporters at the BBB. Two molecules of paliperidone were attached via dimerisation and this leads to inhibition of P-gp and ABC transporters at the BBB. After the uptake and inhibition at the BBB cells, the dimers then converted to paliperidone monomer and delivered into the brain parenchyma. The synthesis allows the entry of paliperidone into the brain without being pumped out by P-gp and ABC transporters [173].

Sobetirome ethanolamide prodrug was developed to stimulate myelin repair in multiple sclerosis. Sobetirome is a thyroid hormone which has limited permeability across the BBB. The synthesis of ester prodrugs of sobetirome will increase the uptake through active (amino acid, glucose and choline transporters) and passive pathways at the endothelial cells, and within the cells, non-specific esterases will cleave the prodrug ester and leaving behind active sobetirome in the brain [174]. The addition of ester molecule on CNS drugs provides a useful strategy to utilise the esterases available in the endothelial cells to convert the prodrug into active drug molecules within the brain parenchyma.

1.3.2.2 Intranasal drug delivery

Intranasal drug delivery has been shown to bypass the BBB and deliver drugs into the brain. The drug needs to be administered into the olfactory region of the nasal cavity (**Figure 1.5**), from where it is believed that the drug traverses the olfactory epithelium and enters the olfactory bulb. The drug is then thought to travel through the olfactory and trigeminal nerves to reach the brain parenchyma [175].

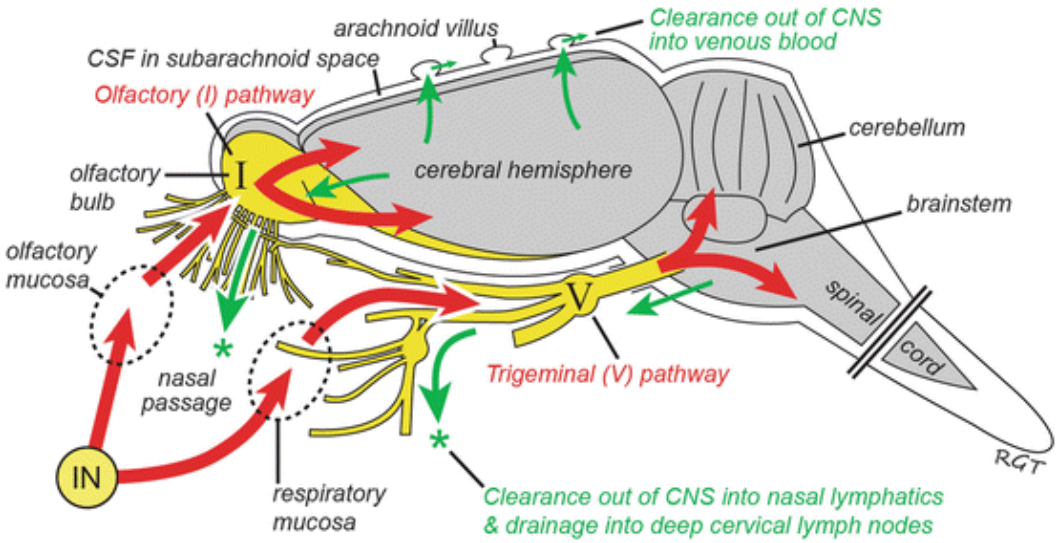

Figure 1.5 Intranasal drug delivery provides drug access of to the brain through olfactory pathway and trigeminal pathway. Reproduced with permission [176].

Intranasal administration of insulin has been investigated for treating Alzheimer's disease [177-179]. The use of intranasal insulin was found to support memory function and improve cognitive impairment in patients with Alzheimer's disease [180]. CPEX Pharmaceuticals has developed their intranasal insulin product (Nasulin®) to deliver the insulin for diabetic management [181, 182]. However, at the same time, the use of nasal insulin was found to support memory function and improve cognitive impairment in patients with Alzheimer's disease [180]. Other studies reported improvements of cognitive function corresponding to a decline in amyloid protein, Aβ42 level in cerebrospinal fluid after intranasal insulin administration [168, 183]. In another study, chloramphenicol acetyltransferase, a bacterial enzyme that catalyses chloramphenicol antibiotic, was successfully delivered into the brain region of rats through intranasal administration within 15 minutes of application [184].

Even though these studies suggest that intranasal administration can be a potential non-invasive therapy for delivering drugs to the brain, there are still challenges in using the intranasal pathways The limitations in using nasal pathway includes the limited

volume for administration, mucociliary clearance, potential enzymatic degradation and small anterior anatomy of the nasal cavity [185-189].

1.3.2.3 Nanoparticles as drug carriers

Nanoparticles are potential drug carriers that have been widely studied for the delivery of drugs into the brain across the BBB [190, 191]. Nanoparticles are 1 to 1000 nm particles in diameter, and can be produced from biodegradable polymers, lipids or a combination of both as shown in **Table 1** and are able to bind or encapsulate drug molecules [192]. The size allows the particles to be endocytosed into the cell via the different pathways discussed in **Section 1.2.2**. The encapsulation of drugs inside the nanoparticles provides protection to drugs from degradation and importantly, can mask undesirable properties of the drug that may prevent uptake into the brain [193]. Nanoparticles can also be modified to provide controlled release properties [194-197] and the surface can be decorated with ligands for site-specific drug targeting, or the charge on the surface can be controlled [198-202].

Poly(lactic-co-glycolic acid (PLGA) and polybutylcyanoacrylate (PBCA) polymers have been used extensively to prepare nanoparticles which can target the BBB. These polymeric nanoparticles have also been surface decorated with surfactants such as Tween 80 and poloxamers, such as Poloxamer 188, to target receptors present on the endothelial cells. PLGA nanoparticles decorated with Poloxamer 188 or alginate hydrogel were able to increase the uptake of doxorubicin, dexamethasone, loperamide, quercetin and cerebrolysin [203-205]. PBCA nanoparticles surface modified with Tween 80 were shown to increase the uptake of dalargin, gemcitabine, kyotorphine, loperamide and gemcitabine into the brain in all groups studied [152, 206-210]. Modifications of other types of

nanoparticles including micelles, liposomes, microcapsules, dendrimers, solid lipid nanoparticle and cerium oxide are shown in **Table 1.1** below. However, despite the extensive studies, the uptake was not being replicated in humans. The scalability and manufacturing issues can be the limitation in producing the formulation at a larger scale. In addition, stability is another concern where in lab setting, the nanoparticles are freshly prepared, and stability might not be an issue [211].

Table 1.1 Nanoparticles developed as drug carriers to target the BBB

Type of nanoparticles		Surface modification	Drug	References
Polymer	PLGA	Poloxamer 188	Doxorubicin	[212]
			Loperamide	[213]
		Alginate hydrogel	Dexamethasone	[203]
		None	Quercetin	[204]
		None	Cerebrolysin	[205]
	PBCA	Tween 80	Dalargin	[206]
			Gemcitabine	[214]
			Kyotorphin	[207]
			Loperamide	[210]
			Rivastigmine	[209, 215]
	Dendrimers	None	No drug used	[216, 217]
Lipid	Micelles	None	Bevacizumab	[208]
	Liposomes	PC:Chol:DSPG	Amphotericin B	[218]
				[219]
		AmBisome		[220]
	Solid lipid	Cationic bovine serum albumin	Doxorubicin	[221]
		None	Atazanavir	[222]
		Transferrin	Quinine	[223]
Others	Cerium oxide	None	Lenalidomide	[224]
	Microcapsules	Sodium alginate	Human endostatin	[225]

PLGA: Poly(lactic-co-glycolic acid), PBCA: polybutylcyanoacrylate

Varying degrees of brain uptake have been reported from nanoparticle uptake studies. Uptake of nanoparticles into the brain are usually observed under fluorescent or electron microscope by fluorescent labelling or with electron dense molecule. Electron dense molecules such as gold, silver or platinum also allow observation and localisation of the nanoparticles in the brain at a cellular level with the aid of electron microscopy. Fluorescently labelled PBCA nanoparticles coated with Tween 80 were observed in mouse brain sections under a fluorescence microscope and confirmed the uptake into the brain of a mouse [226].

The use of fluorescence and electron microscopy can be a challenge in measuring the successful uptake of nanoparticle into the brain. For example, in electron microscopy, the animal needs to be sacrificed and the brain sample needs to go through various preservation and fixation steps. The administration of PEG-amine/galactose coated with gold nanoparticles in rat model was observed primarily in the cytosol of microvascular endothelium in the brain. [227, 228]. Even though the authors concluded that the observation was due to the uptake into the brain, however, there is a concern that the observation of the particle was an artefact from the processing of the tissue sectioning and preservation methods used for electron microscopy techniques. Osmium tetroxide and glutaraldehyde have been found to produce artefacts that look like dense particles in tissue sections [229-231]. Therefore, ideally the uptake of nanoparticles into the brain is best done using live imaging techniques.

1.4 Cubosomes as drug carrier to the brain

Despite various studies conducted on various type of nanoparticles to carry drugs to target the brain, this thesis is interested with the use of lipid-based nanoparticles. Certain amphiphilic lipids that can self-assembled in water to form highly ordered structures can be dispersed in aqueous environment to form lyotropic liquid crystals [232]. There are various types of self-assembled lipid carriers which include liposomes, cubosomes and hexosomes. In the next few sections, the dispersions of lyotropic liquid crystals will be discussed and the advantage of using cubosomes as the drug carrier of option to target the BBB will be reviewed.

1.4.1 Lyotropic liquid crystals

Lyotropic liquid crystals (LLC) are an interesting field to explore in developing lipid-based nanoparticles to target the BBB. Molecules that commonly form LLC phases are amphiphilic with a hydrophilic head and a lipophilic tail that can self-assemble in aqueous environments to form highly ordered structures (mesophases), which have properties in between solid crystals and isotropic liquids [233-235]. Furthermore, these large-scale structures can be dispersed into nanosized particles. LLCs are sensitive to changes in the concentration of amphiphiles or water, where the molecules can change from a less ordered state (micelles) to more ordered state (inverse cubic phase) or vice versa [236]. The flexibility provided by fine-tuning the concentration of amphiphiles and water provides an advantage of using LLCs as self-assembling lipid nanoparticles over polymer-based nanoparticles [237-239]. In the following sections, the lipid self-assembly of LLCs will be discussed, as will the advantages of using cubosomes as a drug carrier to target the brain.

1.4.2 Lipid self-assembly

Amphiphilic molecules such as polar lipids that form LLC can self-assemble and spontaneously form different ordered structures in aqueous environment such as the lamellar, hexagonal and cubic mesophases. Amphiphilic molecules consist of hydrophobic tail and hydrophilic head, which orientate to form lipid bilayers in an aqueous environment. The specific structure or mesophase formed is greatly influenced by the molecular structure of the amphiphiles and can be predicted using the critical packing parameter (CPP). The CPP is a geometrical value that compares the ratio between the volume of hydrophobic liquid tail (*v*), the cross-sectional lipid head area (*a*) and the lipid chain length (*l*) as shown in **Equation 1** below. The CPP can be used to predict the curvature (shape) and the geometry of the whole molecule at the lipid-water interface.

Equation 1 $$\boldsymbol{CPP = \frac{v}{al}}$$

The curvature of lipid monolayers is affected by the amphiphilic lipid structure as shown in **Figure 1.6.** Lipids with CPP value of 1 (Type 0) usually self-assemble into planar or bilayer structures with zero mean curvature. When the value of the CPP is less than one, the polar heads of the lipids form a convex interface and "normal oil in water" morphologies with positive curvature form (Type I). In contrast, when the CPP is more than one, the curvature is towards the aqueous environment, resulting in negative curvature with "inverse water in oil" structures (Type II).

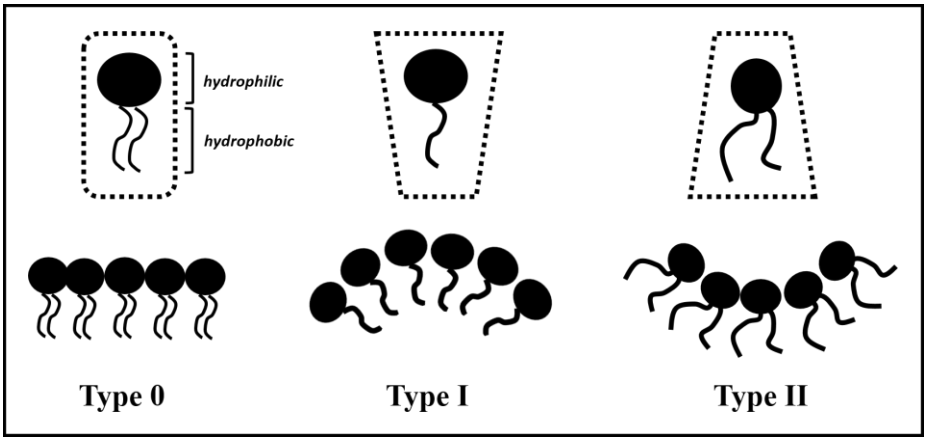

Figure 1.6 Schematic drawings of the curvature of lipid monolayers. Type 0 displays zero curvature with planar structure; Type I shows a monolayer with positive curvature and Type II represents a lipid monolayer with negative curvature.

Figure 1.7 illustrates the formation of different bilayer structures, which are affected by the molecular packing parameter. As the value of the packing parameter (P) increases, the inverted structures are favoured.

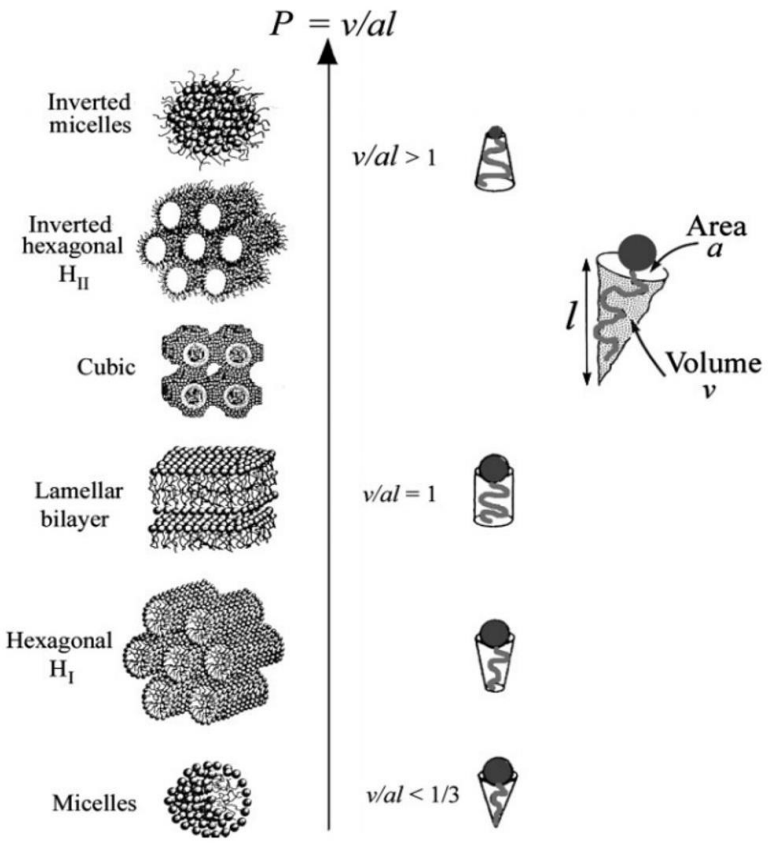

Figure 1.7 Schematic illustration of the structure formation from self-assembly of amphiphilic molecules. The molecular packing parameter (P) formed different curvatures and lead to different structures. P: packing parameter, v: molecular volume, l: length of molecule and a: cross-sectional area of head group (Adapted from [240] with permission).

In addition to lipid molecular structure, changes in temperature, pressure, aqueous environment and additives can also influence phase transition [241]. The mesophase structure can also be affected by the concentration of amphiphiles. At very low amphiphile concentration, the molecules have no specific arrangement and are randomly dispersed throughout the aqueous phase. Increasing the concentration of amphiphile leads to spontaneous assembly into simple vesicles or micelles. The hydrophobic tails from the amphiphiles are repelled by the aqueous phase while the hydrophilic head form the outer surface of the micelles, favouring the aqueous phase. The lamellar phase is often formed after the hexagonal phase and is composed of a layer of amphiphiles arranged in an ordered manner, separated by a layer of aqueous phase. The bicontinuous cubic phase

is formed upon the addition of higher concentrations of amphiphiles to the system [242, 243]. The CPP concept provides a guide in amphiphilic arrangement, but not all amphiphilic lipids will follow the CPP. For example, in GMO, increasing the concentration of GMO leads to the formation of inverse micellar phase followed by lamellar phase [244, 245]. Another example is the lipid phytantriol used in this thesis, where increasing its concentration leads to a more ordered state where the molecules start to form a discontinuous cubic phase and hexagonal phase [246].

1.4.3 Lamellar phase

Lamellar phase, the most commonly studied LLC, is a one-dimensional stack of bilayers that are separated by layers of water [247]. The hydrophobic tails are shielded from the aqueous environment in the bilayers. The fluidity and arrangement of the tails further characterise this phase. In the crystalline lamellar (L_c) phase, the lipid molecules are ordered and changes in external environment, such as in temperature increase, the fluidity of the lipid tails changes. Subsequent heating causes a transition from L_c to a lamellar gel (L_β) phase and continuous heating leads to the formation of the fluid lamellar phase (L_α). At elevated temperatures, the fluid isotropic phase (L_2), which consists of reverse micelles is preferred, while in most phospholipid systems, the hexagonal phase appears before the L_2 phase upon heating [248]. The L_α phase is the most common phase adopted by biological membranes.

In nanoparticle technology for drug delivery, liposomes are the most widely studied lamellar phase. Liposomes are particles made of phospholipids that orientate to form lipid bilayer [249-252]. The lipid arrangement allows the incorporation of hydrophilic drugs in the liposome core and hydrophobic drugs in the lipid bilayer. Liposomes can be surface decorated to increase the delivery to targeted cells (**Figure 1.8**). The addition of

charged lipids, polyethylene glycol and ligands will improve the targeting effect of liposome and reduce the toxicity of the encapsulated drugs [253].

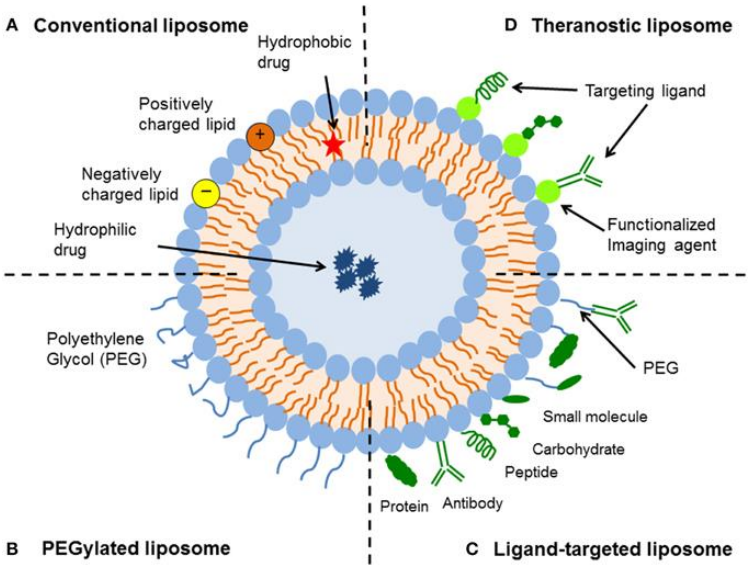

Figure 1.8 Surface modified liposome for drug delivery. Hydrophilic drugs are encapsulated in the aqueous core while hydrophobic drugs in the lipid bilayer. In conventional liposome (A), the lipid bilayer can be made of charged or neutral lipids and cholesterol. Polyethylene glycol (PEG) is added to form PEGylated liposome (B) to provide stability to liposome while ligands such as antibodies, protein and peptides can be added to form ligand-targeted liposome (C) to target selected receptors. Theranostic liposome (D) consists of both targeting ligand and imaging molecule to allow localisation of the liposome after administration. (Reproduced with permission [253]).

Currently, there are several liposomal formulations in the market. Intravenous formulation of liposomes such as Ambisome, Abelcet and Amphotec encapsulate amphotericin B, used to treat severe fungal infection. Several liposomal formulations with doxorubicin are marketed under the brand names Myocet, Caelyx and Doxil, and are used intravenously as chemotherapeutic agents to treat Kaposi's sarcoma, ovarian and breast cancers. In targeting the brain, Depocyt, a cytarabine-encapsulated liposome is used for treating neoplastic and lymphomatous meningitis. The difference in all the liposome formulations lies behind the composition of the lipid bilayers. The surface

decoration of liposomes allows targeting to specific tissues in the body and reduces toxicity of the drug by masking the drugs inside the liposome [253]. Apart from being a drug carrier, liposomes have also been extensively studied for vaccine delivery [254-256]. The advantages of using liposomes as drug carriers and the challenges in translating liposome research to marketed products are widely studied and reviewed by Narang *et. al* [257, 257].

1.4.4 Hexagonal phase

The hexagonal phase consists of a series of cylindrical micelles arranged into a two-dimensional hexagonal lattice, where back-to-back lipid layers separate the cylinders. It can present as the normal hexagonal (H_I) or inverse hexagonal phase (H_{II}). The H_{II} phase occurs at a high temperature as a result of increased chain disorder, where the cylindrical arrangement is entropically more favourable [248]. The dispersions of hexagonal phase in aqueous solution lead to the formation of hexagonal particles called hexosomes [258]. Glycerate based surfactants such as phytanyl glycerate and oleyl glycerate form hexosomes and have shown to have potential in drug delivery [237, 259]. Irinotecan, a highly lipophilic cancer drug molecule was successfully incorporated into hexosomes for cancer therapy [237]. There have been a small number of studies reported on the potential use of hexosomes as a drug carrier to the brain. The addition of cationic lipids in hexosomes dispersions was able to encapsulate plasmid DNA, through electrostatic interaction between the negatively charged DNA, for brain delivery [260, 261].

1.4.5 Bicontinuous cubic phase

The bicontinuous cubic phase is a unique structure and consists of a continuous single lipid bilayer (thickness about 3.5 nm), separating two non-intersecting aqueous

channels with an interfacial area of about 400 m^2/g [258, 262, 263]. The lipid bilayers are organised in a honeycombed structure with two internal aqueous channels that has shown the potential to accommodate various types of drug molecules [264]. The bulk cubic phase is viscous and solid-like, does not display any optical properties under cross-polarised light and categorised as isotropic [235, 265]. The amphiphiles that make up the cubic phase can absorb water, which leads to the formation of a gel-like structure in the bulk phase with a cubic structure. The internal structure and high surface area of the cubic phase allows a high loading of amphiphilic, hydrophobic and hydrophilic drug molecules [266-268].

A few studies have investigated the potential of the cubic phase and cubosomes as drug carriers via different routes of administration (**Table 1.3**). The high viscosity and gel-like structure of the bulk phase provides a suitable structure with adhesive properties for topical and buccal drug delivery of Leu5 enkephalin, cyclosporin A and sulforhodamine drugs [269-271]. The bulk phase can provide slow release properties as the drugs are trapped in the bulk gel and are continuously in contact to the skin and buccal mucosa.

Table 1.2 Examples of studies on cubosomes carrying drug molecules through oral, buccal, topical and intravenous administration

Route of administration	Drug	References
Oral	Cinnarizine	[272]
	Diclofenac	[273]
Buccal	Leu5 enkephalin	[269]
Topical	Cyclosporin A	[270]
	Sulforhodamine	[271]
Intravenous	Camptothecin	[274]

Unfortunately, due to the high viscosity of the bulk gel, it is not suitable for intravenous drug preparation. However, due to its ability to maintain the cubic internal structure in excess water, it can be dispersed to form colloidal dispersions, called cubosomes [275]. There are three common types of cubosomes that have been identified from X-ray crystallographic studies; primitive (*Im3m*), diamond (*Pn3m*) and gyroid (*Ia3d*) in order of increasing curvature as illustrated in **Figure 1.9** [276]. The water content in the system influences the transition of cubosomes from one type to another. In addition, temperature, type of additives and amphiphiles used also play a role in the transition [264]. The inverse cubic phase of phytantriol lipid is reported to be stable in the presence of excess water and this provides various advantages in formulating cubosomes as a drug carrier for intravenous formulation to the brain [246, 277]. The significance of this for this thesis will be discussed in more detail in the next section.

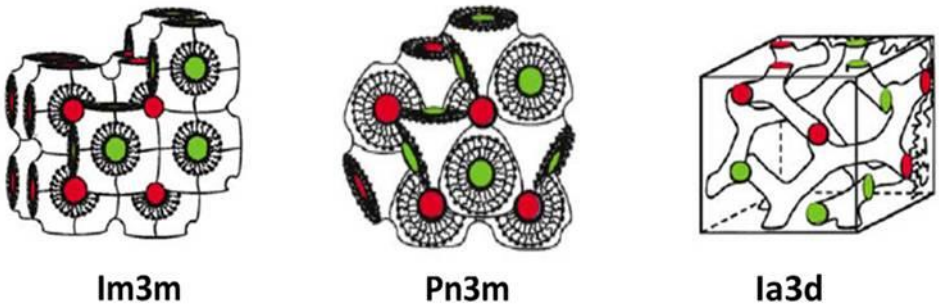

Figure 1.9 Schematic representations of the inverse bicontinuous cubic phases with increasing curvature: *Im3m* (primitive), *Pn3m* (diamond) and *Ia3d* (gyroid). Individual lipids are shown as ball-stick figures, whilst the regions filled with green and red colour represent water channels [278].

1.4.6 The advantages of using cubosomes as drug carrier

Cubosomes have the potential to offer various advantages as drug carriers to cross the BBB. The ability of cubosomes to be stably dispersed in excess water allows the delivery of drugs through intravenous administration [274]. The amphiphilic lipids commonly used in preparing cubosomes formulation have low toxicity [279, 280] and the amphiphilic lipids assembly mimics the lipid orientation in the lipid bilayer within cell membrane [281, 282]. The internal tortuous structures of cubosomes allow a higher drug loading as compared to other lipid nanoparticles such as liposomes [283]. Hydrophobic and hydrophilic drugs can be encapsulated in the lipid bilayer and aqueous core respectively [284-286]. In addition, cubosomes formulation can be modified to produce various encapsulation and release properties of drug molecules. **Figure 1.10** illustrates how the surface of cubosomes may potentially be modified by molecules into the lipid bilayer. To have a desired effect such as to target the encapsulated drug to specific tissues or receptors.

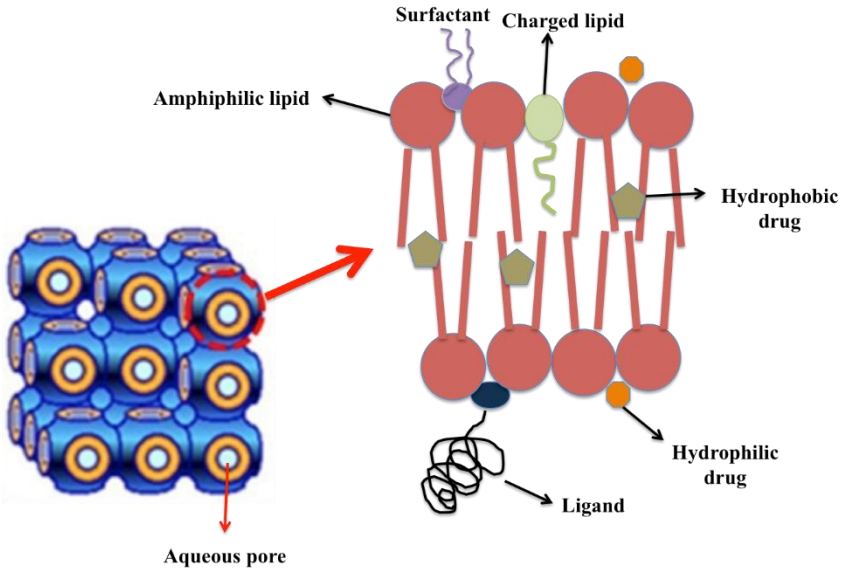

Figure 1.10 Schematic illustration of the internal structure of cubosomes which allow surface modifications with surfactant, charged lipid and the addition of ligands. The tortuous structure of the lipid bilayers and the aqueous pores allow encapsulation of a higher amount of hydrophobic and hydrophilic drug due to the high surface area (Adapted and modified from [287] with permission).

Whilst early studies in cubosome research proposed that due to the nature of its structure, cubosomes may be able to modulate the release of encapsulated drug molecules [264, 288, 289]. However, in 2013, Boyd *et al*. showed that cubosomes produce a burst instead of sustained release of drug *in vitro* [290]. The authors also went on to suggest that the degradation of cubosomes in the body would cause immediate release of the drug molecules. However, this has not been demonstrated to date. Cubosomes still offer various benefits as a drug carrier. The encapsulation of drug within the complex structure of cubosomes has been shown to offer protection against chemical of physical degradation of protein bioactives [291].

The drug release properties of cubosomes are influenced by the structure and changes in the environment. Hydrophilic drugs are encapsulated within the aqueous channels and the release is affected by the size of the channels and the molecular weight of the drugs [237]. Adding specific additives such as octyl glucoside detergent into

cubosome formulation can increase the size of the channel, thus increasing the rate of release [292]. The molecular size of the drugs will also determine whether the drug can be released faster or slower. Meanwhile, lipophilic drug molecules will be trapped within the tortuous lipid bilayer of the cubosomes and the release is affected by the partitioning between the lipid bilayers and the aqueous site [286]. The release rate and properties are affected by various factors such as the type of lipids that make up the cubosomes, the type of drugs, pH, temperature changes, size of aqueous channels and the addition of additives [292-294]. A number of drugs were encapsulated in the cubosomes and shown to have sustained release properties *in vitro*, and were reviewed by Drummond, C previously [258]. Given the contradiction in the literature, [290] more robust methods need to be developed to evaluate the release of drugs from these complex lipid structures.

1.5 Characterisation of lyotropic liquid crystalline dispersions.

There are a number of different techniques which can be used to characterise the physicochemical properties of lyotropic liquid crystalline dispersions. These techniques are discussed in detail below as they will be used in this thesis for formulation of BBB-targeted cubosomes.

1.5.1.1 Dynamic light scattering

Dynamic light scattering has been frequently used in studying colloidal systems. It is a simple and convenient method to study the size, heterogeneity and stability of different types of colloidal dispersions. In this technique, a small solution containing colloidal particles (cubosomes) is placed in the path of a focused laser. The random Brownian motion in the scattered laser causes the intensity to fluctuate (at the detector)

which generates the diffusion coefficients or particle size. The measurement relies on partice concentration, size of particle core and type of ions in the dispersions [295].

1.5.1.2 Small angle X-ray scattering

Scattering techniques provide information on shape, size and nanostructure of bulk and dispersed liquid crystalline systems. The common radiation sources used in scattering are light, X-ray and neutron. In small angle X-ray diffraction (SAXS), a radiation of wavelength λ (usually ~1 Å) is passed through the sample. This is either absorbed or scattered and an X-ray detector measures the intensity of scattering as a function of the scattering angle relative to the incident beam. The scattered intensity from the sample is normalised to non-sample-related scattering (background). The intensity of the scattering (q) is defined as:

Equation 2 $$\boldsymbol{q = \frac{4\pi \sin(\theta/2)}{\lambda}}$$

Where λ is the wavelength of radiation, and 2θ is the scattering angle. The intensity versus scattering angle is plotted (q vs. 2θ) and Bragg peaks are identified. Bragg peaks are specific for a given liquid crystalline phase (**Table 1.3**). However, more than one type of Bragg peaks pattern can occur, and these indicate the presence of a multiple phase system. At least three peaks are needed to differentiate the symmetry aspects with confidence [235].

Table 1.3 Lyotropic liquid crystalline mesophases; the ratio of spacing between Bragg reflections [235]

Mesophase	Descriptor	Peak ratio
Lamellar	L_α, L_β	**1 : 2 : 1 : 2 : 3 : 4 … etc.**
Bicontinuous cubic	**P (*Im3m*)**	**√2 : √4 : √6 : √8 : √10… etc.**
	D (*Pn3m*)	**√2 : √3 : √4 : √6 : √8… etc.**
	G (*Ia3d*)	**√6 : √8 : √14 : √16 : √18 : √20…etc.**
Hexagonal	H_I, H_{II}	**√3 : √4 : √7 : √12…etc.**

P: Primitive, D: Diamond, G: Gyroid

1.5.1.3 Electron microscopy

Electron microscopy (EM) allows direct visualisation of both bulk and dispersed mesophases. Scanning (SEM) and transmission (TEM) techniques are most commonly used depending on the information required.

SEM generates a low-resolution image (10 to 100 nm) but does allow mapping of surface morphological features and characterisation. Cryogenic field emission scanning electron microscopy (cryo-FESEM) has been shown to have better resolution as compared to standard SEM and therefore it is possible to characterise microstructure. It has been successfully used to visualise the structure of dispersed cubosomes and hexosomes particles [296-298]. In cryo-FESEM, samples are snap frozen at very low temperatures in liquid nitrogen or propane and then viewed under the microscope. The main limitation of cryo-FESEM is ice crystal formation during sample preparation [299] which can distort the original structure of the sample. To avoid the ice crystal formation, high pressure freezing technique and metal cryo coating can be applied. However, these techniques can affect the physical condition of the samples and disrupt the structure of particles [300].

TEM is not commonly used to observe cubosomes structure, because of the need to chemically fix the liquid sample. If the sample is subjected to harsh conditions during

fixation, it may change the structure of the original particles. An alternative to this problem is to do physical fixation on the sample by utilising cryo-TEM technique. The sample is subjected to fast cooling and increase in vapour-pressure up to cryogenic temperature, which leads to a vitrified and not a typical frozen sample. The vitrification process leads to formation of a high viscosity, low-vapour-pressure sample [299]. This technology preserves the size, shape and the nature state of the sample at studied concentration and temperature [262]. The image of the original nanostructure is preserved and captured. However, the sample viscosity is a limitation, as very viscous samples are not suitable for cryo-TEM preparation. The sample might not be able to freeze properly to form a thin layer of vitrified sample [299].

1.5.1.4 Cryogenic-electron tomography

Cryogenic electron tomography (cryo-ET) is another method used to image particles in its native state. The samples are processed in a similar manner to cryo-TEM samples as described in **Section 1.5.3**. The vitrified sample (on the grid) undergo minimal chemical and physical changes and the cryogenic processing allows the sample preservation in the native state. During TEM imaging, under cryogenic conditions, the sample is tilted at different angles and the images were collected. To avoid radiation damage due to continuous imaging, a low dose of electron is used (around 50 e^{-1} $Å^{-2}$) and the contrast is increased by defocusing the sample [301]. By applying sub-tomogram averaging to all the tilt series, the information from each image can be combined and averaged to form the 3D structure. Since a large number of images are captured, any specific image at certain tilt angle with poor resolution can be deleted and excluded, without losing any detail information of the structure. Images with high resolution and good signal-to-noise ratio are usually collected at low tilt. Whilst at high tilts, the images

have lower resolution with the risk of structural damage to the sample due to the beam exposure [302].

The advantage of using cryo-ET is that the preservation of the sample is in its original state. This is useful for biological samples such as lipid-based nanoparticles that can be easily damaged by chemical fixation. This technique can offer a better preservation method to allow detailed observation of cubosome particles in the dispersion, without any changes in the structure. The 3D reconstruction from the tilt series will allow the detailed internal and surface structure to be observed instead of 2D form from normal cryo-TEM imaging [303]. It offers a detailed examination of biological particles including virus and bacteria [304]. Cryo-ET technique is important in this thesis as it can showcase the 3D image of the detailed cubosomes structure and cryo fixation provides a better preservation technique as compared to chemical fixation.

1.6 *In vitro* model of the BBB

Various studies have been conducted to develop *in vitro* cell culture models that can mimic *in vivo* properties of the human BBB [305]. The use of immortalised cells allows a larger number of studies to be conducted in a large scale, including nanoparticle uptake studies. Any *in vitro* BBB model should be easy to grow with preservation of transporters and receptors. Cerebral microvessel endothelial cells (CMEC) from bovine origin were isolated in the 1980s to provide a BBB *in vitro* model [306]. Even though these primary brain endothelial cells expressed functional receptors, tight junctions and other key BBB markers, the challenges in getting fresh brain tissues prohibited larger studies.

Recently, an immortalised human BBB cell line, the hCMEC/D3 was developed by a group of scientists in France. Since the development of hCMEC/D3 cells in 2005, more than 100 studies have been published in various areas of neurological research,

using this cell line [305, 307]. The cell line was developed from human temporal lobe microvessels isolated from excised tissue from the brain of an epileptic patient. The cells were enriched and immortalised by lentiviral vector transduction using SV40 large T antigen and the catalytic subunit of human telomerase (hTERT). Specific colony was selected by limited dilution cloning and characterised, which then named as hCMEC/D3 cells. These endothelial cells showed similar morphology to primary brain endothelial cells such as elongated cells and contact inhibition when grown on collagen. This phenotype was maintained and the endothelial markers were retained up until passage 33 [305, 307, 308].

To confirm the suitability of hCMEC/D3 cell as an *in vitro* BBB model, the expression of membrane receptors and transporters were tested using various techniques including quantitative proteomic analysis, immunochemical analysis and RT-PCR analysis [305]. MRP, BCRP and P-gp were found on hCMEC/D3 after an assessment by quantitative proteomic analysis [309-311]. The level of expression was found to be similar to isolated human brain microvessels [309]. P-gp was shown to be expressed up to passage 38 and localised at the apical side of hCMEC/D3 cells. Even though P-gp expression was found to be lower than primary human brain capillary endothelial cell (HBCE), the expression was comparable and inhibited by P-gp inhibitors such as taquidar and vinblastine [311, 312]. High levels of transferrin and Glut-1 receptors were expressed by hCMEC/D3 with similar density to human brain microvessels [309]. Other influx transporters present at hCMEC/D3 cells are LDL-receptors, amino acid transporters, organic ion transporters (OATP) and all members of solute carrier family (SLC) transporters [305]. In order to use hCMEC/D3 cell line to study cubosomes uptake via receptor mediated endocytosis, the presence of these transporters especially LDL-receptors are important.

hCMEC/D3 cell line can offer various advantages in conducting high throughput *in vitro* studies. The cost involved is lower than primary cell culture, and it also retains phenotype, receptors and transporters similar to primary human brain endothelial cell, which makes it a suitable BBB *in vitro* model to be conducted in this thesis for cubosomes toxicity and uptake studies.

The introduction section has outlined the challenges and opportunities in delivering drug to the brain to treat neurological diseases. Given the possibilities for encapsulation and release of drugs of varying properties, together with the ability to modify the surface chemistry using BBB targeting moieties on the surface, cubosomes emerge as a suitable platform as a drug carrier system to improve drug delivery into the brain.

1.7 Thesis hypotheses

A number of hypotheses were developed and tested in this thesis in order to examine the potential of cubosomes as drug carriers to the brain. These were:

1. That cubosomes can be surface decorated with different stabilisers to target receptor-mediated transcytosis at BBB.
2. That cubosomes co-formulated with cationic lipids can target the adsorptive endocytosis pathway at BBB.
3. That cubosomes surface decorated with different stabilisers and cationic lipids can interact and cross the BBB with limited toxicity.

1.8 Aims

In order to investigate the above hypotheses, the aims of this thesis are:

i) To formulate and characterise cubosomes surface decorated with non-ionic stabilisers and charged lipids to understand:
    a) the effect of using non-ionic stabilisers at different concentration on the stability of cubosomes and the internal structure.
    b) the influence of lipid chain length (from charged lipids) on the formation of cubosomes.
    c) the monolayer interactions of charged lipids with the cubic phase forming lipid phytantriol.

ii) To investigate the interaction of surface decorated cubosomes *in vitro* with a human brain endothelial cell line.
    a) by evaluating the toxicity of cubosomes stabilised from non-ionic stabilisers and the addition of charged lipids
    b) by determining the cell uptake of surface decorated cubosomes

iii) To investigate the uptake and toxicity of surface decorated cubosomes into the brain *in vivo* using a zebrafish model by:
    a) evaluating the toxicity effect of surface decorated cubosomes in zebrafish brain
    b) observing and investigating the uptake of cubosomes in the zebrafish midbrain

Chapter 2

General materials and methods

2 General materials and methods

2.1 Materials

Chloroform (HPLC grade), dichloromethane and 1,2-propandiol (propylene glycol) were purchased from Merck (Darmstadt, Germany). Phytantriol (3,7,11,15-tetramethyl-1,2,3-hexadecanetriol, ≥95% purity) was purchased from A & E Connock (Hampshire, England). Lutrol® or Poloxamer 407 (Pluronic F127) was obtained from BASF (Ludwigshafen, Germany). Kolliphor® (Poloxamer 188), cetyltrimethylammonium bromide (CTAB) and Tween 80 (Polysorbate 80) were purchased from Sigma-Aldrich (New Zealand). 1,2-Dioleoyl-3-trimethylammonium-propane (DOTAP), 1,2-dimyristoyl-*sn*-glycero-3-phospho 1'-*rac* glycerol (DMPG) and 1,2-di-O-octadecenyl-3-trimethylammonium propane (DOTMA) were purchased from Avanti Polar Lipids. Inc (Alabama, USA). Octanethiol functionalized 3 nm gold nanoparticle was from Nanoprobes (New York, USA). 1,2-dipalmitoyl-*sn*-glycero-3-phosphoethanolamine-N-(lissamine rhodamine B sulfonyl) (LR) and 1,2-dipalmitoyl-*sn*-glycero-3-phosphoethanolamine-N-(7-nitro-2-1,3-benzoxadiazol-4-yl) (NBD) were purchased from Avanti Polar Lipids Inc (Alabama, USA). All chemicals were used as received. Milli-Q water (ion exchanged, distilled and purified by Millipore, Bedford, MA) was used in all experiments.

2.2 Methods

2.2.1 Preparation and characterisation of cubosome dispersions

2.2.1.1 Preparation of cubosome dispersions

Phytantriol (20 mg/mL), stabilisers (5 to 20% w/w of Pluronic F127, Tween 80 or Poloxamer 188 to phytantriol), and propylene glycol (co-solvent, 54 mg/mL) and where appropriate, CTAB, DOTAP, DOTMA or DMPG (1.4 to 5.3 mol % to phytantriol) were weighed into a glass vial and dissolved completely in sufficient chloroform (typically 5 mL). For preparing tagged cubosomes, NBD (37.3 μM), LR (205.6 mM) or octanethiol functionalized 3 nm gold nanoparticle (0.01 mM) was added to the mixture at this stage. Chloroform was subsequently evaporated under vacuum at 45 °C leaving behind a lipid mixture (liquid precursor). Water (1 mL) was added to the liquid precursor and the mixture was vortex mixed for 10 min to form cubosome dispersion [313].

2.2.1.2 Size, polydispersity and ζ -potential

The particles size distribution and ζ-potential were determined using dynamic light scattering (DLS) (Malvern Zetasizer 3000, Malvern, UK). Measurements were performed at 25 °C and the results presented are the mean of three successive measurements of 100 s of at least three independent experiments, using a refractive index of 1.467 for phytantriol. Samples were diluted with water to adjust the signal level. The average particle size (Z-average), polydispersity index (PDI) and ζ-potential (based on the Smoluchowski model) of the various dispersions were determined [314].

2.2.1.3 Small angle X-ray scattering (SAXS)

Measurements were conducted on the SAXS/WAXS beamline at the Australian Synchrotron (Clayton, VIC) to identify phase structures using previously described methods[315]. Samples were added to 96 well microplate and mounted vertically in the beam path. The 2D SAXS patterns were collected using a Pilatus 1 M (170 mm × 170 mm) detector which was located 960 mm from the sample position, with 2 s exposure and X-ray wavelength of 1.0322 Å. The diffraction patterns were integrated using the Scatterbrain software operating on the beam line and plotted as intensity versus scattering vectors (q) to identify peak ratios as described in order to determine the liquid crystalline structure [265]. The relative positions of the Bragg peaks were used to define the cubic-phase space groups and mean lattice parameter, as discussed in [316].

2.2.1.4 Cryo-transmission electron microscopy (cryo-TEM)

Cubosome dispersions (3 µL) were added to 300 mesh R2/2 Quantifoil grids (Quantifoil GmbH, Germany) that were glow-discharged for 10 s. Excess dispersion was removed by blotting with filter paper (Whatman Nr. 1). Grids were rapidly plunged into liquid ethane and kept near its freezing temperature (-120 °C) in a Reichert KF80 freezing device (C. Reichert Optische Werke, Austria). The samples were stored in liquid nitrogen before loading into a Gatan 914 cryo holder (Gatan Inc, California, U.S.A) and viewed in a JEOL 2200FS transmission electron microscope (JEOL Ltd, Japan) fitted with a TVIPS F416 CMOS camera (TVIPS GmbH, Germany).

2.2.1.5 Cryo-electron tomography (Cryo-ET)

Selected samples from **Section 2.2.1.4** were subjected for Cryo-ET. Automated tilt series images from the grid were acquired using SerialEM software (University of Colorado, Boulder, U.S.A). Tilt angle increments of 1.5 or 2 degrees with the tilt range of -60 to +60 degrees was used [317]. Tomograms were reconstructed and analysed using IMOD software (University of Colorado, Boulder, U.S.A) [318]. Nonlinear anisotropic diffusion was carried out using ETOMO to de-noise the merged tomogram and 3D images were visualised using *Chimera 1.10.2* (University of California) [319].

2.2.2 Langmuir monolayer studies

To study the effect of charged lipids (CTAB, DOTAP, DOTMA and DMPG) on phytantriol lipid monolayer, the interfacial behaviour was investigated at ambient temperature (25 ± 1 °C) using the Langmuir-Blodgett trough (NIMA, Coventry, UK). A surface area of 100 cm^2 and a volume of 50 mL were used. Prior to conducting each experiment, the Teflon trough and barriers were cleaned with dichloromethane and Milli-Q water. After the subphase was added (Milli-Q water), a Wilhelmy paper plate (Whatman's No.1 Chromatography paper, Australia) was connected to the pressure sensor to measure the surface pressure (π).

Single and mixed components of phytantriol and charged lipid were dissolved in chloroform. The concentration of phytantriol was constant (0.5 mg/mL) while the concentration of added component varied. A 20 uL aliquot of the single or mixed component mixture was spread on the subphase using a Hamilton syringe and left for 10 min for the chloroform to evaporate. Compression was applied at a speed of 5 cm^2/min and the π-A isotherms were recorded by the instrument software (Nima 516, KSV Nima,

Finland). Experiments were conducted at room temperature with three replicates. Collapse pressure and limiting area per molecule for each single and mixed component mixture was calculated.

2.2.2.1 Analysis of π-A isotherms

The compression of the monolayer will lead to a stage where the monolayer will collapse. This is known as the collapse pressure where a sudden change in the pressure occurs, the isotherms deviate from the straight line and a plateau of maximum pressure was observed (**Figure 2.6**) [320]. To obtain the experimental limiting molecular area, the rising linear part of the isotherm was extrapolated to zero pressure as shown in **Figure 2.6** and to get the ideal limiting molecular area (A_i) was calculated using additivity rule as **Equation 3** [321, 322].

Equation 3 $$\boldsymbol{A_i = X_{phyt}A_{phyt} + X_{charged\ lipid}A_{charged\ lipid}}$$

Where X_{phyt} is the mole fraction of phytantriol, $X_{charged\ lipid}$ is the mole fraction of charged lipid while A_{phyt} and $A_{charged\ lipid}$ are the experimental limiting molecular area for pure phytantriol and pure charged lipid monolayers respectively. The deviation between the calculated ideal limiting molecular areas to the experimental values were compared to evaluate the miscibility and interaction between the phytantriol and charged lipids in the mixed monolayer [323].

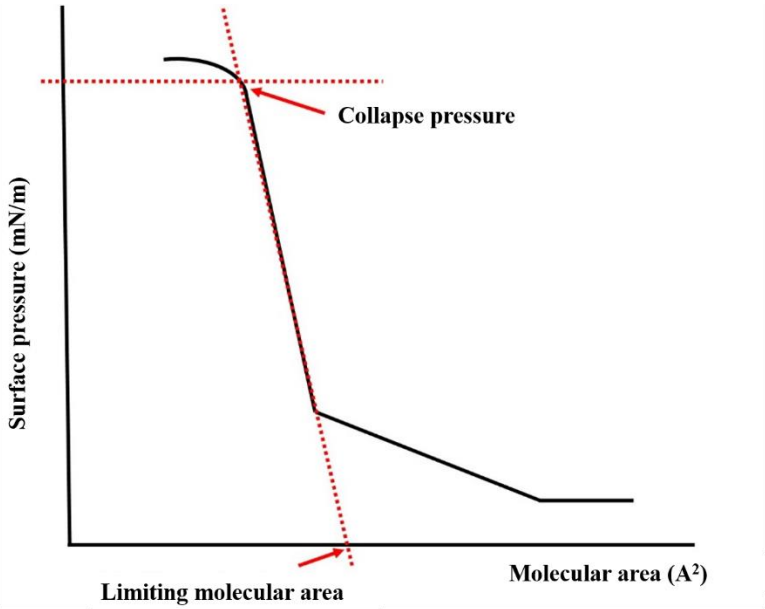

Figure 2.1 Schematic diagram of π-A isotherm showing the extrapolation for the collapse pressure and limiting molecular area.

2.2.3 Cell maintenance

Immortalised human brain capillary endothelial cells (hCMEC/D3) were purchased from Cedarlane, Canada and passage 23 to 34 were used in all experiments. Cells were grown in flask pre-coated collagen type 1 (Falcon™) and grown in EBM-2 medium (Lonza, Basel, Switzerland) supplemented with 5% fetal bovine serum (Life Technologies, NZ), 1% penicillin-streptomycin (Life Technologies, NZ), 1.4 µM hydrocortisone (Sigma-Aldrich), 5 µg/mL ascorbic acid (Sigma-Aldrich), 0.001% chemically defined lipid concentrate (Life Technologies, NZ), 10 mM HEPES (Life Technologies, NZ) and 1 ng/mL human Basic Fibroblast Growth Factor (Sigma-Aldrich). Cells were grown at 37 °C with 5% CO_2 and saturated humidity. Cell culture medium was replaced every 2 to 3 days and studies were conducted when the cells reached 70 to 80% confluency, 3 to 4 days after seeding.

2.2.3.1 Cell viability and uptake studies

For functional assays, cells were seeded on type 1 collagen pre-coated 24 well plates (Falcon™) with the density of 50,000 cells/well. Cells were washed three times with Dubelco's phosphate buffered saline (Invitrogen Corporation) and incubated with fluorescently-labelled cubosomes at various concentrations for 2 h at 37 °C. After that, the media was removed, and cells were washed with FACS buffer to remove any remaining formulation (see **Appendix 1** for FACS buffer recipe). Tryple (Gibco, Denmark) was added to each well and left for 10 min at 37 °C to allow the cells to detach. The cells were re-suspended with FACS buffer and centrifuged for 10 min at 1000 rpm. Supernatants were discarded and the cells were re-suspended in 100 µL of FACS buffer containing 1 µg/mL propidium iodide (PI) for staining the dead cells. Cells were then analysed using flow cytometry to determine the cell viability for toxicity studies and cubosome uptake.

2.2.3.2 Evaluating cell uptake for cubosome surface coated with cationic lipids

To further study the uptake of cubosome modified with charged lipid was through adsorptive endocytosis, the uptake study was repeated. Adsorptive endocytosis is an active process and requires energy. To test the hypothesis that the uptake of cubosome surface modified with cationic lipids is through adsorptive endocytosis, the cells were incubated with cubosome formulation for 2 h at 37 °C and 4 °C. After 2 h of incubation, the uptake at both temperature was analysed using flow cytometer.

To further elucidate that there was an electrostatic interaction between positively charged cationic cubosome, in a separate study, the cells were pre-incubated with poly-L-lysine (931 nM) for 1 h. Then poly-L-lysine was removed, and the cells were washed

with PBS to remove any remaining poly-L-lysine. The cells were then incubated with cubosome formulation at 37 °C for 2 h. The uptake was analysed.

2.2.3.3 Analysis of cubosome toxicity and uptake by flow cytometry

Cell viability and uptake of surface modified cubosomes after 2 h incubation was measured using flow cytometer. The measurement was carried out using FACSCanto™ II flow cytometer (BD Biosciences, California, USA) and data acquired using CellQuestPro software (BD Biosciences). Data analysis was conducted using FlowJo® 7.6 software (Tree Star, Oregon, USA). Typical gating strategy used in data analysis is shown in **Figure 2.2A-C**. Cell viability was defined as the percentage of PI-negative cells out of single cells as PI was used to stain the dead cells. Uptake by the cells was analysed by comparing NBD positive population of live cells treated by cubosome to that of control where the cells were incubated with NBD suspension (without cubosome) at the same concentration of NBD in cubosome formulation. Auto fluorescence of the cells was taken into account by deducting the positive signal from the untreated cells. **Figure 2.2D** shows the signal from auto fluorescence of untreated cells (negative population) while **Figure 2.2E** shows a shift in signal for cells with positive uptake of NBD (positive population).

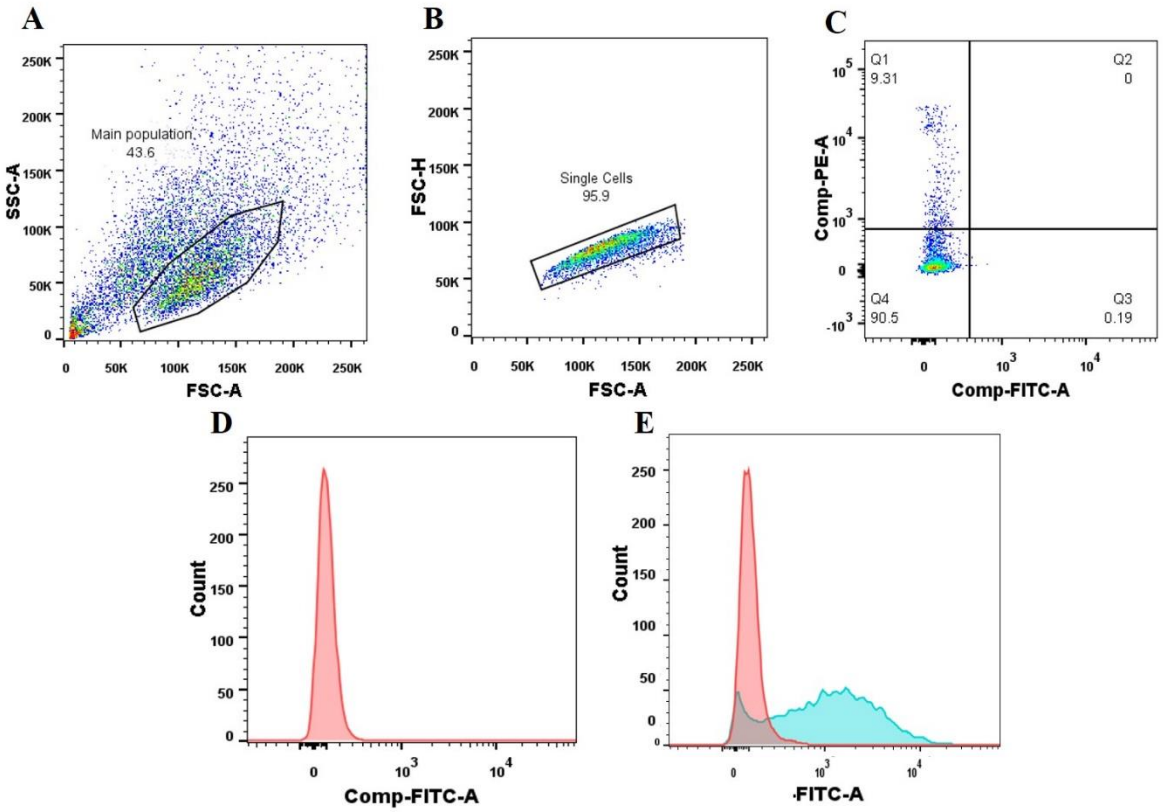

Figure 2.2 Gating strategy for FACS analysis of live cells and NBD positive cells for viability and uptake studies. The cells debris was excluded (A) and doublets removed (B). The gating at (C) is to set the population of live cells (PI-negative) with NBD positive cells, which is located at Q3. The histograms were used to illustrate the untreated cells population (red) under FITC channel (D) and the shift in the signal for NBD positive cells (E) (in blue).

2.2.3.4 Observation of cubosome uptake under fluorescence microscopy

To observe the cellular uptake of cubosome (NBD-labelled) under fluorescence microscope, after 2 hr of incubation with cubosome formulation, the cells were washed with PBS to remove any remaining cubosome in the incubation media. 0.5 mL PBS was added into each well as a buffer and Hoechst 3342 (Thermo Fisher Scientific, US) with concentration of 8.1 µM was prepared with PBS and added into each well. The cells were incubated for 10 min. Then each well was washed three times with PBS to remove the

staining and then incubated with CellMask™ Deep Red Plasma membrane stain (Thermo Fisher Scientific, USA) at 1:1000 dilution for 10 min to stain the plasma membrane. The cells were then washed with PBS to remove the staining. Media was added into each well and cubosomes uptake was observed under fluorescence microscope (Nikon Corp., Japan) fitted with TxRed, DAPI and FITC filter. The images were analysed using ND2 software (Nikon Corp., Japan).

2.2.4 Statistical analysis

The results are expressed as mean ± standard deviation (SD). One-way analysis of variance (ANOVA) with Tukey's multiple comparison's test using Prism 6 (GraphPad Software Inc., USA) was applied. Statistical significance was determined when $p<0.05$.

Chapter 3

Formulation and characterisation of cubosomes that target receptor-mediated endocytosis at BBB

A part of this Chapter was published in:

Azhari, H., Strauss, M., Hook, S., Boyd, B. J., & Rizwan, S. B. (2016). Stabilising cubosomes with Tween 80 as a step towards targeting lipid nanocarriers to the blood–brain barrier. *European Journal of Pharmaceutics and Biopharmaceutics*, *104*, 148-155.

3 Formulation and characterisation of cubosomes that target receptor-mediated endocytosis at BBB.

3.1 Introduction

Nanoparticles decorated with ligands to target BBB have been proposed as a potential method to carry CNS drug molecules into the brain. As discussed in **Chapter 1**, this thesis will focus on the utilisation of cubosome as a drug carrier to target specific pathways at the BBB. This will be achieved by formulating cubosomes which contain molecules that have previously been shown to target the BBB to improve delivery of drugs to the brain. In particular, this chapter focus on targeting cubosomes towards the BBB via receptor-mediated endocytosis. Various receptors present on the endothelial surface to shuttle different endogenous molecules into the brain. The shuttling of molecules through this pathway was discussed in **Section 1.2.3.4** previously. Low density lipoprotein receptor is the receptor of interest in this chapter where cubosomes were formulated specifically to target this receptor at the BBB.

3.1.1 Low density lipoprotein receptors as potential BBB target

Low density lipoprotein (LDL) receptors allow lipoprotein transport from the blood circulation into the cells throughout the body. Lipoproteins are essential carriers of lipid molecules such as cholesterol from the blood circulation into the cells in the form of fatty acyl esters [324]. The cholesteryl esters are hydrolysed into sterols which are important in the construction of cellular membranes, production of steroid hormone and synthesis of bile acid [325, 326]. Lipoproteins require binding with apolipoproteins (Apo) in plasma, which mediate its interaction with LDL-receptors. ApoA to E are present in the

blood stream bind to lipoproteins and facilitate their interaction with the LDL-receptor [327, 328].

To improve the drug delivery to the brain, nanoparticles have been designed to mimic the uptake of lipoproteins across the BBB [329, 330]. In particular, decorating the surface of nanoparticles with ApoE has been shown to facilitate their binding to LDL-receptors and their subsequent transport across the BBB [331-333]. For example, rosmarinic acid, an antioxidant and an anti-inflammatory agent currently being investigated for the treatment of Alzheimer's disease, has limited permeability across the BBB. To overcome poor permeability issues, in one study, rosmarinic acid was conjugated to polyacrylamide-chitosan-poly(lactide-co-glycolide) (PLGA) nanoparticles which were decorated with ApoE [334]. Increase uptake of rosmarinic acid in PLGA nanoparticles was found to halt the degenerative progress on damaged Aβ-neurons in Alzheimer's model in rats, as compared to PLGA nanoparticles without ApoE decoration. This result shows that the addition of ApoE on the PLGA nanoparticles allow the interaction with LDL-receptors at the BBB to promote the uptake into the brain [334].

ApoE conjugated nanoparticles have been used to facilitate delivery of lipophilic drugs that have limited BBB permeability. For example, resveratrol a polyphenol compound that has been identified to have antioxidant, anti-inflammatory, anti-bacterial and neuroprotective effects. It has been shown to decrease pro-inflammatory cytokines in rodent and primate model, which confer neuroprotective effect for Parkinson's, Huntington's and Alzheimer's diseases [335-342]. Resveratrol is highly lipophilic and has poor aqueous solubility, undergoes rapid metabolism, chemical instability, low bioavailability and limited permeability across the BBB [343, 344]. To overcome some of these challenges, in several studies, resveratrol has been encapsulated in solid lipid nanoparticles functionalised with ApoE with the aim that the particles are endocytosed

similar to lipoproteins into the endothelium via LDL-receptors [18, 345-347]. In one study, a 1.8-fold increase uptake of resveratrol by human brain endothelial cells, hCMEC/D3 was reported when formulated into solid lipid nanoparticles functionalised with ApoE, compared to nanoparticles without ApoE [333].

Nanoparticles can also be targeted towards the LDL-receptors by decorating their surface with surfactants. Certain surfactants promote binding with ApoE in the blood plasma, which then facilitated the binding of the nanoparticles to the LDL-receptors. Various surfactants have been investigated and will be discussed in the next section.

3.1.2 Surface coating of nanoparticles with surfactants to target LDL receptors at the BBB

Nanoparticles formulated with polymers such as poly(lactide-co-glycolide (PLGA), poly(butyl cyanoacrylate) (PBCA) and poly(isohexyl cyanoacrylate) (PIHCA) surface decorated with Poloxamer 188, Polysorbate or Tween 20, 40, 60 and 80 have been shown to cross the BBB [348]. These will be discussed in some detail in the subsequent sections.

In one study, PBCA nanoparticles decorated with Tween 80 were used to deliver the anti-nociceptive drug dalargin, which has poor permeability across the BBB, into the mice. Successful delivery of the dalargin was confirmed with a functional anti-nociceptive test in mice due to the effect of dalargin in the brain [349]. However, the addition of surfactants such as Cremophor®, polyxamine 908, Brij®35, Poloxamers 184, 407 and 338 did not result in any significant uptake of dalargin uptake into the brain [350]. Therefore, it was concluded that only certain surfactants are able to bind to ApoE in the plasma to target the LDL-receptors. In certain formulations, the surface coating by the surfactants will affects the interaction with ApoE in the plasma. Moreover, the formation of protein

corona after the intravenous administration of nanoparticles may reduce or deactivate the binding sites of ApoE leading to failure to interact with the LDL-receptors [351, 352].

3.1.2.1 Tween 80 coated nanoparticles

Tween 80 is an amphipathic non-ionic surfactant with fatty acid esters of polyoxyethylene sorbiton monooleate (**Figure 3.1**). The hydrocarbon chain consists of an oleate moiety with double bond, which causes a kink in the structure [353]. It is commonly used in cleaning and pharmaceutical products as a surface stabiliser due to its low cost, availability and biodegradability [354].

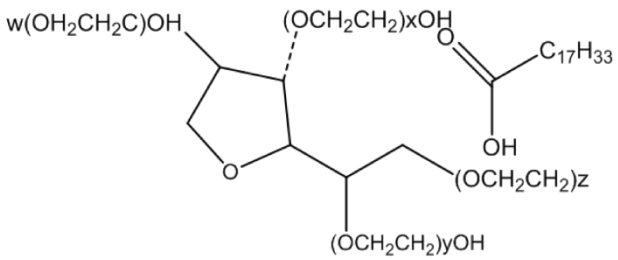

Tween 80 (x + y + z = 20)

Figure 3.1 Chemical structure of Tween 80.

Drugs encapsulated in polymeric nanoparticles functionalised with Tween 80 have been shown to have increased BBB permeability [192]. Evidence suggests that after intravenous administration, plasma lipoproteins ApoB and ApoE binds with Tween 80 moieties on the surface of nanoparticles (as discussed in the previous section). These protein-bound particles then mimic the endogenous transport of LDL to cross the BBB via receptor-mediated transcytosis [355-357]. The BBB-targeting effects of nanoparticles coated with Tween 80 have been reported with varying degrees of success and are summarised in **Table 3.1**. PBCA nanoparticles with Tween 80 are widely studied to target the BBB. Various drugs such as dalargin, kyotorphine and methotrexate have been incorporated into nanoparticles and show some degree of uptake into the brain after administration.

Encapsulation of resveratrol in glyceryl behenate-based solid lipid nanoparticles coated with Tween 80 as the surfactant can lead to an increase in concentration of resveratrol in the rat brain [27]. Even at concentrations as low as 0.1% w/v of Tween 80, significant uptake of nanoparticles has been observed *in vitro* in MDCKII-MDR_1 cells [207]. In addition to lipid-based nanoparticle, inorganic super iron oxide nanoparticles coated with Tween 80 have also been reported to be able to cross the BBB with the assistance of an external magnetic field [358]. These studies show that Tween 80 plays an important role in facilitating the uptake of nanoparticles into the brain.

Table 3.1 Summary of selected studies in which drug has been encapsulated in Tween 80 coated nanoparticles

Drug	Core polymer	Results	References
Dalargin	PBCA	Positive analgesic effect in mice and observation of NP in Purkinje cells under EM	[206]
Dalargin (oral)	PBCA	Significant Dalargin-induced analgesia in tail flick test	[359]
Kyotorphin	PBCA	Central analgesia by hot plate test in mice	[360]
Methotrexate	PBCA	Significant increase in drug concentration in brain tissues and cerebrospinal fluids	[361]
NMDA receptor antagonist MRZ 2/576	PBCA	Prolonged duration of anticonvulsive activity	[362]
Nerve growth factor	PBCA	Improved recognition and memory in Parkinson's disease model	[363]
Anti-HIV agents (stavudine, delavirdine and saquinavir)	PBCA	Increased permeability across HBMECs	[332]
Temozolomide	PBCA	Significant concentration of temozolomide found in the brain	[364]
Tacrine	PBCA	Significant increase in tacrine concentration in the brain	[215]

PBCA: Poly (butyl cyanoacrylate) NP: nanoparticles EM: electron microscope
HBMEC: Human brain-microvascular endothelial cells EEG: electroencephalogram

3.1.2.2 Poloxamer 188 coated nanoparticles

Poloxamer 188 is a triblock copolymer sold under the trade name Pluronic F68® [365]. It is a non-ionic surfactant with poly (ethylene oxide):poly(propylene oxide):poly(ethylene oxide) at a weight ratio of 4:2:4 (**Figure 3.2**) [366]. Poloxamer 188 is a biodegradable polymer that has been widely used to stabilise polymeric and lipid nanoparticles [367, 368]. Poloxamer 188 has demonstrated neuroprotective and anti-inflammatory activities [369, 370]. The uptake of Poloxamer 188 coated nanoparticles into the brain has been shown to be similar to that for Tween 80 coated nanoparticles. ApoB or ApoE are adsorbed on the surface of the nanoparticles which can then bind to LDL-receptors present on the cell surface at the BBB. The nanoparticles are then endocytosed into the cell via receptor-mediated transcytosis [371-373].

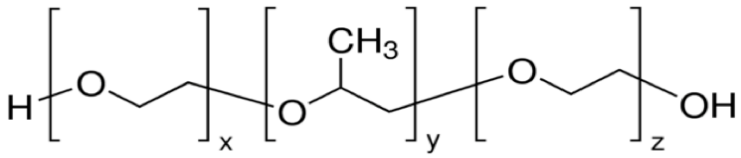

Poloxamer 188 (x: 76, y: 29, z: 76)

Figure 3.2 Chemical structures of Poloxamer 188.

A number of studies on nanoparticles coated with Poloxamer 188 for crossing the BBB are summarised in **Table 3.2**. The nanoparticles were either made from polymers, gelatin or nano-emulsions. Drugs such as loperamide, which is an opioid receptor agonist and a substrate to Pg-p is unable to cross the BBB but has potential as an anti-nociceptive agent. Loperamide was encapsulated in PLGA-PEG-PLGA nanoparticles and coated with Poloxamer 188 and Tween 80. A significant increase in anti-nociceptive effects (<20%) in mice was observed when loperamide was administered in Poloxamer 188 and

Tween 80 coated nanoparticles compared to uncoated nanoparticles [374]. In another study, the oral administration of zolmitriptan, a selective serotonin receptor agonist encapsulated in PLGA nanoparticles coated with Poloxamer 188 had a 14-fold increase in uptake into the mice brain compared to the non-encapsulated drug [375].

Table 3.2 BBB uptake studies with different drugs encapsulated in Poloxamer 188-coated nanoparticles.

Drug	Core polymer	Results	Reference
Campthotecin	SLN	High concentration of campthotecin in the brain (brain AUC ratio)	[376]
Doxorubicin	PBCA	Increase in survival rate of rats with brain tumour	[377]
Loperamide	PLGA	Noticeable nociceptive effect	[378]
Doxorubicin	PLGA	Long term cancer remission in 40% of animals treated	[378]
Doxorubicin	PLGA	Increase uptake in U87 human glioma cell line	[371]
Brain-derived neurotrophic factor (BDNF)	PLGA	Improved cognitive and neurological deficits in mice with traumatic brain injury	[350]
Cilengitide	Gelatin based nanoparticle	Improved median survival period for rats with glioblastoma	[379]
Risperidone	Nanoemulsion	Increase in brain-to-plasma concentration ratios in rats	[380]

SLN: solid lipid nanoparticle AUC: area under curve PBCA: Poly (butylcyanoacrylate) PLGA: poly (lactide-co-glycolide)

A significant number of studies have investigated the ability of nanoparticles prepared from synthetic polymers such as PBCA and coated with Tween 80 and Poloxamer 188 to improve delivery of drug molecules into the brain with varying degree of success. Despite the success, to date their use to transport CNS drugs have not been commercialised yet.

3.1.2.3 Pluronic F127

The non-ionic triblock poloxamer, Pluronic F127 is commonly used to stabilise cubosome dispersions [263]. It has an average molecular weight of 12 600 Da with 67 units of polyethylene oxide (PEO) and 100 units of polypropylene oxide (PPO) (**Figure 3.3**). Pluronic F127 is able to stabilise cubosomes by causing steric hindrance between individual cubosomes to avoid aggregation [381, 382]. The hydrophobic parts of PEO moieties are thought to anchor to the surface of the lipid bilayer and hence influence membrane stability. However, a previous study has shown that a high amount of Pluronic F127 (3.96 mM) is required to cover the surface of cubosomes to produce a stable dispersion [383].

In an *ex-vivo* model of U87 (human glioblastoma) cells, Pluronic F127 co-formulated with angiopep iron oxide nanoparticles was found to significantly increase the delivery of rhodamine 123 (model drug) as observed under a fluorescence microscope [384]. In another study, positive uptake of rhodamine 123 by rat brain endothelial cells was again observed when it was formulated into Pluronic F127 micelles coated on TGPS- D-α-tocopheryl polyethylene glycol succinate [385]. However, both studies were conducted using cell culture model and more robust *in vivo* studies need to be conducted to evaluate the potential of nanoparticles co-formulated with Pluronic F127 in targeting the brain.

Pluronic block copolymers have also been shown to inhibit P-gp and sensitise multidrug resistant (MDR) tumours efflux transporters, [386]. This can increase the uptake of drug into the brain, as a result of the decrease in the efflux of the drug molecules [387, 388]. The mechanism of Pluronic F127 mediated inhibition has been proposed to be indirectly caused by ATP depletion, which is needed for Pg-p to function [385, 386, 389]. This suggests that the uptake of Pluronic F127 coated nanoparticles does not go through the

LDL-receptors at the BBB. In this work, Pluronic F127 serves only as the control, and not specifically to target the LDL receptors.

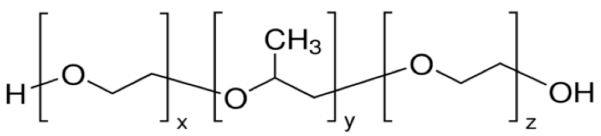

Pluronic F127 (x: 100, y: 65, z: 100)

Figure 3.3 Chemical structures of Pluronic F127

3.1.3 Selecting stabilisers for cubosomes that provide a dual role of colloidal stability and BBB targeting

Cubosome particles are colloidally unstable and require a stabiliser to avoid particle aggregation [383]. In this thesis, the stabilisers Tween 80 and Poloxamer 188 have been selected for investigation not only for their ability to provide colloidal stability to cubosome particles, but also for their potential to facilitate the binding of cubosomes to LDL-receptors at the BBB, as discussed in the preceding section. Pluronic F127, was selected as the control as it is the most commonly used stabiliser for cubosomes and regarded as the "gold standard" stabiliser [390]. In this thesis, Pluronic F127 stabilised cubosomes are not expected to be able to cross the BBB. On the other hand, it is hypothesised that coating cubosomes with Poloxamer 188 and Tween 80 will lead to an increase in the uptake of cubosomes into the brain, as has been previously shown with polymeric nanoparticles coated with the two surfactants [365, 373, 391, 392].

3.2 Hypothesis and aims

The overall aim of this chapter was to develop stable cubosome formulations with the stabilisers Tween 80 and Poloxamer 188 to target receptor-mediated endocytosis pathway at the BBB. The following hypotheses were tested:

Hypothesis 1: That cubosomes could be stabilised using Tween 80 and Poloxamer 188.
Hypothesis 2: That human brain endothelial cells were viable upon exposure to cubosomes.
Hypothesis 3: That cubosomes stabilised with Tween 80 and Poloxamer 188 will lead to its uptake by human brain endothelial cells through LDL-receptor binding via receptor-mediated endocytosis.

In order to investigate the above hypotheses, the following specific aims were conducted:

1) To prepare and characterise the physical properties of cubosomes stabilised with Pluronic F127, Tween 80 and Poloxamer 188.
2) To investigate the toxicity of the stabilisers and cubosomes coated with different stabilisers in human brain endothelial cells, hCMEC/D3.
3) To study the uptake of cubosomes coated with Tween 80 and Poloxamer 188 *in vitro* using hCMEC/D3 cell.

3.3 Results and discussion

3.3.1 Physical characterisation of phytantriol cubosomes stabilised with Poloxamer 188 and Tween 80.

Phytantriol lipid can self-assemble in excess water to form cubic phase at ambient temperature [246]. However, the dispersion of cubic phase in excess water (cubosomes) is not stable and is prone to aggregation over time. The addition of stabilisers can stabilise the dispersion and increase the shelf life [390]. The effect of adding poloxamer (Pluronic F127 and Poloxamer 188) and Tween 80 to phytantriol cubosomes were evaluated and the physical properties of the dispersions were characterised. A sufficient amount of stabiliser must coat the cubosomes surface in order to provide adequate steric repulsion [383, 390]. The cubosomes must retain its internal structure in excess water and to avoid premature release of the encapsulated drug molecules before crossing the BBB. Published bulk phase study of Tween 80 in phytantriol and water show that phytantriol/water mixtures can accommodate up to 20% w/w Tween 80 and still retain its cubic structure [393]. Based on these reports, stabilisers with the concentrations ranging from 5% to 20% w/w (with respect to the lipid phytantriol) were investigated in this chapter.

Cubosome dispersions were freshly prepared using the solvent precursor method, which involves the formulation of a precursor solution of lipid (phytantriol) and stabiliser by the addition of a co-solvent (propylene glycol). The resulting low viscosity precursor solution then can be dispersed into homogeneous dispersions with minimal energy input (vortex mixing) [313]. This method has been shown to be more suitable for proteins and heat labile drugs compared to high energy homogenisation [394], thus allowing a wider range of drug molecules to be encapsulated inside the cubosomes.

3.3.1.1 Effect of poloxamers on the size and nanostructure of phytantriol dispersions

The effect of varying the different concentrations of poloxamers on the size, polydispersity and the nanostructure of the dispersions can be observed in **Table 3.3**. Cubosomes stabilised with Pluronic F127 are usually below 200 nm [395]. Increasing the concentration of Pluronic F127 from 5% to 20% w/w led to a decrease in particle size and more homogeneous particles (PDI <0.09). These results suggest that increasing the concentration of Pluronic F127 promotes better steric stabilisation in phytantriol dispersions. Pluronic F127 is thought to stabilise cubosomes by acting as a detergent in which the hydrophobic PPO moieties anchor to the lipid membrane, while the hydrophilic moieties protrude out and in contact with the aqueous phase. It is also proposed that the PPO and PEO residue can be incorporated into the lipid bilayer within various configurations. The possible configuration is determined by the length of PEO-PPO and the method of mixing the lipid with the poloxamers [396].

It is most likely that the PPO moieties are adsorbed and partially inserted onto the surface of phytantriol lipid while the long PEO chains protrudes out into the aqueous phase providing steric stabilisation (**Figure 3.4**) [397]. Increasing the amount of Pluronic F127 used from 5% to 20% w/w leads to higher adsorption of Pluronic F127 on the surface, thus reducing the interfacial tension between the phytantriol lipid and water. This then leads to the reduction in particle size of the cubosomes and therefore forming more homogeneous particles [398].

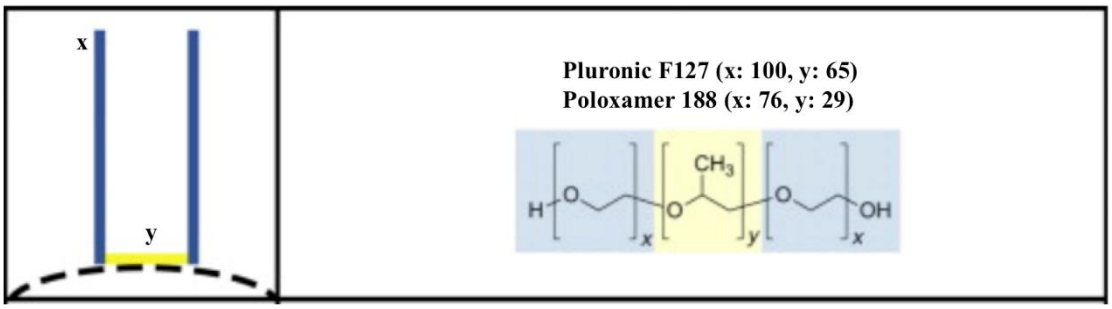

Figure 3.4 The adsorption of poloxamer on the surface of phytantriol cubosomes. The PPO moiety (y) is adsorbed on the surface of cubosomes while PEO chains (x) protrude out to the aqueous phase to exert steric stabilisation. Adapted from [398] with permission.

The suitable size of nanoparticles for intraveneneous administration was proposed to be in between 2 to 200 nm. While too small nanoparticles (<5 nm) can be subjected to renal excretion and clearance from tissues, larger particles might not be able to enter the cells through the desired pathway [399]

In contrast, larger particles (~215 nm) were observed when 20% w/w of Poloxamer 188 was added as compared to 5% w/w (~180 nm), with more heterogeneous particles formed (PDI >0.3) at 20% w/w of Poloxamer 188. Poloxamer 188 has a high surface activity which aids in higher amount of insertion in the phytantriol lipid bilayer within cubosome structure [366, 400]. This leads to an increase in cubosome size as the concentration of Poloxamer added, increases from 5% w/w to 20% w/w. Poloxamer 188 has a shorter PEO-PPO-PEO chain compared to Pluronic F127 (**Figure 3.2 and 3.3**). It is likely that the PPO unit in Poloxamer 188 may adsorb differently onto the phytantriol bilayer as compared to Pluronic F127. Hence for the same concentration used, Poloxamer 188 does not occupy the surface of the cubosomes as densely as Pluronic F127 [396]. However, these results contradict observations reported by Swarnakar *et al.* [401] where the authors found that an increase in the concentration of Poloxamer 188 led to smaller particle size and a more homogeneous dispersion. The conflicting observations can be explained by the method and lipid used in both studies. In this thesis, only a low energy

vortex mixer was used. Swarnakar *et al*. [401] employed high energy ultrasonication for particle formation. In addition, it also used GMO lipid instead of phytantriol. It is possible that this method of dispersion promotes better adsorption of Poloxamer 188 onto phytantriol bilayer, thus a greater reduction in the surface tension which promotes a reduction in particle size and increase in particle homogeneity. The choice of lipid also affects the final dispersion due to the effect of different lipid packing.

Table 3.3 Effect of stabilisers on size, polydispersity index (PDI), internal structure and lattice parameter of cubosome particles. Data presented (size and PDI) are mean ± standard deviation of three independent experiments

Stabilisers (% w/w to phytantriol)	**Average particle size (nm)**	**PDI**	**Internal structure**	**Lattice parameter (Å)**
Pluronic F127				
5%	267.0 ± 3.1	0.22 ± 0.01	*Pn3m*	69
15%	177.5 ± 5.4	0.18 ± 0.01	*Pn3m*	69
20%	176.2 ± 1.1	0.09 ± 0.03	*Pn3m*	66
Poloxamer 188				
5%	179.5 ± 0.3	0.15 ± 0.01	*Pn3m*	67
15%	188.1 ± 1.2	0.29 ± 0.02	*Pn3m*	68
20%	215.3 ± 4.5	0.40 ± 0.00	*Pn3m*	68
Tween 80				
5%	242.9 ± 35.0	0.28 ± 0.00	*Im3m*	102
15%	164.9 ± 1.8	0.13 ± 0.01	*Im3m*	107
20%	204.7 ± 1.1	0.21 ± 0.00	*Im3m*	120

To confirm the internal structure of all the dispersions after the addition of stabilisers, SAXS was conducted and the data is summarised in **Figure 3.5** and **Table 3.3**. All dispersions stabilised with Pluronic F127 and Poloxamer 188 have the *Pn3m* cubic structure with lattice parameter between 66 to 69 Å, as indicated by the presence of three Bragg peaks with spacing ratios of √2: √3: √4. Even though Pluronic F127 has longer PEO and PPO units compared to Poloxamer 188 (76 PPO and 26 PEO), the interaction between both poloxamers and phytantriol bilayer produced cubosomes with

similar internal structure and lattice parameter. It is known that poloxamers with PEO units equal to or greater than 37 usually form *Pn3m* internal cubic structure in phytantriol based systems [398]. The partitioning of the PEO chain from poloxamers into the phytantriol lipid bilayer increases the membrane surface curvature causing the formation of *Pn3m* structure [402].

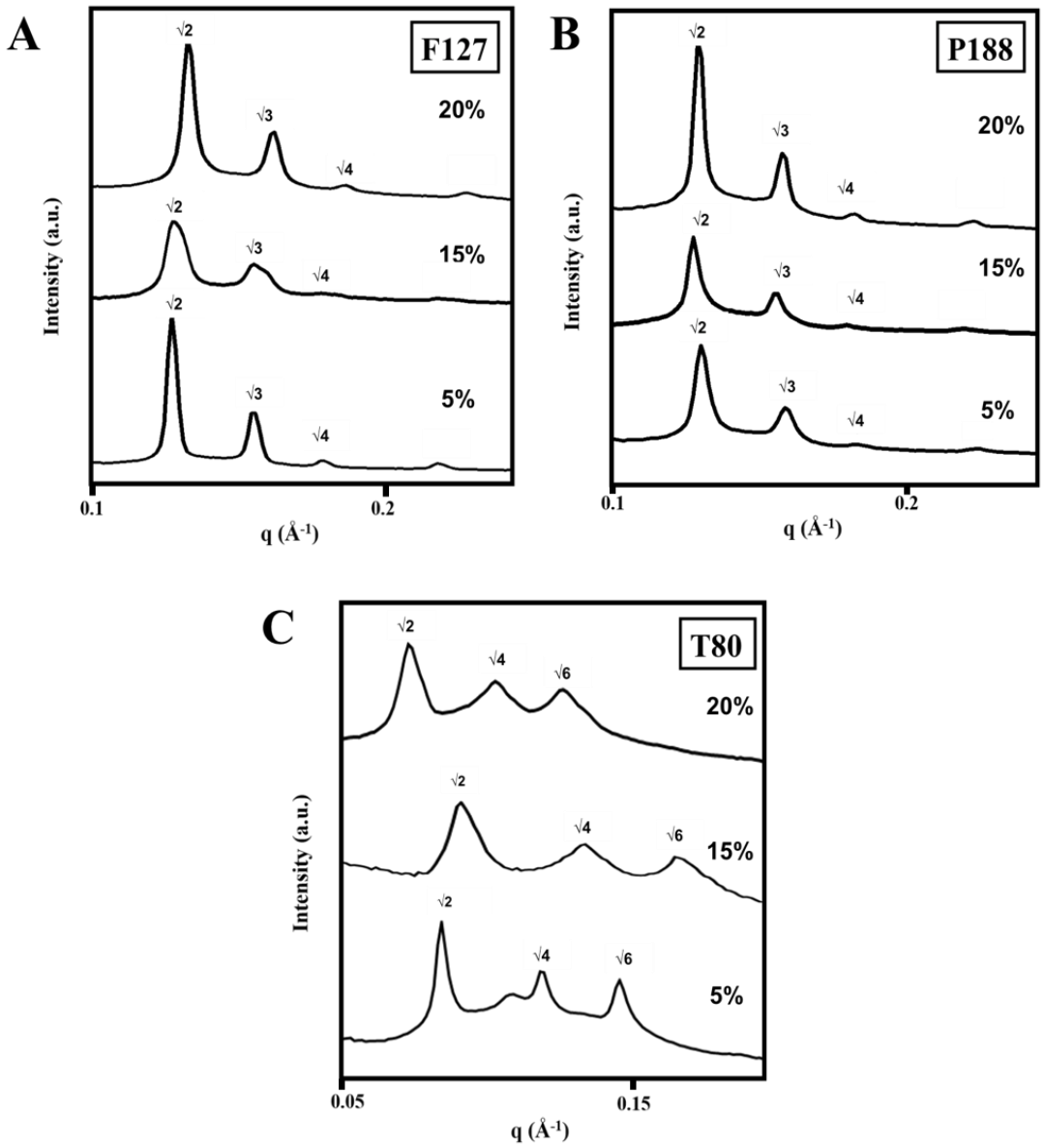

Figure 3.5 SAXS diffraction (intensity versus *q* plots) of cubosomes dispersions stabilised by (A) Pluronic F127 (F127), (B) Poloxamer 188 (P188) and (C) Tween 80 (T80) at 5% to 20% w/w with respect to phytantriol. The plots showing Bragg peaks used to assign phase structure.

In contrast, in GMO-based dispersions, increasing the amount of Pluronic F127 (up to 1% w/w) leads to the change in the internal structure of cubosomes from *Pn3m* to *Im3m* cubic phase. This is because Pluronic F127 is capable of disrupting the internal crystalline structure of GMO cubosomes at higher concentrations [263, 367]. From these results, it can be postulated that the mechanism of steric stabilisation provided by Pluronic F127 is influenced by the cubosome forming lipids, where in phytantriol, the concentration of Pluronic F127 studied (5 to 20% w/w) did not change the internal structure of cubosomes.

3.3.1.2 Effect of Tween 80 on the size and nanostructure of phytantriol dispersions

Increasing Tween 80 concentration from 5% to 20% w/w in the dispersion leads to an increase in particle size. All formulation produced homogeneous dispersions (PDI <0.3) (**Table 3.3**). The internal structure formed was found to be *Im3m* cubic for all the concentrations, as evidenced by the presence of three Bragg peaks with relative positions in the ratio of √2: √4: √6 (**Figure 3.5**). A negative shift in the *q* value was observed when the amount of Tween 80 was increased. This is due to the overall expansion of the cubic phase consistent with the increased hydration as the lattice parameter is increased from 102 to 120 Å. This is consistent with the finding that the increase in Tween 80 content leads to a shift in bulk phase behaviour from *Pn3m* cubic phase to *Im3m* cubic phase and then to lamellar phase [393]. However, the decrease in particle size with increase in Tween 80 concentration up to 15% w/w suggests an interaction between Tween 80 and the cubosomes bilayer leading to a reduction in the interfacial tension.

Upon addition of Tween 80, the hydrophobic PEG unit on the Tween 80 likely interacts with the phytantriol bilayer. The steric effect is likely be caused by the hydrophilic part of the Tween 80, which protrudes out of the phytantriol bilayer (**Figure 3.6**). Increasing the Tween 80 content will increase the adsorption of Tween 80 molecule on the surface of the bilayer which will then increase the thickness of the bilayer and the pore size (lattice parameter). It is also observed that the increase in size of cubosomes after the addition of Tween 80 from 5% to 20% w/w suggests that Tween 80 interacts differently with the cubosomes and increase the overall size at high concentrations.

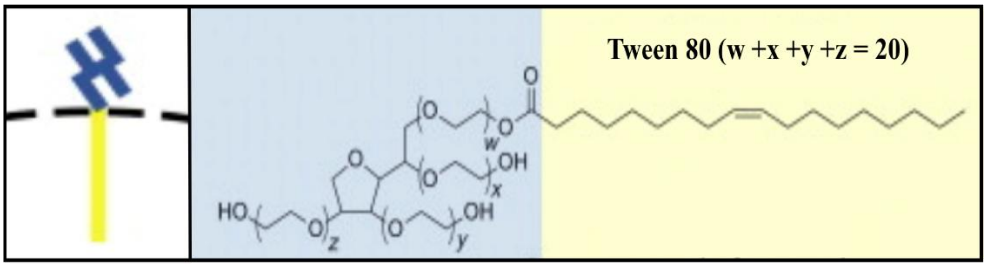

Figure 3.6 The chemical structure of Tween 80 with an illustration of its adsorption on the cubosomes surface. Hydrophobic moiety of Tween 80 (yellow) is inserted into the bilayer through hydrophobic interaction while the hydrophilic moiety (blue) exerts the steric hindrance on the surface of the cubosomes. (Adapted with permission [398]).

The suitable size of nanoparticles for intraveneous administration was proposed to be in between 2 to 200 nm. While too small nanoparticles (<5 nm) can be subjected to renal excretion and clearance from tissues, larger particles might not be able to enter the cells through the desired pathway [399]. However, upon intraveneous administration into the body, the cubosomes and other nanoparticles are subjected to various protein and ionic interaction within the blood content and form protein corona. This might change the overall diameter of the particles and affect the interaction with the cells [403, 404]. Regardless, this thesis did not investigate the effect of particle size on the uptake of cubosomes and only focus on formulation development, followed by uptake studies *in vitro* and *in vivo*.

3.3.1.3 Effect of stabilisers on cubosomes surface charge

From the studies conducted above, 15% w/w of stabiliser was selected for use in subsequent studies. At this concentration, cubosomes stabilised with Pluronic F127 and Poloxamer 188 formed *Pn3m* structure while *Im3m* structure is formed in Tween 80 cubosomes. Even though Pluronic F127, Poloxamer 188, Tween 80 and phytantriol are non-ionic, these interactions lead to negative ζ-potential as shown in **Table 3.4**. The

differences in the charge between different formulation was shown to be significant ($p<0.05$). This has been previously reported and is likely due to the adsorption of hydroxyl ions from water at the phytantriol/water interface [405].

Table 3.4 ζ-potential (mv) of phytantriol cubosomes stabilised with 15% w/w Pluronic F127, Poloxamer 188 and Tween 80. Data presented are mean ± standard deviation of at least three repeated measurements.

Cubosomes	**ζ-potential (mv)**
Pluronic F127	-28.6 ± 0.3
Poloxamer 188	-29.5 ± 0.4
Tween 80	-31.8 ± 0.3

3.3.1.3 Visualisation of the internal nanostructure of cubosomes

Direct structural evidence of cubosomes was obtained using cryo-TEM. This is an advanced microscopy technique for visualising the internal structure of nanoparticles [406]. Cryo-freezing is a crucial step in sample preparation and involves the formation of vitrified ice on the grids which contains the particles. Failure to form a thin layer of vitrified ice leads to the inability to observe the cubosomes particles under cryo-TEM. Due to the limitations of thick ice formation on grids, cubosomes stabilised with Poloxamer 188 could not be frozen for TEM imaging

Cubosomes stabilised with 15% w/w Pluronic 127 formed heterogeneous sized particles (arrowhead) with a size distribution consistent with the results reported in **Table 3.3**. In addition to cubosome particles, vesicles were also observed in the samples as illustrated in **Figure 3.7.** Vesicles as shown in Panel A (arrow) are commonly observed co-exist with cubosomes stabilised with Pluronic F127 [407]. Panel B shows particle with well-arranged cubic lattice periodicity, indicating successful cubosome formation when using 15% w/w Pluronic F127 as a stabiliser. Formation of cubosomes is also supported by the SAXS results presented in **Figure 3.5**.

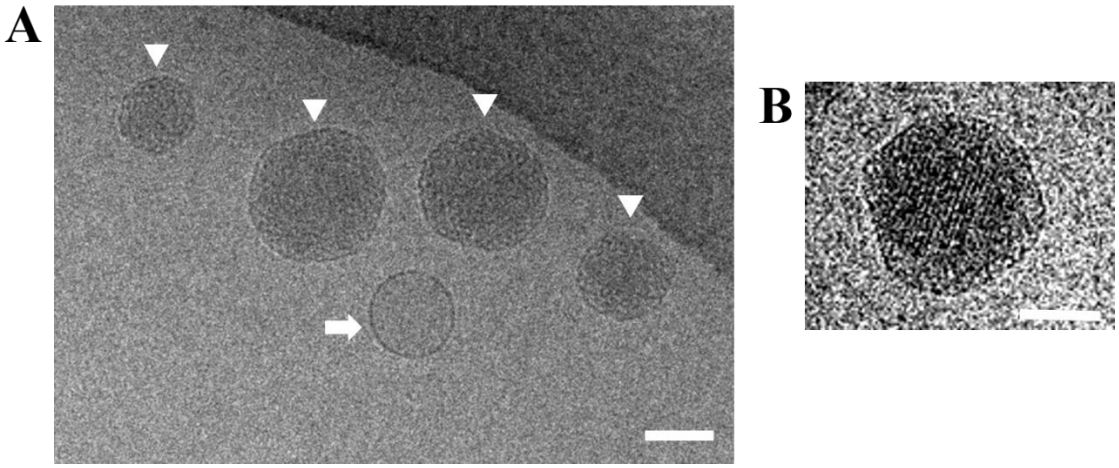

Figure 3.7 Cryo-TEM micrographs of cubosome dispersion stabilised with 15% w/w Pluronic F127. Panel A shows the cubosomes formation (arrow heads) with the presence of a vesicle (arrow). Panel B shows the surface structure of one single cubosome. Scale bar: 100 nm.

Cryo-TEM was also used to investigate the effect of Tween 80 concentration on particle nanostructure. Cryo-TEM tomograms shown in **Figure 3.8** show the nanostructure of particles stabilised 5% to 20% w/w. At 5% w/w Tween 80, a particle with a diameter of about 240 nm were observed (Panel A), while at the higher concentration of 20% w/w Tween 80, relatively more homogeneous dispersions (with about 200 nm particle size) were observed with the appearance of vesicles (Panel C). This observation correlates with the results from the particle size and polydispersity studies in **Section 3.4.1.2** where when 5% and 20% of Tween 80 were used, higher PDI values were recorded (>0.2). Interestingly, the addition of 15% w/w Tween 80 resulted in uniformly-shaped and homogeneously dispersed cubosomes of about 170 nm in size. This shows that increasing the Tween 80 concentration does not necessarily produce more homogeneous dispersions.

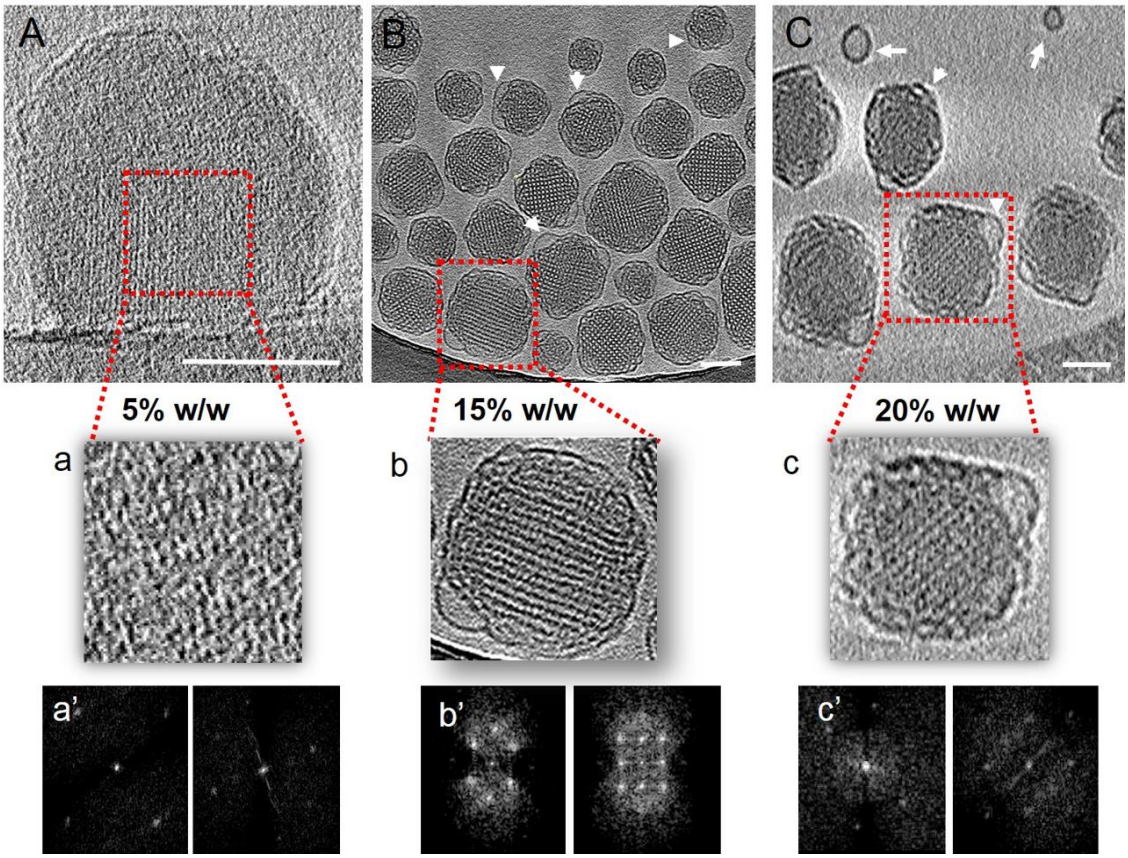

Figure 3.8 Cryo-electron tomograms showing a field of cubosomes embedded in vitrified buffer suspension. Cubosomes were stabilised with (A) 5% w/w, (B) 15% w/w and (C) 20% w/w Tween 80. The presence of a vesicular coat was seen in panel C and indicated by the arrowhead while the vesicles are indicated by the arrows. Panel a-c show the enlarged view of representative cubosomes from the tomogram with their Fast Fourier Transform (Panel a'-c'). Scale bar: 100 nm. (Adapted from [393] and reproduced with permission).

Dispersions stabilised by Tween 80 were further investigated using cryo-electron tomography (cryo-ET) for a more in-depth analysis of the internal cubosome structure. The tomograms for each dispersion are shown in **Figure 3.8**. Panels a to c show the enlarged images of representative cubosomes from Panels A to C, and Panels a' to c' show their Fast Fourier Transform (FFT). The FFT pattern of the particles can provide information on the crystalline structures. From **Figure 3.8**, all the patterns reveal cubic packing and hexagonal symmetry, depending on the angle of rotation. Increasing the

concentration of Tween 80 from 5% w/w to 15% w/w resulted in more homogenous particles with the presence of vesicular coat and the absence of vesicles. A stronger FFT signal and clear symmetry is evident with 15% w/w Tween 80. At the highest concentration studied (20% w/w), the vesicular coats were also observed with the addition of a bilayer coating encapsulating the particles (Panel c). The presence of these vesicular coats is commonly reported in literature [245, 275]. Tween 80 stabilised cubosomes with a concentration of 15% w/w is processed for 3D reconstruction to get a full view of the cubosome.

3.3.1.4 The 3D reconstruction of Tween 80 cubosomes

To observe the 3D structure of cubosomes stabilised with 15% w/w Tween 80, a single cubosome was randomly selected from the tomogram in **Figure 3.9,** Panel A (dotted box) and sliced in x, y and z planes (Panel B). A 3D surface projection of the whole particle is shown in **Figure 3.9,** Panel C. The internal cubosome nanostructure was captured at two different thickness, a 'thick' (Panel D) and a 'thin' slice (Panel E) through the vertical plane. The complex nanoporous structure and the 3D hierarchical organization of the lipid bilayer in a cubosome in its native state is evident in these slices. The surface of the slice in Panel D and E are magnified in Panels *d* and *e*, respectively and the surface is capped in light pink for clarity. Upon further magnification, a distinct bilayer arrangement with uniform water channels (dotted circle) is evident. The periodicity of the water channels shown in **Figure 3.9** (Panel e') was calculated at ~100 Å. The reconstructed 3D images clearly show a tortuous structure with bicontinuous network comprising water channels as previously reported [408].

The findings from physical characterisation and cryo-TEM imaging show that Tween 80 is as effective as Pluronic F127 in stabilising phytantriol cubosomes. The absence of vesicles and the formation of homogeneous particles suggest that 15% w/w is the optimum concentration of Tween 80 to stabilise phytantriol cubosomes [394]. To standardise the formulation preparation from all the stabilisers, the concentration of stabiliser used will be standardised to 15% w/w in subsequent studies.

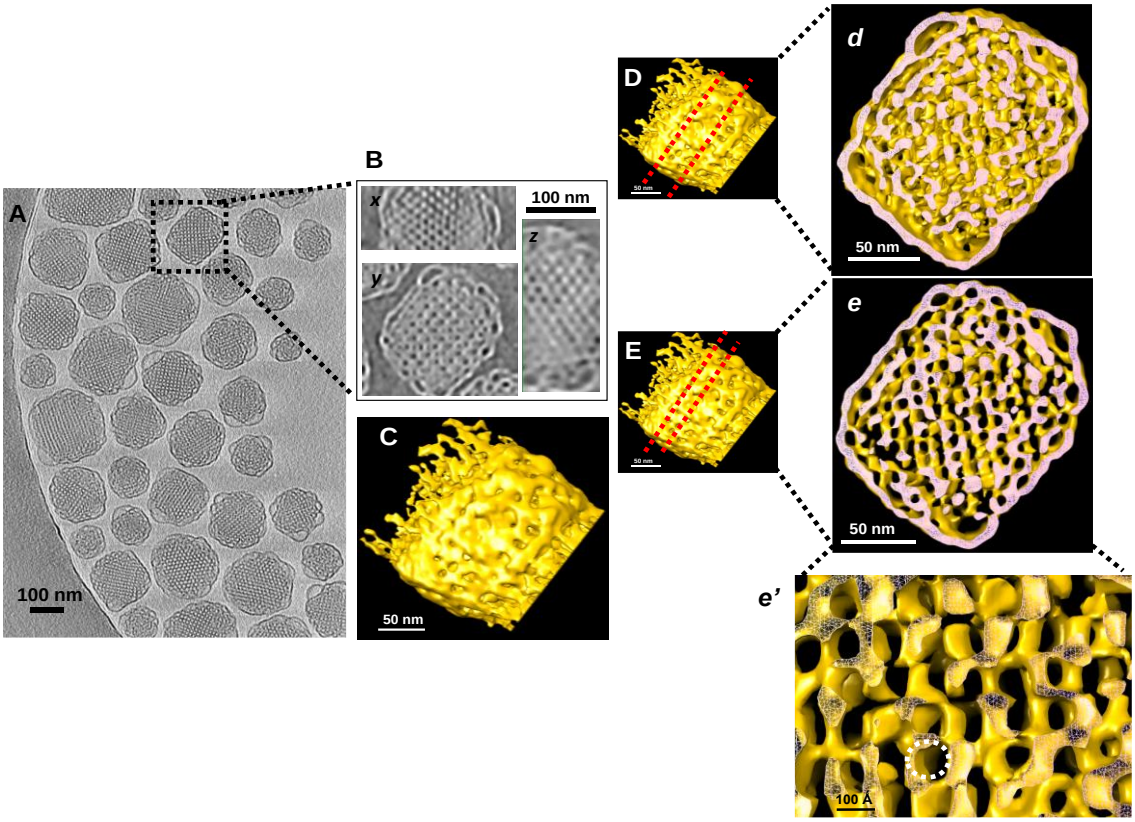

Figure 3.9 A full view cryo-electron tomogram of cubosomes dispersions stabilised with 15% w/w Tween 80 (A). A single cubosome (box) is sliced in x, y and z planes (B) and reconstructed as a 3D image. The surface projection (whole particle) of the reconstructed cubosome is shown in panel C. The reconstructed particles are further 'sliced' tangentially at two different thickness, thick (D) and thin (E) to reveal the internal structure of the particles at different depths, labelled *d* and *e*, respectively. The surface of the particles in Panel *d* and *e* are capped in light pink. Upon magnification of Panel *e*', an internal structure comprised of distinct bilayer arrangement (yellow) with uniform water channels (white circle) is visible. (Adapted from [393] and reproduced with permission).

3.3.2 Toxicity of phytantriol towards hCMEC/D3

To develop a suitable drug carrier to deliver drugs to the brain, it is crucial to consider its toxic effect on the cells of the BBB, in particular the endothelial cells. This is because an observed high drug uptake may not necessarily be due to the successful preparation and targeting of the drug carrier, but because of the BBB being compromised by local toxicity effects. Therefore, it is important to establish that any observed uptake is with a result of the formulation and not due to cellular toxicity from the components of the formulation, which in the case of cubosomes can be due to the lipid phytantriol or the stabilisers.

A preliminary study was conducted to evaluate an appropriate concentration range of cubosomes for use in the *in vitro* uptake study. The concentration of cubosomes studied was reflected to the concentration of phytantriol in the cubosome formulation, and will be referred as phytantriol concentration. The viability of hCMEC/D3 cells after two hours of incubation with increasing doses of phytantriol (8 to 300 µM) was determined and is presented in **Figure 3.10**. At low concentrations of phytantriol (8 to 50 µM), cell viability is over 90%. As the concentration of phytantriol increases from 50 to 300 µM, cell viability declines from about 80% to 40%. From these toxicity results, the concentration of phytantriol used in subsequent *in vitro* studies was set at < 30 µM to achieve at least 80% live cells.

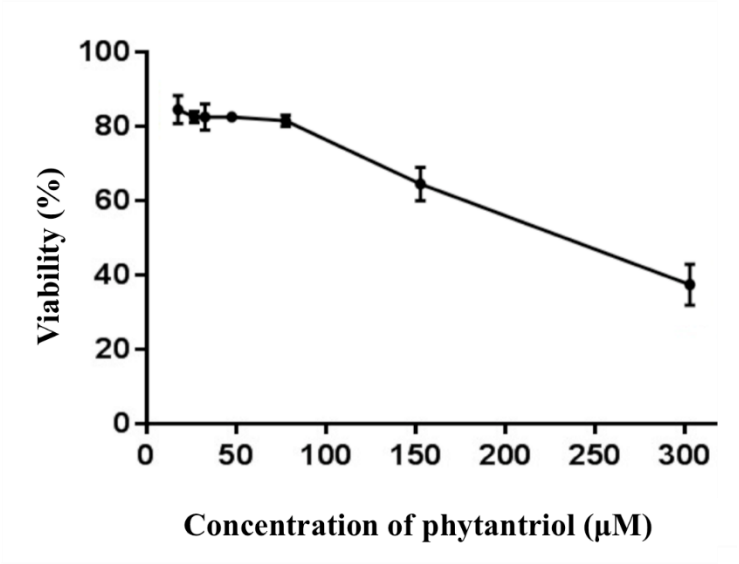

Figure 3.10 Viability of hCMEC/D3 cells (total percentage of PI-negative cells) after incubation with increasing concentration of Pluronic F127 stabilised cubosomes, by using phytantriol concentration (μM) in the cubosome formulation as reference. Data presented are mean ± standard deviation of three independent experiments.

3.3.3 Toxicity of stabilisers towards hCMEC/D3 cells

With the toxicity effects of phytantriol lipid established, this study now focuses on the toxicity of stabilisers used in this thesis. In order to understand the *in vitro* toxicity effect of stabilisers, both stabilisers (0.75 μg to 1.88 μg) as a suspension (without phytantriol lipid) and in cubosome dispersions were studied.

The effect of Pluronic F127, Poloxamer 188 and Tween 80 in a suspension or in cubosomes on the viability of hCMEC/D3 cells are presented in **Figure 3.11** by comparing the cell viability after incubation with stabiliser in suspension. A similar effect on cell viability was observed in all groups studied, however the cellular toxicity was significantly higher ($p<0.05$) when the stabilisers were in a suspension form (dotted line, closed symbols). In cubosome dispersions, the hydrophobic part of the stabilisers is expected to be inserted in the lipid bilayer while the hydrophobic part is protruded out to exert steric stabilisation, as discussed previously. This observation suggests that the

toxicity of the stabilisers might be masked by their incorporation in the phytantriol lipid bilayer within the cubosome structure [409]. The overall toxicity study suggests that cubosome dispersions stabilised with Pluronic F127, Poloxamer 188 and Tween 80 at concentrations up to 38 μM are not toxic to hCMEC/D3 cells.

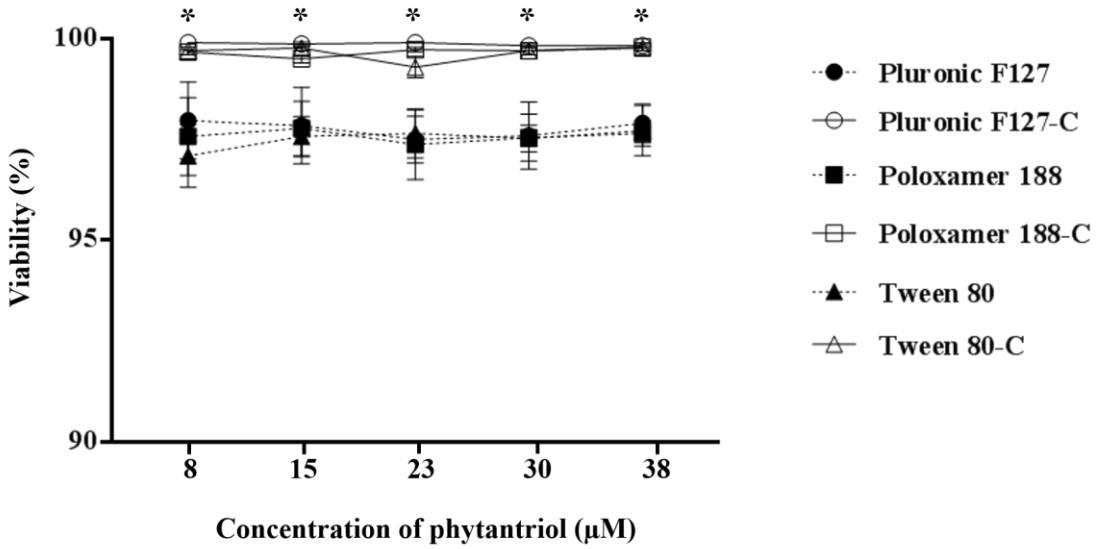

Figure 3.11 Viability (%) of hCMEC/D3 cells after two hours incubation with cubosomes stabilised with Pluronic F127 (open circle), Poloxamer 188 (open square) and Tween 80 (open triangle). The viability of Pluronic F127 (closed circle), Poloxamer 188 (closed square) and Tween 80 (closed triangle) in solution form (dotted line) without cubosomes were also tested in the same way. Data presented are mean ± standard deviation of three independent experiments. *P<0.05 compared to stabilisers (in suspension).

3.3.4 Uptake of cubosomes by hCMEC/D3 cells

3.3.4.1 Uptake of cubosomes coated with Tween 80 and Poloxamer 188

For uptake studies, cubosomes were fluorescently labelled with NBD (refer to **Section 2.2.1.1** for preparation). The cellular uptake of cubosomes by hCMEC/D3 cells were analysed by quantifying NBD positive populations in hCMEC/D3 cells incubated with cubosomes or equal concentration of NBD only as a suspension (control). The analysis was conducted using flow cytometry. The general cell autofluorescence was taken into account and deducted from the total fluorescence measurement.

Figure 3.12 summarises the uptake of cubosomes stabilised by the three different stabilisers. The uptake (%) of cubosome formulations by hCMEC/D3 cells were significantly lower ($p<0.05$) compared to the control group across all concentrations. It is possible that the processing stepps involved in the analysis of cellular uptake using flow cytometry may have led to the loss of positive NBD cells, causing the low level of detection observed. Therefore, fluorescence microscopy was used to visualise uptake of cubosomes by hCMEC/D3 cells. By using fluorescence microscopy, any evidence of cellular uptake can be observed directly without any physical disturbance to the cells.

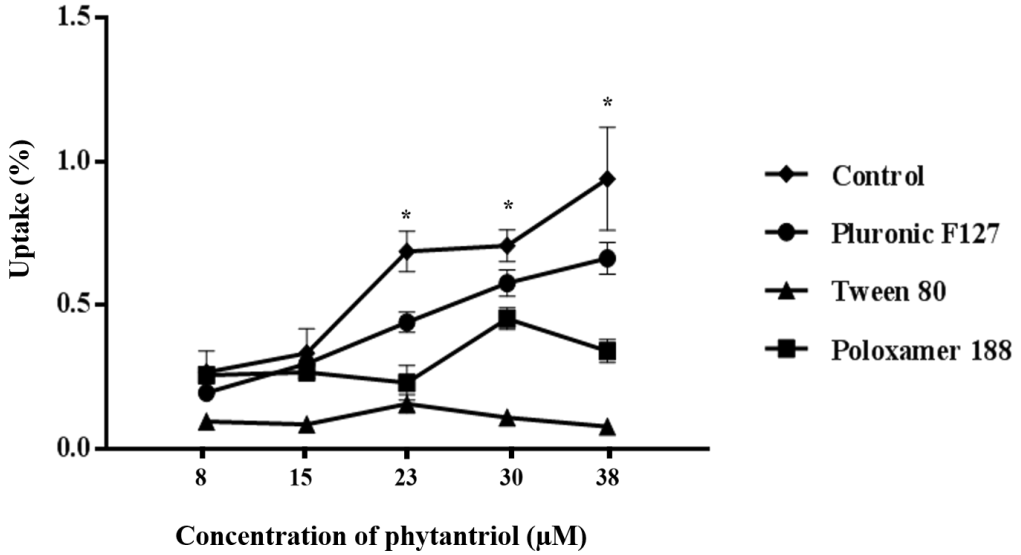

Figure 3.12 Uptake of NBD labelled cubosomes stabilised with Pluronic F127, Poloxamer 188 or Tween 80 with NBD suspension (control) in hCMEC/D3 cells, after two hours of incubation at five different doses. The concentration of NBD in NBD suspension (control) corresponds to the concentration of NBD in cubosome dispersion. Data presented are mean ± standard deviation of three independent experiments. *P<0.05 compared to control (NBD suspension).

In the fluorescence microscopy studies, the concentration of phytantriol was kept constant at 38 µM, and the cubosomes were labelled with NBD. **Figure 3.13** illustrates the presence of NBD in the cells, observed as green spots within the cells after two hours of incubation. The fluorescence signal from NBD was not strong and only low levels of cellular uptake were observed in cells incubated with Pluronic F127, Tween 80 and Poloxamer 188 stabilised cubosomes compared to the control (cells incubated in NBD suspension). This observation is in agreement with the uptake studies using the flow cytometer (**Figure 3.12**).

Even though hCMEC/D3 cells have been shown to express LDL-receptors on their cell surface [305, 309] however, uptake by the LDL-receptor requires the binding with apolipoproteins. In the *in vitro* environment, the lack of apolipoproteins in the cell media

might be a reason for the poor cellular uptake observed in Tween 80 and Poloxamer 188 cubosomes [305, 355, 410, 411]. In order to optimise the interaction between Tween 80 and Poloxamer 188 cubosomes with LDL-receptors, the cubosomes can be pre-incubated with ApoE or the cell culture media can be conditioned with ApoE solution.

Another limitation in the uptake might be due to the incubation period of cubosomes with hCMEC/D3 cells. Other studies with positive uptake utilising LDL*-receptors were conducted with incubation for 24 hours or more. However, under static cell culture condition, a longer incubation time might force the cell to endocytose the particles due to the gravity effect. Cells that divide rapidly are prone to endocytose particles that were exposed on their cell membrane for a long period [305, 307, 412-416]. In short, longer incubation might give false positive uptake [417].

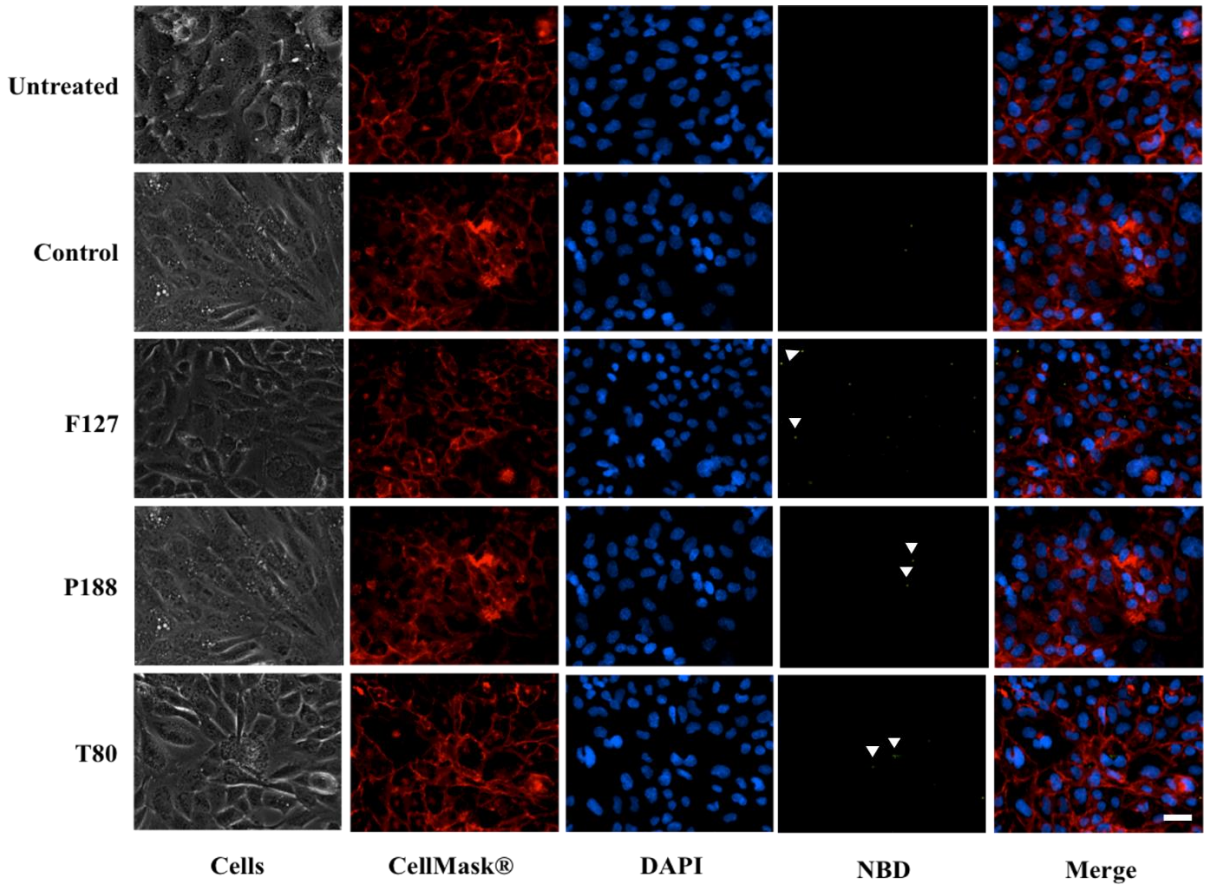

Figure 3.13 Micrographs showing uptake of NBD tagged cubosomes stabilised with 15 % w/w Pluronic F127 (F127), Poloxamer 188 (P188) and Tween 80 (T80), under fluorescence microscope. Cubosomes concentrations were selected at 38 µM of phytantriol. Cell membranes were stained with CellMask® (Texas red filter), nucleus was stained by Hoercht 33258 (DAPI-blue) for live cells and FITC channel was used to observe the green fluorescence from NBD. Positive uptake (NBD) was observed from the presence of green fluorescence spots (arrowhead). Scale bar: 10 µm.

3.4 Conclusion

Cubosomes stabilised with three different stabilisers with BBB-targeting potential were successfully formulated and their uptake by human brain endothelial cells, hCMEC/D3 was investigated.

The cell toxicity of all cubosome formulations was observed to be concentration dependent and not affected by the type of stabilisers. However, to the contrary of the hypothesis that Tween 80 and Poloxamer 188 stabilised cubosomes will be endocytosed into the hCMEC/D3 cells, only a very low cellular uptake (<1%) was observed in the formulations studied. This is probably due to lack of ApoE in the media which is necessary to facilitate interaction with the LDL-receptor for subsequent endocytosis by endothelial cells.

In the next chapter, cubosomes with a positive surface charge to target the adsorptive endocytosis pathway at the BBB will be formulated and their uptake by hCMEC/D3 cells investigated.

Chapter 4

Cationic cubosomes to target adsorptive endocytosis at the BBB

4 Cationic cubosomes to target adsorptive endocytosis at the BBB.

4.1 Introduction

There are several uptake pathways at the BBB that can be utilised to deliver nanoparticles to the brain, including adsorptive endocytosis transport which will be explored in this chapter using cubosomes. As discussed in **Section 1.2.2.5**, adsorptive endocytosis provides a mechanism for positively charged endogenous and exogenous macromolecules and particles to enter endothelial cells through electrostatic interaction. In the following sections, the literature regarding the mechanism of adsorptive endocytosis for nanoparticle uptake into the brain, the use of charged lipids to surface coat nanoparticles to target this pathway and the current information on monolayer interactions between phytantriol and charged lipids will be reviewed.

4.1.1 Adsorptive endocytosis transport at the BBB.

The endothelial cell membrane has a highly negative surface charge that creates a repulsive effect on anionic molecules, while attracting cationic molecules, predominantly through electrostatic interactions. Designing nanoparticles with positively charged surfaces can induce uptake across the negatively charged cell membrane through electrostatic interactions [201, 418, 419].

The negative charge present on endothelial cells, at the luminal, abluminal and the basement membrane is illustrated in **Figure 4.1**. The cell membrane is surrounded by a specific glycoprotein called glycocalyx, which is composed of heparan sulfate proteoglycans (HSPG) and sialo-glycoconjugates that exerts the negative charge on the endothelial cells [420-422]. The two major forms of HSPG are syndecan and glypican where the luminal side has a larger proportion of glypican. Meanwhile, the abluminal side of

the cell membrane is made up of mixed proteoglycans, HSPG and chondroitin sulfate proteoglycans (CSPG). The basement membrane consists of HSPG and a different type of CPSG, which is the perlecan. The anionic charge presented on both luminal and abluminal surfaces is affected by the distribution of glypican, where the charge is more negative at the luminal side due to higher amount of glypican [423].

Overall, the net negative charge decreases from the luminal to abluminal and finally basement membrane [423]. This effect was observed and confirmed by examining the localisation of cationic colloidal gold at the BBB, with more intense staining being detected on the luminal surface of the endothelial cells [420].

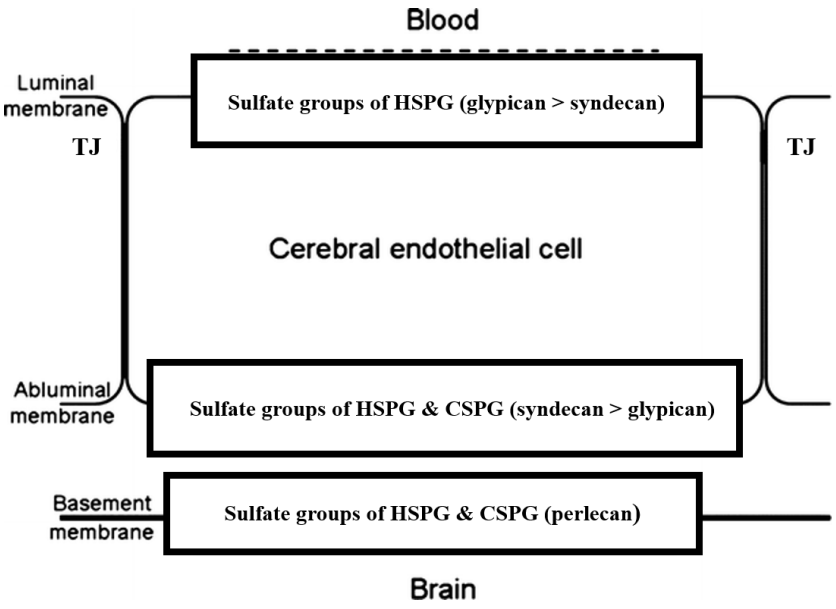

Figure 4.1 The endothelial cell and basement membrane components with different distribution of proteoglycans. The overall negative charge of the cell membrane and the basement membrane allows the uptake of cationic molecules through the electrostatic attraction followed by adsorptive endocytosis. HSPG: heparan sulfate proteoglycans; CSPGs: chondroitin sulfate proteoglycans and TJ: tight junctions. (Adapted from [423] with permission).

The overall anionic charge on the cell can therefore facilitate the shuttling of cationic molecules from the cell surface, all the way through the brain interstitium. For example, ebitaride, an adrenocorticotropic hormone analogue developed for treating Alzheimer's disease, has a positive net charge at physiological pH and can cross the BBB using this adsorptive endocytosis pathway [424]. However, not all positively charged molecules enter the brain through the same pathway. Positively charged drugs such as amantadine, enter the brain via the cationic amino acid transporter [425]. Large peptides and proteins like histone and avidin with positively charged surface have a greater tendency to cross the BBB through the electrostatic pathway [423, 426].

4.1.2 Cationic nanoparticles for drug delivery to the brain.

Developing nanoparticles with positive surface charge via the addition of positively charged molecules or ligands on their surface can improve drug delivery across the BBB. For example, in one study, the addition of a hexamethylediamine group on albumin and antibodies to modify their charge (positive charge) has led to an increase in the uptake to the brain (rats) within 10 minutes of subcutaneous administration, as compared to native albumin and antibodies [427].

The addition of specific cationic ligands known as cell penetrating peptides (CPP), which are cationic peptides with a maximum of 30 residues in length, have been widely investigated for their capacity to increase uptake of liposomes and the delivery of small-molecule drugs, proteins, peptides and oligonucleotides [428-433].

Docetaxel loaded in nanoparticles conjugated with angiopep-2 and activatable cell-penetrating peptide (ACP) has increased drug localisation at glioma site [434]. Albumin nanoparticles carrying doxorubicin prepared with the addition of cationic albumin and mannose modified albumin showed dual targeting to glioblastoma from mannose binding to the glucose receptor and the electrostatic interactions from cationic albumin in bEnd.3 cells, U87MG glioblastoma cells and spheroids [201]. This shows that adding specific cationic moieties to the nanoparticle surface, can increase their delivery into the brain cells. However, since adsorptive endocytosis pathway is non-selective, and all cell membranes are negatively charged (not just the BBB), the uptake of positively charged nanoparticles will also occur at other non-target tissues.

4.1.3 Cationic cubosomes to target the BBB

The addition of specific molecules to change the overall cubosomes charge to a net positive charge in order to target adsorptive endocytosis has been reported [435]. This chapter will explore the potential of adding cationic lipids into phytantriol cubosome formulations to target the adsorptive endocytosis pathway at the BBB. It was hypothesised that cationic lipids with long hydrocarbon tails and hydrophilic heads will most likely be inserted in between the phytantriol lipid bilayer within the cubosome particle and change the ζ-potential and surface charge of the particle. Single and double chain cationic lipids were studied to evaluate the effect of chain number and length on the formation of cubosomes and on cellular interactions such as uptake and toxicity. Three different cationic lipids (single and double chain) with quaternary ammonium head groups were selected to prepare cationic cubosomes while an anionic lipid was selected for the control group (**Figure 4.2**).

CTAB

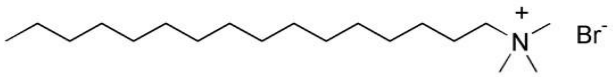

DOTAP

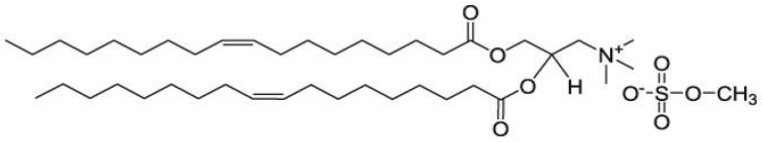

DOTMA

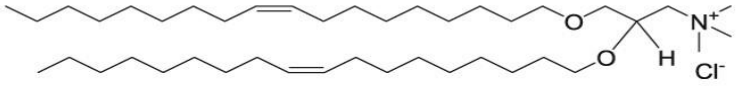

DMPG

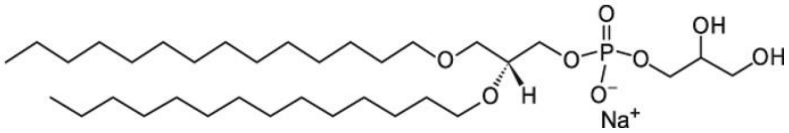

Figure 4.2 Chemical structures of single chain cationic lipid, cetyltrimethylammonium bromide (CTAB), double chain cationic lipid, 1,2-Dioleoyl-3-trimethylammonium-propane (DOTAP), 1,2-di-O-octadecenyl-3-trimethylammonium propane (DOTMA) and anionic lipid 1,2-di-O-tetradecyl-***sn***-glycero-3-phospho-(1'-***rac***-glycerol) (DMPG).

4.1.3.1 Cetyltrimethylammonium bromide

Cetyltrimethylammonium bromide (CTAB) is a single-tailed monocationic surfactant with quaternary amine group (**Figure 4.2**). It has been used as a stabilising agent in nanoparticle preparations [436] due to its miscibility with other amphiphilic molecules. Moreover, the addition of CTAB with other surfactants has been shown to favour the formation of different nanostructures including lamellar, hexagonal and bicontinuous cubic phases [437-442]. This suggests that CTAB can be incorporated into cubosome formulations. However, the addition of cationic lipids into nanoparticle formulations can also lead to cellular toxicity [443-445]. Therefore, it is important to determine an optimum concentration of CTAB that imparts a positive charge to the cubosome surface but does not cause cell toxicity.

4.1.3.2 1,2-Dioleoyl-3-trimethylammonium-propane (DOTAP)

DOTAP (**Figure 4.2**) is a double-tailed cationic lipid which has been commonly used as a cationic additive in nanoparticle formulation to improve cell uptake and gene transfection [446-449]. It has double monounsaturated carbon chains and a monocationic head group. The presence of ester bond makes DOTAP biodegradable. This characteristic was reported to reduce the cell toxicity as compared to single-tailed cationic lipid like CTAB [450, 451]. Interestingly, DOTAP has been shown to improve gene transfection in nude mice regardless of the type of nanoparticle used [452, 453]. These results suggest that the interaction of the nanoparticle with cells was influenced by the positive charge exerted by DOTAP and not the type of nanoparticle.

4.1.3.3 1,2-di-O-octadecenyl-3-trimethylammonium propane (DOTMA)

DOTMA is another double chain cationic lipid commonly used to form lipid-DNA complexes due to the electrostatic interactions between negatively charged DNA and positively charged DOTMA for gene transfection studies with a similar structure to DOTAP (**Figure 4.2)** [454, 455]. DOTMA has a similar structure to DOTAP and the mixtures of DOTMA with neutral phospholipids has been shown to result in the spontaneous formation of multilamellar liposomes upon sonication [456, 457].

DOTAP and DOTMA are selected in this thesis as double chain cationic lipids to formulate cationic cubosomes and compared with CTAB cubosomes for the uptake across BBB. Both DOTAP and DOTMA have quaternary ammonium group and unsaturated double chain hydrophobic domain. However, they have different linkages between the long alkyl chain and trimethyl ammonium headgroup, where two ether bonds are present in DOTMA while two ester bonds in DOTAP [458]. In gene transfection studies, the differences in the linkage plays an important role where ether linkage from DOTMA promotes a higher efficacy in gene transfection [458-460]. The influence of structural differences of these cationic lipids on their uptake by brain endothelial cells will be investigated in this thesis.

4.1.3.4 1,2-di-O-tetradecyl-*sn*-glycero-3-phospho-(1'-*rac*-glycerol) (DMPG)

1,2-di-O-tetradecyl-*sn*-glycero-3-phospho-(1'-*rac*-glycerol) or dimyristoylphosphatidylglycerol (DMPG) is an anionic, double-tailed phospholipid with a negatively charged head group (**Figure 4.2**). DMPG has been added to liposomes to increase the biological activity of *cis*-Bis-neodecanoato-trans-R,R-1,2-diaminocyclohexane platinum (II) (NDDP), a lipophilic cisplatin analogue anti-tumour

agent, to target liver cancer [461]. While cationic lipids have been known to cause cell toxicity, anionic lipids are less toxic [462]. It was hypothesised that the addition of this anionic lipid to the cubosomes will not lead to uptake via adsorptive endocytosis pathway and this will therefore act as a control for the *in vitro* studies. It was hypothesised that any cellular uptake of anionic cubosomess into cells might therefore occur through passive mechanisms or via receptor or carrier mediated pathway [463].

4.1.5 The interaction of phytantriol lipid bilayers with charged lipids

The addition of charged lipids may influence the stability of the phytantriol lipid bilayer in cubosomes. In order to form stable cubosome dispersions, the added charged lipid needs to be miscible with phytantriol [464-466] and is expected to be inserted in between the phytantriol lipid bilayer, due to the nature of the hydrophilic head and hydrophobic tails from the charged lipids as illustrated in **Figure 4.3**. An optimum concentration of charged lipids needs to be added to avoid disruption of the bilayer and causing any structural change or affecting the stability of cubosomes. Possible interactions between charged lipids and the phytantriol bilayer was investigated in this thesis using a lipid monolayer model. These are representative models for studying liposomes as the bilayers are considered an approximate superimposition of two monolayers [467, 468]. The monolayer studies are discussed in more detail below.

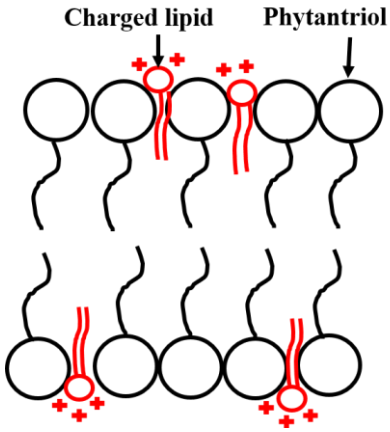

Figure 4.3 Illustration on the insertion of amphiphilic charged lipids into phytantriol bilayer.

4.1.5.1 Langmuir monolayer study

Pure and mixed lipid monolayers can be studied using a Langmuir-Blodgett trough to understand interactions and miscibility within lipid monolayers when charged lipids are introduced into the system. Theoretically, amphiphilic lipid molecules such as phytantriol are expected to accommodate and orientate at the water/air interface and form a stable film which is known as a Langmuir monolayer [469, 470]. The miscibility between phytantriol and charged lipids and their impact on monolayer stability can be examined by Langmuir trough studies. It is important to know the miscibility of charged lipids with phytantriol before formulating them into cubosomes, as these two components have to be miscible in order to form a stable dispersion and allow the charged lipids to express the charge on cubosome surface [471].

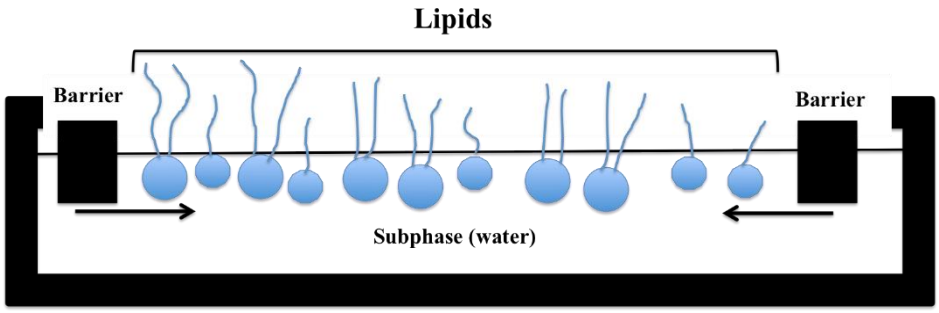

Figure 4.4 Illustration of Langmuir-Blodgett trough showing the lipid was added on the water surface and the barriers are moved (in the direction of the arrows) to slowly compress the monolayer.

In order to examine this, molecular area and surface pressure isotherms are plotted to obtain information on the orientation, dimensional properties and molecular interactions between molecules in single and mixed components monolayers [471]. To construct the isotherm of a single lipid component (e.g. phytantriol) or mixed components (e.g. phytantriol with charged lipids), the lipids (in solvent) are added on the

subphase (water), and the solvent is evaporated. The barriers then slowly compress the monolayer (**Figure 4.4**) and the pressure isotherm is plotted. **Figure 4.5** shows the surface area of the monolayer slowly reducing upon compression which then cause an increase in the surface pressure. As the surface area of the monolayer decreases further, the monolayer changes from gaseous phase (G) and into the liquid phase. The intermolecular interactions between the molecules led to a more ordered orientation of the molecules on the interphase. The proximity and orientation of molecules determines the liquid expanded (LE) and liquid condensed (LC) states. Meanwhile, the plateau region of LC + LE indicates rearrangement of the molecules into a more ordered monolayer as the barriers are compressed. In the solid state (S), the amphiphilic molecules are closely packed, and the hydrophobic tails are arranged in parallel. Further compression leads to the collapse of the monolayer and is shown as a break in the isotherm, as illustrated by red dotted line in **Figure 4.5**. Monolayer packing and molecular orientation can be affected by the presence of unsaturated bonds, polar head groups, steric hindrance and hydrophilic interactions between the molecules [471]. The structural effects of the selected lipid can be explained by the theory of critical packing parameter from **Section 1.4.1**.

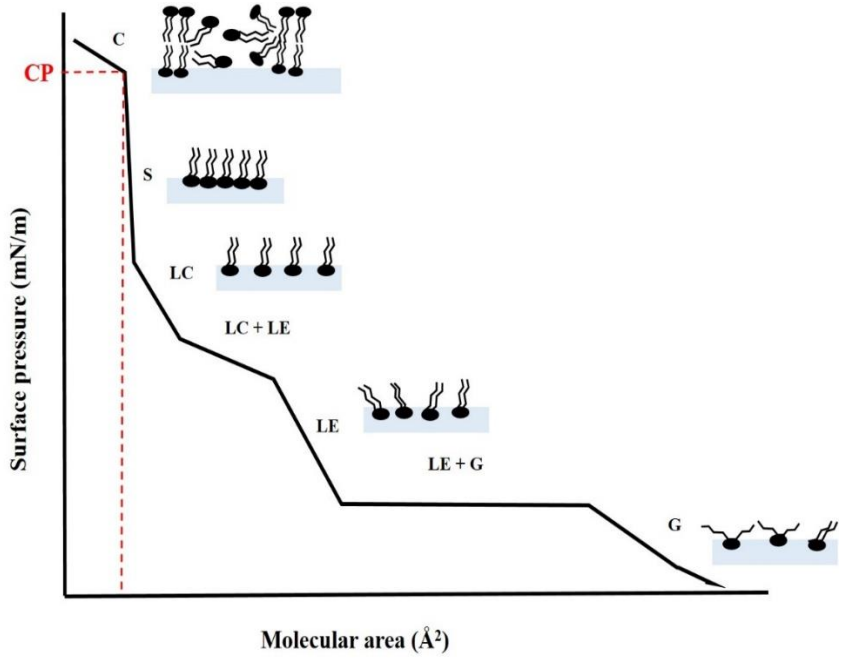

Figure 4.5 Langmuir isotherm that exhibits the different phases adapted by lipids at a monolayer; G: gaseous, LE: liquid extended, LC: liquid condensed and S: solid with schematic drawings of molecular arrangements of the different phases of lipids at interphase. The red dotted line shows the collapse pressure (CP) of the monolayer when the monolayer finally collapsed (Adapted from [471]).

The miscibility of two lipids in a system can be investigated from the isotherm where the collapse pressure in mixed monolayer of two lipids being related to miscibility. The addition of a second lipid into the monolayer can cause a reduction in the collapse pressure, as the mixed monolayer is more compressible than a single lipid monolayer [322]. A mixed monolayer with single collapse pressure is indicative that the two lipids are miscible [472], while two separate collapse points indicate there is lack of interaction between the lipids and that the two components are immiscible. In this case, each of the components will separate from the mixture and result in two collapse points corresponding to their respective individual collapse pressures [473].

Deviations from the limiting molecular areas can be calculated from the isotherms to further evaluate the miscibility of mixed monolayers. A detailed analysis of the

isotherm and the calculation of the limiting molecular areas was presented in the method section (**Section 2.2.4**). The deviation is calculated from the differences in calculated (from the experiment) versus ideal molecular area. A negative deviation indicates a non-ideal behaviour of the mixed monolayer where there are attractive forces between the lipids, indicating the lipids are miscible. Meanwhile, positive deviation in the calculated molecular areas in mixed monolayers shows an ideal behaviour and that the monolayers are immiscible. Repulsive forces usually occur due to interactions between the head groups of the two lipids and can lead to immiscibility [323, 474]. If the lipids are immiscible, they will separate during the preparation and cubosomes with positively charged surface will not be formed.

4.2 Hypothesis and aims

The overarching aim of this chapter is to develop cationic cubosomes to target the adsorptive endocytosis pathway at the BBB, as a potential drug delivery pathway to the brain. Hence, the hypotheses for this chapter are:

Hypothesis 1: That double chain cationic lipid will have a greater impact on the stability of phytantriol monolayer as compared to single chain cationic lipid.

Hypothesis 2: That single and double chain cationic lipids can be added into cubosomes formulation to form positively charged cubosomes.

Hypothesis 3: That the chain length from cationic lipids will affect the toxicity *in vitro*.

Hypothesis 4: That the addition of cationic lipids will lead to increased cellular uptake *in vitro* through the adsorptive endocytosis pathway.

To investigate the above hypotheses, the following experiments were conducted. The:

1) investigation of the stability and miscibility of phytantriol monolayer after the addition of single and double chain charged lipids;
2) investigation of the physicochemical properties of cubosomes after the addition of single and double chain charged lipids;
3) evaluation of the cellular toxicity of cubosomes after the addition of single and double chain charged lipids in hCMEC/D3 cells, in comparison to the free solution of charged lipids; and the
4) evaluation of cellular uptake of cubosomes after the addition of single and double chain charged lipids.

Pluronic F127 was used as a stabiliser in all cubosome formulations at a concentration of 15% w/w (to phytantriol), based on the results in **Chapter 3**. Since this

chapter aimed to study the effect of cationic cubosomes on the interaction with hCMEC/D3 cells, cubosomes stabilised by Pluronic F127 were used because it is not expected to cross the BBB, and the effect of adding cationic lipids can be studied.

4.3 Results and discussion

4.3.1 Effect of adding single and double chain charged lipids on phytantriol monolayer formation.

To predict the effect of adding a cationic lipid to cubosome formulations, the interactions between phytantriol and selected cationic lipids in a monolayer were studied using a Langmuir monolayer trough.

Pure phytantriol had a typical phospholipid isotherm as shown in **Figure 4.6**. Referring to **Figure 4.5** previously, the lipid oriented in an expanded state and showed a transition at about 65 $Å^2$ from the liquid condensed to the solid state before the monolayer collapsed at 42.3 ± 3.6 mN/m. The collapse pressure for pure phytantriol was similar to the published value of 42.4 ± 1.4 mN/m [475]. The addition of DOTAP, CTAB and DMPG at the selected concentration had no significant impact on the stability of phytantriol ($p>0.05$), as observed from the collapse pressures (**Table 4.1**). In contrast, the addition of DOTMA to phytantriol led to a significant reduction ($p<0.05$) in collapse pressure (30.9 ± 0.5 mN/m), which indicates a reduction in stability of phytantriol monolayer.

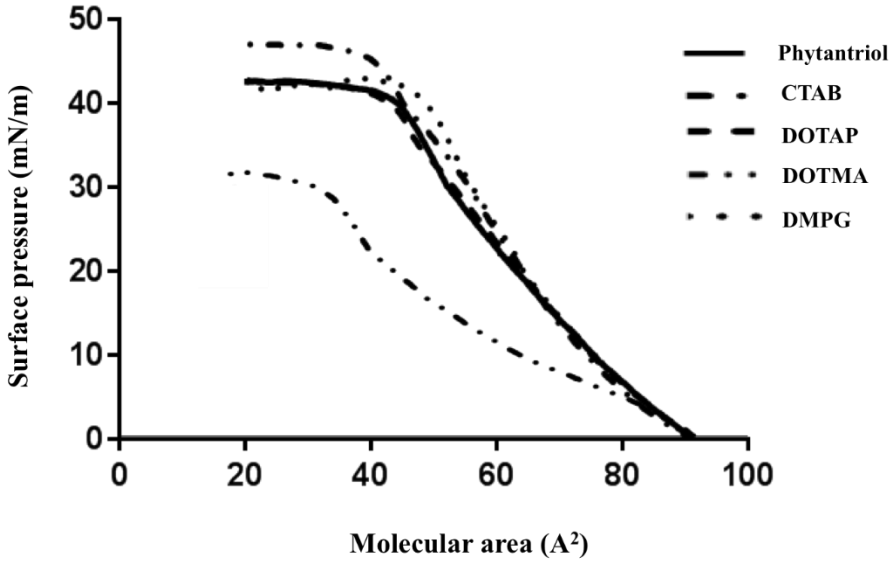

Figure 4.6 π-A isotherm for pure phytantriol and mixed monolayer of phytantriol with CTAB, DOTAP, DOTMA and DMPG from Langmuir monolayer studies. The isotherms are the average of three independent experiments.

Interestingly, as observed from the limiting molecular areas (**Table 4.1**), the addition of DOTMA to phytantriol lead to an experimental area of 52.5 $Å^2$/molecule while phytantriol plus CTAB, DOTAP and DMPG resulted in areas of 58.4, 60.9 and 58.7 $Å^2$/molecule, respectively. DOTMA has a smaller head group as compared to DOTAP and DMPG and was expected to have less of an impact on phytantriol monolayer. However, it is possible that the packing properties of DOTMA were influenced by the small head group and hydrophobic interaction from the long double chain lipids, which led to a densely packed lipid monolayer, a lower molecular area and a less stable monolayer as observed from the reduction in collapse pressure after the addition of DOTMA [476].

Table 4.1 Experimental and calculated ideal limiting molecular area (Å^2) of phytantriol, mixed monolayers of phytantriol and charged lipids at water-air-interface with the deviation from ideality.

Charged lipid (1.4 mol%)	**Experimental limiting molecular area (Å^2/molecule)**	**Ideal limiting molecular area (Å^2/molecule)**	**Deviation from ideality (%)**	**Collapse pressure (mN/m)**
0% (Phytantriol)	61.6 ± 3.9	-	-	42.3 ± 3.6
CTAB	58.4 ± 4.0	61.1	-4.4	46.1 ± 0.35
DOTAP	60.9 ± 0.1	62.7	-2.8	42.3 ± 0.35
DOTMA	52.5 ± 11.8	62.8	-16.4	30.9 ± 0.5
DMPG	58.7 ± 1.2	61.5	-4.6	42.9 ± 1.9

4.3.2 Miscibility of phytantriol mixed monolayers

In order to formulate cubosome dispersion with charged lipids, the lipids must be miscible with phytantriol. Non-miscible components will have two collapse pressures where the lipids have no interaction and are immiscible, hence the components will separate from the monolayer and show two collapse pressures [472, 473]. The miscibility of phytantriol monolayer with CTAB, DOTAP, DOTMA and DMPG can be observed from the presence of a single collapse pressure as illustrated in **Figure 4.6**.

To further evaluate the miscibility of the mixed monolayer, the experimental limiting molecular area was calculated and compared to the ideal limiting molecular area. **Table 4.1** above summarised the limiting molecular areas for the isotherms and the deviation from ideality. Negative deviation indicates miscibility of the components in the mixed monolayers while positive deviation shows that there was lack of interaction between the lipids, and the mixture has low miscibility [477, 478]. At the studied concentration, the addition of all charged lipids resulted in a negative deviation from

ideality which indicates there was interaction between the lipid and lead to miscibility. These results corroborate with the value from the collapse pressure, which confirms the molecular interaction between the charged lipids with phytantriol monolayer leads to the miscibility in the monolayer. The addition of DOTMA again had the largest impact on the deviation from ideality. This further suggests the miscibility of DOTMA with phytantriol monolayer might be from the smaller head group as compared to DOTAP and DMPG.

The Langmuir monolayer study can assist in predicting the bilayer stability in cubosome formation. However, the monolayer study only represents a layer of the lipid, while cubosomes are formed by multiple lipid bilayers [471]. Nevertheless, the Langmuir monolayer studies showed that the addition of charged lipids at 1.4 mol% to phytantriol monolayer had a minimal impact on monolayer stability and that the lipids were miscible, although DOTMA might have a higher interaction with phytantriol lipid layer.

4.3.3 Physicochemical properties of cubosomes with the addition of single and double chain cationic lipids.

Cubosomes formulated with the addition of 1.4 mol% of cationic lipids were prepared and the effects on particle size and homogeneity evaluated (**Table 4.2**). The average size for all formulations was less than 200 nm and all the cubosome formulations were homogenous based on having a PDI value of less than 0.3. As expected, the addition of cationic lipids, CTAB, DOTAP and DOTMA led to highly positively charged particles with ζ-potential of 45.2 to 45.7 mV. The addition of the anionic lipid, DMPG increased the negative charge to -31.0 ± 0.2 mV, as compared to the control, which was Pluronic F127 stabilised cubosomes without any cationic lipids) from **Section 3.4.1.3** (**Table 3.5**), which had a charge of –28.6 ± 0.3 mV.

Table 4.2 Particle size (Z-average) and polydispersity index (PDI) for cubosomes stabilised with 15% w/w Pluronic F127 ± lipids. Data presented are the mean ± standard deviation of three independent experiments.

Charged lipid	**Average particle size (nm)**	**PDI**	**ζ-potential (mV)**	**Internal structure**	**Lattice parameter (Å)**
Control	177.5 ± 5.4	0.18 ± 0.01	-28.6 ± 0.3	*Pn3m*	69
CTAB	176.7 ± 2.4	0.242 ± 0.292	46.2 ± 0.2	*Pn3m*	71
DOTAP	201.8 ± 1.1	0.174 ± 0.014	45.7 ± 0.8	*Pn3m*	71
DOTMA	158.1 ± 3.6	0.090 ± 0.026	45.5 ± 2.9	*Pn3m*	74
DMPG	193.5 ± 2.1	0.248 ± 0.002	-31.0 ± 0.2	*Pn3m*	74

To confirm the internal structure of the charged cubosome dispersions, diffraction patterns were obtained and are summarised in **Figure 4.7** and **Table 4.2.** When 1.4 mol% of CTAB, DOTAP, DOTMA or DMPG was added, the internal structure of cubosomes was recorded to be *Pn3m* cubic with lattice parameter between 70.5 to 74.1 Å. The increase in the lattice parameter (swelling) after the addition of charged lipids was consistent with previous studies [435, 479]. The formation of *Pn3m* cubic phase was confirmed by the presence of three Bragg peaks with spacing ratio of √2: √3: √4 as observed in **Figure 4.7.** These results show that the addition of single and double chain charged lipids at studied concentration (1.4 mol%) is sufficient to induce a positive surface charge on particles, thereby facilitating adsorptive endocytosis, without disrupting the internal structure of the cubosomes.

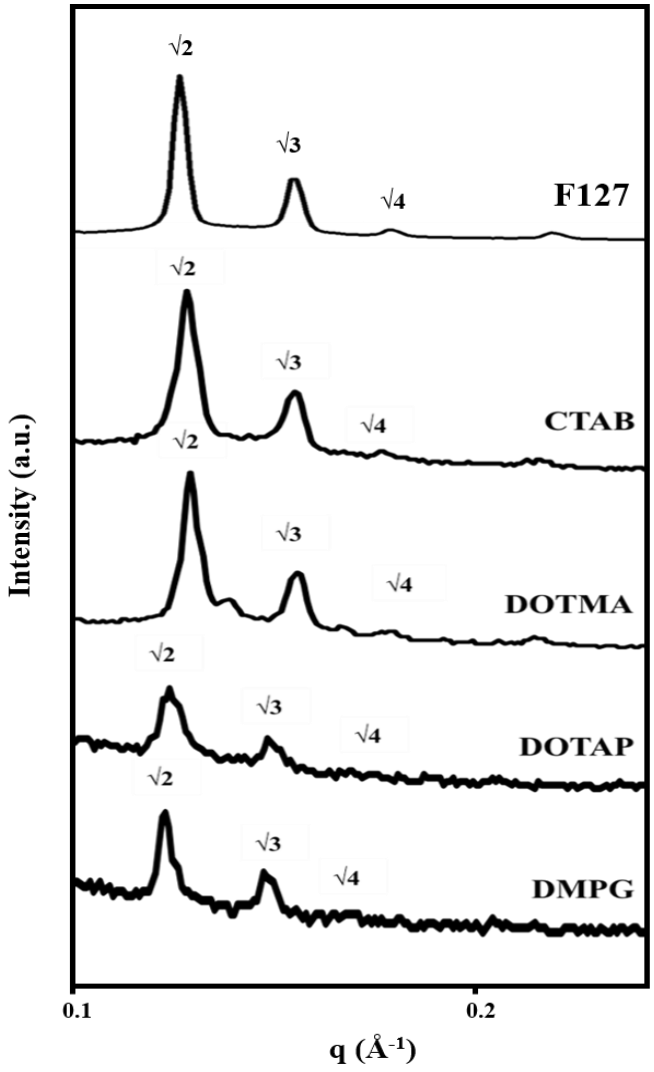

Figure 4.7 SAXS diffraction (intensity versus q plots) of phytantriol cubosome dispersions stabilised by 15% w/w Pluronic F127 without any additives (F127) and with the addition of CTAB, DOTAP, DOTMA and DMPG at 1.4 mol %. The Bragg peaks at √2: √3: √4 confirm the formation of *Pn3m* cubic structure.

Electron microscopy was carried out (**Figure 4.8**) to confirm the homogeneity and to visualise the nanostructure of cubosome particles. Under electron microscopy, a heterogeneous distribution of particles was observed in the CTAB, DOTAP and DOTMA cubosome formulations. The image from DMPG cubosomes is not available due to the failure in freezing the samples for cryo-TEM observation. Adding DOTAP and DOTMA produced a number of vesicles (arrow) with some of the cubosomes having vesicular

coats surrounding the cubosomes (arrowhead). The formation of vesicles is commonly reported for cubosomes stabilised with Pluronic F127 [245, 382, 407]. These vesicles are believed to be the precursors for cubosomes that eventually transform into cubosomes [245, 480, 481].

The presence of vesicles was not observed under SAXS analysis (**Figure 4.7**) because the signal for vesicles are usually weak as compared to the signals from cubosomes. Hence, in the dispersion that contains a mixture of cubosomes and vesicles, the scattering signals for the vesicles are being masked and did not appear as an individual peak [482, 483]. However, direct observation under electron microscopy can illustrate the presence of vesicles in the dispersion. Vesicles formation in DOTAP and DOTMA cubosomes can be explained from their molecular structure. The presence of unsaturated double chain led to a decrease in the lipid curvature hence spontaneously transforming the phytantriol lipid bilayer into lamellar phase [238, 484, 485]. DOTAP has a larger headgroup compared to DOTMA and this leads to further decrease in the curvature. The molecular structure of DOTAP leads to the presence of a larger number of vesicles in the dispersion as compared to DOTMA cubosomes [486].

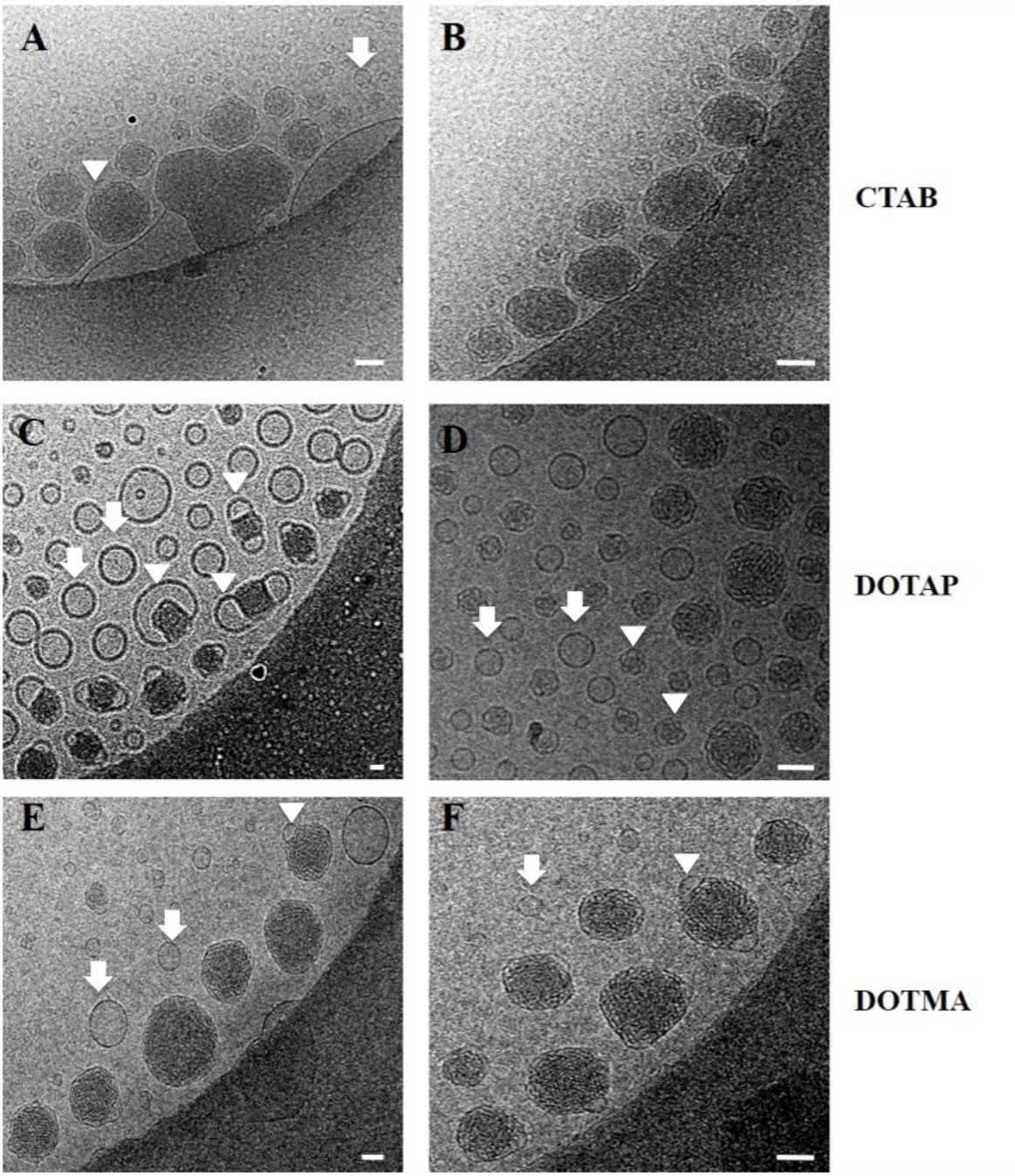

Figure 4.8 Cryo-TEM micrographs of cubosomes dispersions stabilised with phytantriol and added with CTAB (Panel A-B), DOTAP (Panel C-D) and DOTMA (Panel E-F). The arrows indicate the vesicles formation while the arrowhead showing the vesicular coats surrounding cubosomes. Scale bar: 100 nm.

DOTAP and DOTMA cubosomes were further analysed by cryo-ET. The tomogram in **Figure 4.9** (Panel A) illustrates the vesicles (Panel a") observed in DOTAP cubosomes dispersion as having "onion" like layers under Fast Fourier Transform (FFT) analysis (Panel iii). These vesicles are most likely liposome like structures with the lipid bilayer forming the outer vesicle layer [395]. The "budding" off structures surrounding cubosomes were also apparent under cryo-ET. This might indicate the process of cubosome formation in the dispersion [487-489]. Meanwhile, FFT analysis of the DOTAP (Panel i and ii) and DOTMA (Panel iv and v) cubosomes show cubic packing and hexagonal symmetry depending on the axis of rotation. DOTMA cubosomes (Panel B) also showed cubosomes with vesicles surrounding the particles.

Overall, even though the dispersion was observed to be heterogeneous, it can be concluded that adding 1.4 mol% of charged lipids to Pluronic F127 stabilised cubosomes did not change the internal structure of Pluronic F127 stabilised cubosomes but was able to change the surface charge. This observation allows the use of the formulation at studied concentration, for further *in vitro* and *in vivo* studies.

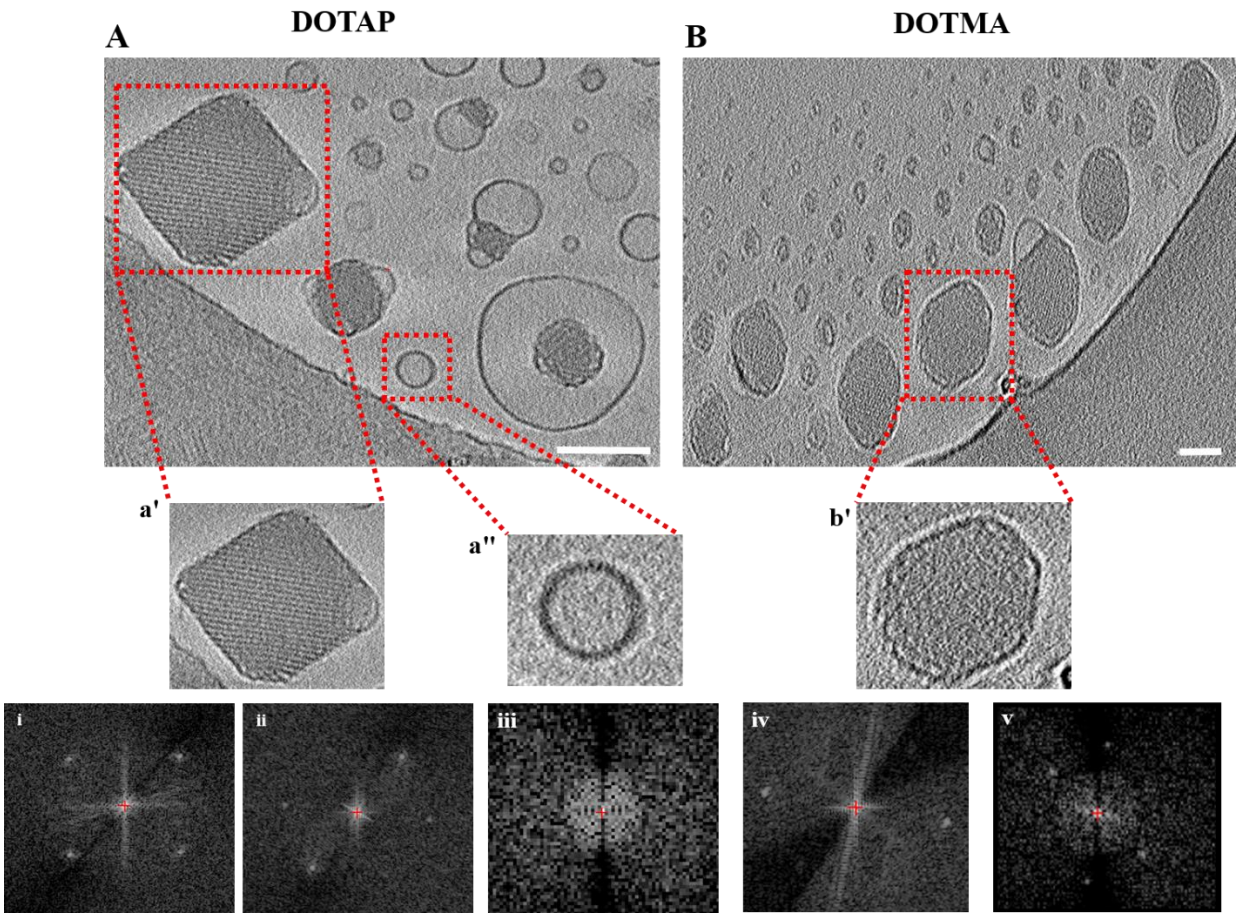

Figure 4.9 Cryo-electron tomograms showing field of cubosomes embedded in vitrified buffer suspension. Cubosomes were added with 1.4 mol% (A) DOTAP and (B) DOTMA. Panel a', a" and b' show the enlarged view of representative cubosomes from the tomogram with their Fast Fourier Transform in (Panel i-v). Arrows indicate the "budding off" structure observed outside the cubosomes. Scale bar: 100 nm.

4.3.4 Toxicity of charged cubosomes in hCMEC/D3 cells.

As cationic lipids are associated with cell toxicity, it is important to determine whether the addition of cationic lipids in cubosomes results in cellular uptake due to adsorptive-mediated endocytosis, and not from passive diffusion across the cell as a result of local cell toxicity [490, 491]. Therefore, cubosome toxicity was studied with flow cytometery where cells were incubated with cationic cubosomes and their respective cationic lipids in a suspension (no cubosomes) at different concentrations (**Figure 4.10**). The suspensions were included in the study to investigate whether the toxicity of charged lipids was different in suspensions versus within cubosome formulations.

Cell toxicity was evaluated after two hours of incubation with the formulations and the percentage of live cells was measured. There was no concentration dependent toxicity observed in all formulations studied with cell viability being approximately 98 to 99% in cells treated with cubosomes containing charged lipids. The low toxicity recorded might be due to the low concentration of charged lipids added into cubosomes formulation (1.4 mol%) where in gene transfection study, the amount of charged lipids added are 2 to 3 times higher [492, 493].

Interestingly, from **Figure 4.10**, it was observed that the cell viability significantly decreased to about 96 to 97% ($p<0.05$) when the charged lipids are in suspension form (dotted line, closed symbols) as compared to cubosome formulations (solid line, open symbols). Even though the difference between charged lipids in suspension and within cubosome formulation is less than 2%, it is possible that the toxicity of charged lipids was being masked by cubosome formation. This could suggest that the charged lipids were inserted in between the phytantriol lipid bilayer in cubosome particles. This insertion has been proposed for liposomes co-formulated with cationic lipids where the lipids were inserted in between the lipid bilayers [494-496] in which the

presence of hydrophobic chain within the molecule assists the insertion of charged lipids into the lipid bilayer [497].

In addition, there was no impact on cell viability relating to the type of lipid added (single versus double chain cationic lipids). Overall, this viability study suggests that, at the concentration of charged lipids used in this thesis, toxicity is less than 5% therefore any change in cell uptake following cubosome modification will most likely be from the cellular interaction of cubosomes with the cell membrane, and not from the cellular toxicity. Moreover, this also showed that the addition of cationic lipids at studied concentration is not toxic to the cells.

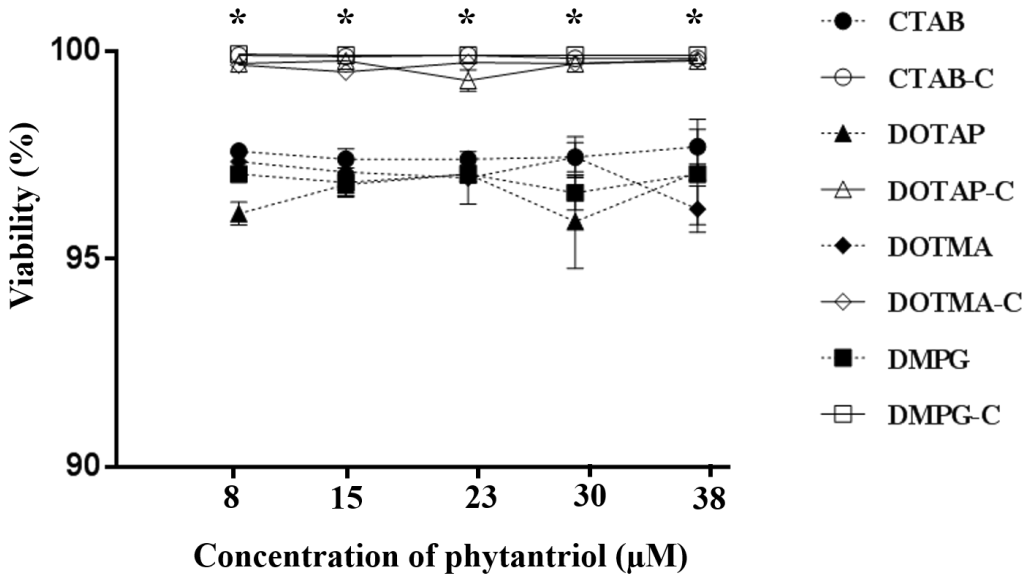

Figure 4.10 Viability (%) of hCMEC/D3 cells after two hours incubation with increasing concentration of cubosomes stabilised with 15% w/w Pluronic F127 and containing 1.4 mol% of CTAB (CTAB-C), DOTAP (DOTAP-C), DOTMA (DOTMA-C) and DMPG (DMPG-C). Toxicity of all the charged lipids (in suspensions, dotted line) were studied at concentrations corresponding to those present in their respective cubosome dispersions and compared against toxicity from Pluronic F127 stabilised cubosomes containing 1.4 mol% of charged lipids (solid line). Data presented are mean ± standard deviation of three independent experiments. The difference in viability is statistically significant (*$p<0.05$) for all formulations at all concentrations.

4.3.5 Uptake of cationic cubosomes by hCMEC/D3 cells

The addition of cationic lipids into cubosome formulation was shown to produce positively charged cubosomes. To test the hypothesis that cellular uptake of cubosomes is influenced by the positive surface charge, DMPG (anionic lipid) cubosomes which are negatively charged were used as a negative control. Meanwhile, the uptake of Pluronic F127 stabilised cubosomes (no additive) was used as a control to evaluate the absence of charged lipids in the cubosomes on cell uptake. All cubosomes were fluorescently labelled with NBD (as in **Chapter 3**) for the detection by flow cytometry. Uptake of all formulations was compared to the uptake of Pluronic F127 stabilised cubosomes.

There was a significant increase in the observed uptake of cationic cubosomes containing DOTAP and DOTMA ($p<0.05$) as compared to DMPG and Pluronic F127 stabilised cubosomes (**Figure 4.11**). There was a trend of dose dependent uptake in DOTAP and DOTMA cubosomes. Cubosomes with single chain cationic lipid, CTAB had no significant increase in uptake at all concentrations. At the concentration of 38 μM (of phytantriol), the uptake of DOTAP and DOTMA cubosomes were about 17 times higher than CTAB, DMPG and Pluronic F127 stabilised cubosomes (without additives).

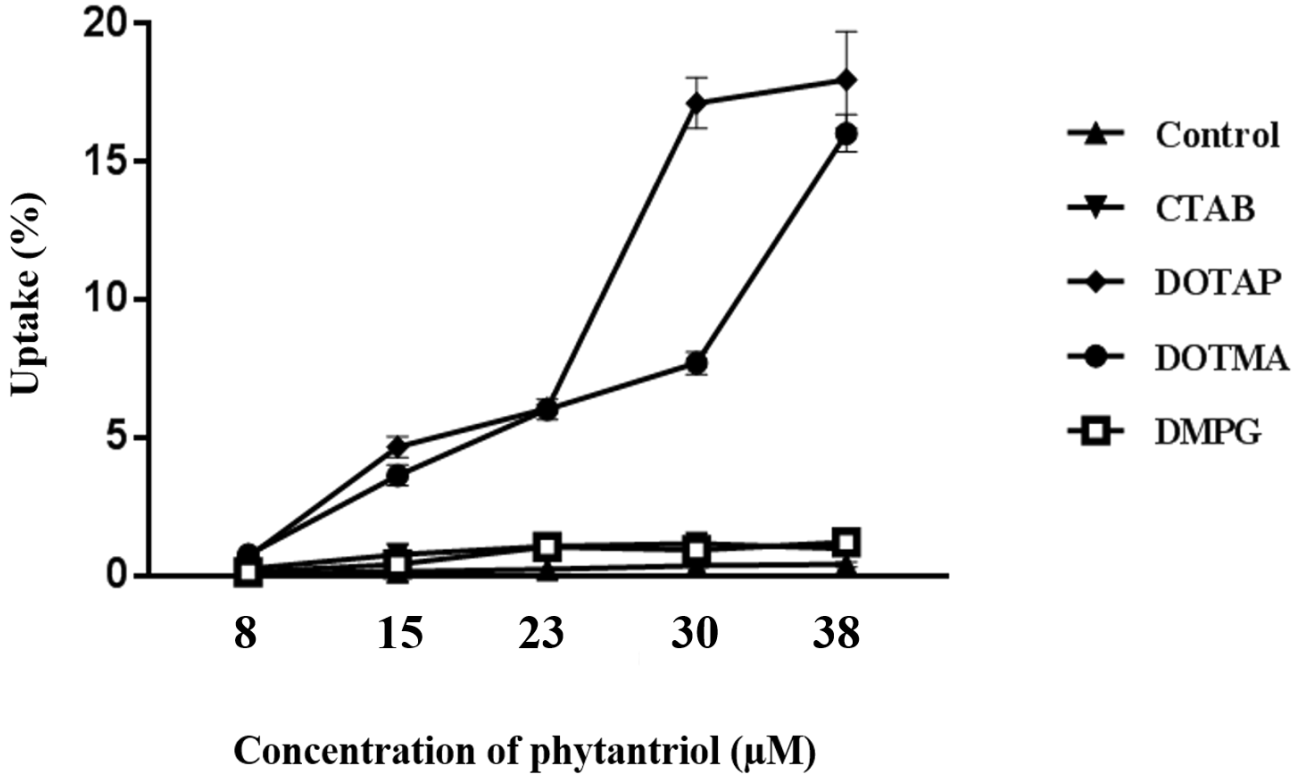

Figure 4.11 Uptake (%) by hCMEC/D3 cells after two hour incubation with Pluronic F127 stabilised cubosomes without additive (control), CTAB cubosomes (CTAB), DOTAP cubosomes (DOTAP), DOTMA cubosomes (DOTMA) and DMPG cubosomes (DMPG). All the cubosomes were stabilised with 15% w/w Pluronic F127 and fluorescently labelled with NBD fluorescence tag. Data presented are mean ± standard deviation of three independent experiments. *P<0.05 compared to the uptake of control.

In order to visually observe the uptake of cationic cubosomes, the uptake studies were repeated with hCMEC/D3 cells and 38 µM (of phytantriol) of cubosomes, with analysis via fluorescence microscopy (**Figure 4.12**). The cubosomes were labelled with NBD and cell membrane with CellMask®. Increased NBD fluorescence was observed in cells cultured with DOTAP cubosomes, followed by DOTMA cubosomes. Lower uptake was observed in CTAB and DMPG cubosomes treated cells. However, it was uncertain that the fluorescence molecules were inside the cells or adhered on the surface of the cell membrane. While confocal microscopy technique can be a solution for this issue, NBD molecule is subjected to bleaching effect from the laser exposure from the confocal imaging. The bleaching effect on NBD can affect the intensity of the signal and might lead to insufficient fluorescence detection.

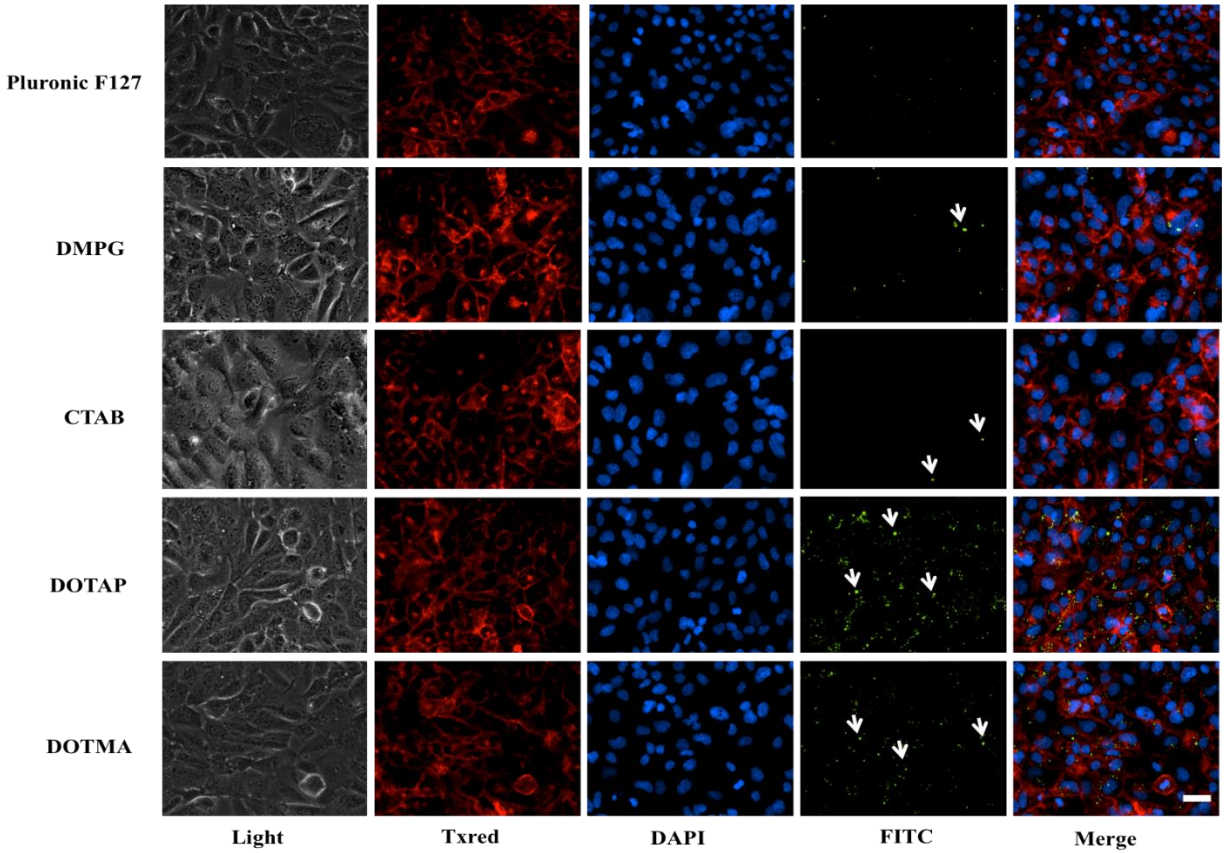

Figure 4.12 Micrograph showing uptake of NBD tagged cubosomes stabilised with 15% w/w Pluronic F127 +/- CTAB, DOTAP, DOTMA and DMPG at 1.4 mol%. Cells were incubated with 38 μM of cubosomes for two hours. Cell membrane was stained by CellMask® (Txred), nucleus was stained by Hoercht 33258 (DAPI-blue) and NBD positive was observed under FITC channel. Positive uptake was observed from the presence of green fluorescence spots showed by the white arrows. Scale bar: 10 μm.

The uptake of cationic cubosomes is likely to be through adsorptive endocytosis pathway, where uptake should be inhibited by lowering the temperature (energy dependent uptake) or pre-coating the cell membrane with positively charged molecule in order to prevent the electrostatic interaction between the cationic cubosomes and the anionic cell membrane.

Cells were therefore incubated with cubosomes at 37 °C and 4 °C for two hours. **Figure 4.13** shows that there was a reduction in uptake for cubosomes in all groups at 4 °C. The reduction in uptake was about 2-fold for DOTAP and DOTMA cubosomes at 4 °C. The inhibition at 4 °C is associated with the reduction in energy dependent endocytosis thus decreasing the uptake through non-specific adsorptive endocytosis pathway [498-501]. However, at the same time, other transport pathways at the endothelial cells also utilise the ATP and the uptake will be inhibited at low temperature. For example, carrier mediated endocytosis such as glucose transporter at the BBB requires energy to function and transport glucose into the brain [118, 502]. The uptake recorded at 4 °C was not completely inhibited. There is a chance that the cubosomes were associated and adsorbed on the cell membrane (without internalisation) and detected by flow cytometer as positive uptake. Therefore, to further test whether uptake of charged cubosomes was from adsorptive endocytosis pathway, cells were pre-incubated with positively charged poly-L-lysine for 60 minutes to neutralise some of the positive charge on the cell membrane.

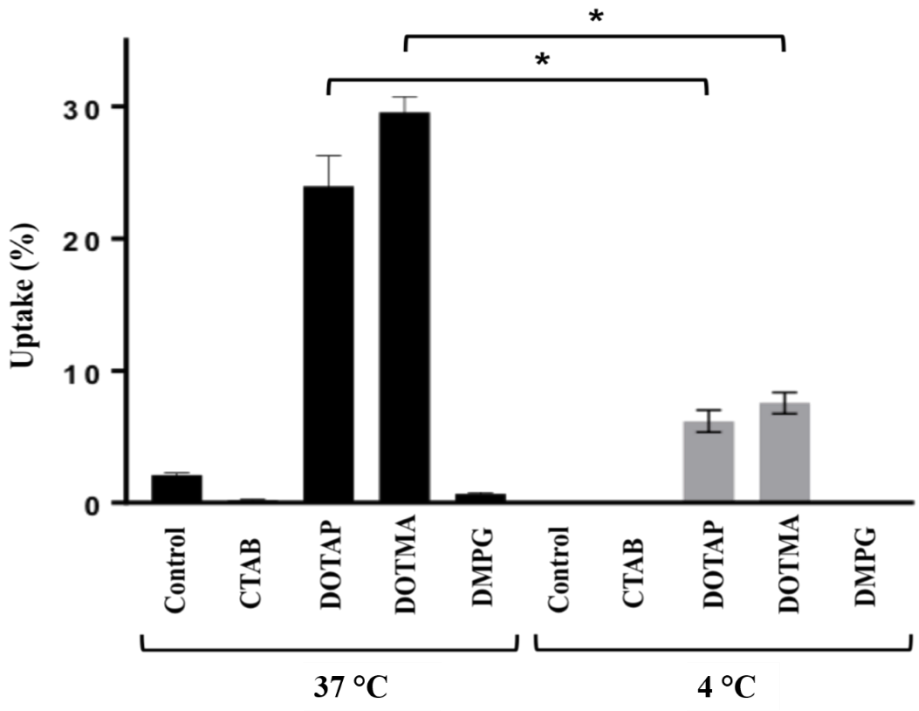

Figure 4.13 Uptake (%) by hCMEC/D3 cells after two hours incubation with cubosomes (38 μM of phytantriol) stabilised with 15% w/w Pluronic F127 +/- CTAB, DOTAP, DOTMA and DMPG at two different temperatures (37 °C and 4 °C). Data presented are mean ± standard deviation of three independent experiments. *P<0.001 compared to incubation at 37 °C.

Following pre-incubation with positively charged poly-L-lysine, cells were incubated with cubosomes for two hours before uptake was analysed by flow cytometry (**Figure 4.14**). Uptake was significantly reduced when the cells were pre-treated with poly-L-lysine ($p<0.05$ for DOTAP and DOTMA) with an approximate 3-fold reduction in uptake for cells treated with DOTAP and DOTMA cubosomes. The aim of pre-incubation with positively charged poly-L-lysine was that through electrostatic interactions it would coat the negatively charged surface on the cell membrane. The coating would neutralise some of the negative charge on the cell membrane, hence reducing cubosomes uptake through adsorptive endocytosis pathway. This data supports the hypothesis that the uptake of cubosomes, modified through the addition of the double chain cationic lipids, DOTAP and DOTMA, was through adsorptive endocytosis.

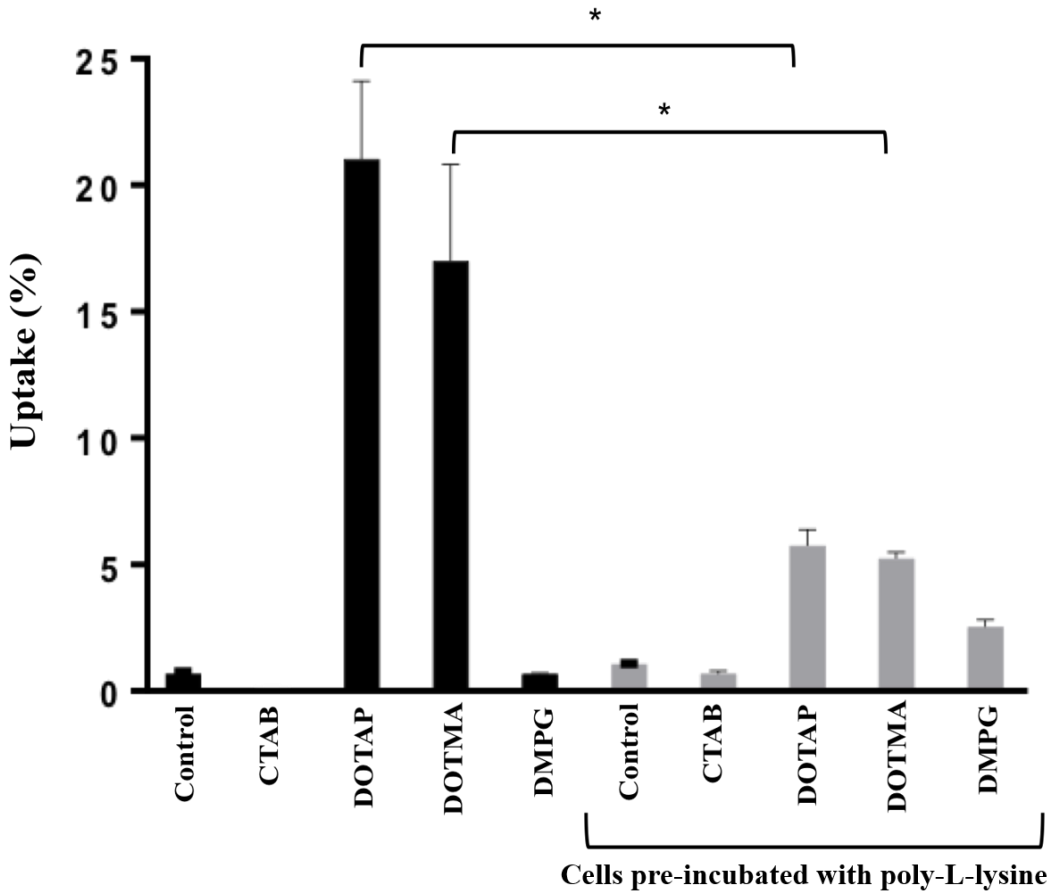

Figure 4.14 Uptake (%) by hCMEC/D3 cells after two hours incubation with cubosomes stabilised with 15% w/w Pluronic F127 without additives (control) and with the addition of charged lipids. The concentration selected for each cubosome dispersion was 38 µM of phytantriol. The uptake was compared to cells pre-incubated with 931 nM poly-L-lysine. Data presented are mean ± standard deviation of three independents experiments. *P<0.001 compared to incubation without poly-L-lysine.

The significantly high cellular uptake of DOTAP and DOTMA cubosomes can be explained by the effect of; cubosomes charge, chain length and hydrophobicity of charged lipids. Firstly, the cationic charge exerted by the addition of the cationic lipids DOTAP and DOTMA likely promotes electrostatic interactions with the cell membrane as supported by the poly-L-lysine studies. This non-specific interaction promotes endocytosis of cubosomes into the cell through the adsorptive endocytosis pathway. This is in agreement with published studies reporting that adding cationic lipids into liposomal formulation increases gene transfection in the cells [503-505]. Similarly, the use of cell penetrating peptide and cationic lipids were shown to promote the uptake into the cell through adsorptive endocytosis pathway [506, 507].

Even though the charges for DOTAP, DOTMA and CTAB cubosomes are between 45 to 46 mV, the difference in surface charge might be too small to show any significant effect in the uptake. Meanwhile, for cubosomes modified with DMPG, there was a lack of uptake observed. The negative charge (-31 mV) on the surface of DMPG cubosomes suggests that there will be repulsion with the negatively charged cell membrane.

However, among the cationic cubosomes, DOTAP and DOTMA cubosomes showed significantly higher uptake than the CTAB cubosomes (about 15 times higher). This suggests that chain length and the chemical structure of the cationic lipids might play a significant role in the uptake process. The presence of (1) hydrocarbon chains adjacent to the head group, (2) hydrocarbon chains connected to the backbone by the ether bonds and (3) two oleyl chains that acts as the hydrophobic anchor, were reported to increase the efficacy of gene transfection by DOTAP and DOTMA liposomes [458]. In addition, the long and double hydrocarbon chains from DOTAP and DOTMA increase the hydrophobicity of the particles and contributes to higher uptake, due to the lipidic

nature of the cell membrane [508]. This favour the partitioning of DOTAP and DOTMA cubosomes, from the presence of double chain hydrophobic tails compared to single chain in CTAB. Alternatively, CTAB as a highly water-soluble molecule might partition out of the cubosomes and interact with the cell membrane and neutralise the effect on the surface, which then reduce the cationic character of the cubosomes, which further impact the chance of uptake into the cell.

In addition, the difference in the linkage bonds between DOTMA and DOTAP was proposed to affect the uptake efficiency into the cell [458]. The two ester bonds in DOTAP exhibited a 10 times higher gene transfection *in vitro* compared to DOTMA with two ether bonds as the linkage [203, 460, 509]. However, in this chapter, the differences in the uptake between DOTAP and DOTMA was not significant at any of the concentrations studied. Thus, the overall observation from this *in vitro* uptake study is the increase uptake of cationic cubosomes was affected by the chain length of the double chain cationic lipids that affects the hydrophobicity, which promotes interaction with the cell membrane.

4.4 Conclusion

In order to target the adsorptive endocytosis pathway, positively charged cubosomes were formulated by adding single or double chain cationic lipids into Pluronic F127 stabilised cubosomes. The addition of charged lipids should not interfere with the stability of the phytantriol lipid layer and the lipid mixture should be miscible. Langmuir monolayer studies have shown that the addition of CTAB, DOTAP and DMPG did not affect the stability of the phytantriol monolayer while DOTMA reduced the collapse pressure by 30% ($p<0.05$). The reduction in collapse pressure reflects the change in limiting area per molecule observed after adding DOTMA. The hydrophobic interaction between the long double chains from DOTMA with phytantriol lipid layer might lead to a formation of dense mixed monolayer, which makes the phytantriol monolayer less stable after DOTMA addition [476]. CTAB, DOTAP, DOTMA and DMPG lipids were shown to be miscible with phytantriol, as observed from the negative deviation in the limiting molecular area and the single collapse pressure in each mixed monolayer.

Cationic cubosomes were successfully formulated at a concentration of 1.4 mol% of CTAB, DOTAP and DOTMA with Pluronic F127 stabilised cubosomes. All the formulations formed cubosomes with *Pn3m* internal structure and a lattice parameter around 70 to 74 Å. The addition of charged lipids at this concentration did not change the internal structure of Pluronic F127 stabilised cubosomes. This might suggest that the charged lipids had a minimal impact on the stability of phytantriol bilayer in cubosomes formulation.

Pluronic F127 stabilised cubosomes, modified through the addition of 1.4 mol% of charged lipids had low toxicity to hCMEC/D3 cells. It appears that by incorporating the cationic lipids into the cubosome formulation, the cytotoxicity effect of the cationic lipids is masked to some degree. The increased uptake of cubosomes containing DOTAP

and DOTMA was not associated with cellular toxicity and was likely due to adsorptive endocytosis uptake through electrostatic interaction between the cationic cubosomes and the anionic cell membrane. It was shown that the uptake was energy dependent and that it could be inhibited through partial neutralisation of the cell membrane (with cationic poly-L-lysine), supporting the hypothesis that uptake was via adsorptive endocytosis. The lack of increased uptake of cationic cubosomes containing the single chain lipid CTAB might be due to the presence of a different linker as compared to DOTAP and DOTMA and length of the hydrocarbon chain [468, 510]. It can be concluded that the positive uptake observed in hCMEC/D3 cells, is influenced by the positive surface charge of cubosomes, the linker group and the chain length of the cationic lipids. In **Chapter 5**, further uptake studies will be conducted using an *in vivo* model to understand and evaluate the potential of using cationic cubosomes to target the BBB.

Chapter 5

In vivo brain uptake of cubosomes in a zebrafish model

5 *In vivo* brain uptake of cubosomes in a zebrafish model

5.1 Introduction

Cubosomes with BBB targeting moieties Tween 80 and Poloxamer 188 were prepared and characterised in **Chapter 3** and **Chapter 4** to target receptor-mediated endocytosis, while cationic lipids were incorporated into cubosomes to target adsorptive endocytosis. In **Chapter 3**, *in vitro* studies with hCMEC/D3 cells suggested that the addition of Tween 80 and Poloxamer 188 into cubosome formulations do not lead to significant uptake by human brain endothelial cells. In contrast, positively charged cubosomes formed through the addition of double chain cationic lipids (DOTAP and DOTMA) lead to significant cellular uptake via adsorptive endocytosis. Given *in vitro* studies do not represent the *in vivo* environment, due to the static nature of the cell culture and lack of plasma proteins, which in the case of Tween 80 is essential for receptor-mediated endocytosis, an investigation using a suitable *in vivo* BBB model is needed.

Various *in vivo* models have been used to predict the uptake of nanoparticles into the brain. The mouse model is the most commonly used BBB model due to similarities in the transporters, receptors and cell properties to the human BBB [511]. Unfortunately, mouse models can be costly and labour intensive, therefore hindering high throughput screening in uptake studies. The zebrafish model was therefore chosen as a BBB model and is discussed in more detail below.

5.1.1 Zebrafish as an *in vivo* model in drug development

Zebrafish (*Danio rerio*) originate from Southeast Asia and have been widely utilised in various fields of study, especially in molecular genetics and developmental biology [512, 513]. Zebrafish have been reported to be 200 to 1000 times cheaper than mammalian models and the cost can be as low as 1% of that of rodents [514, 515].

Zebrafish offer several advantages as an animal model over the mouse model. It has been reported that 70% of their genes are similar to those in human and they can therefore be a suitable *in vivo* model for certain genetic or developmental studies [516]. The advantages of zebrafish model over the mouse model in drug development studies are summarised in **Table 5.1**. Zebrafish are a small size vertebrate and only occupy a small space for living. The husbandry of zebrafish is simple and a single medium size fish tank can accommodate about 50 to 60 adult zebrafish. The larvae and embryo only require as low as 50 µL of liquid to survive [517]. In contrast, fewer than 10 mice can live together in a medium sized cage. Zebrafish have a fast reproduction rate with approximately 10 days breeding cycle and a fish produces from 50 to 300 eggs at a time, while a single mouse produces around 10 pups in a single breeding. Zebrafish will take about 24 hours after fertilisation to develop into larvae, while the gestation period for mice is about 21 days [517, 518]

The large number of offspring and shorter gestation period significantly reduces maintenance cost and offers options for high throughput screening of high cost molecules [518-521]. Furthermore, since the larvae are about 3 to 8 mm length, this allows experiment to be conducted in 96 well plates using the adapted cell culture-based method [516, 522-525].

Table 5.1 Key differences between the zebrafish model and mouse model [517, 526, 527].

Zebrafish	**Mouse**
Vertebrate	Mammal
Small space to live (60 fish per medium tank)	Large space needed (<10 mice per medium cage)
Low cost	High cost
Breeding cycle every 10 days, 50 to 300 eggs at a time	Breeds 3 times throughout life, ≤ 10 pups every pregnancy
External fertilisation	Placental viviparity
Transparent larvae	Not transparent
No prostate, mammary glands or lungs	Have similar organs to human

Zebrafish eggs are fertilised externally and the embryos survive and grow outside the parent's body. Meanwhile, the reproductive mode for mice is placental viviparity, where the pups grow inside the mother until birth. In zebrafish, manipulations can be conducted during the gestational period by treating the embryo and development can be observed through the transparent skin [517, 518]. The transparent skin allows live imaging to be conducted without the need to sacrifice or dissect the animal [528].

In zebrafish, organogenesis begins as early as 24 h.p.f (hours post fertilisation) with the organs being fully developed at about 5 d.p.f. (days post fertilisation) [524]. Zebrafish also matures quickly but has a longer life span than mice and therefore can be used to study aging [514]. The stages of zebrafish life are summarised in **Table 5.2**.

Table 5.2 Stages of zebrafish life from fertilisation until death [529].

Age	**Stage**
0 to 72 h.p.f	Pre-hatching (embryo)
72 to 120 h.p.f	Post-hatching
1 to 29 d.p.f	Larvae Start swimming at 5 d.p.f
30 to 89 d.p.f	Juvenile
90 d.p.f to 2 years	Adult Sexually active after 90 to 120 d.p.f
> 2 years	Aged fish (to study aging)
4 to 5 year old	Death

In the first few hours after fertilisation, the embryo can be injected with DNA or RNA to genetically modify the embryo, so it will develop into a specific adult transgenic line. In addition, disease models can be induced in the early hours of fertilisation and since the embryo is transparent, the changes in the organ development can be observed under a microscope [530, 531]. A number of transgenic lines used for drug discovery studies have been developed, for example the *Tg(fli1a:EGFP)* fish which expresses green fluorescent protein in all endothelial cells [520, 532]. Another transgenic line, *Tg(flk:nsmcherry)* is similar but the endothelial cells have red fluorescence instead.

It must be acknowledged that zebrafish are an incomplete mammalian model as they do not have organs such as lungs, skin, prostate and mammary glands [517]. Nonetheless, zebrafish are cost-effective and versatile model in various field. It is widely studied in toxicological studies that requires high throughput screening. The similarity of organs in zebrafish and human allow different toxicological studies to be conducted to screen a large number of toxic compounds. A detailed discussion on neurotoxic compounds and toxicological studies in zebrafish was conducted and reviewed [533] and will not be discussed here.

Zebrafish is a highly useful and ethical model that can bridge the gap between *in vitro* and higher animal studies as illustrated in **Figure 5.1** below [523]. Using this model allows adherence to the 3R principles (replacement, reduction and refinement) in ethical research. As a non-vertebrate model, zebrafish is an attractive alternative to the mammalian model as it is a less sentient species (replacement) [516]. By only using larvae, we can avoid the use of adult zebrafish without sacrificing reliability (reduction). The study also reduces animal distress by minimising the procedures involved (refinement). In addition, the live-imaging technique allows non-invasive quantification step and lesser sample processing [534].

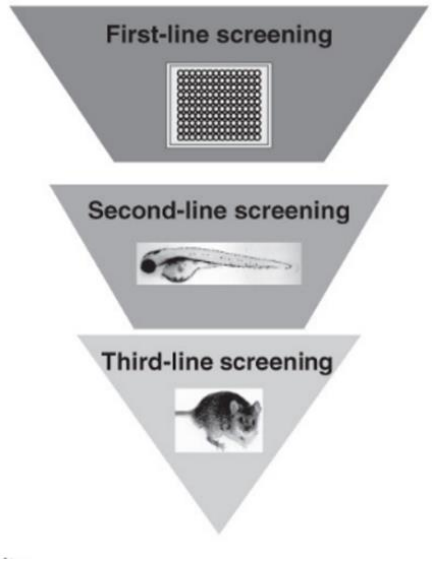

Figure 5.1 Zebrafish model as a bridge between cell culture method (first-line screening) and higher vertebrate animal model (third-line screening) (Adapted from [523] with permission).

5.1.2 Zebrafish as a model for the BBB

Zebrafish have been widely used and this model is used to study the uptake of cubosomes across the BBB as the central nervous system and brain development between zebrafish and mammals are similar [535].

In order to use zebrafish as the BBB model for the uptake of cubosomes into the brain, the zebrafish brain needs to express similar receptors, transporters and neurotransmitter to that of the mammal brain [514]. **Table 5.3** outlines in detail the development of the CNS in zebrafish. After fertilisation, the brain starts to develop at 3 d.p.f signified by the formation of transporters and TJs. ATP binding cassette (ABC) transporters are also found in the brain and they have been shown to behave in a similar fashion to those in the mammalian brain [536, 537]. Claudin-5 and ZO-1 have also been detected at the zebrafish brain at 3 d.p.f. [530, 538, 539].

Table 5.3 Zebrafish brain development at different stages of life.

Age	Development	References
6 h.p.f	Formation of neural plate	**537, 540**
10 h.p.f	End of gastrulation Formation of neural tube followed by spinal cord	
24 h.p.f	Formation of olfactory nerve, primary neurons, forebrain, hindbrain and midbrain	**541, 542**
28 h.p.f	Major vessels and angiogenesis are fully developed	**517**
48 h.p.f	Brain ventricles and optic nerve	**543-545**
2 to 3 d.p.f	Neurons secreting neurotransmitter and tight junctions formed	**533, 538, 539**
4 d.p.f	Oligocytes, astrocytes, Schwann cells and glial cells	**544, 546**
6 d.p.f	Development of complex circulatory system	**512**
8 d.p.f	Efflux transporter fully functional	**537, 547**
10 d.p.f	BBB fully functional and formed Tight junction fully formed and function similarly to human Complete development of feet process of pericytes and astrocytes	**520, 538, 548**

Even though the BBB starts to develop at 3 d.p.f, it is only at 10 d.p.f that the BBB is fully developed and functional [538, 548], thus any nanoparticle uptake studies (into the brain) should be carried out after 10 d.p.f. However, some studies have started earlier at 5 to 6 d.p.f. In one of these studies, doxorubicin and paclitaxel encapsulated in exosomes were shown to enter the brain region of the zebrafish based on the observation of fluorescence signal inside the zebrafish brain [549]. In another study, transferrin conjugated carbon dots were observed to be able to cross the BBB and enter the zebrafish brain after intravenous injection. The appearance of fluorescently-labelled carbon dots in the central canal suggests the potential use of transferrin conjugated nanoparticles to target the receptor-mediated pathway at the BBB [550]. As these studies were carried out in

larvae below the age where the BBB is thought to be fully developed [538, 548, 551], there is an uncertainty to whether the positive uptake was due to the nanoparticle design or the BBB not being fully developed, hence leaky to nanoparticles.

To date, larvae after 10 d.p.f have not been used to study nanoparticle transport across the BBB. This might be due to the fact that larvae develop pigmentation as they age. At 12 to 14 d.p.f, significant pigmentation appears on the skin reducing optical transparency, therefore preventing direct imaging of the brain. However, for brain uptake studied use of larvae younger than 10 d.p.f which do not have a fully developed BBB will most likely lead to unreliable results due to the leakiness at the BBB. Hence, this thesis uses larvae of 10 to 12 d.p.f to study the uptake and toxicity of cubosomes. Since the BBB has been reported to be fully developed at 10 d.p.f [520, 538, 548], it can be concluded that any cubosomes uptake reported in this thesis is likely due to endocytosis, and not from the BBB being leaky. To circumvent the interference in imaging cause by the pigmentation on the skin, the larvae are oriented laterally, where the midbrain area can be clearly observed and imaged (see **Figure 5.3** under **Section 5.3.3**).

5.1.3 Observing the uptake of cubosomes using confocal microscopy

Real-time live imaging of the uptake of nanoparticles into the brain has been a challenge with animal models such as mice, due to their size and anatomy. Positron emission tomography, magnetic resonance imaging and computer tomography have been used to image the whole brain [552, 553]. However, the resolution from these techniques is insufficient to provide detailed information on individual cells and nanoparticles. While fluorescence, confocal and two-photon microscopy can offer higher resolution [554], the depth of penetration is limited to a sample thickness of less than 1 mm [555]. While this limits the option to image the whole brain of rodents, it can be used on zebrafish larvae because of their small size and thickness.

Confocal microscopy is used in this thesis to view the uptake of cubosomes in the zebrafish brain, as it offers several significant advantages over fluorescence microscopy. Firstly, zebrafish larvae have a thickness of about 0.5 to 1.0 mm, so imaging with a fluorescence microscope can produce high background noises due to signals being collected above and below the plane of focus [556, 557]. The depth of illumination is also limited thus reducing the image quality [558]. Even though the area of interest can be focused to increase the contrast, non-specific background fluorescence reduces the quality of the image which may cause inaccurate interpretations of nanoparticle uptake [559, 560]. The pinhole in the confocal microscope focuses light onto the sample and removes background interference and out of focus glow (**Figure 5.2**). The captured images have a higher resolution with less artefacts caused by light scattering. In addition, confocal imaging allows optical sectioning of the sample along the z-axis. The images can be captured at different depths through the sample and collectively translated into a 3D structure. This provides information on the uptake of nanoparticles at different depths of the brain [561-565]. However, samples imaged using both fluorescence and confocal imaging

can suffer from photo bleaching [566-569]. It is important to minimise the exposure time and avoid excessive bleaching that can lead to data misinterpretation.

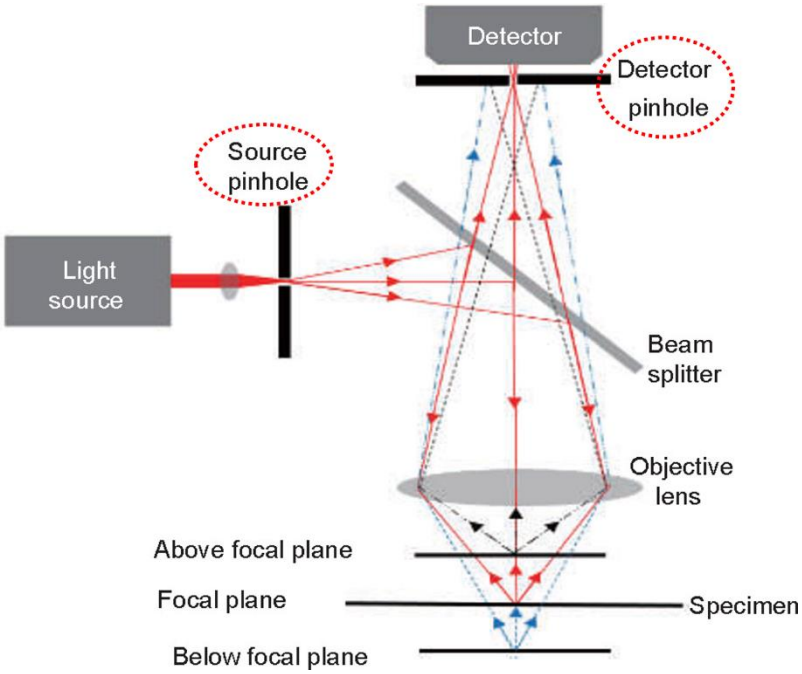

Figure 5.2 Schematic diagram of a confocal microscopy showing the location of the pinhole; at the light source and the detector (circled in red). The detector pinhole allows the light source from the focal plane to be detected while blocking the light from above and below the plane. (Reproduced with permission from [570]).

5.2 Hypothesis and aims

The overall objective of this chapter is to investigate the uptake and toxicity of surface modified cubosomes using zebrafish. The hypotheses tested were, that:

Hypothesis 1: cubosomes stabilised with Tween 80 and Poloxamer 188 have increased uptake into the zebrafish midbrain due to the interaction with ApoE (see **Section 3.1.2**)

Hypothesis 2: gold-labelled cubosomes can be used to investigate the localisation of cubosomes in the brain.

Hypothesis 3: cubosomes containing double chain cationic lipids, DOTAP and DOTMA will have a higher uptake into the zebrafish midbrain compared to cubosomes with single chain cationic lipid based on cell uptake studies in **Section 4.3.5**.

Hypothesis 4: the uptake of cubosomes into the midbrain is not driven by their toxicity at the BBB.

To explore the hypotheses above, the following aims were investigated:

1) The uptake of cubosomes stabilised with Tween 80 and Poloxamer 188 into the zebrafish brain.

2) The distribution of gold-labelled cubosomes in the zebrafish brain at the ultrastructural level.

3) The uptake of cubosomes surface decorated with single chain (CTAB) and double chain (DOTAP and DOTMA) cationic lipids into the zebrafish brain.

4) The toxicity of cubosomes at the zebrafish midbrain.

5.3 Materials and methods

5.3.1 Materials

Octanethiol functionalized 3 nm gold nanoparticles was purchased from Nanoprobes (New York, USA). 1,2-dipalmitoyl-*sn*-glycero-3-phosphoethanolamine-N-(lissamine rhodamine B sulfonyl) was purchased from Avanti Polar Lipids. Inc (Alabama, USA). Milli-Q water (ion exchanged, distilled and purified by Millipore, Bedford, MA) was used in all experiments.

5.3.2 Preparation and characterisation of modified cubosomes tagged with lipid dye and gold nanoparticles

Tween 80, Poloxamer 188, Pluronic F127 and cationic cubosomes were prepared as described in **Section 2.2.1.1** and 0.01% w/w of lissamine rhodamine PE (LR) or 89.3 nM octanethiol functionalized 3 nm gold nanoparticles were added to the chloroform before the evaporation step. Particle size and polydispersity index were measured as described in **Section 2.2.1.1** and SAXS analysis was conducted as outlined in **Section 2.2.1.2**.

5.3.3 Zebrafish husbandry and experimental procedure

Adult zebrafish were kept in a flow-through system with UV-treated water and maintained at 24 to 30 °C, pH 7.0 to 8.0 and conductivity of 200 to 1000 $\mu S^{1.}$ Adult fish were mated by leaving a breeding pair in the dark, overnight. Zebrafish usually lay their eggs in the first two hours after the lights are switched on the next morning. The embryos were collected and kept in an E3 solution (0.17 mM KCl, 5 mM NaCl, 0.33 mM MgSO4, 0.33 mM CaCl2, and 0.1% Methylene Blue) in a petri dish at 28 °C. Larvae were fed

with dry food ZM-000 (Zebrafish Management Ltd (ZM), UK) and rotifer (plankton) starting on 5 d.p.f. All experiments were carried out at 10 to 12 d.p.f.

Zebrafish larvae were anaesthetised with 0.2 mg/mL tricaine (ethyl 3-aminobenzoate methanesulfonate, Sigma-Aldrich) and mounted laterally on a depression slide with 10 mg/mL warmed agar solution (Sigma-Aldrich). Control solutions or modified cubosomes (labelled with LR or gold nanoparticles) were injected intravenously (5 nL) using a microinjection gauge into the common cardinal vein with the aid of a dissecting stereomicroscope (Leica, Switzerland).

The zebrafish brain consists of three different regions; forebrain, midbrain and hindbrain [571]. Since the studies were conducted on 10 to 12 d.p.f larvae, the midbrain region is selected to observe and quantify cubosomes uptake as it represents the largest region of the brain in the zebrafish. The location of the midbrain also facilitates clear imaging without interference from skin pigmentation that starts to develop from day 8 to 9 d.p.f [572, 573].

Three different transgenic zebrafish lines were used in order to study the toxicity of cubosomes towards the BBB and their uptake into the brain and neurons. The *Tg(fli1a:EGFP)* transgenic line was selected to study brain uptake as it expresses the green fluorescence protein in the endothelial cells. **Figure 5.3** shows the expression of green fluorescence protein under fluorescence microscopy, where the lining of the blood vessels (endothelial cells) are green. The area of interest, the midbrain, where uptake of cubosomes was quantifies is outlined by the white dotted line.

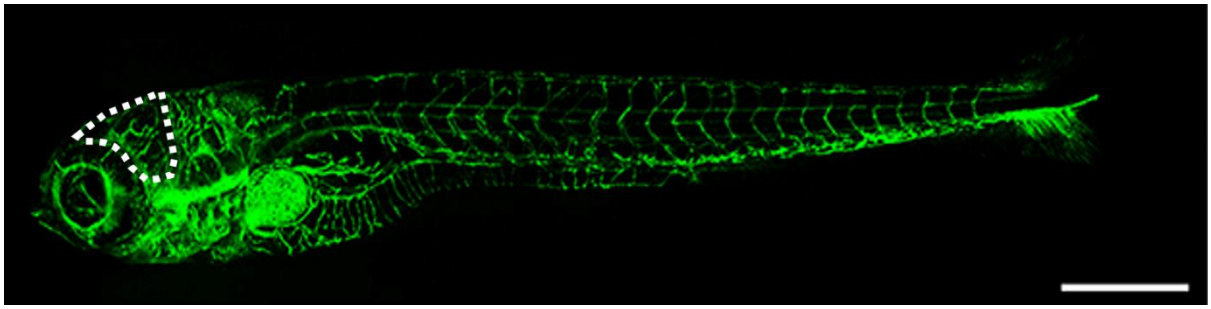

Figure 5.3 The transgenic zebrafish line, *Tg(fli1a:EGFP)* with blood vessels which fluoresce in green under fluorescence microscope. The dotted white line illustrates the midbrain region. Scale bar: 500 µm [532].

The *Tg(sox10:EGFP)* transgenic line was chosen because the neurons in this line express the green fluorescence protein. In this line, the accumulation of LR-labelled cubosomes (which fluoresce in red) in the green fluorescing neurons can be observed. This was used to investigate whether cubosomes which enter the brain are taken up by neurons.

Finally, to evaluate any toxic effects of cubosomes in the midbrain, zebrafish were exposed to acridine orange dye (which has a green fluorescence) which is used as the apoptotic cell marker. Therefore the *Tg(flk:nsmcherry)* zebrafish line which expresses the mcherry fluorescence protein (fluorescence in red) along the blood vessels was used [131, 574].

5.3.4 Live imaging of cubosome uptake using confocal microscope

To observe the uptake of cubosomes in the midbrain of the zebrafish, *Tg(fli1a:EGFP)* and *Tg(sox10:EGFP)* larvae were anaesthetised with 0.2 mg/mL of tricaine and mounted laterally on a depression slide using 1.5 % warmed agar solution. The larvae were injected with 5 nL of cubosome formulations and observed under the confocal microscope.

Following the injection of cubosomes, the midbrain was observed, and confocal images were captured using a Nikon C2 Si confocal microscope (Nikon Corp., Japan). Only single time point imaging was undertaken to avoid bleaching effect on the fluorescence label (LR). After 120 min post injection, 20 stacks of z-series were collected (thickness: 2 µm each) without any image saturation. To avoid image saturation, an image acquisition software (Nikon Corp., Japan) was used (while setting up the acquisition parameters) to monitor the intensity values [575-577]. To observe the green fluorescence, FITC filter (ex 488/em 509 nm) was used and for LR, Texas red filter (ex 545/em 572 nm) was used. To analyse the uptake of LR-labelled cubosomes into the midbrain, each z-stack was analysed individually using ImageJ software (National Institutes of Health, NIH). The midbrain area was selected, and a threshold was applied to identify the fluorescent blood vessels in the brain. Thresholding is a method which divides the image into two classes of pixels so that the blood vessels or neurons (fluoresce in green) and LR which fluoresce in red can be differentiated. This differentiation allows the quantification of fluorescence intensity from LR which are located outside the blood vessel, which indicates the uptake of uptake into the brain.

In *Tg(fli1a:EGFP)* larvae, the fluorescence was quantified using the "integrated density" measurement, where it measures the total sum of the pixel values for all 20 z-stacks in the midbrain area [578-580]. The fluorescence intensity in the brain of zebrafish that were administered with LR-labelled cubosomes was compared to that of zebrafish administered LR formulated as suspension (no cubosome control). The experiments were conducted on a total of at least 15 zebrafish larvae in each experimental group on separate days, and the images were analysed. The cubosome formulations were freshly prepared on the day of injection.

5.3.5 Toxicity analysis

To determine whether the administration of cubosomes was causing any toxicity in the midbrain of the zebrafish larvae, acridine orange staining was carried out. *Tg(flk1:mcherry)* zebrafish larvae were anaesthetised with 0.2 mg/mL tricaine, mounted laterally and injected with 5 nL of cubosome dispersions, DMSO (80%) as positive control or saline as the negative control. Immediately following this, 5 nL of 1 mg/mL acridine orange solution was injected intravenously into the larvae and after a period of two hours, the midbrain area was imaged using a Nikon C2 Si confocal microscope (Nikon Corp., Japan). The images were qualitatively analysed using ImageJ software to detect the presence of fluorescent acridine orange.

5.3.6 Uptake of gold-labelled cubosomes

For uptake studies with gold-labelled cubosomes, only Tween 80 cubosomes was studied as this formulation showed uptake into the brain without any associated toxicity. Day 10 larvae were anaesthetised with 0.2 mg/mL tricaine and fixed in agar. The larvae were then injected intravenously with 5 nL of 15% w/w Tween 80 stabilised cubosomes labelled with gold nanoparticle, gold nanoparticle suspension or 15% Tween 80 stabilised cubosomes. Two hours after injection, the agar was broken open using a scalpel and the larvae were transferred into a 5 mL tube for fixation.

Microwave processing has been reported to improve the diffusion of fixative chemicals into larvae and improve ultrastructural observation under TEM [50, 581]. A Pelco BioWave Pro Laboratory microwave oven fitted with a ColdSpot heating reduction system (Ted Pella Inc, Redding, California, USA) was used to maintain the temperature at 23 °C throughout the processing. The processing steps were adapted from [582] with

slight modification. The first two cycles involved fixing the larvae with 2.5% EM grade glutaraldehyde (Sigma-Aldrich, New Zealand) in 0.1 M cacodylate buffer (Sigma-Aldrich, New Zealand) and microwave heating at 100 W under vacuum (2 psi) at a cycle of two min on-off-on. Then the larvae were then rinsed with 0.1 M cacodylate buffer for 10 min followed by microwave heating at 250 W without vacuum for 40 sec. After that, the vacuum was switched on and larvae were fixed with 1% osmium tetroxide (Sigma-Aldrich, New Zealand) buffered with 0.1 M cacodylate buffer and microwaved for two min on-off-on cycle at 100 W. This step was repeated twice without changing the solution. The larvae were then rinsed with double-distilled water in the fume hood for 10 min and were microwaved for 40 sec at 250 W to remove the osmium solution. Next, 2% uranyl acetate (Sigma-Aldrich, New Zealand) in double-distilled water was added and again the larvae were microwaved for one min on-off-on cycle at 150 W for tertiary fixation. The samples were then rinsed for 10 min followed by microwave for 40 sec at 250 W with double-distilled water. The samples were then enhanced using enbloc staining technique with 2% uranyl acetate in 50% ethanol (to enhance TEM images contrast) and then microwave heated at 150 W with vacuum in a two min on-off-on-off cycle. The larvae were then dehydrated by using increasing ethanol concentrations from 50 to 100% and microwaved for 40 sec at 250 W without vacuum. The larvae were infiltrated with epoxy resin in four steps described below, with three min of microwave heating at 250 W and vacuum after each step:

Step 1: 1 part resin : 2 parts 100% ethanol

Step 2: 2 parts resin : 1 part 100% ethanol

Step 3: 100% resin

Step 4: 100% resin

5.3.7 Sectioning

The resin block was remounted and ultra-thin sections (80 nm sections) were obtained using a Reichert-Jung Ultracut E ultramicrotome (C. Reichert AG, Vienna, Austria). The sections were fixed on Formvar carbon coated 100 mesh copper grids and viewed under TEM, Philips CM100 BioTWIN with LaB6 emitter (Philips/FEI Corporation, Eindhoven, Holland). Images of the brain ultrastructure at the midbrain region were captured using MegaView lll digital camera (Olympus Soft Imaging Solutions GmbH, Münster, Germany).

5.3.8 Energy dispersive X-ray spectroscopy (EDS)

The presence of gold particles in the midbrain was confirmed by X-ray analysis using a JOEL 2300F EDS (Joel Ltd, Tokyo, Japan). Grids with the brain section were mounted and area with dense gold nanoparticles was analysed and compared to the reference spectrum in order to confirm the presence of gold.

5.3.9 Statistical analysis

The results are expressed as the mean ± standard deviation (SD). One-way analysis of variance (ANOVA) with Tukey's multiple comparison's test using Prism 6 (GraphPad Software Inc., USA) was applied. Statistical significance was determined when $p<0.05$.

5.4 Results and discussion

5.4.1 Uptake of Tween 80 and Poloxamer 188 stabilised cubosomes in the zebrafish brain.

Zebrafish larvae were injected intravenously with Tween 80 or Poloxamer 188 stabilised cubosomes, fluorescently-labelled with lissamine rhodamine (LR) to investigate the potential of these two stabilisers to target cubosomes to the BBB. The uptake of cubosomes (formulation described in **Chapter 3**) in the midbrain was analysed by quantifying the fluorescence of LR presented as integrated density (g/cm), two hours post injection. **Figure 5.4** summarises the uptake of different cubosome formulations and a LR suspension as the control. The presence of red fluorescent signal in the midbrain region outside the blood vessels, suggests that the LR-labelled cubosomes crossed the BBB and entered the brain parenchyma (**Figure 5.5**).

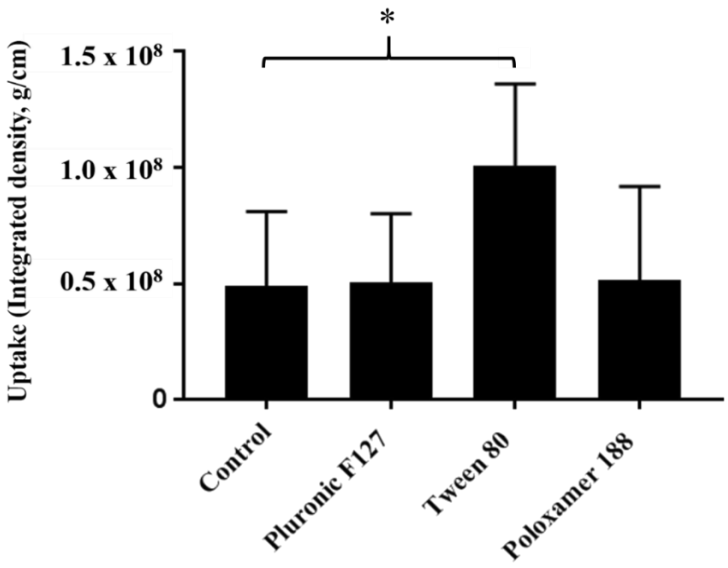

Figure 5.4 Uptake of LR in the midbrain from LR-labelled cubosomes expressed as integrated density (g/cm) and compared against control (LR suspension). Data presented are the mean ± standard deviation of uptake of LR in 10 to 20 larvae per group. *P<0.05 compared to control.

A two-fold increase in the fluorescence was detected in the midbrain of zebrafish injected with Tween 80 cubosomes ($p<0.05$) compared to thecontrol and other groups (**Figure 5.4**). Zebrafish injected with Poloxamer 188 or Pluronic F127 cubosomes showed no significant increase in the uptake as compared to control (LR suspension). **Figure 5.5** further illustrates the uptake of cubosomes in the midbrain region. A strong fluorescence signal was observed in the midbrain region of larvae injected with Tween 80 cubosomes, while lack of signal observed in the other treatment groups.

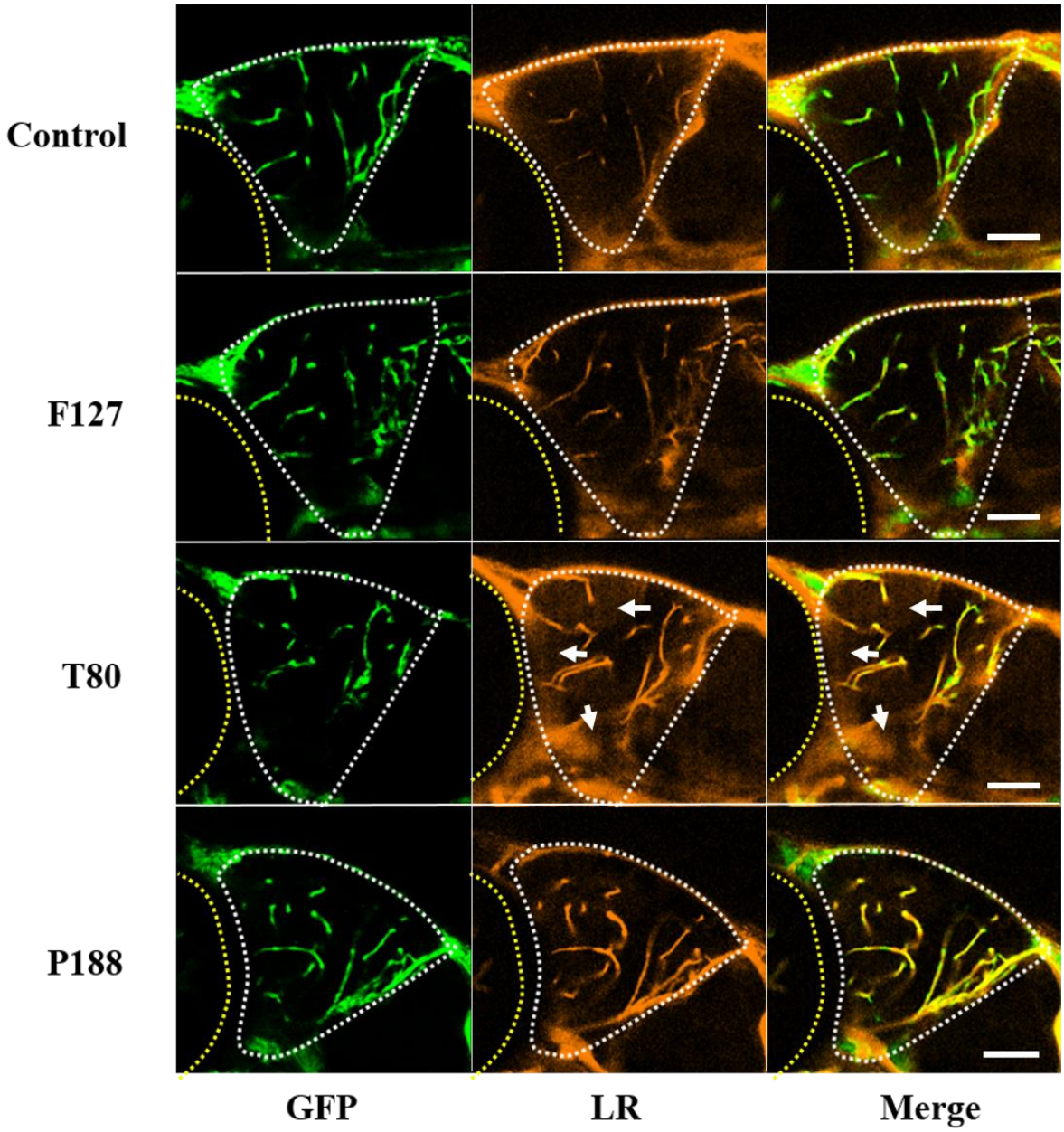

Figure 5.5 Representative confocal micrographs of *Tg(fli1a:EGFP)* larvae 120 min after injection with Pluronic F127 (F127), Tween 80 (T80) and Poloxamer 188 (P188) cubosomes fluorescently labelled with LR. The yellow dotted line outlines the eye region while the white dotted line indicates the midbrain region. LR fluorescence in the midbrain is highlighted within the white dotted areas and indicated by the arrows. The GFP panels show green fluorescence from the blood vessels in the midbrain while the LR panels show fluorescence from LR while the merge panels show the area of LR fluorescence outside the blood vessel (arrows). The uptake of LR is compared against the uptake of control (LR suspension). Scale bar: 50 µm.

To observe whether the cubosomes accumulated in the neurons, the above study was replicated in *Tg(sox10:EGFP)* larvae, where the neurons fluoresce in green (**Figure 5.6).** No LR accumulation in the neurons was detected for any of the cubosome formulations studied. Even though the brain uptake of Tween 80 cubosomes was statistically significant in the previous study, lack of fluorescence was observed inside the neurons, suggests that their uptake into the brain is not specifically localised to neurons. Similarly, in zebrafish injected with Poloxamer 188 and Pluronic F127 cubosomes, lack of LR fluorescence in the neurons was observed. PBCA nanoparticles surface coated with Tween 80 were used to deliver β-galactosidase into the brain and were found to be localised in the neurons. The uptake of this protein (540 kDa) was proposed to be via LDL-receptors present at the BBB and neurons [583]. As **Figure 5.6** shows, poor signal associated with LR is detected in the neurons when Tween 80 cubosomes are used. To overcome this problem, the microscope can be adjusted to induce higher fluorescence intensity by increasing the intensity of the laser on the larvae. However, this can cause bleaching of the fluorescence molecules, leadings to misinterpretation of data [584].

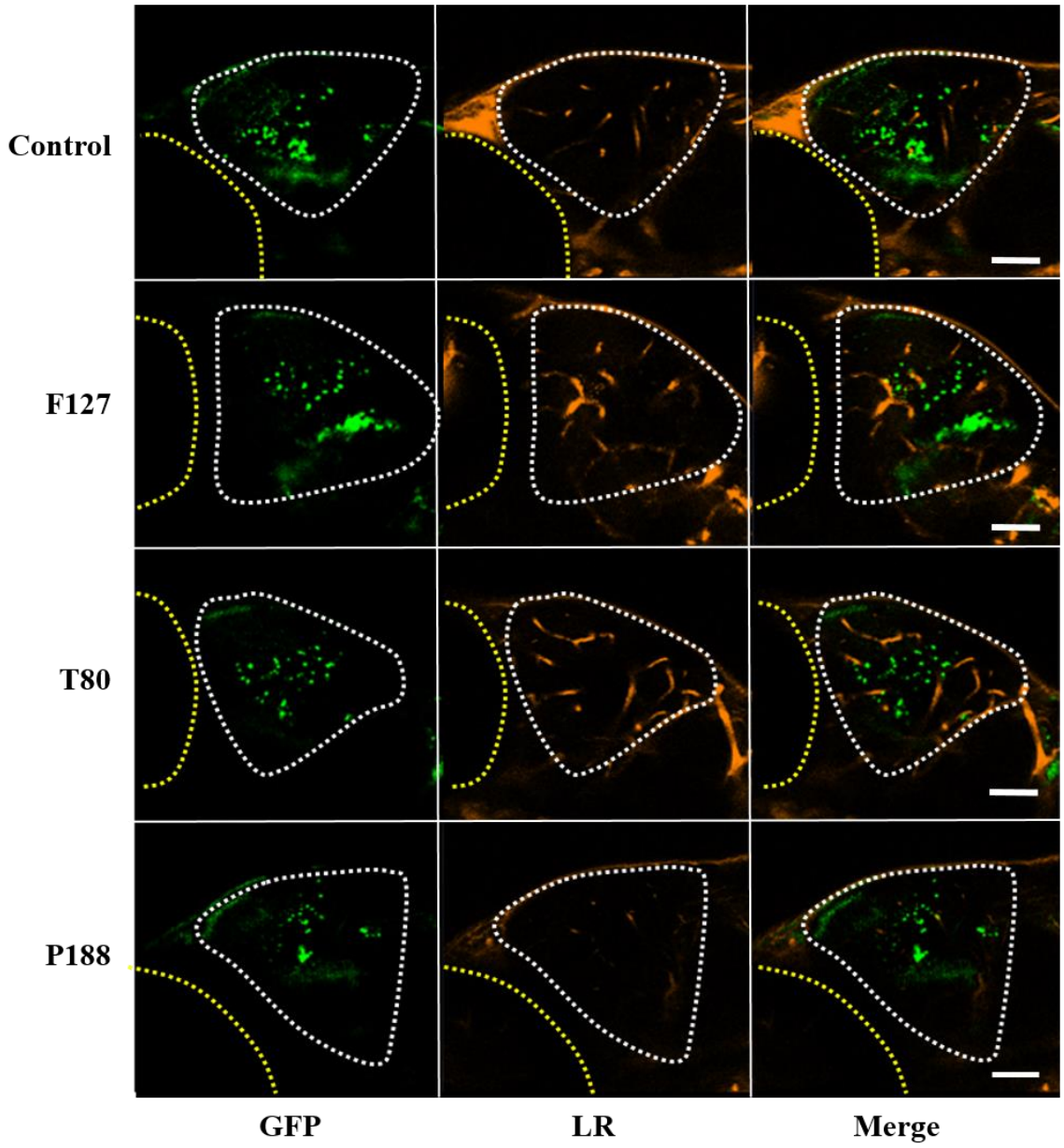

Figure 5.6 Confocal micrographs of the midbrain of (*Tg(sox10:EGFP)* zebrafish larvae, 120 min after intravenous injection with Pluronic F127 (F127), Tween 80 (T80) and Poloxamer 188 (P188) cubosomes labelled with LR. The yellow dotted line outlines the eye region while the white dotted line indicates the midbrain region. The uptake of LR suspension was used as the control. The GFP panel indicates the location of neurons which fluoresce in green while the LR panel indicates the LR, which fluorescence in red. The merge panels combine the GFP and LR panels to show any overlap of green and red fluorescence which might indicate neuronal uptake. Scale bar: 50 µm.

The uptake of cubosomes across the BBB is crucial to transport drug molecules into the brain parenchyma. Here, the addition of Tween 80 to cubosomes resulted in an increased uptake of the fluorescent molecule, LR into the brain, without any significant accumulation observed in the neurons. Previous literature suggests that coating nanoparticles with Tween 80 or Poloxamer 188 can lead to an increase in their uptake across BBB. Polymeric nanoparticles coated with Tween 80 have been shown to promote the uptake of encapsulated dalargin and doxorubicin into the brain [27, 585, 586]. The uptake of Tween 80 and Poloxamer 188 coated nanoparticles were proposed to be facilitated by the adsorption of Tween 80 and Poloxamer 188 moieties to ApoE in the plasma [192]. The complexes then interact with LDL-receptors (particularly LDL-receptor related protein 1, LRP) on the endothelial cells at the BBB followed by endocytosis into the cells. Drugs encapsulated in the nanoparticles might be released inside the cells or transcytosed across the cell into the brain parenchyma (**Figure 5.7**). The surfactant coating of nanoparticles might reduce the clearance rate by reticuloendothelial system and prolong the circulation time in the blood, hence allowing sufficient interaction time between nanoparticles and LDL-receptors [350].

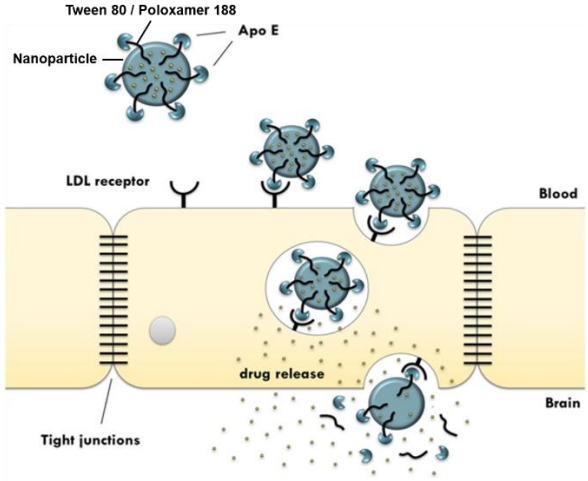

Figure 5.7 Illustration on the proposed uptake mechanism of Tween 80/Poloxamer 188 surface coated nanoparticles into the brain via LDL receptors (Adapted from [330] with permission).

The presence of LR observed in the midbrain region does not necessarily indicate the presence of cubosomes in the brain. It is possible that the cubosomes are broken down after internalisation into the endothelial cells and only the LR molecule is exocytosed out and into brain parenchyma. However, as observed from the LR suspension (control), the presence of cubosomes is necessary for the increased uptake of LR. The quantification of the LR signal in the midbrain region indicates that Tween 80 cubosomes have the potential to cross the BBB or facilitate the uptake of other molecules into the brain. These studies are however unable to provide information on the fate and exact localisation of Tween 80 cubosomes within the brain.

There was insignificant uptake of Poloxamer 188 cubosomes into the midbrain or neurons of the zebrafish. This is in disagreement with studies that show polymeric nanoparticles surface decorated with Poloxamer 188 can increase uptake of molecules into the brain through the same mechanism proposed for Tween 80 coated nanoparticles [347, 350].

In liposomal formulation, Poloxamer 188 was inserted the bilayer due to the interaction of the PEO moiety with both the hydrophobic tails and hydrophilic head of the lipids that form liposomes [587], rather than adsorption on the surface [400]. At the interface, the insertion of Poloxamer 188 can force the lipid molecules to pack tightly causing membrane compression [400, 588]. However, 80% of the Poloxamer 188 chain consists of PEO moieties which increase the hydrophilicity. There is a possibility that a large amount of Poloxamer 188 added in the cubosome formulation are not inserted in the phytantriol lipid layer, but instead form aggregates and micelles in the dispersion [589]. Previously in **Chapter 3** (**Table 3.4**), Poloxamer 188 cubosomes were found to have higher PDI value when compared to the other cubosome formulations, which might indicate the formation of micelles in the dispersion. Therefore, it is possible that the

amount of Poloxamer 188 added to the cubosomes was sufficient to exert steric stabilisation on the surface, but not enough to allow for interactions with ApoE, which then lead to lack of uptake through LDL receptors at the BBB [352, 371, 404, 590, 591]. There is a possibility that in cubosomes, Poloxamer 188 molecules are packed within the phytantriol lipid bilayer, with only a low amount protruding out to interact with ApoE in the plasma. The distribution of Poloxamer 188 on the internal and external interface might affect the successful interaction with ApoE.

In this chapter, the same amount of Poloxamer and Tween 80 were added into the cubosome formulations. The PPO-PEO chain length in Poloxamer 188 might exert a different effect on the phytantriol lipid as compared to polyoxyethylene sorbiton and alkyl chain in Tween 80 [400, 592]. To further investigate the potential of Poloxamer 188 as a cubosome stabiliser for BBB targeting, future studies should explore a wider concentration of Poloxamer 188.

5.4.2 Ultrastructural localisation of Tween 80 cubosomes

In order to observe the fate of Tween 80 cubosomes in the brain at the ultrastructural level, Tween 80 cubosomes were labelled with gold nanoparticles and their localisation in the midbrain was observed under electron microscopy.

5.4.2.1 Characterisation of gold-labelled cubosomes

Gold functionalised with octanethiol (89.3 nM) was added to Tween 80 cubosomes in order to label the cubosomes to allow detection by electron microscopy. Gold has a high atomic weight (197 amu) and can provide contrast upon interaction with electron waves under electron microscope [593]. Hydrophobic octanethiol chain conjugated to gold particle (**Figure 5.8**) mimics the structure of phytantriol lipid. The hydrophobic tail allows its insertion between the lipid bilayers within the cubosome structure [594]. The gold nanoparticles are expected to be fully inserted into the bilayer. The addition of gold nanoparticles with less than 5 nm diameter into the phospholipid bilayer did not disrupt the bilayer, however, if the gold particles were larger than 5 nm in diameter, they may not fit in the bilayer and can alter the structure [595]. Since this study used 3 nm sized gold nanoparticles, it was expected that they would be inserted within the phytantriol bilayer without disrupting the internal structure [596].

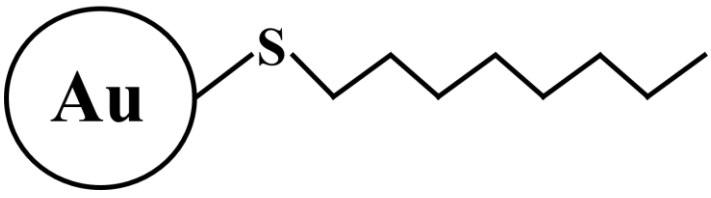

Figure 5.85 Schematic illustration on the chemical structure of gold functionalised with octanethiol.

The addition of gold nanoparticles at the studied concentration led to an increase on the size ($p<0.05$) and polydispersity of the Tween 80 cubosomes as shown in **Table 5.4**. The gold nanoparticle was proposed to be inserted into the lipid bilayer within the cubosomes which caused an increase in size. The internal structure of cubosomes is maintained as *Im3m* cubic structure, which is confirmed by the presence of Bragg peaks with peak position in a ratio of $\sqrt{2}:\sqrt{4}:\sqrt{6}$ (**Table 5.4, Figure 5.9A**).

Table 5.4 Characterisation of Tween 80 cubosomes and gold-labelled Tween 80 cubosomes.

Formulation	**Average size (nm)**	**PDI**	**Internal structure**
Tween 80	164.9 ± 1.8	0.13 ± 0.10	*Im3m*
Gold-labelled Tween 80	196.0 ± 2.5	0.25 ± 0.02	*Im3m*

Tween 80 cubosomes labelled with gold nanoparticles were analysed by EM to determine whether the gold nanoparticles were successfully encapsulated within the cubosome structure (**Figure 5.9B).** Electron-dense nanoparticles are visible inside the cubosome structure indicating the successful addition of gold nanoparticles into Tween 80 cubosomes.

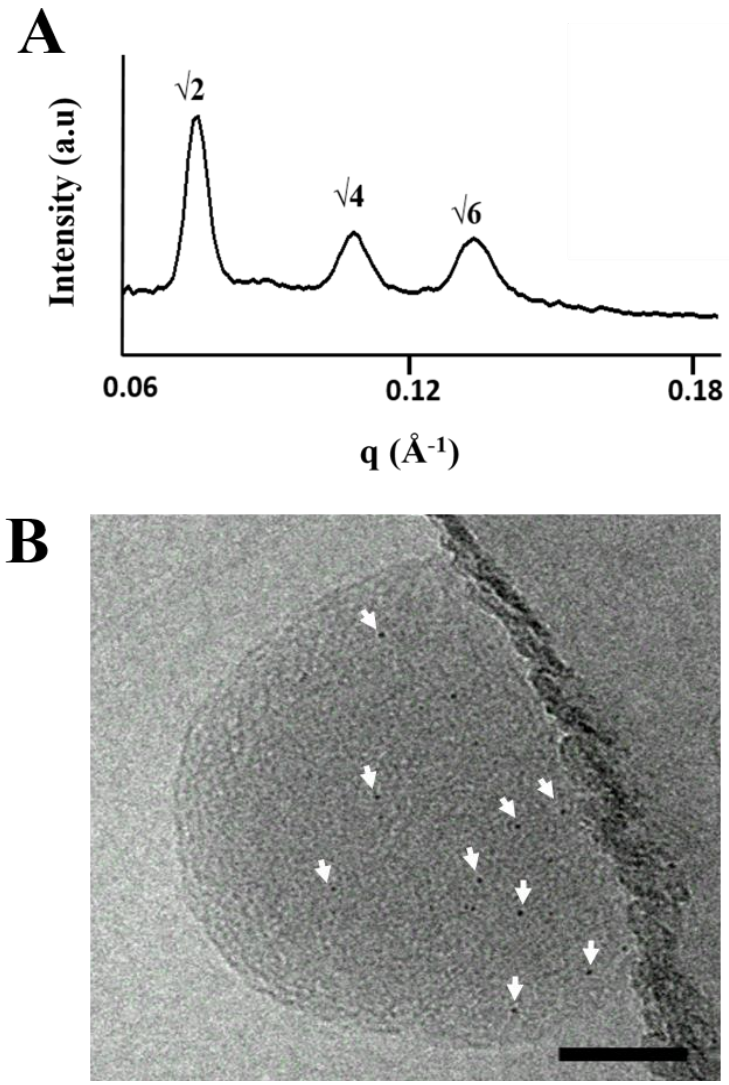

Figure 5.9 (A) SAXS diffractogram of Tween 80 stabilised cubosomes after the addition of gold nanoparticles indicating formation of *Im3m* cubosomes. The incorporation of gold nanoparticles into Tween 80 cubosomes is shown in (B) from cryo-TEM imaging. The arrows are pointing at the of gold particles inside the cubosomes. Scale bar: 50 nm.

5.4.2.2 Fate of gold-labelled Tween 80 cubosomes

The midbrain sections were examined 120 min after intravenous administration of cubosomes. All sections were imaged without any staining to allow for clear imaging of the gold nanoparticles and to prevent artefacts related to lead citrate and uranyl acetate staining [597-599]. There is evidence of dense nanoparticles in the brain tissue of zebrafish larvae injected with Tween 80 cubosomes, suggesting the presence of gold nanoparticles in the brain parenchyma (**Figure 5.10d and e**). The data suggests that gold nanoparticles are able to leave the blood vessels, translocate across the endothelial cells and enter the brain parenchyma (**Figure 5.10f**). Interestingly, the gold suspension was unable to enter the brain, again suggesting the presence of cubosomes facilitates uptake of gold nanoparticles (**Figure 5.10c**). To confirm that the dense particles are not artefacts, the brain sections from untreated larvae (**Figure 5.10a**) and from larvae treated with Tween 80 cubosomes (without gold label) (**Figure 5.10b**) were investigated. With no dense particles observed, therefore, the circular dense and black structures visible in the images (**panel d, e and f**) are proposed to be the gold nanoparticles and not from the cubosomes. It is unlikely to observe intact cubosomes under TEM due to the lipidic nature of cubosomes which can be destroyed after the processing and fixation [600, 601].

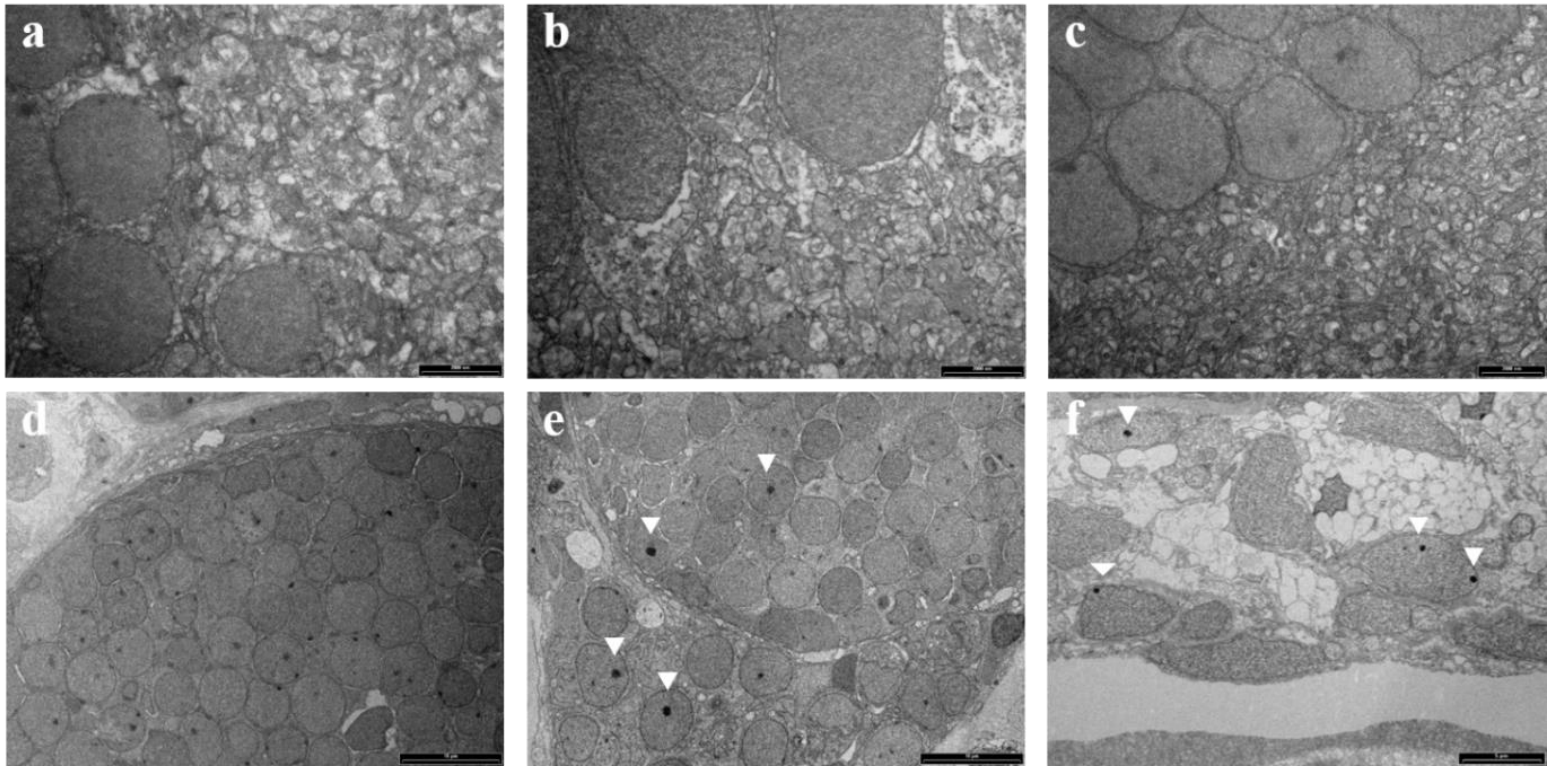

Figure 5.10 Representative electron micrographs of zebrafish larvae midbrain. Larvae that were untreated (a) or injected with Tween 80 cubosomes (b) or a gold suspension (c) showed no evidence of gold particles in the brain. Electron micrographs from larvae injected with Tween 80 cubosomes labelled with gold nanoparticles showed the presence of dense black particles (white arrowheads) as in panel e and f and cells adjacent to the blood vessel (panel f). Scale bar: 2 µm

In order to confirm that the dense particles are gold nanoparticles, the chemical composition was analysed by EDS. From the micrograph in **Figure 5.11A**, two particles from the brain section were analysed (**Figure 5.11B** and **Figure 5.11C**). The expected elemental peaks for gold are indicated by the arrows. Unfortunately, the specific peaks for gold were not clearly detected. The lack of signal might be due to the low acceleration voltage and the size of gold nanoparticles used in the study which is only 3 nm in diameter [602]. Previously, 15 kv was used to detect 10 nm gold particles using EDS [603]. To get a stronger signal for smaller gold particles, a higher accelerating voltage must be applied. However, this is avoided in this study as it could lead to sample damage and contribute to inaccurate peaks detected [604]. Using an EDS detector with a higher sensitivity would allow the detection of small particles at a lower kV and this should be considered in future studies.

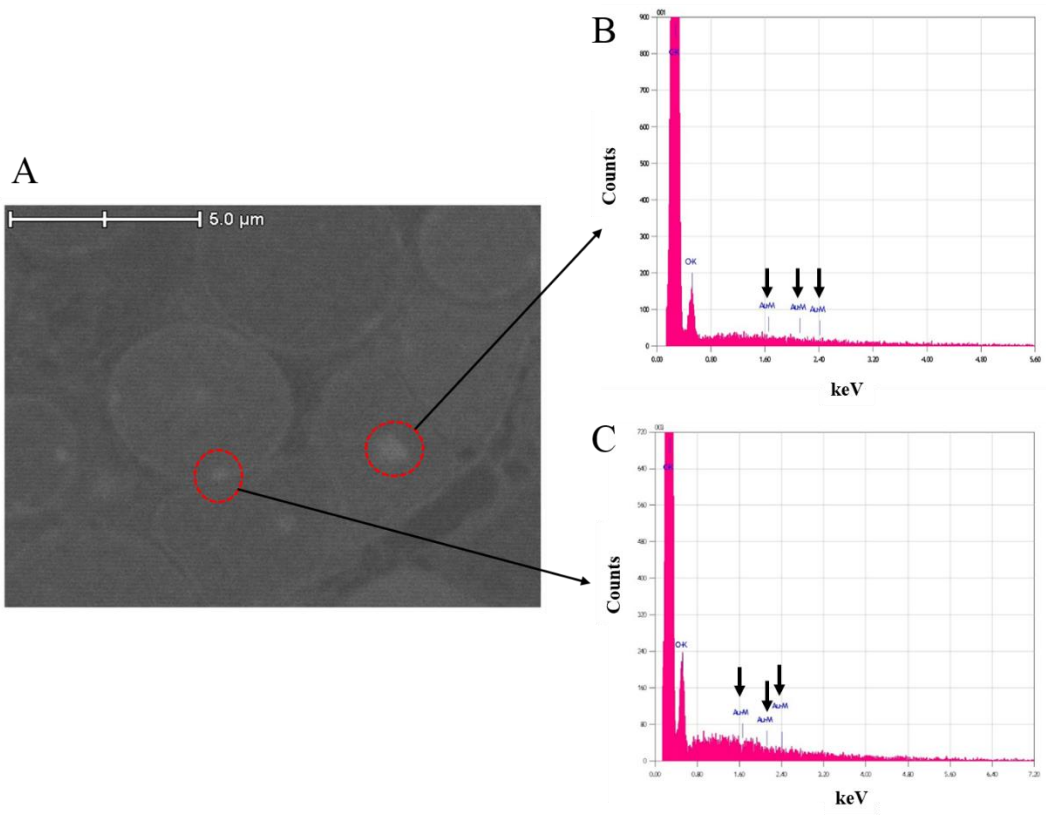

Figure 5.11 EDS spectra from two different spots in (A) were analysed and presented in (B) and (C). Arrows indicate the position of expected peaks for gold nanoparticles. Scale bar: 5 µm.

Overall, the microscopic examination of gold-tagged Tween 80 cubosomes suggests that there was uptake of gold nanoparticles into the midbrain region of the zebrafish even though intact cubosomes were not observed. It is possible that as the sections were unstained, the phytantriol lipid from cubosomes did not provide enough contrast for it to be detected under TEM. Negative staining could provide sufficient contrast to observe phospholipids and lipid structure within the cells [601, 605, 606]. However, it is likely that then the tissues in the brain (which also have a high lipid content) might obscure the cubosomes causing inability to distinguish their differences [607, 608]. It is therefore still uncertain that if, after the uptake into the brain, the cubosomes maintain their initial structure or if they are subjected to intracellular degradation. As cholesterol and lipid taken up into the brain are subjected to cellular metabolism before being utilised

by the brain cells [609], it is possible that Tween 80 cubosomes are also being metabolised after uptake, leaving behind gold particles which can be observed as dense particles under TEM.

5.4.3 Evaluation of cationic cubosomes uptake in the brain

In **Chapter 4**, positively charged cubosomes were successfully formulated and characterised. From the *in vitro* uptake studies using hCMEC/D3 cells, the addition of double chain cationic lipids, DOTAP and DOTMA into cubosomes led to increased cellular uptake. In order to further investigate the potential of using cationic cubosomes to target the BBB, they were fluorescently labelled with LR and uptake into the zebrafish brain was investigated (**Figure 5.12**).

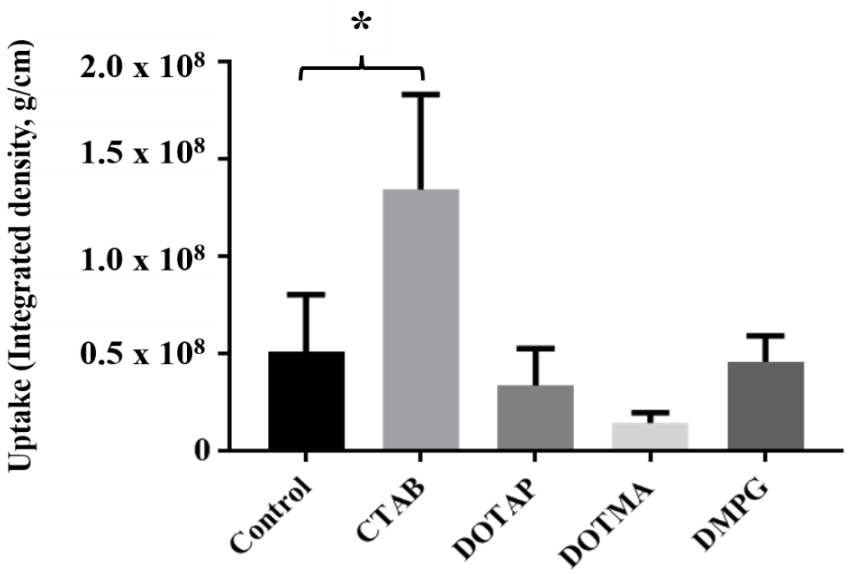

Figure 5.12 Uptake of LR in the zebrafish midbrain from LR-labelled charged cubosomes in the midbrain, expressed as integrated density (g/cm) and compared against control (LR-labelled Pluronic F127 stabilised cubosomes without additives). Data presented are mean ± standard deviation of LR uptake in 10 to 20 larvae per group. *P<0.05 compared to control.

Interestingly, the addition of the single chain cationic lipid, CTAB into Pluronic F127 cubosomes results in the highest uptake into zebrafish midbrain, with about a three-fold increase as compared to the control (LR-labelled Pluronic F127 cubosomes). No increase in LR uptake was observed for double chain cationic lipid, DOTAP and DOTMA cubosomes. Uptake of LR in all groups was imaged and presented in **Figure 5.13**. The signal from LR is clearly observed in the brain of zebrafish treated with CTAB cubosomes, while lack of signal from LR was observed with LR-labelled DOTAP and DOTMA cubosomes, which indicates lack of uptake in these two groups.

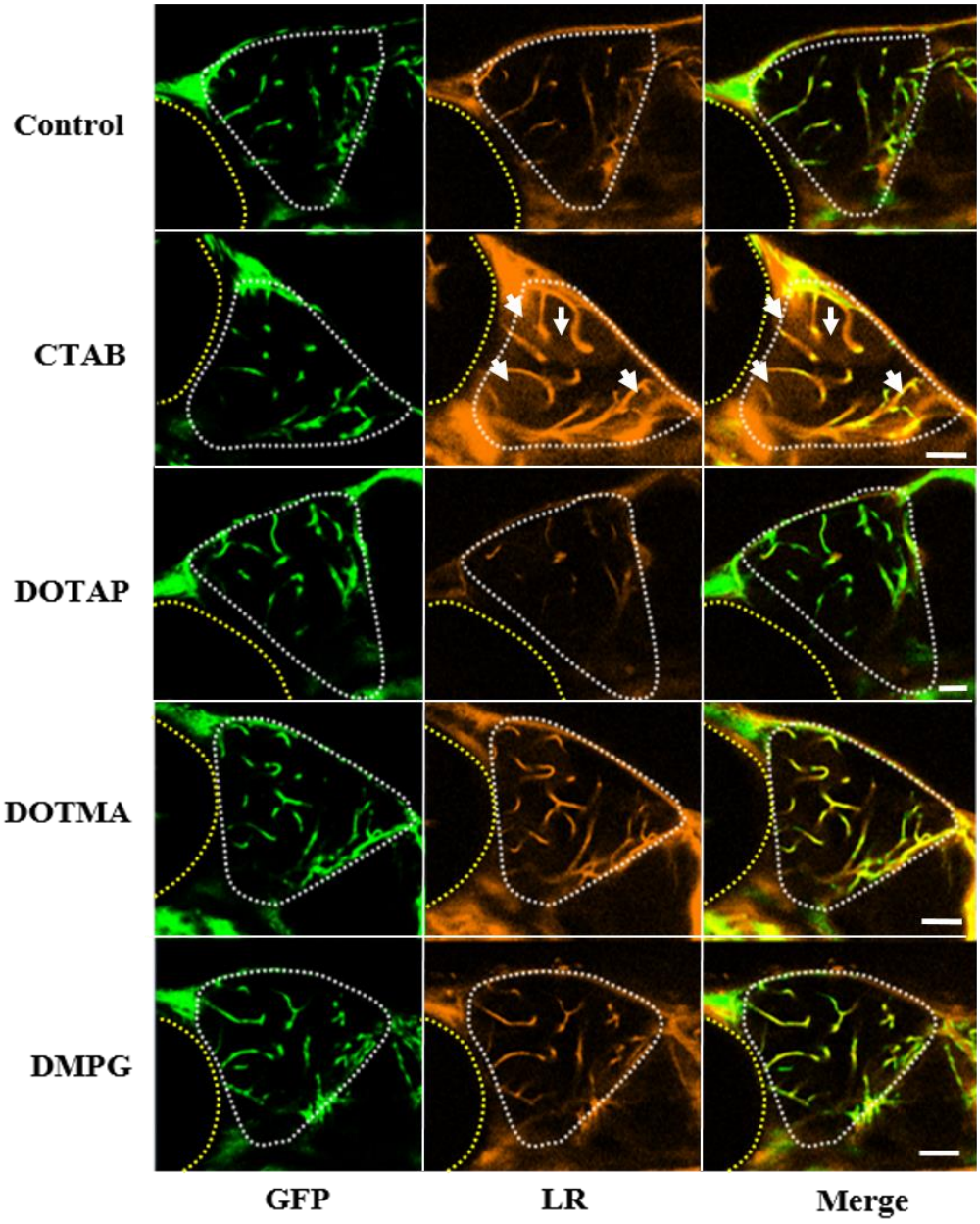

Figure 5.13 Representative confocal micrographs of zebrafish larvae treated with CTAB, DOTAP, DOTMA and DMPG cubosomes fluorescently labelled with LR. The dotted yellow line outlines the eye region while the white dotted line outlines the midbrain region. The GFP panel show green fluorescence indicating the blood vessels, while the LR panels show the fluorescence from LR. The uptake of LR was observed to be within the midbrain region, as evident by the presence of red fluorescence outside the blood vessel (indicated by the arrows). The merge panels show the overlap of GFP and LR panels to illustrate the presence of LR outside the blood vessels. The uptake of cubosomes is compared against the uptake from control (LR-labelled Pluronic F127 stabilised cubosomes). Scale bar: 50 μm.

Further investigation was conducted to observe whether cationic cubosomes localise in the neurons (**Figure 5.14).** No LR was observed in the neurons for any formulation groups studied. This suggests that the uptake of CTAB cubosomes which previously observed, does not localise in the neurons. The positive charge on the surface of cubosomes most likely retards the diffusion of cationic cubosomes further away from the blood vessels after successful internalisation. The extracellular space within the brain parenchyma has an anionic charge that hinder the free diffusion of cationic cubosomes [610-612].

While the *in vitro* studies in **Chapter 4** show increased cellular uptake for DOTAP and DOTMA cubosomes, the *in vivo* studies suggest that only CTAB cubosomes were able to cross the BBB and enter the brain. This is an interesting observation which suggests that the difference in conditions of the cell cultures and *in vivo* models can significantly influence nanoparticle uptake [613, 614]. The *in vitro* model lacks the ADME (absorption, distribution, metabolism and elimination) properties as compared to studies using live animal (*in vivo*) [615]. In addition, the flow properties of *in vitro* and *in vivo* might lead to different cubosomes uptake [616]. Cell culture is a static model where a simple concentration gradient and the gravity will cause full interaction between cubosomes and the hCMEC/D3 cells [617, 618].

It is possible that the presence of double chain cationic lipids DOTMA and DOTAP on the surface of cubosomes leads to protein corona formation in plasma *in vivo* which then neutralises the surface charge and thereby reducing interactions with the negatively charged endothelial cell membrane at BBB [619, 620]. Another possibility is that the double chain DOTAP and DOTMA increases the clearance rate of cubosomes from blood, which then reduces contact time between the endothelial cells and the cubosomes, thus limiting successful uptake [621, 622]. In contrast, previous studies have shown that the

addition of DOTAP and DOTMA into polymeric nanoparticles can increase gene transfection. The type of nanoparticles used might play a role in the adsorptive endocytosis process *in vivo*, which suggests that not all positively charged nanoparticles will lead to positive cellular uptake [351, 623-625].

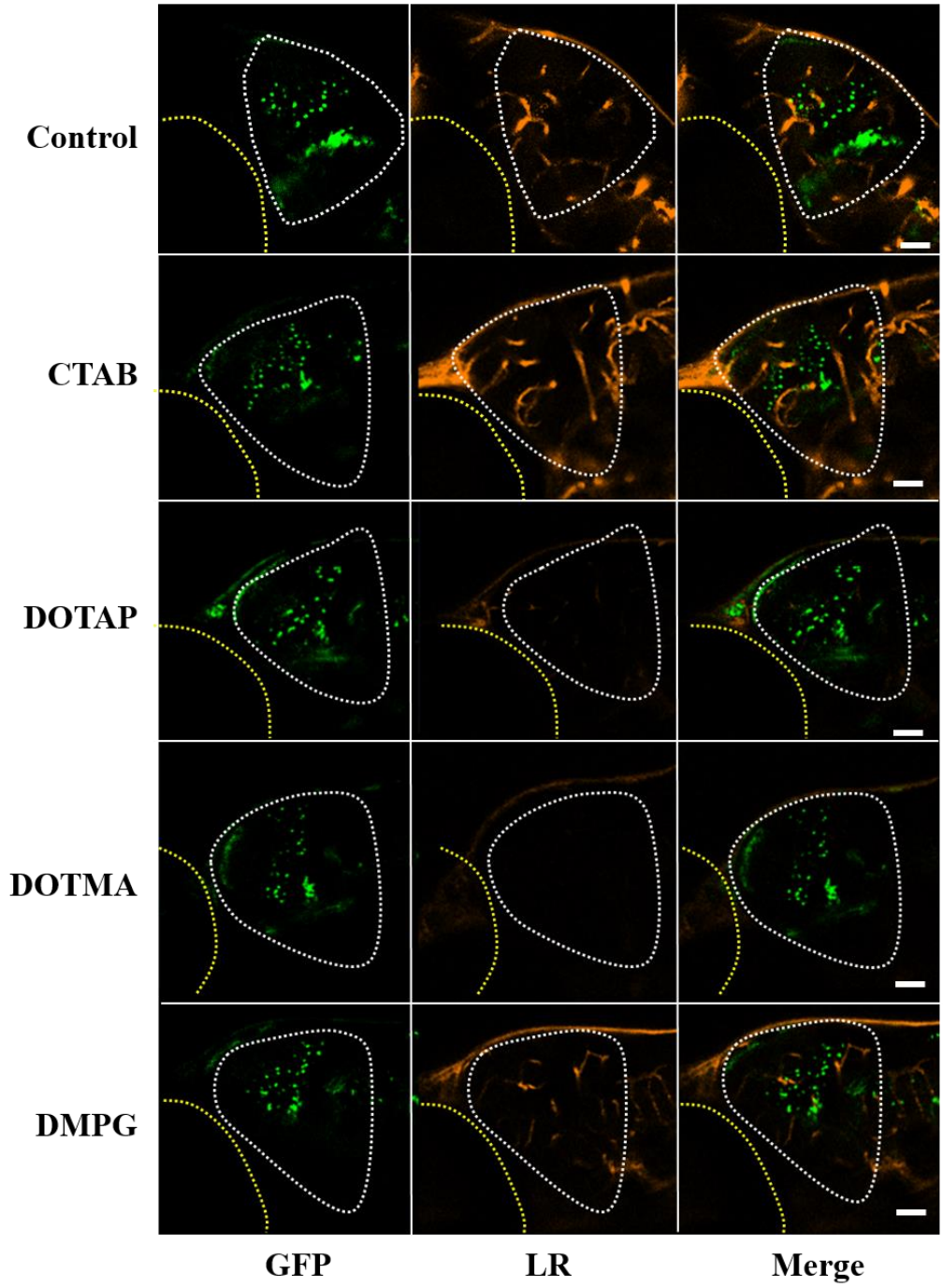

Figure 5.14 Confocal micrographs of zebrafish midbrain with the neurons fluorescence in green (GFP). The yellow dotted line shows the eye while the white dotted line outlines the midbrain region. LR-labelled CTAB, DOTAP, DOTMA and DMPG cubosomes were injected and the midbrain was observed 120 min after injection. The presence of LR signal in the neurons was compared to the control (LR-labelled Pluronic F127 stabilised cubosomes without additives). Scale bar: 50 µm.

5.4.4 Toxicity of surface modified cubosomes in the brain

The *in vivo* toxicity assay in the zebrafish brain was conducted to investigate whether any uptake of cubosomes into the brain could be a result of local toxicity. Acridine orange is a positively charged molecule that selectively binds to nucleic acids, and it enters cells that have compromised membrane permeability. Acridine orange will stain cells that are in late apoptosis or necrosis [626-628]. To evaluate cell apoptosis post cubosomes administration, the midbrain region was observed 120 min after administering cubosome formulations and acridine orange (AO) solution. **Figure 5.15** illustrates the toxic effect of administering cubosomes stabilised with Pluronic F127, Poloxamer 188 and Tween 80 to the midbrain region. DMSO was injected into zebrafish larvae as a positive control. The presence of green fluorescence signal in the DMSO treated group comes from acridine orange molecules that have crossed from the damaged blood vessel and permeated into the apoptotic cells, as indicated by the arrows. The green fluorescence observed in panel AO for Tween 80 and Poloxamer 188 groups show fluorescence signal from acridine orange which was restricted inside the blood vessel and no signal was detected in the brain parenchyma (outside the blood vessel). In the "merge" panel, the overlap between the red fluorescence (mcherry panel) and acridine orange (AO panel) confirmed that acridine orange did not cross the blood vessel and enter the brain parenchyma, which suggests that there were no local toxicity effects by Tween 80 and Poloxamer 188 cubosomes in the midbrain region. These observations suggest that these cubosomes have low toxicity in the midbrain and it also suggests that the uptake of Tween 80 cubosomes into the brain was not caused by cellular damage [629, 630].

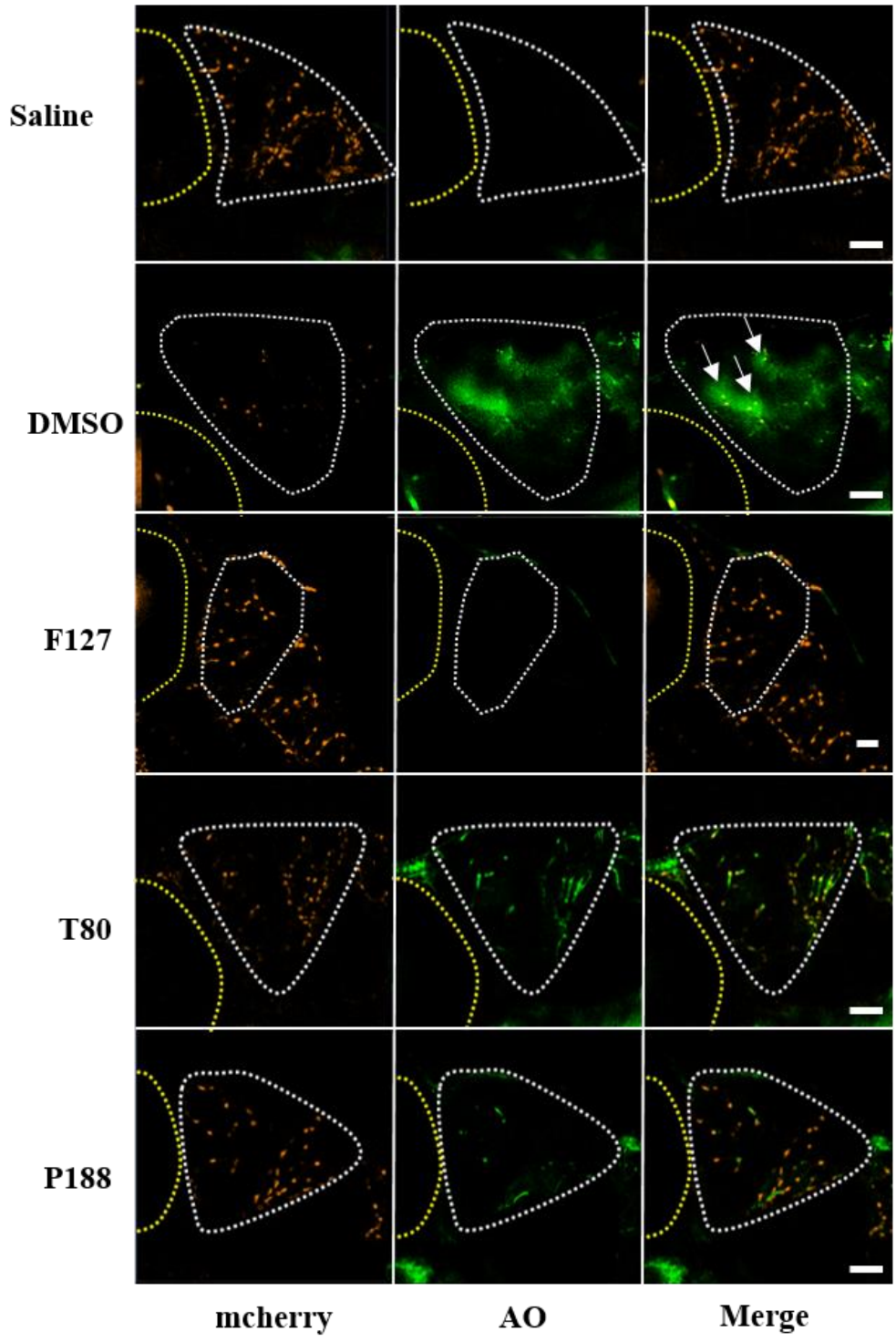

Figure 5.15 Representative confocal micrographs showing toxicity of cubosomes in the midbrain region using acridine orange (AO) assay. Apoptotic cells stained with AO were observed as green fluorescence under confocal microscope. Zebrafish treated with Pluronic F127 (F127), Tween 80 (T80) and Poloxamer 188 (P188) stabilised cubosomes were imaged 120 min after injection. Saline was injected to illustrate negative toxicity and DMSO as positive control to induce toxicity (arrows). Scale bar: 50 µm.

The same analysis was carried out following administration of the charged cubosomes (**Figure 5.16**). Larvae treated with CTAB cubosomes showed the most obvious sign of brain toxicity where the green fluorescence signal from AO can be clearly observed in the midbrain region. In larvae treated with DOTAP and DOTMA cubosomes, the green signal was limited to the blood vessel.

These observations suggest that the addition of single chain cationic lipids at the studied concentrations can cause toxicity at the brain. The toxicity of single chain cationic lipid is higher than that of double chain cationic lipids in agreement with previous reports in the literature [451, 631-633]. The lipid structure of charged lipids added affected the toxicity level of the formulated cationic cubosomes. It was reported that the single chain CTAB increases the toxicity from its aliphatic chain. The hydrophobic tail causes disruption of the cell membrane bilayer, which leads to an increase in membrane fluidity and causing the cell membrane to collapse [634-636]. This reduces the integrity of the cell membrane and allows the acridine orange molecule to permeate the cell and observed as the toxicity.

The uptake of CTAB cubosomes observed previously might therefore be due at least in part to cellular toxicity and damage at the BBB, which would allow the cubosomes to enter the brain [637, 638]. However, since the toxicity studies were conducted within two hours of cubosomes administration, the toxicity can be from acute effect [462, 639]. Acute toxicity can be temporary and the leakiness associated with the toxicity can be resumed after a while. This toxicity can possibly assist in shuttling drug molecules into the brain for a short duration [612]. Future investigation should be undertaken to understand the type of toxicity involved when using CTAB cubosomes. The toxicity effect can be evaluated from cell lysis, transient TJ opening, DNA damage or programmed cell death [637]. To quantify acute toxicity, mitochondrial activity assay can be conducted while for chronic toxicity, quantification of reactive oxygen species and DNA damage can be

carried out [640, 641]. Also, further investigation needs to be conducted to determine whether a lower concentration of CTAB can be used, one that promotes uptake without undue toxicity.

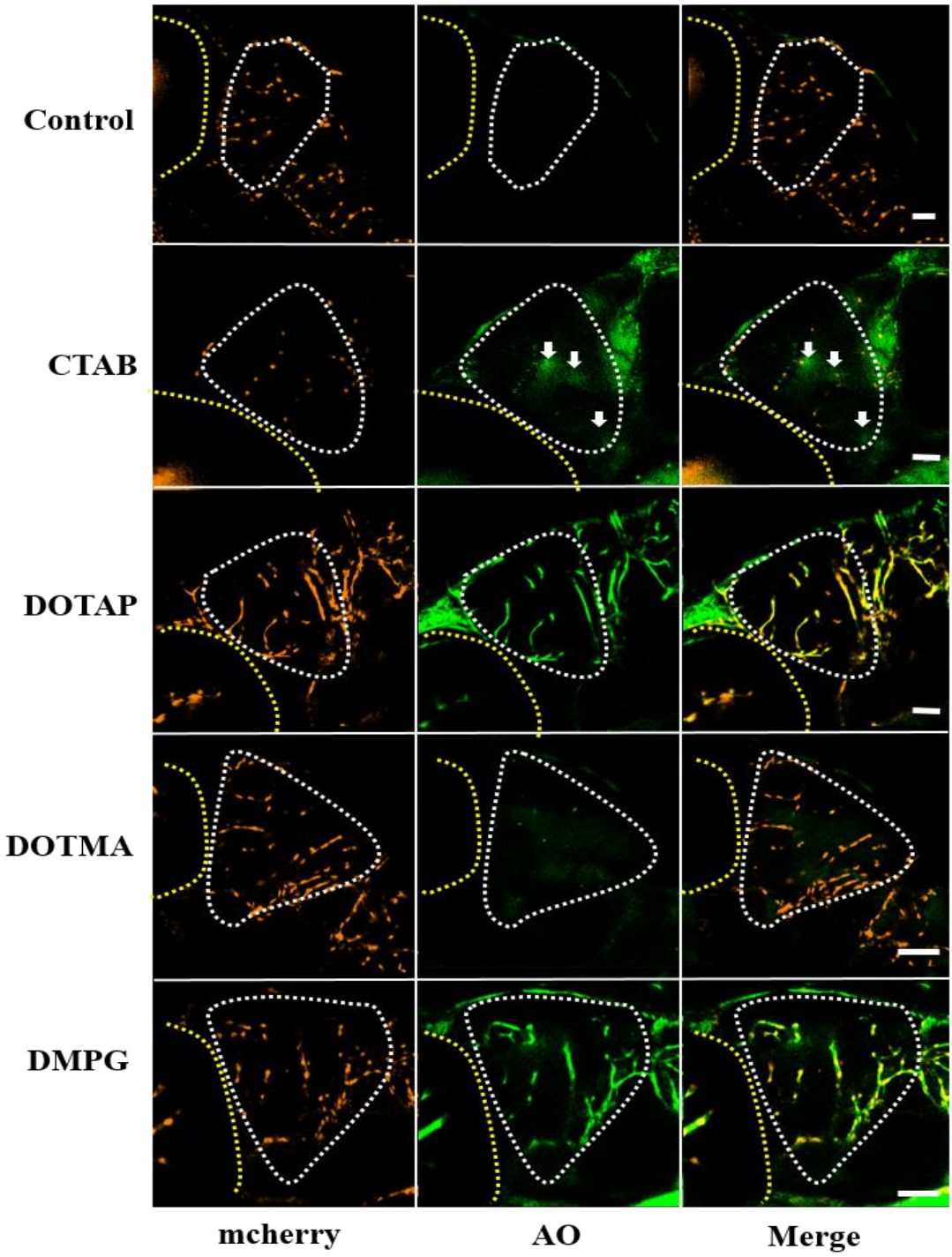

Figure 5.16 Confocal images of the midbrain section (white dashed line) showing the toxicity of charged cubosomes in *Tg(flk:nmscherry)*. The blood vessels fluoresce in red (mcherry). Yellow dashed line outlines the eye and white arrows point to the positive toxicity region in the zebrafish. The toxicity effects are compared against the control (Pluronic F127 stabilised cubosomes). Scale bar: 50 µm.

5.5 Conclusion

In conclusion, the studies outlined in this chapter illustrates the uptake and toxicity of cubosomes in the midbrain section of zebrafish larvae. The addition of Tween 80 into the cubosome formulation can promote its uptake into the midbrain. This most likely via its interaction with LDL-receptors at the BBB [391, 642-646]. Even though the uptake into the brain was observed under confocal and electron microscope, there was no neuronal accumulation of Tween 80 cubosomes. Moreover, at this point, it is unclear whether the Tween 80 cubosomes enter the midbrain as intact particles or whether there is degradation of the cubosome structure which then releases the fluorescence label or gold nanoparticles. Further studies can be conducted by incorporating CNS drug molecules into Tween 80 cubosomes and then evaluating its clinical effects or drug accumulation in the brain.

Another important issue to consider is that the addition of Poloxamer 188 to cubosome formulations failed to promote its uptake into the brain. It is unclear whether the Poloxamer 188 concentration studied in this chapter is insufficient to coat the surface of the cubosomes for interaction with ApoE at the BBB or whether the plasma interaction with Poloxamer 188 cubosomes led to formation of a corona, which prevents interaction with LDL receptors. More studies need to be conducted to determine if the concentration of Poloxamer 188 influences uptake of cubosomes into the brain.

The addition of double tailed charged lipids into cubosomes failed to cause any significant uptake into the brain. Only cubosomes modified with the single chain cationic lipid, CTAB was able to cross the BBB but without any neuronal accumulation. Unfortunately, the uptake of CTAB cubosomes was related to the increase in toxicity at the midbrain region. Local toxicity effects might cause the BBB to be leaky, which then allow the CTAB cubosomes to enter the brain. Future studies should be conducted to

determine if the concentration of CTAB can be optimised such that it exerts a positive surface charge with minimum brain toxicity. However, even with the limitations described in this study, Tween 80 cubosomes are found to be a promising drug carrier to encapsulate CNS drug molecules to target the BBB.

Chapter 6

General discussion and conclusions

6 General discussion and conclusions

The BBB remains a challenge in treating CNS diseases. This biological interface between the blood and the brain restricts the uptake of therapeutic drugs into the brain and thus hinders drugs from reaching the desired therapeutic concentrations in the brain [20]. As such, this thesis looked into the possibility of using lipid-based nanoparticles called cubosomes, in which their surfaces were decorated with varied moieties, primarily to target the uptake across BBB. Cubosomes were selected as a drug carrier due to the structural benefits they have to offer. The unique tortuous structure of cubosomes allows the encapsulation of lipophilic, hydrophilic, and amphiphilic drug molecules. The high drug loading observed in these nanoparticles is largely due to the high surface area. Furthermore, encapsulation of drugs within the cubosome structure has been shown to shelter and protect the drug from chemical degradation [264, 487, 647, 648]. In comparison to several other nanoparticles, cubosomes can be easily prepared from lipids and surfactants, which happen to be commercially available.

In this thesis, cubosomes were formulated using the lipid phytantriol, together with several specific BBB-targeting molecules, and their potential uptake by brain endothelial cells *in vitro* and *in* vivo in a zebrafish model was investigated. The overall hypothesis of the thesis was that the addition of certain molecules, which are known to target the BBB, on the surface of cubosomes would alter the surface properties to enable cubosomes to be targeted to endothelial cells of BBB. Although several uptake pathways are available, which are used by endogenous molecules to maintain brain homeostasis [20, 71], this thesis only investigated two pathways, which are: 1) receptor-mediated endocytosis (through LDL receptors) and 2) adsorptive endocytosis.

In several prior studies, polymeric nanoparticles have been conjugated with BBB-targeting moieties in order to cross the BBB [373, 649]. Inclusion of specific surfactants and

ligands, particularly on the surface of polymeric nanoparticles appeared to promote internalisation into the cell through a specific pathway at the BBB. Encapsulation of loperamide, dopamine and doxorubicin in specific polymeric nanoparticles resulted in successful uptake into the brain, especially due to surface modification of the nanoparticles [371, 644, 650]. As such, this thesis focused on adding Tween 80 and Poloxamer 188 on the surface of cubosomes to target the receptor-mediated pathway at the BBB. The second part of this thesis aimed to target cubosomes to the BBB via adsorptive mediated pathway. In order to target this particular pathway, the surface of phytantriol cubosomes was also decorated with cationic lipids to ascertain that they too become positively charged.

Characteristics of surface modified cubosomes

In finding effective drug nanocarriers for successful delivery of drug molecules, several physicochemical characteristics of the drug carrier are often investigated during the optimisation [57, 586, 651, 652]. Whilst the size and dispersity of the various cubosomes were investigated as part of formulation optimization, a study looking at the effect of cubosome size on its uptake by endothelial cells was not conducted. Only the influence of targeting ligands and surface characteristics on endothelial cell uptake were investigated. **Chapter 3** outlines the use of Tween 80 and Polysorbate 188 in phytantriol cubosomes, which had been used as stabilisers and ligands to target the BBB. It was hypothesised that the addition of these stabilisers would facilitate the uptake of cubosomes via LDL-receptors at the endothelial cells [392]. This is due to the interaction between the stabiliser and ApoE in the plasma which leads to binding to LDL-receptors, thus the uptake into brain endothelial cells [649].

Previously, polymeric nanoparticles with their surfaces coated with these surfactants promoted uptake across BBB [192]. However, this thesis describes for the first time the use of a complex lipid-based carrier, the cubosome to target the brain. The flexibility in controlling the internal structure of cubosomes by changes in additives, temperature and pressure provides the extra advantages in using this type of drug carrier over other lipid-based carriers such as liposomes or micelles [258, 262, 394]. This thesis has produced cubosomes with the addition of Poloxamer 188 and Tween 80, which functioned as stabilisers. The internal structures of the resulting cubosomes were influenced by Tween 80 and Poloxamer 188, and led to the formation of *Pn3m* and *Im3m* cubic structures, respectively. This is most likely a result of their respective influence on lipid packing and curvature as has been previously reported for other lipid systems [395].

Both the internal structure and the morphology of Tween 80 cubosomes were clearly observed under cryo-TEM. The images displayed the lattice structure inside the cubosomes, along with clear illustrations of aqueous channels within the structure. The tortuosity within the structure offers a large surface area to encapsulate the drug molecules [648]. Furthermore, the arrangement of lipid bilayers enables the encapsulation of lipophilic drug molecules, while the aqueous pores accommodate hydrophilic molecules. Additionally, amphiphilic molecules are also inserted between the lipid bilayers and the aqueous channels [267]. It is therefore anticipated that highly lipophilic or hydrophilic drugs that fail to cross the BBB can be encapsulated within cubosomes, and with coating of specific ligands on the surface, the cubosomes can transport the drug molecules across the BBB.

Apart from adding BBB-targeting ligands on the cubosomes, the surface properties of the cubosomes was altered by inducing a cationic charge. Cationic cubosomes offer a potential to target the BBB via the adsorptive mediated pathway [425,

[465, 653]. In a prior study, nanoparticles, such as liposomes, were co-formulated with cationic molecules to deliver DNA in gene transfection [464]. As such, positively-charged liposomes were bound to negatively charged DNA and simultaneously promoted uptake into cell via adsorptive endocytosis pathway [631]. **Chapter 4** presents the preparation and the characterisation of cubosomes by including single- (CTAB) and double-chain (DOTAP and DOTMA) cationic lipids with the objective of preparing positively charged cubosomes. Varied cationic lipids were used to determine the impacts of single and dual chain lengths on the stability of cubosome. Overall, the stability of phytantriol monolayer was differently affected by its interaction with cationic lipids. DOTMA with double ether linkage caused a greater impact on phytantriol stability, in comparison to that of DOTAP, most likely as a result of its ester linkage [458]. In contrast, CTAB and DOTAP exhibited a similar effect on monolayer stability. Interestingly, despite of the variances in chain length and linkage, they all appeared to be miscible with the phytantriol bilayer. This suggests that at studied concentration, these lipids can be inserted into phytantriol bilayer within the cubosomes structure.

The addition of cationic lipids into phytantriol cubosomes which were stabilised with Pluronic F127 did not significantly alter the internal cubic structure but did result in additional vesicles in the formulation. Furthermore, while the amount of charged lipids used did not alter the internal structure, it had been sufficient to exert a positive charge on the nanoparticle surface. The observation of vesicles that co-exist with cubosomes is in agreement with those reported in the literature [262, 395]. These vesicles are thought to function as the precursors of cubosomes, whereby they fuse and form a single cubosome. But it is also likely that they are vesicles formed from the cationic lipids. The amphiphilic structure of the cationic lipids can form micelles and vesicles in water. The excess cationic lipids in the formulation that were not inserted in the cubosomes, will assemble

into vesicles as observed. Overall, cationic cubosomes were successfully formulated and insignificant difference was detected between adding single- and adding double-chain cationic lipids to the final structure of cubosomes.

The characterisation steps involved in formulating the cubosomes had been crucial in order to assure the type and the characteristics of the nanoparticles formed. Recently, Tween 80 was found to not only stabilise cubosomes, but also to have successfully crossed the BBB, thus displaying a positive clinical effect via *in vivo* from the restoration of cognitive function in Alzheimer's model (in rats). Nevertheless, the study failed to verify if the studied particles were indeed cubosomes mainly due to lack of characterisation [654]. Therefore, characterisation sheds light on the correlation between the attributes of cubosome and its uptake into the brain.

Fate of cubosomes in the brain

The inclusion of Tween 80 and Poloxamer 188 as stabilisers for cubosomes had been aimed to serve as BBB-targeting moieties at LDL receptors, as demonstrated by several prior studies [20]. Tween 80 and Poloxamer 188 cubosomes demonstrated low levels of uptake in the *in vitro* hCMEC/D3 cells, a human endothelial model of the BBB. Although the hCMEC/D3 cells express LDL receptors on their cell membranes [305, 416, 655], the cell culture media does not contain any ApoE for the interaction between Tween 80 and Poloxamer 188. This *in vitro* model is inadequate for demonstrating the potential exerted by cubosomes to target BBB. Hence, the potential in using cubosomes to deliver drug was investigated *in vivo* in zebrafish.

The advantages of using zebrafish have been discussed in detail in **Chapter 5**, and this model was used to screen the potential of cubosome formulations to target BBB. Interestingly, even though Poloxamer 188 coated nanoparticles have shown evidence of

brain uptake [365, 374], only Tween 80 cubosomes showed significant uptake into the brain. It is likely that the concentration of Poloxamer 188 applied in this thesis was insufficient to completely coat the surface of cubosomes which affected the ability of cubosomes to interact with ApoE molecules in the plasma [590].

The fluorescent molecules found in the midbrain region of zebrafish larvae showed that Tween 80 cubosomes can indeed function as a promising drug carrier. This finding is further supported by the localisation of gold nanoparticles that came from the gold-tagged Tween 80 cubosomes in the midbrain region, upon observation under electron microscope. The encapsulation of lipophilic dye, such as dil and nile red, in nanoparticles, has been related to premature release after *in vivo* administration [656, 657]. Nonetheless, in this thesis a combination of fluorescent molecule and gold nanoparticles conjugated with lipid tails were used. These molecules were expected to have been inserted within the phytantriol bilayers found within cubosomes and released only when the cubosome structure was broken apart. At this point, it is uncertain if Tween 80 cubosomes had remained intact after entering the brain or if the cubosomes had broken apart to leave behind the fluorescent molecules and the gold particles, as observed. Moreover, due to the lipidic nature of cubosomes, it is possible that after the successful internalisation into the cells, the Tween 80 cubosomes degraded and released the fluorescent molecules or the gold particles [288, 658]. Even if the cubosomes did not remain intact after the uptake into the brain, it still can serve as a potential drug carrier. The degradation of cubosomes would eventually release the drugs encapsulated within the cubosomes structure, once the cubosomes have successfully entered the brain and reach the brain parenchyma.

On the other hand, the cationic cubosomes displayed varied uptake properties for *in vitro* versus *in vivo* studies. It had been fascinating to note that cubosomes with double-

chain cationic lipids; DOTAP and DOTMA, exhibited increment in their uptake under *in vitro* studies, but not for *in vivo*. On the contrary, while CTAB cubosomes showed low uptake in *in vitro* studies, a significant increase in brain uptake had been recorded after administration was performed into the zebrafish larvae. Unfortunately, the uptake was linked with the local toxicity at the brain. This observation signifies that the cationic cubosomes might behave differently under *in vitro* versus *in vivo* approaches. This is because; the presence of various proteins and molecules in the plasma could have led to the formation of protein corona, which may possibly mask or neutralise the positive charges on the surface of cubosomes [147, 659, 660]. This has the potential to inhibit the electrostatic interaction with the negatively charged cell membranes found at BBB, thus lead to failure in uptake.

It is important to note that DOTAP and DOTMA cubosomes exerted lower levels of toxicity, in comparison to that of CTAB cubosomes. This observation is in parallel with prior studies, where single-chain cationic lipids have been reported to cause higher levels of toxicity, when compared to that of double-chain cationic lipids [631, 661]. Even though a positive uptake had been noted for CTAB cubosomes, they may be unsuitable for formulating cationic cubosomes, primarily due to the toxicity effect. Hence, it is worthwhile to further probe into the possibility of applying higher concentrations of DOTAP and DOTMA to formulate cationic cubosomes in targeting BBB, as they showcase lower levels of toxicity in cells.

Overall, the significance of conducting *in vitro* and *in vivo* studies that determines cubosome formulation suitability is conducted towards targeting BBB. The observations derived from *in vitro* studies may be inconclusive to exhibit the potential formulation of cubosomes for further studies, while the *in vivo* studies, on the other hand, may offer sufficient information regarding the actual scenario upon administration in human.

Future direction

Despite of all the extensive studies conducted previously, only a number of nanoparticles have been successfully translated into the clinic, and in this case, liposomes appear to be the most commonly applied nanoparticles. To date, neither nanoparticle surface decorated with Tween 80 nor any cubosome formulation has managed to reach the market for targeting drugs to the BBB. Therefore, in order to translate these formulations into pharmaceutical products, more research work is required for investigating the implementation of cubosomes as effective CNS drug carrier.

This thesis only studied the uptake of surface modified cubosomes within a specific brain region (midbrain). However, receptor-mediated endocytosis through LDL-receptors and adsorptive endocytosis via electrostatic interaction on the cell membrane can also occur at the other organ of the body. LDL-receptors are highly expressed in the liver and used to transport cholesterol molecules into the cells [662], while the cell membranes are negatively charged and can attract cationic molecules on their surface. In the future, it will be crucial to study the biodistribution of surface modified cubosomes and investigate the organ accumulation of these cubosomes.

Even though cubosomes can offer high drug loading capacity, the properties related to drug release from cubosomes need to be further explored. The presence of aqueous pores within the structure of cubosomes may allow encapsulation of hydrophilic drugs, but it is also important to determine if the drugs may possibly be released prior to reaching the target organ. It is important to take note that the water channels can lead to uncontrolled release of drugs into the blood system even before the cubosomes can reach the brain. These drugs can possibly cause peripheral side effects as they are released within the peripheral drug circulation. On the other hand, lipophilic or amphiphilic drugs may be more suitable for encapsulation within cubosomes. The tortuosity of phytantriol

lipid bilayer within the cubosomes structure can trap these drug molecules, thus hindering premature release of drug into the blood system. Upon entering the brain and being degraded, the drugs encapsulated within the cubosome structure are released in the brain parenchyma to treat CNS diseases.

In addition, as this thesis employed fluorescent molecules and gold nanoparticles as labels for the cubosomes, future studies can replace these molecules with CNS drugs like phenytoin to determine their clinical effects *in vivo*. It is significant to investigate the biodistribution of encapsulated drug molecules within the system of the body to further comprehend the localisation of cubosomes upon administration. Accumulation of the drug molecules in liver and kidneys also suggest an insight about the fate of cubosomes [663, 664]. Another possible suggestion refers to conjugating the CNS drug molecules with fluorescent molecules in the attempt to observe the location of cubosomes, aside from measuring the clinical effect from the drugs. Furthermore, it is important to characterise the drug encapsulated in cubosomes, mainly due to the interference of these drug molecules with phytantriol packing in the lipid bilayer, aside from potential alteration in its internal structure that may lead to formation of a different structure [435]. Moreover, the inclusion of buffer or salt solution into the lamellar phase seemed to modify the structure into cubic phase [479, 665], whereas the size and the structure of the additives (including drugs) may transform the internal structure.

Towards scaling up the formulation for mass production, a more sophisticated method is required. Vortex mixer with low heat production has been proven to generate homogenous cubosome dispersions, but one drawback of this technique is the use of solvent, thus projecting adequacy for small-scale production. As such, high energy ultrasonication has been proposed as an alternative to produce cubosomes in a larger scale as this particular approach omits the use of solvent for manufacturing [395, 407].

Nevertheless, due to the excessive generation of heat, its suitability is questioned for delivering of drug molecules or protein, which possesses a certain level of heat tolerance or are heat labile [313]. Therefore, further research works are sought to look into suitable CNS drug molecules that can be encapsulated in cubosomes through ultrasonication method.

In the attempt to translate the formulations into clinical applications, the dispersion requires long term stability and sterility. As cubosome dispersion requires an aqueous state, adding preservatives can extend the shelf life, aside from inhibiting microbial growth. Hydrophilic preservatives can be included into the dispersed phase (water) to protect the formulation. Nonetheless, it is imminent to comprehend that the preservatives might influence the stability of cubosomes or modify its internal structure [666]. Non-ionic preservatives with low molecular weight, thus, may be a good alternative to address the disruption that may occur within the cubosome structure.

Another option is to freeze dry and store the cubosomes in powder form so as to ease reconstitution when required [273, 667]. However, this particular technique may cause changes to its internal structure, especially upon reconstitution. Hence, further characterisation and formulation development need to be carried out in order to generate a suitable cubosome formulation to expand its shelf life for clinical use without disrupting the structure and stability.

In conclusion, the development of surface modified cubosomes was undertaken in this thesis with Tween 80, which successfully stabilised the cubosomes that possess the potential to target BBB with limited toxicity. Nevertheless, these cubosomes are still at its initial stage to assertively conclude that the addition of Poloxamer 188 and cationic lipids into cubosomes does not offer any advantage to target the brain. With that, further investigations are demanded in seeking the right concentration that can target the brain

with minimum toxicity. Nevertheless, the outcomes from Tween 80 cubosomes deserve future investigations in a larger animal model to show that this formulation can be used as a carrier for CNS drug delivery to target the brain.

7 Appendix 1

FACS buffer

Sodium azide	0.9 g
Foetal bovine serum (FBS)	20 g
PBS	to 1000 mL

8 References

1. Thakur, K.T., E. Albanese, P. Giannakopoulos, et al., *Neurological Disorders*, in *Mental, Neurological, and Substance Use Disorders: Disease Control Priorities, Third Edition (Volume 4)*, V. Patel, et al., Editors. 2016, The International Bank for Reconstruction and Development / The World Bank Washington (DC).
2. Hebert, L.E., P.A. Scherr, J.L. Bienias, D.A. Bennett, and D.A. Evans, *Alzheimer disease in the us population: Prevalence estimates using the 2000 census.* Archives of Neurology, 2003. **60**(8): p. 1119-1122.
3. Dorsey, E.R., R. Constantinescu, J.P. Thompson, et al., *Projected number of people with Parkinson disease in the most populous nations, 2005 through 2030.* Neurology, 2007. **68**(5): p. 384-386.
4. Albert, S.M., *Projecting neurologic disease burden: Difficult but critical.* Neurology, 2007. **68**(5): p. 322-323.
5. Hirtz, D., D.J. Thurman, K. Gwinn-Hardy, et al., *How common are the "common" neurologic disorders?* Neurology, 2007. **68**(5): p. 326-337.
6. Gabathuler, R., *Approaches to transport therapeutic drugs across the blood-brain barrier to treat brain diseases.* Neurobiology of Disease, 2010. **37**(1): p. 48-57.
7. Begley, D.J., *ABC Transporters and the Blood-Brain Barrier.* Current Pharmaceutical Design, 2004. **10**(12): p. 1295-1312.
8. Muller, R.H. and C.M. Keck, *Challenges and solutions for the delivery of biotech drugs – a review of drug nanocrystal technology and lipid nanoparticles.* Journal of Biotechnology, 2004. **113**(1): p. 151-170.
9. Abbott, N.J., *Blood-brain barrier structure and function and the challenges for CNS drug delivery.* Journal of Inherited Metabolic Disease, 2013. **36**(3): p. 437-449.
10. Neves, V., F. Aires-da-Silva, S. Corte-Real, and M.A.R.B. Castanho, *Antibody Approaches To Treat Brain Diseases.* Trends in Biotechnology, 2016. **34**(1): p. 36-48.
11. Gholamin, S., S.S. Mitra, A.H. Feroze, et al., *Disrupting the CD47-SIRPα anti-phagocytic axis by a humanized anti-CD47 antibody is an efficacious treatment for malignant pediatric brain tumors.* Science Translational Medicine, 2017. **9**(381).
12. Hinrich, A.J., F.M. Jodelka, J.L. Chang, et al., *Therapeutic correction of ApoER2 splicing in Alzheimer's disease mice using antisense oligonucleotides.* EMBO Molecular Medicine, 2016. **8**(4): p. 328-345.
13. Fernández-de Retana, S., A. Montañola, P. Marazuela, et al., *Intravenous treatment with human recombinant ApoA-I Milano reduces beta amyloid cerebral deposition in the APP23-transgenic mouse model of Alzheimer's disease.* Neurobiology of Aging, 2017. **60**(Supplement C): p. 116-128.
14. Pardridge, W.M., *Drug and gene delivery to the brain: The vascular route.* Neuron, 2002. **36**(4): p. 555-558.
15. Gomes, M.J., C. Fernandes, S. Martins, F. Borges, and B. Sarmento, *Tailoring Lipid and Polymeric Nanoparticles as siRNA Carriers towards the Blood-Brain Barrier – from Targeting to Safe Administration.* Journal of Neuroimmune Pharmacology, 2017. **12**(1): p. 107-119.

16. von Roemeling, C., W. Jiang, C.K. Chan, I.L. Weissman, and B.Y.S. Kim, *Breaking Down the Barriers to Precision Cancer Nanomedicine.* Trends in Biotechnology, 2017. **35**(2): p. 159-171.
17. Aaron, C.A., P. Balabhaskar, P. Kapil, and M. Samir, *Clinical and commercial translation of advanced polymeric nanoparticle systems: opportunities and material challenges.* Translational Materials Research, 2017. **4**(1): p. 014001.
18. Portioli, C., M. Bovi, D. Benati, et al., *Novel functionalization strategies of polymeric nanoparticles as carriers for brain medications.* Journal of Biomedical Materials Research - Part A, 2017. **105**(3): p. 847-858.
19. Zhang, G.L., L.K. Chen, X.Y. Guo, et al., *Nanoparticle-mediated Drug Delivery Systems (DDS) in the Central Nervous System.* Current Organic Chemistry, 2017. **21**(3): p. 272-283.
20. Kreuter, J., *Drug delivery to the central nervous system by polymeric nanoparticles: What do we know?* Advanced Drug Delivery Reviews, 2014. **71**: p. 2-14.
21. Alyautdin, R., I. Khalin, M.I. Nafeeza, M.H. Haron, and D. Kuznetsov, *Nanoscale drug delivery systems and the blood-brain barrier.* International Journal of Nanomedicine, 2014. **9**(1): p. 795-811.
22. Johnsen, K.B. and T. Moos, *Revisiting nanoparticle technology for blood-brain barrier transport: Unfolding at the endothelial gate improves the fate of transferrin receptor-targeted liposomes.* Journal of Controlled Release, 2016. **222**: p. 32-46.
23. Gastaldi, L., L. Battaglia, E. Peira, et al., *Solid lipid nanoparticles as vehicles of drugs to the brain: Current state of the art.* European Journal of Pharmaceutics and Biopharmaceutics, 2014. **87**(3): p. 433-444.
24. Song, X.-l., S. Liu, Y. Jiang, et al., *Targeting vincristine plus tetrandrine liposomes modified with DSPE-PEG2000-transferrin in treatment of brain glioma.* European Journal of Pharmaceutical Sciences, 2017. **96**: p. 129-140.
25. Sonali, R.P. Singh, N. Singh, et al., *Transferrin liposomes of docetaxel for brain-targeted cancer applications: formulation and brain theranostics.* Drug Delivery, 2016. **23**(4): p. 1261-1271.
26. Geszke-Moritz, M. and M. Moritz, *Solid lipid nanoparticles as attractive drug vehicles: Composition, properties and therapeutic strategies.* Materials Science and Engineering: C, 2016. **68**: p. 982-994.
27. Jose, S., S.S. Anju, T.A. Cinu, et al., *In vivo pharmacokinetics and biodistribution of resveratrol-loaded solid lipid nanoparticles for brain delivery.* International Journal of Pharmaceutics, 2014. **474**(1): p. 6-13.
28. Kuo, Y.-C. and I.H. Wang, *Enhanced delivery of etoposide across the blood–brain barrier to restrain brain tumor growth using melanotransferrin antibody- and tamoxifen-conjugated solid lipid nanoparticles.* Journal of Drug Targeting, 2016. **24**(7): p. 645-654.
29. Lok, J., P. Gupta, S. Guo, et al., *Cell–cell Signaling in the Neurovascular Unit.* Neurochemical Research, 2007. **32**(12): p. 2032-2045.
30. Hawkins, B.T. and T.P. Davis, *The Blood-Brain Barrier/Neurovascular Unit in Health and Disease.* Pharmacological Reviews, 2005. **57**(2): p. 173-185.
31. Engelhardt, B. and L. Sorokin, *The blood–brain and the blood–cerebrospinal fluid barriers: function and dysfunction.* Seminars in Immunopathology, 2009. **31**(4): p. 497-511.
32. Lochhead, J.J., P.T. Ronaldson, and T.P. Davis, *Hypoxic Stress and Inflammatory Pain Disrupt Blood-Brain Barrier Tight Junctions: Implications for Drug*

Delivery to the Central Nervous System. The AAPS Journal, 2017. **19**(4): p. 910-920.
33. Hancoock, B.M., T.A. Weston, C.W. Renken, and K.S. Doran, *The Role of Astrocytes in Blood-Brain Barrier Function During Bacterial Infection.* The FASEB Journal, 2016. **30**(1 Supplement): p. 1204.3.
34. Hindle, S., R. Munji, E. Dolghih, et al., *Evolutionarily Conserved Roles For Blood-Brain Barrier Xenobiotic Transporters In Endogenous Steroid Partitioning And Behavior.* bioRxiv, 2017.
35. Abbott, N.J. and I.A. Romero, *Transporting therapeutics across the blood-brain barrier.* Molecular Medicine Today, 1996. **2**(3): p. 106-113.
36. Begley, D.J. and M.W. Brightman, *Structural and functional aspects of the blood-brain barrier*, in *Peptide Transport and Delivery into the Central Nervous System*, L. Prokai and K. Prokai-Tatrai, Editors. 2003, Birkhäuser Basel: Basel. p. 39-78.
37. Lalatsa, A., A.G. Schätzlein, and I.F. Uchegbu, *Drug Delivery Across the Blood–Brain Barrier-5.50*. 2011: Elsevier B.V. 657-667.
38. Abbott, N.J., L. Ronnback, and E. Hansson, *Astrocyte-endothelial interactions at the blood-brain barrier.* Nat Rev Neurosci, 2006. **7**(1): p. 41-53.
39. Ballabh, P., A. Braun, and M. Nedergaard, *The blood–brain barrier: an overview: Structure, regulation, and clinical implications.* Neurobiology of Disease, 2004. **16**(1): p. 1-13.
40. Hartsock, A. and W.J. Nelson, *Adherens and tight junctions: Structure, function and connections to the actin cytoskeleton.* Biochimica et Biophysica Acta (BBA) - Biomembranes, 2008. **1778**(3): p. 660-669.
41. Prasad, S. and L. Cucullo, *Pericytes and Astrocytes Crosstalk: Understanding Perivascular Synergism at the BBB.* The FASEB Journal, 2013. **27**(1 Supplement): p. lb720.
42. Armulik, A., G. Genove, M. Mae, et al., *Pericytes regulate the blood-brain barrier.* Nature, 2010. **468**(7323): p. 557-561.
43. Fricker, G. and D.S. Miller, *Modulation of Drug Transporters at the Blood-Brain Barrier.* Pharmacology, 2004. **70**(4): p. 169-176.
44. Rist, R.J., I.A. Romero, M.W.K. Chan, et al., *F-actin cytoskeleton and sucrose permeability of immortalised rat brain microvascular endothelial cell monolayers: effects of cyclic AMP and astrocytic factors.* Brain Research, 1997. **768**(1-2): p. 10-18.
45. Janzer, R.C. and M.C. Raff, *Astrocytes induce blood–brain barrier properties in endothelial cells.* Nature, 1987. **325**(6101): p. 253-257.
46. Abbott, N.J., *Astrocyte-endothelial interactions and blood-brain barrier permeability.* J Anat, 2002. **200**.
47. Arthur, F.E., R.R. Shivers, and P.D. Bowman, *Astrocyte-mediated induction of tight junctions in brain capillary endothelium - an efficient in vitro model.* Developmental Brain Research, 1987. **36**(1): p. 155-159.
48. Lo, E.H. and G.A. Rosenberg, *The Neurovascular Unit in Health and Disease.* Introduction, 2009. **40**(3 suppl 1): p. S2-S3.
49. Pardridge, W.M., *CSF, blood-brain barrier, and brain drug delivery.* Expert Opinion on Drug Delivery, 2016. **13**(7): p. 963-975.
50. Morris, A.W.J., M.M. Sharp, N.J. Albargothy, et al., *Vascular basement membranes as pathways for the passage of fluid into and out of the brain.* Acta Neuropathologica, 2016. **131**(5): p. 725-736.

51. Kapp, E., S.F. Malan, and S.L. Sampson, *Small Molecule Efflux Pump Inhibitors in Mycobacterium tuberculosis: a Rational Drug Design Perspective.* Mini Rev Med Chem, 2017.
52. Fitzpatrick, A.W.P., S. Llabrés, A. Neuberger, et al., *Structure of the MacAB–TolC ABC-type tripartite multidrug efflux pump.* Nature Microbiology, 2017. **2**: p. 17070.
53. Cecchelli, R., V. Berezowski, S. Lundquist, et al., *Modelling of the blood–brain barrier in drug discovery and development.* Nat Rev Drug Discov, 2007. **6**.
54. Chen, Q., L. Jiang, C. Li, et al., *Haemodynamics-Driven Developmental Pruning of Brain Vasculature in Zebrafish.* PLoS Biol, 2012. **10**(8): p. e1001374.
55. Nitta, T., M. Hata, S. Gotoh, et al., *Size-selective loosening of the blood-brain barrier in claudin-5-deficient mice.* J Cell Biol, 2003. **161**.
56. Banks, W.A., *Characteristics of compounds that cross the blood-brain barrier.* BMC Neurology, 2009. **9**(1): p. S3.
57. Yanagida, K., C.H. Liu, G. Faraco, et al., *Size-selective opening of the blood–brain barrier by targeting endothelial sphingosine 1–phosphate receptor 1.* Proceedings of the National Academy of Sciences, 2017. **114**(17): p. 4531-4536.
58. Yin, Y., L. Cao, H. Ge, et al., *L-Borneol induces transient opening of the blood–brain barrier and enhances the therapeutic effect of cisplatin.* NeuroReport, 2017. **28**(9): p. 506-513.
59. Xihui, G., W. Yuan-Cheng, L. Yikang, et al., *Nanoagonist-mediated endothelial tight junction opening: A strategy for safely increasing brain drug delivery in mice.* Journal of Cerebral Blood Flow & Metabolism, 2017. **37**(4): p. 1410-1424.
60. Kuo, Y.C. and P.R. Chou, *Neuroprotection against degeneration of sk-N-mc cells using neuron growth factor-encapsulated liposomes with surface cereport and transferrin.* J Pharm Sci, 2014. **103**(8): p. 2484-97.
61. Wahl, M., L. Schilling, A. Unterberg, and A. Baethmann, *Autacoids as Mediators of Vasogenic Brain Oedema*, in *New Concepts of a Blood—Brain Barrier*, J. Greenwood, D.J. Begley, and M.B. Segal, Editors. 1995, Springer US: Boston, MA. p. 147-157.
62. Mackic, J.B., M. Stins, S. Jovanovic, et al., *Cereport™ (RMP-7) Increases the Permeability of Human Brain Microvascular Endothelial Cell Monolayers1.* Pharmaceutical Research, 1999. **16**(9): p. 1360-1365.
63. Doctrow, S.R., S.M. Abelleira, L.A. Curry, et al., *The bradykinin analog RMP-7 increases intracellular free calcium levels in rat brain microvascular endothelial cells.* Journal of Pharmacology and Experimental Therapeutics, 1994. **271**(1): p. 229-237.
64. Bocsik, A., F.R. Walter, A. Gyebrovszki, et al., *Reversible Opening of Intercellular Junctions of Intestinal Epithelial and Brain Endothelial Cells With Tight Junction Modulator Peptides.* Journal of Pharmaceutical Sciences, 2016. **105**(2): p. 754-765.
65. Deli, M.A., *Potential use of tight junction modulators to reversibly open membranous barriers and improve drug delivery.* Biochimica et Biophysica Acta (BBA) - Biomembranes, 2009. **1788**(4): p. 892-910.
66. Gopalakrishnan, S., N. Pandey, A.P. Tamiz, et al., *Mechanism of action of ZOT-derived peptide AT-1002, a tight junction regulator and absorption enhancer.* International Journal of Pharmaceutics, 2009. **365**(1): p. 121-130.
67. O'Keeffe, E. and M. Campbell, *Modulating the paracellular pathway at the blood–brain barrier: current and future approaches for drug delivery to the CNS.* Drug Discovery Today: Technologies, 2016. **20**: p. 35-39.

68. González-Mariscal, L., Y. Posadas, J. Miranda, et al., *Strategies that Target Tight Junctions for Enhanced Drug Delivery.* Current Pharmaceutical Design, 2016. **22**(35): p. 5313-5346.
69. Tajes, M., E. Ramos-Fernández, X. Weng-Jiang, et al., *The blood-brain barrier: Structure, function and therapeutic approaches to cross it.* Molecular Membrane Biology, 2014. **31**(5): p. 152-167.
70. Stockwell, J., N. Abdi, X. Lu, O. Maheshwari, and C. Taghibiglou, *Novel central nervous system drug delivery systems.* Chemical Biology and Drug Design, 2014. **83**(5): p. 507-520.
71. Lalatsa, A., A.G. Schatzlein, and I.F. Uchegbu, *Strategies to deliver peptide drugs to the brain.* Molecular Pharmaceutics, 2014. **11**(4): p. 1081-1093.
72. Janmey, P.A. and P.K.J. Kinnunen, *Biophysical properties of lipids and dynamic membranes.* Trends in Cell Biology, 2006. **16**(10): p. 538-546.
73. Perisa, D., L. Rohrer, A. Kaech, and A. von Eckardstein, *Itinerary of high density lipoproteins in endothelial cells.* Biochimica et Biophysica Acta (BBA) - Molecular and Cell Biology of Lipids, 2016. **1861**(2): p. 98-107.
74. Clark, D.E., *Rapid calculation of polar molecular surface area and its application to the prediction of transport phenomena. 2. Prediction of blood–brain barrier penetration.* Journal of Pharmaceutical Sciences, 1999. **88**(8): p. 815-821.
75. Loscher, W. and H. Potschka, *Role of drug efflux transporters in the brain for drug disposition and treatment of brain diseases.* Prog Neurobiol, 2005. **76**(1): p. 22 - 76.
76. Begley, D.J., *ABC transporters and the blood-brain barrier.* Curr Pharm Des, 2004. **10**.
77. Miller, D.S., B. Bauer, and A.M.S. Hartz, *Modulation of P-Glycoprotein at the Blood-Brain Barrier: Opportunities to Improve Central Nervous System Pharmacotherapy.* Pharmacological Reviews, 2008. **60**(2): p. 196-209.
78. Kusuhara, H. and Y. Sugiyama, *Efflux transport systems for drugs at the blood–brain barrier and blood–cerebrospinal fluid barrier (Part 1).* Drug Discovery Today, 2001. **6**(3): p. 150-156.
79. Van Vliet, E.A., R. Van Schaik, P.M. Edelbroek, et al., *Inhibition of the Multidrug Transporter P-Glycoprotein Improves Seizure Control in Phenytoin-treated Chronic Epileptic Rats.* Epilepsia, 2006. **47**(4): p. 672-680.
80. Monica, A.S., J.L. Moore, and W.M. James, *Use of Verapamil as a Potential P-Glycoprotein Inhibitor in a Patient with Refractory Epilepsy.* Annals of Pharmacotherapy, 2004. **38**(10): p. 1631-1634.
81. Pettersson, M., X. Hou, M. Kuhn, et al., *Quantitative Assessment of the Impact of Fluorine Substitution on P-Glycoprotein (P-gp) Mediated Efflux, Permeability, Lipophilicity, and Metabolic Stability.* Journal of Medicinal Chemistry, 2016. **59**(11): p. 5284-5296.
82. Wood, W.G., W.E. Mőller, and G.P. Eckert, *Statins and Neuroprotection: Basic Pharmacology Needed.* Molecular Neurobiology, 2014. **50**(1): p. 214-220.
83. Auclair, D., J.J. Hopwood, D.A. Brooks, J.F. Lemontt, and A.C. Crawley, *Replacement therapy for mucopolysaccharidosis type VI: advantages of early onset of therapy.* Mol Genet Metab, 2003. **78**.
84. Jackson, S., N.M. Anders, A. Mangraviti, et al., *The effect of regadenoson-induced transient disruption of the blood–brain barrier on temozolomide delivery to normal rat brain.* Journal of Neuro-Oncology, 2016. **126**(3): p. 433-439.

85. Portnow, J., B. Badie, M. Chen, et al., *The Neuropharmacokinetics of Temozolomide in Patients with Resectable Brain Tumors: Potential Implications for the Current Approach to Chemoradiation.* Clinical Cancer Research, 2009. **15**(22): p. 7092-7098.
86. Buhr, C., M. Gössl, R. Erbel, and H. Eggebrecht, *Regadenoson in the detection of coronary artery disease.* Vascular Health and Risk Management, 2008. **4**(2): p. 337-340.
87. Banks, W.A., *From blood-brain barrier to blood-brain interface: New opportunities for CNS drug delivery.* Nature Reviews Drug Discovery, 2016. **15**(4): p. 275-292.
88. Nicita, F., A. Spalice, L. Papetti, et al., *Efficacy of verapamil as an adjunctive treatment in children with drug-resistant epilepsy: A pilot study.* Seizure, 2014. **23**(1): p. 36-40.
89. Gao, B., S.R. Vavricka, P.J. Meier, and B. Stieger, *Differential cellular expression of organic anion transporting peptides OATP1A2 and OATP2B1 in the human retina and brain: implications for carrier-mediated transport of neuropeptides and neurosteriods in the CNS.* Pflügers Archiv - European Journal of Physiology, 2015. **467**(7): p. 1481-1493.
90. Storga, D., K. Vrecko, J.G.D. Birkmayer, and G. Reibnegger, *Monoaminergic neurotransmitters, their precursors and metabolites in brains of Alzheimer patients.* Neuroscience Letters, 1996. **203**(1): p. 29-32.
91. Wurtman, R.J., F. Hefti, and E. Melamed, *Precursor control of neurotransmitter synthesis.* Pharmacological Reviews, 1980. **32**(4): p. 315-335.
92. Suarez, L.M., O. Solis, C. Aguado, R. Lujan, and R. Moratalla, *L-DOPA Oppositely Regulates Synaptic Strength and Spine Morphology in D1 and D2 Striatal Projection Neurons in Dyskinesia.* Cerebral Cortex, 2016. **26**(11): p. 4253-4264.
93. Miguelez, C., S. Navailles, P. De Deurwaerdère, and L. Ugedo, *The acute and long-term L-DOPA effects are independent from changes in the activity of dorsal raphe serotonergic neurons in 6-OHDA lesioned rats.* British Journal of Pharmacology, 2016. **173**(13): p. 2135-2146.
94. Schlagenhauf, F., Q.J.M. Huys, L. Deserno, et al., *Striatal dysfunction during reversal learning in unmedicated schizophrenia patients.* NeuroImage, 2014. **89**(Supplement C): p. 171-180.
95. Kim, H.K., A.C. Andreazza, P.Y. Yeung, C. Isaacs-Trepanier, and L.T. Young, *Oxidation and nitration in dopaminergic areas of the prefrontal cortex from patients with bipolar disorder and schizophrenia.* Journal of Psychiatry & Neuroscience : JPN, 2014. **39**(4): p. 276-285.
96. Pincus, J.H. and K. Barry, *Protein redistribution diet restores motor function in patients with dopa-resistant "off" periods.* Neurology, 1988. **38**(3): p. 481-3.
97. Agus, D.B., S.S. Gambhir, W.M. Pardridge, et al., *Vitamin C crosses the blood-brain barrier in the oxidized form through the glucose transporters.* Journal of Clinical Investigation, 1997. **100**(11): p. 2842-2848.
98. Halmos, T., M. Santarromana, K. Antonakis, and D. Scherman, *Synthesis of glucose-chlorambucil derivatives and their recognition by the human GLUT1 glucose transporter.* European Journal of Pharmacology, 1996. **318**(2): p. 477-484.
99. Betzer, O., N. Perets, A. Angel, et al., *In Vivo Neuroimaging of Exosomes Using Gold Nanoparticles.* ACS Nano, 2017. **11**(11): p. 10883-10893.

100. Patching, S.G., *Glucose Transporters at the Blood-Brain Barrier: Function, Regulation and Gateways for Drug Delivery.* Molecular Neurobiology, 2017. **54**(2): p. 1046-1077.
101. Zhang, T.T., W. Li, G. Meng, P. Wang, and W. Liao, *Strategies for transporting nanoparticles across the blood-brain barrier.* Biomaterials Science, 2016. **4**(2): p. 219-229.
102. Pardridge, W.M., *Blood-brain barrier transport of nutrients.* Nutrition Reviews, 1986. **44 Suppl**: p. 15-25.
103. MOUSAVI, S.A., L. MALERØD, T. BERG, and R. KJEKEN, *Clathrin-dependent endocytosis.* Biochemical Journal, 2004. **377**(1): p. 1-16.
104. Abbott, N.J., A.A.K. Patabendige, D.E.M. Dolman, S.R. Yusof, and D.J. Begley, *Structure and function of the blood-brain barrier.* Neurobiology of Disease, 2010. **37**(1): p. 13-25.
105. Pardridge, W.M., *Receptor-mediated peptide transport through the blood-brain barrier.* Endocrine Reviews, 1986. **7**(3): p. 314-330.
106. Pardridge, W.M., *Molecular Trojan horses for blood-brain barrier drug delivery.* Discovery medicine, 2006. **6**(34): p. 139-143.
107. Pardridge, W.M., *Blood-brain barrier delivery.* Drug Discovery Today, 2007. **12**(1-2): p. 54-61.
108. Huwyler, J. and W.M. Pardridge, *Examination of blood-brain barrier transferrin receptor by confocal fluorescent microscopy of unfixed isolated rat brain capillaries.* Journal of Neurochemistry, 1998. **70**(2): p. 883-886.
109. Pardridge, W.M., *Strategies for Delivery of Drugs Through the Blood-Brain Barrier*, in *Annual Reports in Medicinal Chemistry*. 1985. p. 305-313.
110. Skarlatos, S., T. Yoshikawa, and W.M. Pardridge, *Transport of [125I]transferrin through the rat blood-brain barrier.* Brain Research, 1995. **683**(2): p. 164-171.
111. Yemisci, M., S. Caban, E. Fernandez-Megia, et al., *Preparation and Characterization of Biocompatible Chitosan Nanoparticles for Targeted Brain Delivery of Peptides*, in *Neurotrophic Factors: Methods and Protocols*, S.D. Skaper, Editor. 2018, Springer New York: New York, NY. p. 443-454.
112. Chow, B.W. and C. Gu, *The Molecular Constituents of the Blood–Brain Barrier.* Trends in Neurosciences, 2015. **38**(10): p. 598-608.
113. Masliah, E. and B. Spencer, *Overcoming the Obstacle of the Blood–Brain Barrier for Delivery of Alzheimer's Disease Therapeutics*, in *Protein Folding Disorders of the Central Nervous System*. 2017, WORLD SCIENTIFIC. p. 249-265.
114. Molino, Y., M. David, K. Varini, et al., *Use of LDL receptor–targeting peptide vectors for in vitro and in vivo cargo transport across the blood-brain barrier.* The FASEB Journal, 2017. **31**(5): p. 1807-1827.
115. Grabrucker, A.M., B. Ruozi, D. Belletti, et al., *Nanoparticle transport across the blood brain barrier.* Tissue Barriers, 2016. **4**(1): p. 18.
116. Chhabra, R., B. Ruozi, A. Vilella, et al., *Application of polymeric nanoparticles for CNS targeted zinc delivery in vivo.* CNS and Neurological Disorders - Drug Targets, 2015. **14**(8): p. 1041-1053.
117. Abbott, N.J., *Physiology of the blood-brain barrier and its consequences for drug transport to the brain*, in *International Congress Series*. 2005. p. 3-18.
118. Tsuji, A. and I. Tamai, *Carrier-mediated or specialized transport of drugs across the blood–brain barrier.* Advanced Drug Delivery Reviews, 1999. **36**(2–3): p. 277-290.

119. Pardridge, W.M., *Transport of small molecules through the blood-brain barrier: biology and methodology.* Advanced Drug Delivery Reviews, 1995. **15**(1): p. 5-36.
120. Terasaki, T., S. Takakuwa, A. Saheki, et al., *Absorptive-Mediated Endocytosis of an Adrenocorticotropic Hormone (ACTH) Analogue, Ebiratide, into the Blood–Brain Barrier: Studies with Monolayers of Primary Cultured Bovine Brain Capillary Endothelial Cells.* Pharmaceutical Research, 1992. **9**(4): p. 529-534.
121. Terasaki, T. and W.M. Pardridge, *Preface: Targeted drug delivery to the brain (blood-brain barrier, efflux, endothelium, biological transport).* Journal of Drug Targeting, 2000. **8**(6): p. 353-355.
122. Glascock, J.J., E.Y. Osman, T.H. Coady, et al., *Delivery of Therapeutic Agents Through Intracerebroventricular (ICV) and Intravenous (IV) Injection in Mice.* Journal of Visualized Experiments : JoVE, 2011(56): p. 2968.
123. Louveau, A., I. Smirnov, T.J. Keyes, et al., *Structural and functional features of central nervous system lymphatic vessels.* Nature, 2015. **523**: p. 337.
124. Kim, H.S., N.K. Lee, D. Yoo, et al., *Lowering the concentration affects the migration and viability of intracerebroventricular-delivered human mesenchymal stem cells.* Biochemical and Biophysical Research Communications, 2017. **493**(1): p. 751-757.
125. Souza, L.C., C.R. Jesse, M.S. Antunes, et al., *Indoleamine-2,3-dioxygenase mediates neurobehavioral alterations induced by an intracerebroventricular injection of amyloid-β1-42 peptide in mice.* Brain, Behavior, and Immunity, 2016. **56**(Supplement C): p. 363-377.
126. Shultz, S.R., N.A.B. Aziz, L. Yang, et al., *Intracerebroventricular injection of propionic acid, an enteric metabolite implicated in autism, induces social abnormalities that do not differ between seizure-prone (FAST) and seizure-resistant (SLOW) rats.* Behavioural Brain Research, 2015. **278**(Supplement C): p. 542-548.
127. Yan, X.-g., B.-h. Cheng, X. Wang, et al., *Lateral intracerebroventricular injection of Apelin-13 inhibits apoptosis after cerebral ischemia/reperfusion injury.* Neural Regeneration Research, 2015. **10**(5): p. 766-771.
128. Scarlett, J.M., J.M. Rojas, M.E. Matsen, et al., *Central injection of fibroblast growth factor 1 induces sustained remission of diabetic hyperglycemia in rodents.* Nature Medicine, 2016. **22**: p. 800.
129. Suzuki, S., A.J. Li, T. Akaike, and T. Imamura, *Intracerebroventricular infusion of fibroblast growth factor-1 increases Fos immunoreactivity in periventricular astrocytes in rat hypothalamus.* Neurosci Lett, 2001. **300**(1): p. 29-32.
130. Zhang, C., J. Chen, C. Feng, et al., *Intranasal nanoparticles of basic fibroblast growth factor for brain delivery to treat Alzheimer's disease.* International Journal of Pharmaceutics, 2014. **461**(1): p. 192-202.
131. Zhao, Y.-Z., M. Lin, Q. Lin, et al., *Intranasal delivery of bFGF with nanoliposomes enhances in vivo neuroprotection and neural injury recovery in a rodent stroke model.* Journal of Controlled Release, 2016. **224**(Supplement C): p. 165-175.
132. Wang, P., Y. Xue, X. Shang, and Y. Liu, *Diphtheria Toxin Mutant CRM197-Mediated Transcytosis across Blood–Brain Barrier In Vitro.* Cellular and Molecular Neurobiology, 2010. **30**(5): p. 717-725.
133. Bao, X., I. Pastan, D.D. Bigner, and V. Chandramohan, *EGFR/EGFRvIII-targeted immunotoxin therapy for the treatment of glioblastomas via convection-enhanced delivery.* Receptors & clinical investigation, 2016. **3**(4): p. e1430.

134. Azar, J., J. Elacqua, D. Peñaranda, and A. Stone, *Modeling Carmustine Diffusion from Gliadel® Wafers in the Brain to Optimize Cancer Treatment and Minimize Damage to Healthy Tissue.* 2016.
135. Gey, L., M. Gernert, and W. Löscher, *Continuous bilateral infusion of vigabatrin into the subthalamic nucleus: Effects on seizure threshold and GABA metabolism in two rat models.* Neurobiology of Disease, 2016. **91**: p. 194-208.
136. Dill, P., A.N. Datta, P. Weber, and J. Schneider, *Are vigabatrin induced T2 hyperintensities in cranial MRI associated with acute encephalopathy and extrapyramidal symptoms?* European Journal of Paediatric Neurology, 2013. **17**(3): p. 311-315.
137. Pardridge, W.M., *The Blood-Brain Barrier: Bottleneck in Brain Drug Development.* NeuroRX, 2005. **2**(1): p. 3-14.
138. Gangwar, R., A.S. Meena, P.K. Shukla, et al., *Calcium-mediated oxidative stress: a common mechanism in tight junction disruption by different types of cellular stress.* Biochemical Journal, 2017. **474**(5): p. 731-749.
139. Meena, A.S., R. Gangwar, P.K. Shukla, et al., *Ca2+-Induced Mitochondrial Oxidative Stress Mediates Disruption of Intestinal Epithelial Tight Junction: Activation of a Similar Signaling Cascade in Colon by Chronic Restraint Stress.* The FASEB Journal, 2016. **30**(1 Supplement): p. 1250.8.
140. Chakraborty, S., C.G. Filippi, T. Wong, et al., *Superselective intraarterial cerebral infusion of cetuximab after osmotic blood/brain barrier disruption for recurrent malignant glioma: phase I study.* Journal of Neuro-Oncology, 2016. **128**(3): p. 405-415.
141. McGregor, J.M., S.D. Bell, N.D. Doolittle, T.P. Murillo, and E.A. Neuwelt, *Chapter 10 - Blood-Brain Barrier Disruption Chemotherapy A2 - Newton, Herbert B,* in *Handbook of Brain Tumor Chemotherapy, Molecular Therapeutics, and Immunotherapy (Second Edition)*. 2018, Academic Press. p. 145-153.
142. Saunders, N.R., M.D. Habgood, K. Møllgård, and K.M. Dziegielewska, *The biological significance of brain barrier mechanisms: Help or hindrance in drug delivery to the central nervous system?* F1000Research, 2016. **5**.
143. Zhou, J., K.-B. Atsina, B.T. Himes, G.W. Strohbehn, and W.M. Saltzman, *Novel Delivery Strategies for Glioblastoma.* Cancer journal (Sudbury, Mass.), 2012. **18**(1): p. 10.1097/PPO.0b013e318244d8ae.
144. Sampson, J.H., G. Akabani, G.E. Archer, et al., *Intracerebral infusion of an EGFR-targeted toxin in recurrent malignant brain tumors.* Neuro-Oncology, 2008. **10**(3): p. 320-329.
145. Lam, M.F., M.G. Thomas, and C.R.P. Lind, *Neurosurgical convection-enhanced delivery of treatments for Parkinson's disease.* Journal of Clinical Neuroscience, 2011. **18**(9): p. 1163-1167.
146. Stiles, D.K., Z. Zhang, P. Ge, et al., *Widespread suppression of huntingtin with convection-enhanced delivery of siRNA.* Experimental Neurology, 2012. **233**(1): p. 463-471.
147. Carlos, S., A. Camilo, C. Cherry, et al., *Lipid microbubbles as a vehicle for targeted drug delivery using focused ultrasound-induced blood–brain barrier opening.* Journal of Cerebral Blood Flow & Metabolism, 2017. **37**(4): p. 1236-1250.
148. Wu, S.-K., P.-C. Chu, W.-Y. Chai, et al., *Characterization of Different Microbubbles in Assisting Focused Ultrasound-Induced Blood-Brain Barrier Opening.* Scientific Reports, 2017. **7**: p. 46689.

149. Sheikov, N., N. McDannold, N. Vykhodtseva, F. Jolesz, and K. Hynynen, *Cellular mechanisms of the blood-brain barrier opening induced by ultrasound in presence of microbubbles.* Ultrasound Med Biol, 2004. **30**(7): p. 979-89.
150. Hynynen, K., N. McDannold, N. Vykhodtseva, and F.A. Jolesz, *Noninvasive MR imaging-guided focal opening of the blood-brain barrier in rabbits.* Radiology, 2001. **220**(3): p. 640-6.
151. Vykhodtseva, N.I., K. Hynynen, and C. Damianou, *Histologic effects of high intensity pulsed ultrasound exposure with subharmonic emission in rabbit brain in vivo.* Ultrasound Med Biol, 1995. **21**(7): p. 969-79.
152. Wang, F., Y. Cheng, J. Mei, et al., *Focused ultrasound microbubble destruction-mediated changes in blood-brain barrier permeability assessed by contrast-enhanced magnetic resonance imaging.* J Ultrasound Med, 2009. **28**(11): p. 1501-9.
153. Fan, C.-H., C.-Y. Ting, H.-J. Lin, et al., *SPIO-conjugated, doxorubicin-loaded microbubbles for concurrent MRI and focused-ultrasound enhanced brain-tumor drug delivery.* Biomaterials, 2013. **34**(14): p. 3706-3715.
154. Niu, C., Z. Wang, G. Lu, et al., *Doxorubicin loaded superparamagnetic PLGA-iron oxide multifunctional microbubbles for dual-mode US/MR imaging and therapy of metastasis in lymph nodes.* Biomaterials, 2013. **34**(9): p. 2307-2317.
155. Kheirolomoom, A., P.A. Dayton, A.F.H. Lum, et al., *Acoustically-active microbubbles conjugated to liposomes: Characterization of a proposed drug delivery vehicle.* Journal of Controlled Release, 2007. **118**(3): p. 275-284.
156. Yue, P., L. Gao, X. Wang, X. Ding, and J. Teng, *Ultrasound-triggered effects of the microbubbles coupled to GDNF- and Nurr1-loaded PEGylated liposomes in a rat model of Parkinson's disease.* Journal of Cellular Biochemistry, 2018. **0**(0).
157. Dasgupta, A., M. Liu, T. Ojha, et al., *Ultrasound-mediated drug delivery to the brain: principles, progress and prospects.* Drug Discovery Today: Technologies, 2016. **20**(Supplement C): p. 41-48.
158. Yang, F.-Y., W.-M. Fu, W.-S. Chen, W.-L. Yeh, and W.-L. Lin, *Quantitative evaluation of the use of microbubbles with transcranial focused ultrasound on blood–brain-barrier disruption.* Ultrasonics Sonochemistry, 2008. **15**(4): p. 636-643.
159. Samiotaki, G., F. Vlachos, Y.-S. Tung, and E.E. Konofagou, *A quantitative pressure and microbubble-size dependence study of focused ultrasound-induced blood-brain barrier opening reversibility in vivo using MRI.* Magnetic Resonance in Medicine, 2012. **67**(3): p. 769-777.
160. Cho, H., H.-Y. Lee, M. Han, et al., *Localized Down-regulation of P-glycoprotein by Focused Ultrasound and Microbubbles induced Blood-Brain Barrier Disruption in Rat Brain.* Scientific Reports, 2016. **6**: p. 31201.
161. Kinoshita, M., N. McDannold, F.A. Jolesz, and K. Hynynen, *Noninvasive localized delivery of Herceptin to the mouse brain by MRI-guided focused ultrasound-induced blood–brain barrier disruption.* Proceedings of the National Academy of Sciences, 2006. **103**(31): p. 11719-11723.
162. Wei, K.-C., P.-C. Chu, H.-Y.J. Wang, et al., *Focused Ultrasound-Induced Blood–Brain Barrier Opening to Enhance Temozolomide Delivery for Glioblastoma Treatment: A Preclinical Study.* PLOS ONE, 2013. **8**(3): p. e58995.
163. Jordão, J.F., E. Thévenot, K. Markham-Coultes, et al., *Amyloid-β plaque reduction, endogenous antibody delivery and glial activation by brain-targeted, transcranial focused ultrasound.* Experimental Neurology, 2013. **248**(Supplement C): p. 16-29.

164. Park, J., Y. Zhang, N. Vykhodtseva, F.A. Jolesz, and N.J. McDannold, *The kinetics of blood brain barrier permeability and targeted doxorubicin delivery into brain induced by focused ultrasound.* Journal of Controlled Release, 2012. **162**(1): p. 134-142.
165. Zhang, J.Y., J.F. Diao, Q.L. Lü, and C.Y. Wu, *Research progress in in vitro models for assessing drug transport across blood-brain barrier.* Chinese Journal of New Drugs, 2015. **24**(21): p. 2453-2458.
166. Vukelja, S.J., S.P. Anthony, J.C. Arseneau, et al., *Phase 1 study of escalating-dose OncoGel (ReGel/paclitaxel) depot injection, a controlled-release formulation of paclitaxel, for local management of superficial solid tumor lesions.* Anticancer Drugs, 2007. **18**(3): p. 283-9.
167. DiMeco, F., K.W. Li, B.M. Tyler, et al., *Local delivery of mitoxantrone for the treatment of malignant brain tumors in rats.* J Neurosurg, 2002. **97**(5): p. 1173-8.
168. Craft, S., L.D. Baker, T.J. Montine, and et al., *Intranasal insulin therapy for alzheimer disease and amnestic mild cognitive impairment: A pilot clinical trial.* Archives of Neurology, 2012. **69**(1): p. 29-38.
169. Vlieghe, P. and M. Khrestchatisky, *Medicinal Chemistry Based Approaches and Nanotechnology-Based Systems to Improve CNS Drug Targeting and Delivery.* Medicinal Research Reviews, 2013. **33**(3): p. 457-516.
170. Peura, L., K. Malmioja, K. Laine, et al., *Large Amino Acid Transporter 1 (LAT1) Prodrugs of Valproic Acid: New Prodrug Design Ideas for Central Nervous System Delivery.* Molecular Pharmaceutics, 2011. **8**(5): p. 1857-1866.
171. Pardridge, W.M., *CNS drug design based on principles of blood-brain barrier transport.* Journal of Neurochemistry, 1998. **70**(5): p. 1781-1792.
172. Hersh, D.S., A.S. Wadajkar, N.B. Roberts, et al., *Evolving drug delivery strategies to overcome the blood brain barrier.* Current Pharmaceutical Design, 2016. **22**(9): p. 1177-1193.
173. Bohn, K., A. Lange, J. Chmielewski, and C.A. Hrycyna, *Dual Modulation of Human P-Glycoprotein and ABCG2 with Prodrug Dimers of the Atypical Antipsychotic Agent Paliperidone in a Model of the Blood–Brain Barrier.* Molecular Pharmaceutics, 2017. **14**(4): p. 1107-1119.
174. Placzek, A.T., S.J. Ferrara, M.D. Hartley, et al., *Sobetirome prodrug esters with enhanced blood–brain barrier permeability.* Bioorganic & Medicinal Chemistry, 2016. **24**(22): p. 5842-5854.
175. Chapman, C.D., W.H. Frey, S. Craft, et al., *Intranasal Treatment of Central Nervous System Dysfunction in Humans.* Pharmaceutical Research, 2013. **30**(10): p. 2475-2484.
176. Lochhead, J.J. and R.G. Thorne, *Intranasal Drug Delivery to the Brain*, in *Drug Delivery to the Brain: Physiological Concepts, Methodologies and Approaches*, M. Hammarlund-Udenaes, E.C.M. de Lange, and R.G. Thorne, Editors. 2014, Springer New York: New York, NY. p. 401-431.
177. Kojima, T., M. Kondoh, T. Keira, et al., *Claudin-binder C-CPE mutants enhance permeability of insulin across human nasal epithelial cells.* Drug Delivery, 2016. **23**(8): p. 2703-2710.
178. Hölscher, C., *First clinical data of the neuroprotective effects of nasal insulin application in patients with Alzheimer's disease.* Alzheimer's & Dementia, 2014. **10**(1, Supplement): p. S33-S37.

179. Rosenbloom, M.H., T.R. Barclay, M. Pyle, et al., *A Single-Dose Pilot Trial of Intranasal Rapid-Acting Insulin in Apolipoprotein E4 Carriers with Mild–Moderate Alzheimer's Disease.* CNS Drugs, 2014. **28**(12): p. 1185-1189.
180. Shah, R.B., M. Patel, D.M. Maahs, and V.N. Shah, *Insulin delivery methods: Past, present and future.* International Journal of Pharmaceutical Investigation, 2016. **6**(1): p. 1-9.
181. Illum, L., *Nasal drug delivery — Recent developments and future prospects.* Journal of Controlled Release, 2012. **161**(2): p. 254-263.
182. Robert, S., M. Thomas, S. Leon, M. Michael, and S. Poul, *Comparison Pharmacokinetics of Two Concentrations (0.7% and 1.0%) of Nasulin™, an Ultra-Rapid-Acting Intranasal Insulin Formulation.* Journal of Diabetes Science and Technology, 2010. **4**(3): p. 603-609.
183. Benedict, C., W.H. Frey Ii, H.B. Schiöth, et al., *Intranasal insulin as a therapeutic option in the treatment of cognitive impairments.* Experimental Gerontology, 2011. **46**(2–3): p. 112-115.
184. Appu, A.P., P. Arun, J.K.S. Krishnan, J.R. Moffett, and A.M.A. Namboodiri, *Rapid intranasal delivery of chloramphenicol acetyltransferase in the active form to different brain regions as a model for enzyme therapy in the CNS.* Journal of Neuroscience Methods, 2016. **259**: p. 129-134.
185. Djupesland, P.G., *Nasal drug delivery devices: characteristics and performance in a clinical perspective—a review.* Drug Delivery and Translational Research, 2013. **3**(1): p. 42-62.
186. Soane, R.J., M. Frier, A.C. Perkins, et al., *Evaluation of the clearance characteristics of bioadhesive systems in humans.* International Journal of Pharmaceutics, 1999. **178**(1): p. 55-65.
187. Neutra, M.R. and P.A. Kozlowski, *Mucosal vaccines: the promise and the challenge.* Nat Rev Immunol, 2006. **6**(2): p. 148-158.
188. Holmgren, J., C. Czerkinsky, K. Eriksson, and A. Mharandi, *Mucosal immunisation and adjuvants: a brief overview of recent advances and challenges.* Vaccine, 2003. **21**: p. S89-S95.
189. Illum, L., *Nasal drug delivery—possibilities, problems and solutions.* Journal of Controlled Release, 2003. **87**(1): p. 187-198.
190. Vilella, A., G. Tosi, A.M. Grabrucker, et al., *Insight on the fate of CNS-targeted nanoparticles. Part I: Rab5-dependent cell-specific uptake and distribution.* Journal of Controlled Release, 2014. **174**(0): p. 195-201.
191. Li, H., T.Y. Tsui, and W. Ma, *Intracellular delivery of molecular cargo using cell-penetrating peptides and the combination strategies.* International Journal of Molecular Sciences, 2015. **16**(8): p. 19518-19536.
192. Kreuter, J., *Mechanism of polymeric nanoparticle-based drug transport across the blood-brain barrier (BBB).* Journal of Microencapsulation, 2013. **30**(1): p. 49-54.
193. Zhang, L., F.X. Gu, J.M. Chan, et al., *Nanoparticles in Medicine: Therapeutic Applications and Developments.* Clinical Pharmacology & Therapeutics, 2008. **83**(5): p. 761-769.
194. Zhong, J., S. Yang, L. Wen, and D. Xing, *Imaging-guided photoacoustic drug release and synergistic chemo-photoacoustic therapy with paclitaxel-containing nanoparticles.* Journal of Controlled Release, 2016. **226**(Supplement C): p. 77-87.
195. Lei, Y., Y. Hamada, J. Li, et al., *Targeted tumor delivery and controlled release of neuronal drugs with ferritin nanoparticles to regulate pancreatic cancer*

progression. Journal of Controlled Release, 2016. **232**(Supplement C): p. 131-142.
196. Deng, R., M.J. Derry, C.J. Mable, Y. Ning, and S.P. Armes, *Using Dynamic Covalent Chemistry To Drive Morphological Transitions: Controlled Release of Encapsulated Nanoparticles from Block Copolymer Vesicles.* Journal of the American Chemical Society, 2017. **139**(22): p. 7616-7623.
197. Yu, E., A. Lo, L. Jiang, et al., *Improved controlled release of protein from expanded-pore mesoporous silica nanoparticles modified with co-functionalized poly(n-isopropylacrylamide) and poly(ethylene glycol) (PNIPAM-PEG).* Colloids and Surfaces B: Biointerfaces, 2017. **149**(Supplement C): p. 297-300.
198. Liu, R., S. Wang, S. Fang, et al., *Liquid Crystalline Nanoparticles as an Ophthalmic Delivery System for Tetrandrine: Development, Characterization, and In Vitro and In Vivo Evaluation.* Nanoscale Research Letters, 2016. **11**(1): p. 254.
199. Serna, N., M.V. Céspedes, P. Saccardo, et al., *Rational engineering of single-chain polypeptides into protein-only, BBB-targeted nanoparticles.* Nanomedicine: Nanotechnology, Biology and Medicine, 2016. **12**(5): p. 1241-1251.
200. Cao, Z.-T., Z.-Y. Chen, C.-Y. Sun, et al., *Overcoming tumor resistance to cisplatin by cationic lipid-assisted prodrug nanoparticles.* Biomaterials, 2016. **94**(Supplement C): p. 9-19.
201. Byeon, H.J., L.Q. Thao, S. Lee, et al., *Doxorubicin-loaded nanoparticles consisted of cationic- and mannose-modified-albumins for dual-targeting in brain tumors.* Journal of Controlled Release, 2016. **225**(Supplement C): p. 301-313.
202. Monaco, I., F. Arena, S. Biffi, et al., *Synthesis of Lipophilic Core–Shell Fe3O4@SiO2@Au Nanoparticles and Polymeric Entrapment into Nanomicelles: A Novel Nanosystem for in Vivo Active Targeting and Magnetic Resonance–Photoacoustic Dual Imaging.* Bioconjugate Chemistry, 2017. **28**(5): p. 1382-1390.
203. Kim, D.-H. and D.C. Martin, *Sustained release of dexamethasone from hydrophilic matrices using PLGA nanoparticles for neural drug delivery.* Biomaterials, 2006. **27**(15): p. 3031-3037.
204. Ghosh, A., A.K. Mandal, S. Sarkar, S. Panda, and N. Das, *Nanoencapsulation of quercetin enhances its dietary efficacy in combating arsenic-induced oxidative damage in liver and brain of rats.* Life Sciences, 2009. **84**(3–4): p. 75-80.
205. Ruozi, B., D. Belletti, H.S. Sharma, et al., *PLGA Nanoparticles Loaded Cerebrolysin: Studies on Their Preparation and Investigation of the Effect of Storage and Serum Stability with Reference to Traumatic Brain Injury.* Molecular Neurobiology, 2015. **52**(2): p. 899-912.
206. Kreuter, J., R.N. Alyautdin, D.A. Kharkevich, and A.A. Ivanov, *Passage of peptides through the blood-brain barrier with colloidal polymer particles (nanoparticles).* Brain Research, 1995. **674**(1): p. 171-174.
207. Trapani, A., N. Denora, G. Iacobellis, et al., *Methotrexate-Loaded Chitosan- and Glycolchitosan-Based Nanoparticles: A Promising Strategy for the Administration of the Anticancer Drug to Brain Tumors.* AAPS PharmSciTech, 2011. **12**(4): p. 1302-1311.
208. Kuroda, J.-i., J.-i. Kuratsu, M. Yasunaga, et al., *Antitumor Effect of NK012, a 7-Ethyl-10-Hydroxycamptothecin–Incorporating Polymeric Micelle, on U87MG Orthotopic Glioblastoma in Mice Compared with Irinotecan Hydrochloride in*

Combination with Bevacizumab. Clinical Cancer Research, 2010. **16**(2): p. 521-529.
209. Liu, H., J. Ni, and R. Wang, *In vitro release performance and analgesic activity of endomorphin-1 loaded nanoparticles.* Pharmazie, 2006. **61**(5): p. 450-452.
210. Alyautdin, R., V. Petrov, K. Langer, et al., *Delivery of Loperamide Across the Blood-Brain Barrier with Polysorbate 80-Coated Polybutylcyanoacrylate Nanoparticles.* Pharmaceutical Research, 1997. **14**(3): p. 325-328.
211. Bobo, D., K.J. Robinson, J. Islam, K.J. Thurecht, and S.R. Corrie, *Nanoparticle-Based Medicines: A Review of FDA-Approved Materials and Clinical Trials to Date.* Pharmaceutical Research, 2016. **33**(10): p. 2373-2387.
212. Wohlfart, S., A.S. Khalansky, S. Gelperina, D. Begley, and J. Kreuter, *Kinetics of transport of doxorubicin bound to nanoparticles across the blood–brain barrier.* Journal of Controlled Release, 2011. **154**(1): p. 103-107.
213. Wohlfart, S., A.S. Khalansky, S. Gelperina, et al., *Efficient Chemotherapy of Rat Glioblastoma Using Doxorubicin-Loaded PLGA Nanoparticles with Different Stabilizers.* PLoS ONE, 2011. **6**(5): p. e19121.
214. Wang, C.-X., L.-S. Huang, L.-B. Hou, et al., *Antitumor effects of polysorbate-80 coated gemcitabine polybutylcyanoacrylate nanoparticles in vitro and its pharmacodynamics in vivo on C6 glioma cells of a brain tumor model.* Brain Research, 2009. **1261**: p. 91-99.
215. Wilson, B., M.K. Samanta, K. Santhi, et al., *Poly(n-butylcyanoacrylate) nanoparticles coated with polysorbate 80 for the targeted delivery of rivastigmine into the brain to treat Alzheimer's disease.* Brain Research, 2008. **1200**: p. 159-168.
216. Albertazzi, L., L. Gherardini, M. Brondi, et al., *In Vivo Distribution and Toxicity of PAMAM Dendrimers in the Central Nervous System Depend on Their Surface Chemistry.* Molecular Pharmaceutics, 2013. **10**(1): p. 249-260.
217. Yan, H., J. Wang, P. Yi, et al., *Imaging brain tumor by dendrimer-based optical/paramagnetic nanoprobe across the blood-brain barrier.* Chemical Communications, 2011. **47**(28): p. 8130-8132.
218. Clemons, K.V., R.A. Sobel, P.L. Williams, D. Pappagianis, and D.A. Stevens, *Efficacy of Intravenous Liposomal Amphotericin B (AmBisome) against Coccidioidal Meningitis in Rabbits.* Antimicrobial Agents and Chemotherapy, 2002. **46**(8): p. 2420-2426.
219. Groll, A.H., N. Giri, V. Petraitis, et al., *Comparative Efficacy and Distribution of Lipid Formulations of Amphotericin B in Experimental Candida albicans Infection of the Central Nervous System.* The Journal of Infectious Diseases, 2000. **182**(1): p. 274-282.
220. Takemoto, K., Y. Yamamoto, and Y. Ueda, *Influence of the Progression of Cryptococcal Meningitis on Brain Penetration and Efficacy of AmBisome in a Murine Model.* Chemotherapy, 2006. **52**(6): p. 271-278.
221. Agarwal, A., H. Agrawal, S. Tiwari, S. Jain, and G.P. Agrawal, *Cationic ligand appended nanoconstructs: A prospective strategy for brain targeting.* International Journal of Pharmaceutics, 2011. **421**(1): p. 189-201.
222. Chattopadhyay, N., J. Zastre, H.-L. Wong, X.Y. Wu, and R. Bendayan, *Solid Lipid Nanoparticles Enhance the Delivery of the HIV Protease Inhibitor, Atazanavir, by a Human Brain Endothelial Cell Line.* Pharmaceutical Research, 2008. **25**(10): p. 2262-2271.

223. Gupta, Y., A. Jain, and S.K. Jain, *Transferrin-conjugated solid lipid nanoparticles for enhanced delivery of quinine dihydrochloride to the brain.* Journal of Pharmacy and Pharmacology, 2007. **59**(7): p. 935-940.
224. Eitan, E., E.R. Hutchison, N.H. Greig, et al., *Combination therapy with lenalidomide and nanoceria ameliorates CNS autoimmunity.* Experimental Neurology, 2015. **273**: p. 151-160.
225. Read, T.-A., M. Farhadi, R. Bjerkvig, et al., *Intravital Microscopy Reveals Novel Antivascular and Antitumor Effects of Endostatin Delivered Locally by Alginate-encapsulated Cells.* Cancer Research, 2001. **61**(18): p. 6830-6837.
226. Koffie, R.M., C.T. Farrar, L.-J. Saidi, et al., *Nanoparticles enhance brain delivery of blood–brain barrier-impermeable probes for in vivo optical and magnetic resonance imaging.* Proceedings of the National Academy of Sciences, 2011. **108**(46): p. 18837-18842.
227. Gromnicova, R., M. Kaya, I.A. Romero, et al., *Transport of Gold Nanoparticles by Vascular Endothelium from Different Human Tissues.* Plos One, 2016. **11**(8): p. 17.
228. Gromnicova, R., C.U. Yilmaz, N. Orhan, et al., *Localization and mobility of glucose-coated gold nanoparticles within the brain.* Nanomedicine, 2016. **11**(6): p. 617-625.
229. Smith, M.W. and M. Gumbleton, *Endocytosis at the blood–brain barrier: From basic understanding to drug delivery strategies.* Journal of Drug Targeting, 2006. **14**(4): p. 191-214.
230. Hasty, D.L. and E.D. Hay, *Freeze-fracture studies of the developing cell surface. II. Particle-free membrane blisters on glutaraldehyde-fixed corneal fibroblasts are artefacts.* The Journal of Cell Biology, 1978. **78**(3): p. 756-768.
231. Peters, T. and C.A. Ashley, *AN ARTEFACT IN RADIOAUTOGRAPHY DUE TO BINDING OF FREE AMINO ACIDS TO TISSUES BY FIXATIVES.* The Journal of Cell Biology, 1967. **33**(1): p. 53-60.
232. Torchilin, V.P., *Structure and design of polymeric surfactant-based drug delivery systems.* Journal of Controlled Release, 2001. **73**(2–3): p. 137-172.
233. Friberg, S., *Lyotropic liquid crystals.* Naturwissenschaften, 1977. **64**(12): p. 612-618.
234. Mely, B., J. Charvolin, and P. Keller, *Disorder of lipid chains as a function of their lateral packing in lyotropic liquid crystals.* Chemistry and Physics of Lipids, 1975. **15**(2): p. 161-173.
235. Hyde, S.T., *Bicontinuous structures in lyotropic liquid crystals and crystalline hyperbolic surfaces.* Current Opinion in Solid State and Materials Science, 1996. **1**(5): p. 653-662.
236. Blackmore, E.S. and G.J. Tiddy, *Phase behaviour and lyotropic liquid crystals in cationic surfactant–water systems.* Journal of the Chemical Society, Faraday Transactions 2: Molecular and Chemical Physics, 1988. **84**(8): p. 1115-1127.
237. Boyd, B.J., D.V. Whittaker, S.-M. Khoo, and G. Davey, *Lyotropic liquid crystalline phases formed from glycerate surfactants as sustained release drug delivery systems.* International Journal of Pharmaceutics, 2006. **309**(1): p. 218-226.
238. Mulet, X., B.J. Boyd, and C.J. Drummond, *Advances in drug delivery and medical imaging using colloidal lyotropic liquid crystalline dispersions.* Journal of Colloid and Interface Science, 2013. **393**(0): p. 1-20.
239. Tadwee, I., S. Shahi, V. Ramteke, and I. Syed, *Liquid crystals pharmaceutical application: A review.* Int. J. Pharm. Res. Allied Sci, 2012. **1**: p. 6-11.

240. Mouritsen, O.G., *Lipids, curvature, and nano-medicine.* European Journal of Lipid Science and Technology, 2011. **113**(10): p. 1174-1187.
241. Venugopal, E., S.K. Bhat, J.J. Vallooran, and R. Mezzenga, *Phase Behavior of Lipid–Based Lyotropic Liquid Crystals in Presence of Colloidal Nanoparticles.* Langmuir, 2011. **27**(16): p. 9792-9800.
242. Kaasgaard, T. and C.J. Drummond, *Ordered 2-D and 3-D nanostructured amphiphile self-assembly materials stable in excess solvent.* Physical Chemistry Chemical Physics, 2006. **8**(43): p. 4957-4975.
243. Chen, Z., T.L. Greaves, C. Fong, R.A. Caruso, and C.J. Drummond, *Lyotropic liquid crystalline phase behaviour in amphiphile-protic ionic liquid systems.* Physical Chemistry Chemical Physics, 2012. **14**(11): p. 3825-3836.
244. Pitzalis, P., M. Monduzzi, N. Krog, et al., *Characterization of the Liquid−Crystalline Phases in the Glycerol Monooleate/Diglycerol Monooleate/Water System.* Langmuir, 2000. **16**(15): p. 6358-6365.
245. Gustafsson, J., H. Ljusberg-Wahren, M. Almgren, and K. Larsson, *Submicron Particles of Reversed Lipid Phases in Water Stabilized by a Nonionic Amphiphilic Polymer.* Langmuir, 1997. **13**(26): p. 6964-6971.
246. Barauskas, J. and T. Landh, *Phase Behavior of the Phytantriol/Water System.* Langmuir, 2003. **19**(23): p. 9562-9565.
247. Milak, S. and A. Zimmer, *Glycerol monooleate liquid crystalline phases used in drug delivery systems.* International Journal of Pharmaceutics, 2015. **478**(2): p. 569-587.
248. Seddon, A.M., *Chapter Six - Recent Developments in the Production, Analysis, and Applications of Cubic Phases Formed by Lipids*, in *Advances in Planar Lipid Bilayers and Liposomes*, A. Iglič and C.V. Kulkarni, Editors. 2013, Academic Press. p. 147-180.
249. Allen, T.M. and P.R. Cullis, *Liposomal drug delivery systems: From concept to clinical applications.* Advanced Drug Delivery Reviews, 2013. **65**(1): p. 36-48.
250. Kraft, J.C., J.P. Freeling, Z. Wang, and R.J.Y. Ho, *Emerging Research and Clinical Development Trends of Liposome and Lipid Nanoparticle Drug Delivery Systems.* Journal of Pharmaceutical Sciences, 2014. **103**(1): p. 29-52.
251. Akbarzadeh, A., R. Rezaei-Sadabady, S. Davaran, et al., *Liposome: classification, preparation, and applications.* Nanoscale Research Letters, 2013. **8**(1): p. 102.
252. Akbarzadeh, A., D. Asgari, N. Zarghami, R. Mohammad, and S. Davaran, *Preparation and in vitro evaluation of doxorubicin-loaded Fe3O4 magnetic nanoparticles modified with biocompatible co-polymers.* Int J Nanomedicine, 2012. **7**.
253. Sercombe, L., T. Veerati, F. Moheimani, et al., *Advances and Challenges of Liposome Assisted Drug Delivery.* Frontiers in Pharmacology, 2015. **6**(286).
254. Iwama, T., T. Uchida, Y. Sawada, et al., *Vaccination with liposome-coupled glypican-3-derived epitope peptide stimulates cytotoxic T lymphocytes and inhibits GPC3-expressing tumor growth in mice.* Biochemical and biophysical research communications, 2016. **469**(1): p. 138-143.
255. Wang, C., P. Liu, Y. Zhuang, et al., *Lymphatic-targeted cationic liposomes: a robust vaccine adjuvant for promoting long-term immunological memory.* Vaccine, 2014. **32**(42): p. 5475-5483.
256. Schwendener, R.A., *Liposomes as vaccine delivery systems: a review of the recent advances.* Therapeutic advances in vaccines, 2014. **2**(6): p. 159-182.

257. Narang, A.S., R.-K. Chang, and M.A. Hussain, *Pharmaceutical Development and Regulatory Considerations for Nanoparticles and Nanoparticulate Drug Delivery Systems.* Journal of Pharmaceutical Sciences, 2013. **102**(11): p. 3867-3882.
258. Drummond, C.J. and C. Fong, *Surfactant self-assembly objects as novel drug delivery vehicles.* Current Opinion in Colloid & Interface Science, 1999. **4**(6): p. 449-456.
259. Fong, C., I. Krodkiewska, D. Wells, et al., *Submicron Dispersions of Hexosomes Based on Novel Glycerate Surfactants.* Australian Journal of Chemistry, 2005. **58**(9): p. 683-687.
260. Angelov, B., V.M. Garamus, M. Drechsler, and A. Angelova, *Structural analysis of nanoparticulate carriers for encapsulation of macromolecular drugs.* Journal of Molecular Liquids, 2017. **235**(Supplement C): p. 83-89.
261. Angelova, A., V.M. Garamus, B. Angelov, et al., *Advances in structural design of lipid-based nanoparticle carriers for delivery of macromolecular drugs, phytochemicals and anti-tumor agents.* Advances in Colloid and Interface Science, 2017. **249**(Supplement C): p. 331-345.
262. Spicer, P.T., *Progress in liquid crystalline dispersions: Cubosomes.* Current Opinion in Colloid & Interface Science, 2005. **10**(5): p. 274-279.
263. Yaghmur, A. and O. Glatter, *Characterization and potential applications of nanostructured aqueous dispersions.* Advances in Colloid and Interface Science, 2009. **147**: p. 333-342.
264. Karami, Z. and M. Hamidi, *Cubosomes: remarkable drug delivery potential.* Drug Discovery Today, 2016. **21**(5): p. 789-801.
265. Hyde, S.T., *Identification of lyotropic liquid crystalline mesophases.* 2001.
266. van 't Hag, L., H.-H. Shen, J. Lu, et al., *Deconvoluting the Effect of the Hydrophobic and Hydrophilic Domains of an Amphiphilic Integral Membrane Protein in Lipid Bicontinuous Cubic Mesophases.* Langmuir, 2015. **31**(44): p. 12025-12034.
267. Hartnett, T.E., A.J. O'Connor, and K. Ladewig, *Cubosomes and other potential ocular drug delivery vehicles for macromolecular therapeutics.* Expert Opinion on Drug Delivery, 2015. **12**(9): p. 1513-1526.
268. Gontsarik, M., M.T. Buhmann, A. Yaghmur, et al., *Antimicrobial Peptide-Driven Colloidal Transformations in Liquid-Crystalline Nanocarriers.* The Journal of Physical Chemistry Letters, 2016. **7**(17): p. 3482-3486.
269. Lee, H.J., B. Engelhardt, J. Lesley, U. Bickel, and W.M. Pardridge, *Targeting Rat Anti-Mouse Transferrin Receptor Monoclonal Antibodies through Blood-Brain Barrier in Mouse.* Journal of Pharmacology and Experimental Therapeutics, 2000. **292**(3): p. 1048-1052.
270. Lopes, L.B., J.L.C. Lopes, D.C.R. Oliveira, et al., *Liquid crystalline phases of monoolein and water for topical delivery of cyclosporin A: Characterization and study of in vitro and in vivo delivery.* European Journal of Pharmaceutics and Biopharmaceutics, 2006. **63**(2): p. 146-155.
271. Bender, J., C. Simonsson, M. Smedh, S. Engström, and M.B. Ericson, *Lipid cubic phases in topical drug delivery: Visualization of skin distribution using two-photon microscopy.* Journal of Controlled Release, 2008. **129**(3): p. 163-169.
272. Joyce, P., R. Yasmin, A. Bhatt, et al., *Comparison across Three Hybrid Lipid-Based Drug Delivery Systems for Improving the Oral Absorption of the Poorly Water-Soluble Weak Base Cinnarizine.* Molecular Pharmaceutics, 2017. **14**(11): p. 4008-4018.

273. Nasr, M. and M. Dawoud, *Sorbitol based powder precursor of cubosomes as an oral delivery system for improved bioavailability of poorly water soluble drugs.* Journal of Drug Delivery Science and Technology, 2016. **35**(Supplement C): p. 106-113.
274. Ranneh, A.-H., Y. Iwao, S. Noguchi, T. Oka, and S. Itai, *The use of surfactants to enhance the solubility and stability of the water-insoluble anticancer drug SN38 into liquid crystalline phase nanoparticles.* International journal of pharmaceutics, 2016. **515**(1-2): p. 501-505.
275. Gustafsson, J., H. Ljusberg-Wahren, M. Almgren, and K. Larsson, *Cubic Lipid−Water Phase Dispersed into Submicron Particles.* Langmuir, 1996. **12**(20): p. 4611-4613.
276. Zabara, A. and R. Mezzenga, *Controlling molecular transport and sustained drug release in lipid-based liquid crystalline mesophases.* Journal of Controlled Release, 2014. **188**(0): p. 31-43.
277. Akbar, S., A. Anwar, A. Ayish, J.M. Elliott, and A.M. Squires, *Phytantriol based smart nano-carriers for drug delivery applications.* European Journal of Pharmaceutical Sciences, 2017. **101**(Supplement C): p. 31-42.
278. Caffrey, M., *Membrane protein crystallization.* Journal of Structural Biology, 2003. **142**(1): p. 108-132.
279. Zhai, J., T.M. Hinton, L.J. Waddington, et al., *Lipid–PEG Conjugates Sterically Stabilize and Reduce the Toxicity of Phytantriol-Based Lyotropic Liquid Crystalline Nanoparticles.* Langmuir, 2015. **31**(39): p. 10871-10880.
280. Hinton, T.M., F. Grusche, D. Acharya, et al., *Bicontinuous cubic phase nanoparticle lipid chemistry affects toxicity in cultured cells.* Toxicology Research, 2014. **3**(1): p. 11-22.
281. Düzgüneş, N. and S. Nir, *Mechanisms and kinetics of liposome–cell interactions.* Advanced drug delivery reviews, 1999. **40**(1-2): p. 3-18.
282. McMahon, H.T. and J.L. Gallop, *Membrane curvature and mechanisms of dynamic cell membrane remodelling.* Nature, 2005. **438**(7068): p. 590.
283. Rizwan, S.B., T. Hanley, B.J. Boyd, T. Rades, and S. Hook, *Liquid crystalline systems of phytantriol and glyceryl monooleate containing a hydrophilic protein: Characterisation, swelling and release kinetics.* Journal of Pharmaceutical Sciences, 2009. **98**(11): p. 4191-4204.
284. Kojarunchitt, T., S. Baldursdottir, Y.-D. Dong, et al., *Modified thermoresponsive Poloxamer 407 and chitosan sol–gels as potential sustained-release vaccine delivery systems.* European Journal of Pharmaceutics and Biopharmaceutics, 2015. **89**: p. 74-81.
285. Kojarunchitt, T., S. Hook, S. Rizwan, T. Rades, and S. Baldursdottir, *Development and characterisation of modified poloxamer 407 thermoresponsive depot systems containing cubosomes.* International journal of pharmaceutics, 2011. **408**(1-2): p. 20-26.
286. Szlezak, M., D. Nieciecka, A. Joniec, et al., *Monoolein Cubic Phase Gels and Cubosomes Doped with Magnetic Nanoparticles–Hybrid Materials for Controlled Drug Release.* ACS Applied Materials & Interfaces, 2017. **9**(3): p. 2796-2805.
287. Puri, A., K. Loomis, B. Smith, et al., *Lipid-Based Nanoparticles as Pharmaceutical Drug Carriers: From Concepts to Clinic.* Critical reviews in therapeutic drug carrier systems, 2009. **26**(6): p. 523-580.
288. Nguyen, T.-H., T. Hanley, C.J.H. Porter, and B.J. Boyd, *Nanostructured liquid crystalline particles provide long duration sustained-release effect for a poorly*

water soluble drug after oral administration. Journal of Controlled Release, 2011. **153**(2): p. 180-186.
289. Garg, G., S. Saraf, and S. Saraf, *Cubosomes: An Overview*. Biological and Pharmaceutical Bulletin, 2007. **30**(2): p. 350-353.
290. Boyd, B.J., *Characterisation of drug release from cubosomes using the pressure ultrafiltration method.* International Journal of Pharmaceutics, 2003. **260**(2): p. 239-247.
291. Rizwan, S.B., W.T. McBurney, K. Young, et al., *Cubosomes containing the adjuvants imiquimod and monophosphoryl lipid A stimulate robust cellular and humoral immune responses.* Journal of Controlled Release, 2013. **165**(1): p. 16-21.
292. Nazaruk, E., A. Majkowska-Pilip, and R. Bilewicz, *Lipidic Cubic-Phase Nanoparticles—Cubosomes for Efficient Drug Delivery to Cancer Cells.* ChemPlusChem, 2017. **82**(4): p. 570-575.
293. Lee, K.W.Y., T.-H. Nguyen, T. Hanley, and B.J. Boyd, *Nanostructure of liquid crystalline matrix determines in vitro sustained release and in vivo oral absorption kinetics for hydrophilic model drugs.* International Journal of Pharmaceutics, 2009. **365**(1): p. 190-199.
294. Phan, S., W.-K. Fong, N. Kirby, T. Hanley, and B.J. Boyd, *Evaluating the link between self-assembled mesophase structure and drug release.* International Journal of Pharmaceutics, 2011. **421**(1): p. 176-182.
295. Bryant, G., C. Abeynayake, and J.C. Thomas, *Improved Particle Size Distribution Measurements Using Multiangle Dynamic Light Scattering. 2. Refinements and Applications.* Langmuir, 1996. **12**(26): p. 6224-6228.
296. Rizwan, S.B., Y.D. Dong, B.J. Boyd, T. Rades, and S. Hook, *Characterisation of bicontinuous cubic liquid crystalline systems of phytantriol and water using cryo field emission scanning electron microscopy (cryo FESEM).* Micron, 2007. **38**(5): p. 478-485.
297. Yamashita, M., K. Kameyama, R. Kobayashi, et al., *Observation of an Emulsion Microstructure with Cryo-FESEM.* Journal of Electron Microscopy, 1996. **45**(5): p. 461-462.
298. Boyd, B.J., S.B. Rizwan, Y.-D. Dong, S. Hook, and T. Rades, *Self-Assembled Geometric Liquid-Crystalline Nanoparticles Imaged in Three Dimensions: Hexosomes Are Not Necessarily Flat Hexagonal Prisms.* Langmuir, 2007. **23**(25): p. 12461-12464.
299. Talmon, Y., *The study of nanostructured liquids by cryogenic-temperature electron microscopy — A status report.* Journal of Molecular Liquids, 2015. **210**: p. 2-8.
300. Erlandsen, S.L., C. Ottenwaelter, C. Frethem, and Y. Chen, *Cryo field emission scanning electron microscopy.* BioTechniques, 2001. **31**(2): p. 300-305.
301. Karuppasamy, M., F. Karimi Nejadasl, M. Vulovic, A.J. Koster, and R.B. Ravelli, *Radiation damage in single-particle cryo-electron microscopy: effects of dose and dose rate.* J Synchrotron Radiat, 2011. **18**(Pt 3): p. 398-412.
302. Pfeffer, S., M. Khoshouei, R. Danev, and F. Förster, *Towards High Resolution in Cryo-Electron Tomography Subtomogram Analysis.* Microscopy and Microanalysis, 2017. **23**(S1): p. 812-813.
303. Medalia, O., I. Weber, A.S. Frangakis, et al., *Macromolecular Architecture in Eukaryotic Cells Visualized by Cryoelectron Tomography.* Science, 2002. **298**(5596): p. 1209-1213.

304. Lučić, V., A. Leis, and W. Baumeister, *Cryo-electron tomography of cells: connecting structure and function.* Histochemistry and Cell Biology, 2008. **130**(2): p. 185.
305. Weksler, B., I. Romero, and P.-O. Couraud, *The hCMEC/D3 cell line as a model of the human blood brain barrier.* Fluids and Barriers of the CNS, 2013. **10**(1): p. 16.
306. Bowman, P.D., S.R. Ennis, K.E. Rarey, A.L. Betz, and G.W. Goldstein, *Brain microvessel endothelial cells in tissue culture: a model for study of blood–brain barrier permeability.* Ann Neurol, 1983. **14**.
307. Weksler, B.B., E.A. Subileau, N. Perrière, et al., *Blood-brain barrier-specific properties of a human adult brain endothelial cell line.* The FASEB Journal, 2005. **19**(13): p. 1872-1874.
308. Mkrtchyan, H., S. Scheler, I. Klein, et al., *Molecular cytogenetic characterization of the human cerebral microvessel endothelial cell line hCMEC/D3.* Cytogenet Genome Res, 2009. **126**(4): p. 313-7.
309. Ohtsuki, S., C. Ikeda, Y. Uchida, et al., *Quantitative targeted absolute proteomic analysis of transporters, receptors and junction proteins for validation of human cerebral microvascular endothelial cell line hCMEC/D3 as a human blood-brain barrier model.* Mol Pharm, 2013. **10**(1): p. 289-96.
310. Carl, S.M., D.J. Lindley, P.O. Couraud, et al., *ABC and SLC Transporter Expression and Pot Substrate Characterization across the Human CMEC/D3 Blood−Brain Barrier Cell Line.* Molecular Pharmaceutics, 2010. **7**(4): p. 1057-1068.
311. Dauchy, S., F. Miller, P.O. Couraud, et al., *Expression and transcriptional regulation of ABC transporters and cytochromes P450 in hCMEC/D3 human cerebral microvascular endothelial cells.* Biochem Pharmacol, 2009. **77**(5): p. 897-909.
312. Tai, L.M., P.S. Reddy, M.A. Lopez-Ramirez, et al., *Polarized P-glycoprotein expression by the immortalised human brain endothelial cell line, hCMEC/D3, restricts apical-to-basolateral permeability to rhodamine 123.* Brain Research, 2009. **1292**(0): p. 14-24.
313. Rizwan, S.B., D. Assmus, A. Boehnke, et al., *Preparation of phytantriol cubosomes by solvent precursor dilution for the delivery of protein vaccines.* European Journal of Pharmaceutics and Biopharmaceutics, 2011. **79**(1): p. 15-22.
314. Kissa, E., *Dispersions: characterization, testing, and measurement*. Vol. 84. 1999: CRC Press.
315. Kirby, N.M., S.T. Mudie, A.M. Hawley, et al., *A low-background-intensity focusing small-angle X-ray scattering undulator beamline.* Journal of Applied Crystallography, 2013. **46**(6): p. 1670-1680.
316. Dong, Y.-D., I. Larson, T. Hanley, and B.J. Boyd, *Bulk and Dispersed Aqueous Phase Behavior of Phytantriol: Effect of Vitamin E Acetate and F127 Polymer on Liquid Crystal Nanostructure.* Langmuir, 2006. **22**(23): p. 9512-9518.
317. Mastronarde, D.N., *Automated electron microscope tomography using robust prediction of specimen movements.* Journal of Structural Biology, 2005. **152**(1): p. 36-51.
318. Kremer, J.R., D.N. Mastronarde, and J.R. McIntosh, *Computer visualization of three-dimensional image data using IMOD.* J Struct Biol, 1996. **116**(1): p. 71-6.
319. Frangakis, A.S. and R. Hegerl, *Noise reduction in electron tomographic reconstructions using nonlinear anisotropic diffusion.* J Struct Biol, 2001. **135**(3): p. 239-50.

320. Kwok, D.Y., B. Tadros, H. Deol, et al., *Axisymmetric Drop Shape Analysis as a Film Balance: Rate Dependence of the Collapse Pressure and Molecular Area at Close Packing of 1-Octadecanol Monolayers.* Langmuir, 1996. **12**(7): p. 1851-1859.
321. Miyoshi, T. and S. Kato, *Detailed Analysis of the Surface Area and Elasticity in the Saturated 1,2-Diacylphosphatidylcholine/Cholesterol Binary Monolayer System.* Langmuir, 2015. **31**(33): p. 9086-9096.
322. de Paula Rigoletto, T., M.E.D. Zaniquelli, M.H.A. Santana, and L.G. de la Torre, *Surface miscibility of EPC/DOTAP/DOPE in binary and ternary mixed monolayers.* Colloids and Surfaces B: Biointerfaces, 2011. **83**(2): p. 260-269.
323. Dynarowicz-Łątka, P. and K. Kita, *Molecular interaction in mixed monolayers at the air/water interface.* Advances in Colloid and Interface Science, 1999. **79**(1): p. 1-17.
324. Vacca, I., *Shuttling lipids across bacterial membranes.* Nature Reviews Microbiology, 2017. **15**: p. 319.
325. Schneider, W.J., *Chapter 17 - Lipoprotein Receptors A2 - Ridgway, Neale D*, in *Biochemistry of Lipids, Lipoproteins and Membranes (Sixth Edition)*, R.S. McLeod, Editor. 2016, Elsevier: Boston. p. 489-518.
326. Iaea, D.B., S. Mao, F.W. Lund, and F.R. Maxfield, *Role of STARD4 in sterol transport between the endocytic recycling compartment and the plasma membrane.* Molecular Biology of the Cell, 2017. **28**(8): p. 1111-1122.
327. Weers, P.M., L.M. Kakutani, J.V. Horn, and V. Narayanaswami, *Chimera of Apolipophorin III and C-terminal Domain of Apolipoprotein E to Study Apolipoprotein Structure Function.* Biophysical Journal, 2017. **112**(3): p. 87a.
328. Yeh, F.L., Y. Wang, I. Tom, L.C. Gonzalez, and M. Sheng, *TREM2 Binds to Apolipoproteins, Including APOE and CLU/APOJ, and Thereby Facilitates Uptake of Amyloid-Beta by Microglia.* Neuron, 2016. **91**(2): p. 328-340.
329. Meng, F., S. Asghar, Y. Xu, et al., *Design and evaluation of lipoprotein resembling curcumin-encapsulated protein-free nanostructured lipid carrier for brain targeting.* International Journal of Pharmaceutics, 2016. **506**(1): p. 46-56.
330. Ana Rute, N., Q. Joana Fontes, W. Babette, et al., *Solid lipid nanoparticles as a vehicle for brain-targeted drug delivery: two new strategies of functionalization with apolipoprotein E.* Nanotechnology, 2015. **26**(49): p. 495103.
331. Neves, A.R., J.F. Queiroz, B. Weksler, et al., *Solid lipid nanoparticles as a vehicle for brain-targeted drug delivery: two new strategies of functionalization with apolipoprotein E.* Nanotechnology, 2015. **26**(49): p. 495103.
332. Kuo, Y.-C. and F.-L. Su, *Transport of stavudine, delavirdine, and saquinavir across the blood–brain barrier by polybutylcyanoacrylate, methylmethacrylate-sulfopropylmethacrylate, and solid lipid nanoparticles.* International Journal of Pharmaceutics, 2007. **340**(1): p. 143-152.
333. Neves, A.R., J.F. Queiroz, and S. Reis, *Brain-targeted delivery of resveratrol using solid lipid nanoparticles functionalized with apolipoprotein E.* Journal of Nanobiotechnology, 2016. **14**(1).
334. Kuo, Y.-C. and R. Rajesh, *Targeted delivery of rosmarinic acid across the blood–brain barrier for neuronal rescue using polyacrylamide-chitosan-poly(lactide-co-glycolide) nanoparticles with surface cross-reacting material 197 and apolipoprotein E.* International Journal of Pharmaceutics, 2017. **528**(1): p. 228-241.

335. Bernier, M., D. Wahl, A. Ali, et al., *Resveratrol supplementation confers neuroprotection in cortical brain tissue of nonhuman primates fed a high-fat/sucrose diet.* Aging (Albany NY), 2016. **8**(5): p. 899-914.
336. Khodaie, N., N. Tajuddin, R.M. Mitchell, E.J. Neafsey, and M.A. Collins, *Combinatorial Preconditioning of Rat Brain Cultures with Subprotective Ethanol and Resveratrol Concentrations Promotes Synergistic Neuroprotection.* Neurotoxicity Research, 2018.
337. Gueguen, N., V. Desquiret-Dumas, G. Leman, et al., *Resveratrol Directly Binds to Mitochondrial Complex I and Increases Oxidative Stress in Brain Mitochondria of Aged Mice.* PLOS ONE, 2015. **10**(12): p. e0144290.
338. Abdel-Aleem, G.A., E.F. Khaleel, D.G. Mostafa, and L.K. Elberier, *Neuroprotective effect of resveratrol against brain ischemia reperfusion injury in rats entails reduction of DJ-1 protein expression and activation of PI3K/Akt/GSK3b survival pathway.* Archives of Physiology and Biochemistry, 2016. **122**(4): p. 200-213.
339. Marambaud, P., H. Zhao, and P. Davies, *Resveratrol Promotes Clearance of Alzheimer's Disease Amyloid-β Peptides.* Journal of Biological Chemistry, 2005. **280**(45): p. 37377-37382.
340. Ge, J.-F., J.-P. Qiao, C.-C. Qi, C.-W. Wang, and J.-N. Zhou, *The binding of resveratrol to monomer and fibril amyloid beta.* Neurochemistry International, 2012. **61**(7): p. 1192-1201.
341. *Nanoparticle-mediated delivery of therapeutic genes: focus on miRNA therapeutics.* Expert Opinion on Drug Delivery, 2013: p. 1.
342. Wu, W.J., J. Li, L. Wu, et al., *Ophthalmic delivery of brinzolamide by liquid crystalline nanoparticles: in vitro and in vivo evaluation.* AAPS PharmSciTech, 2013. **14**.
343. Amri, A., J.C. Chaumeil, S. Sfar, and C. Charrueau, *Administration of resveratrol: What formulation solutions to bioavailability limitations?* Journal of Controlled Release, 2012. **158**(2): p. 182-193.
344. R. Neves, A., M. Lucio, J. L.C. Lima, and S. Reis, *Resveratrol in Medicinal Chemistry: A Critical Review of its Pharmacokinetics, Drug-Delivery, and Membrane Interactions.* Current Medicinal Chemistry, 2012. **19**(11): p. 1663-1681.
345. Michaelis, K., M.M. Hoffmann, S. Dreis, et al., *Covalent Linkage of Apolipoprotein E to Albumin Nanoparticles Strongly Enhances Drug Transport into the Brain.* Journal of Pharmacology and Experimental Therapeutics, 2006. **317**(3): p. 1246-1253.
346. Dal Magro, R., F. Ornaghi, I. Cambianica, et al., *ApoE-modified solid lipid nanoparticles: A feasible strategy to cross the blood-brain barrier.* Journal of Controlled Release, 2017. **249**: p. 103-110.
347. Ćurić, A., J.P. Möschwitzer, and G. Fricker, *Development and characterization of novel highly-loaded itraconazole poly(butyl cyanoacrylate) polymeric nanoparticles.* European Journal of Pharmaceutics and Biopharmaceutics, 2017. **114**(Supplement C): p. 175-185.
348. Wohlfart, S., S. Gelperina, and J. Kreuter, *Transport of drugs across the blood–brain barrier by nanoparticles.* Journal of Controlled Release, 2012. **161**(2): p. 264-273.
349. Olivier, J.-C., L. Fenart, R. Chauvet, et al., *Indirect Evidence that Drug Brain Targeting Using Polysorbate 80-Coated Polybutylcyanoacrylate Nanoparticles Is Related to Toxicity.* Pharmaceutical Research, 1999. **16**(12): p. 1836-1842.

350. Khalin, I., R. Alyautdin, T.W. Wong, et al., *Brain-derived neurotrophic factor delivered to the brain using poly (lactide-co-glycolide) nanoparticles improves neurological and cognitive outcome in mice with traumatic brain injury.* Drug Delivery, 2016. **23**(9): p. 3520-3528.
351. Ritz, S., S. Schottler, N. Kotman, et al., *Protein corona of nanoparticles: distinct proteins regulate the cellular uptake.* Biomacromolecules, 2015. **16**(4): p. 1311-21.
352. Schöttler, S., G. Becker, S. Winzen, et al., *Protein adsorption is required for stealth effect of poly(ethylene glycol)- and poly(phosphoester)-coated nanocarriers.* Nature Nanotechnology, 2016. **11**: p. 372.
353. Kerwin, B.A., *Polysorbates 20 and 80 used in the formulation of protein biotherapeutics: Structure and degradation pathways.* Journal of Pharmaceutical Sciences, 2008. **97**(8): p. 2924-2935.
354. Alyautdin, R.N., E.B. Tezikov, P. Ramge, et al., *Significant entry of tubocurarine into the brain of rats by adsorption to polysorbate 80–coated polybutylcyanoacrylate nanoparticles: An in situ brain perfusion study.* Journal of Microencapsulation, 1998. **15**(1): p. 67-74.
355. Kreuter, J., D. Shamenkov, V. Petrov, et al., *Apolipoprotein-mediated Transport of Nanoparticle-bound Drugs Across the Blood-Brain Barrier.* Journal of Drug Targeting, 2002. **10**(4): p. 317-325.
356. Kreuter, J., T. Hekmatara, S. Dreis, et al., *Covalent attachment of apolipoprotein A-I and apolipoprotein B-100 to albumin nanoparticles enables drug transport into the brain.* Journal of Controlled Release, 2007. **118**(1): p. 54-58.
357. Wagner, S., A. Zensi, S.L. Wien, et al., *Uptake mechanism of ApoE-modified nanoparticles on brain capillary endothelial cells as a blood-brain barrier model.* PloS one, 2012. **7**(3): p. e32568.
358. Huang, Y., B. Zhang, S. Xie, et al., *Superparamagnetic Iron Oxide Nanoparticles Modified with Tween 80 Pass through the Intact Blood–Brain Barrier in Rats under Magnetic Field.* ACS Applied Materials & Interfaces, 2016. **8**(18): p. 11336-11341.
359. Das, D. and S. Lin, *Double-coated poly (butylcynanoacrylate) nanoparticulate delivery systems for brain targeting of dalargin via oral administration.* Journal of Pharmaceutical Sciences, 2005. **94**(6): p. 1343-1353.
360. Schroeder, A., D.A. Heller, M.M. Winslow, et al., *Treating metastatic cancer with nanotechnology.* Nature Reviews Cancer, 2012. **12**(1): p. 39-50.
361. Gao, H., *Progress and perspectives on targeting nanoparticles for brain drug delivery.* Acta Pharmaceutica Sinica B, 2016. **6**(4): p. 268-286.
362. Friese, A., E. Seiller, G. Quack, B. Lorenz, and J. Kreuter, *Increase of the duration of the anticonvulsive activity of a novel NMDA receptor antagonist using poly(butylcyanoacrylate) nanoparticles as a parenteral controlled release system.* European Journal of Pharmaceutics and Biopharmaceutics, 2000. **49**(2): p. 103-109.
363. Kurakhmaeva, K.B., I.A. Djindjikhashvili, V.E. Petrov, et al., *Brain targeting of nerve growth factor using poly(butyl cyanoacrylate) nanoparticles.* Journal of Drug Targeting, 2009. **17**(8): p. 564-574.
364. Tian, Y., Y. Shen, and J.S. Tu, *Advance in development of non-ionic surafctants in brain-targeted drug delivery systems.* Chinese Journal of New Drugs, 2015. **24**(2): p. 166-170.

365. Yan, F., C. Zhang, Y. Zheng, et al., *The effect of poloxamer 188 on nanoparticle morphology, size, cancer cell uptake, and cytotoxicity.* Nanomedicine: Nanotechnology, Biology and Medicine, 2010. **6**(1): p. 170-178.
366. Maskarinec, S.A., J. Hannig, R.C. Lee, and K.Y.C. Lee, *Direct Observation of Poloxamer 188 Insertion into Lipid Monolayers.* Biophysical Journal, 2002. **82**(3): p. 1453-1459.
367. Chong, J.Y., X. Mulet, L.J. Waddington, B.J. Boyd, and C.J. Drummond, *Steric stabilisation of self-assembled cubic lyotropic liquid crystalline nanoparticles: high throughput evaluation of triblock polyethylene oxide-polypropylene oxide-polyethylene oxide copolymers.* Soft Matter, 2011. **7**(10): p. 4768-4777.
368. Jain, D., R. Athawale, A. Bajaj, et al., *Studies on stabilization mechanism and stealth effect of poloxamer 188 onto PLGA nanoparticles.* Colloids and Surfaces B: Biointerfaces, 2013. **109**: p. 59-67.
369. Sandra B. Cadichon, Hoang M. Le, David A. Wright, et al., *Neuroprotective effect of the surfactant poloxamer 188 in a model of intracranial hemorrhage in rats.* Journal of Neurosurgery: Pediatrics, 2007. **106**(1): p. 36-40.
370. Serbest, G., J. Horwitz, and K. Barbee, *The Effect of Poloxamer-188 on Neuronal Cell Recovery from Mechanical Injury.* Journal of Neurotrauma, 2005. **22**(1): p. 119-132.
371. Malinovskaya, Y., P. Melnikov, V. Baklaushev, et al., *Delivery of doxorubicin-loaded PLGA nanoparticles into U87 human glioblastoma cells.* International Journal of Pharmaceutics, 2017. **524**(1–2): p. 77-90.
372. Cai, Q., L. Wang, G. Deng, et al., *Systemic delivery to central nervous system by engineered PLGA nanoparticles.* American Journal of Translational Research, 2016. **8**(2): p. 749-764.
373. Dong, H., L. Tian, M. Gao, et al., *Promising galactose-decorated biodegradable poloxamer 188-PLGA diblock copolymer nanoparticles of resibufogenin for enhancing liver cancer therapy.* Drug Delivery, 2017. **24**(1): p. 1302-1316.
374. Yung-Chu, C., H. Wen-Yuan, L. Wen-Fu, and Z. Ding-Tai, *Effects of surface modification of PLGA-PEG-PLGA nanoparticles on loperamide delivery efficiency across the blood–brain barrier.* Journal of Biomaterials Applications, 2013. **27**(7): p. 909-922.
375. Girotra, P., S.K. Singh, and G. Kumar, *Development of zolmitriptan loaded PLGA/poloxamer nanoparticles for migraine using quality by design approach.* International Journal of Biological Macromolecules, 2016. **85**(Supplement C): p. 92-101.
376. Yang, S.C., L.F. Lu, Y. Cai, et al., *Body distribution in mice of intravenously injected camptothecin solid lipid nanoparticles and targeting effect on brain.* Journal of Controlled Release, 1999. **59**(3): p. 299-307.
377. Petri, B., A. Bootz, A. Khalansky, et al., *Chemotherapy of brain tumour using doxorubicin bound to surfactant-coated poly(butyl cyanoacrylate) nanoparticles: Revisiting the role of surfactants.* Journal of Controlled Release, 2007. **117**(1): p. 51-58.
378. Gelperina, S., O. Maksimenko, A. Khalansky, et al., *Drug delivery to the brain using surfactant-coated poly(lactide-co-glycolide) nanoparticles: Influence of the formulation parameters.* European Journal of Pharmaceutics and Biopharmaceutics, 2010. **74**(2): p. 157-163.
379. Zhao, Y.-Z., Q. Lin, H.L. Wong, et al., *Glioma-targeted therapy using Cilengitide nanoparticles combined with UTMD enhanced delivery.* Journal of Controlled Release, 2016. **224**: p. 112-125.

380. Đorđević, S.M., N.D. Cekić, M.M. Savić, et al., *Parenteral nanoemulsions as promising carriers for brain delivery of risperidone: Design, characterization and in vivo pharmacokinetic evaluation.* International Journal of Pharmaceutics, 2015. **493**(1): p. 40-54.
381. Yaghmur, A., L. De Campo, L. Sagalowicz, M.E. Leser, and O. Glatter, *Control of the internal structure of MLO-based isasomes by the addition of diglycerol monooleate and soybean phosphatidylcholine.* Langmuir, 2006. **22**(24): p. 9919-9927.
382. Yaghmur, A., L. De Campo, L. Sagalowicz, M.E. Leser, and O. Glatter, *Emulsified microemulsions and oil-containing liquid crystalline phases.* Langmuir, 2005. **21**(2): p. 569-577.
383. Chong, J.Y.T., X. Mulet, L.J. Waddington, B.J. Boyd, and C.J. Drummond, *High-Throughput Discovery of Novel Steric Stabilizers for Cubic Lyotropic Liquid Crystal Nanoparticle Dispersions.* Langmuir, 2012. **28**(25): p. 9223-9232.
384. Chen, G.-J., Y.-Z. Su, C. Hsu, et al., *Angiopep-pluronic F127-conjugated superparamagnetic iron oxide nanoparticles as nanotheranostic agents for BBB targeting.* Journal of Materials Chemistry B, 2014. **2**(34): p. 5666-5675.
385. Meng, J., V. Agrahari, and I. Youm, *Advances in Targeted Drug Delivery Approaches for the Central Nervous System Tumors: The Inspiration of Nanobiotechnology.* Journal of Neuroimmune Pharmacology, 2017. **12**(1): p. 84-98.
386. Alakhova, D.Y., N.Y. Rapoport, E.V. Batrakova, et al., *Differential metabolic responses to pluronic in MDR and non-MDR cells: A novel pathway for chemosensitization of drug resistant cancers.* Journal of Controlled Release, 2010. **142**(1): p. 89-100.
387. Batrakova, E.V., T.Y. Dorodnych, E.Y. Klinskii, et al., *Anthracycline antibiotics non-covalently incorporated into the block copolymer micelles: in vivo evaluation of anti-cancer activity.* Br J Cancer, 1996. **74**(10): p. 1545-1552.
388. Venne, A., S. Li, R. Mandeville, A. Kabanov, and V. Alakhov, *Hypersensitizing Effect of Pluronic L61 on Cytotoxic Activity, Transport, and Subcellular Distribution of Doxorubicin in Multiple Drug-resistant Cells.* Cancer Research, 1996. **56**(16): p. 3626-3629.
389. Dehghan Kelishady, P., E. Saadat, F. Ravar, H. Akbari, and F. Dorkoosh, *Pluronic F127 polymeric micelles for co-delivery of paclitaxel and lapatinib against metastatic breast cancer: preparation, optimization and in vitro evaluation.* Pharmaceutical Development and Technology, 2015. **20**(8): p. 1009-1017.
390. Chong, J.Y.T., X. Mulet, B.J. Boyd, and C.J. Drummond, *Chapter Five - Steric Stabilizers for Cubic Phase Lyotropic Liquid Crystal Nanodispersions (Cubosomes)*, in *Advances in Planar Lipid Bilayers and Liposomes*, A. Iglič, C.V. Kulkarni, and M. Rappolt, Editors. 2015, Academic Press. p. 131-187.
391. Huang, Y., Y. Tao, R. Li, and Q.W. Xu, *Evaluation of drug delivery to central nervous system in vivo.* Chinese Journal of New Drugs, 2016. **25**(9): p. 1013-1017.
392. Sun, W., C. Xie, H. Wang, and Y. Hu, *Specific role of polysorbate 80 coating on the targeting of nanoparticles to the brain.* Biomaterials, 2004. **25**(15): p. 3065-3071.
393. Azhari, H., M. Strauss, S. Hook, B.J. Boyd, and S.B. Rizwan, *Stabilising cubosomes with Tween 80 as a step towards targeting lipid nanocarriers to the blood-brain barrier.* Eur J Pharm Biopharm, 2016. **104**: p. 148-55.

394. Barauskas, J., M. Johnsson, F. Joabsson, and F. Tiberg, *Cubic Phase Nanoparticles (Cubosome†): Principles for Controlling Size, Structure, and Stability.* Langmuir, 2005. **21**(6): p. 2569-2577.
395. Akhlaghi, S.P., I.R. Ribeiro, B.J. Boyd, and W. Loh, *Impact of preparation method and variables on the internal structure, morphology, and presence of liposomes in phytantriol-Pluronic® F127 cubosomes.* Colloids and Surfaces B: Biointerfaces, 2016. **145**(Supplement C): p. 845-853.
396. Johnsson, M., M. Silvander, G. Karlsson, and K. Edwards, *Effect of PEO−PPO−PEO Triblock Copolymers on Structure and Stability of Phosphatidylcholine Liposomes.* Langmuir, 1999. **15**(19): p. 6314-6325.
397. Tilley, A.J., C.J. Drummond, and B.J. Boyd, *Disposition and association of the steric stabilizer Pluronic® F127 in lyotropic liquid crystalline nanostructured particle dispersions.* Journal of Colloid and Interface Science, 2013. **392**: p. 288-296.
398. Chong, J.Y.T., X. Mulet, A. Postma, et al., *Novel RAFT amphiphilic brush copolymer steric stabilisers for cubosomes: poly(octadecyl acrylate)-block-poly(polyethylene glycol methyl ether acrylate).* Soft Matter, 2014. **10**(35): p. 6666-6676.
399. Jo, D.H., J.H. Kim, T.G. Lee, and J.H. Kim, *Size, surface charge, and shape determine therapeutic effects of nanoparticles on brain and retinal diseases.* Nanomedicine: Nanotechnology, Biology and Medicine, 2015. **11**(7): p. 1603-1611.
400. Wu, G., J. Majewski, C. Ege, et al., *Interaction between Lipid Monolayers and Poloxamer 188: An X-Ray Reflectivity and Diffraction Study.* Biophysical Journal, 2005. **89**(5): p. 3159-3173.
401. Swarnakar, N.K., K. Thanki, and S. Jain, *Lyotropic Liquid Crystalline Nanoparticles of CoQ10: Implication of Lipase Digestibility on Oral Bioavailability, in Vivo antioxidant activity, and in Vitro–in Vivo Relationships.* Molecular Pharmaceutics, 2014. **11**(5): p. 1435-1449.
402. Van Gorkom, L.C.M., S.Q. Nie, and R.M. Epand, *Hydrophobic lipid additives affect membrane stability and phase behavior of N-monomethyldioleoylphosphatidylethanolamine.* Biochemistry, 1992. **31**(3): p. 671-677.
403. Meng, F.F., S. Asghar, Y.R. Xu, et al., *Design and evaluation of lipoprotein resembling curcumin-encapsulated protein-free nanostructured lipid carrier for brain targeting.* International Journal of Pharmaceutics, 2016. **506**(1-2): p. 46-56.
404. Bertrand, N., P. Grenier, M. Mahmoudi, et al., *Mechanistic understanding of in vivo protein corona formation on polymeric nanoparticles and impact on pharmacokinetics.* Nature Communications, 2017. **8**(1): p. 777.
405. Karraker, K.A. and C.J. Radke, *Disjoining pressures, zeta potentials and surface tensions of aqueous non-ionic surfactant/electrolyte solutions: theory and comparison to experiment.* Advances in Colloid and Interface Science, 2002. **96**(1): p. 231-264.
406. Demurtas, D., P. Guichard, I. Martiel, et al., *Direct visualization of dispersed lipid bicontinuous cubic phases by cryo-electron tomography.* Nature Communications, 2015. **6**: p. 8915.
407. Spicer, P.T., K.L. Hayden, M.L. Lynch, A. Ofori-Boateng, and J.L. Burns, *Novel Process for Producing Cubic Liquid Crystalline Nanoparticles (Cubosomes).* Langmuir, 2001. **17**(19): p. 5748-5756.

408. Angelov, B., A. Angelova, M. Drechsler, et al., *Identification of large channels in cationic PEGylated cubosome nanoparticles by synchrotron radiation SAXS and Cryo-TEM imaging.* Soft Matter, 2015. **11**(18): p. 3686-3692.
409. Müller, R.H., D. Rühl, S. Runge, K. Schulze-Forster, and W. Mehnert, *Cytotoxicity of Solid Lipid Nanoparticles as a Function of the Lipid Matrix and the Surfactant.* Pharmaceutical Research, 1997. **14**(4): p. 458-462.
410. Poller, B., H. Gutmann, S. Krähenbühl, et al., *The human brain endothelial cell line hCMEC/D3 as a human blood-brain barrier model for drug transport studies.* Journal of Neurochemistry, 2008. **107**(5): p. 1358-1368.
411. Rahimi, M., E.P. Ng, K. Bakhtiari, et al., *Zeolite Nanoparticles for Selective Sorption of Plasma Proteins.* Scientific Reports, 2015. **5**.
412. Åberg, C., J.A. Kim, A. Salvati, and K.A. Dawson, *Theoretical framework for nanoparticle uptake and accumulation kinetics in dividing cell populations.* EPL (Europhysics Letters), 2013. **101**(3): p. 38007.
413. Jordan, A., R. Scholz, P. Wust, et al., *Endocytosis of dextran and silan-coated magnetite nanoparticles and the effect of intracellular hyperthermia on human mammary carcinoma cells in vitro.* Journal of Magnetism and Magnetic Materials, 1999. **194**(1): p. 185-196.
414. Vu, K., B. Weksler, I. Romero, P.-O. Couraud, and A. Gelli, *Immortalized Human Brain Endothelial Cell Line HCMEC/D3 as a Model of the Blood-Brain Barrier Facilitates In Vitro Studies of Central Nervous System Infection by Cryptococcus neoformans.* Eukaryotic Cell, 2009. **8**(11): p. 1803-1807.
415. Ponka, P. and C.N. Lok, *The transferrin receptor: role in health and disease.* The International Journal of Biochemistry & Cell Biology, 1999. **31**(10): p. 1111-1137.
416. van Rooy, I., E. Mastrobattista, G. Storm, W.E. Hennink, and R.M. Schiffelers, *Comparison of five different targeting ligands to enhance accumulation of liposomes into the brain.* Journal of Controlled Release, 2011. **150**(1): p. 30-36.
417. Trono, J.D., K. Mizuno, N. Yusa, et al., *Size, Concentration and Incubation Time Dependence of Gold Nanoparticle Uptake into Pancreas Cancer Cells and its Future Application to X-ray Drug Delivery System.* Journal of Radiation Research, 2011. **52**(1): p. 103-109.
418. Lu, W., J. Wan, Z. She, and X. Jiang, *Brain delivery property and accelerated blood clearance of cationic albumin conjugated pegylated nanoparticle.* Journal of Controlled Release, 2007. **118**(1): p. 38-53.
419. Ghadiri, M., E. Vasheghani-Farahani, F. Atyabi, et al., *Transferrin-conjugated magnetic dextran-spermine nanoparticles for targeted drug transport across blood-brain barrier.* Journal of Biomedical Materials Research Part A, 2017. **105**(10): p. 2851-2864.
420. Vorbrodt, A.W., *Ultracytochemical characterization of anionic sites in the wall of brain capillaries.* J Neurocytol, 1989. **18**(3): p. 359-68.
421. Dhami, N.K., R.S. Pandey, U.K. Jain, R. Chandra, and J. Madan, *Non-aggregated protamine-coated poly(lactide-co-glycolide) nanoparticles of cisplatin crossed blood–brain barrier, enhanced drug delivery and improved therapeutic index in glioblastoma cells: in vitro studies.* Journal of Microencapsulation, 2014. **31**(7): p. 685-693.
422. Goulatis, L.I. and E.V. Shusta, *Protein engineering approaches for regulating blood–brain barrier transcytosis.* Current Opinion in Structural Biology, 2017. **45**(Supplement C): p. 109-115.

423. Hervé, F., N. Ghinea, and J.-M. Scherrmann, *CNS delivery via adsorptive transcytosis.* The AAPS journal, 2008. **10**(3): p. 455-472.
424. Shimura, T., S. Tabata, T. Ohnishi, T. Terasaki, and A. Tsuji, *Transport mechanism of a new behaviorally highly potent adrenocorticotropic hormone (ACTH) analog, ebiratide, through the blood-brain barrier.* Journal of Pharmacology and Experimental Therapeutics, 1991. **258**(2): p. 459-465.
425. Suzuki, H. and Y.H. Bae, *Evaluation of drug penetration with cationic micelles and their penetration mechanism using an in vitro tumor model.* Biomaterials, 2016. **98**(Supplement C): p. 120-130.
426. Tamai, I., Y. Sai, H. Kobayashi, et al., *Structure-Internalization Relationship for Adsorptive-Mediated Endocytosis of Basic Peptides at the Blood-Brain Barrier.* Journal of Pharmacology and Experimental Therapeutics, 1997. **280**(1): p. 410-415.
427. Triguero, D., J. Buciak, and W.M. Pardridge, *Capillary Depletion Method for Quantification of Blood–Brain Barrier Transport of Circulating Peptides and Plasma Proteins.* Journal of Neurochemistry, 1990. **54**(6): p. 1882-1888.
428. Lindgren, M., K. Rosenthal-Aizman, K. Saar, et al., *Overcoming methotrexate resistance in breast cancer tumour cells by the use of a new cell-penetrating peptide.* Biochem Pharmacol, 2006. **71**(4): p. 416-25.
429. Morris, M.C., J. Depollier, J. Mery, F. Heitz, and G. Divita, *A peptide carrier for the delivery of biologically active proteins into mammalian cells.* Nat Biotechnol, 2001. **19**(12): p. 1173-6.
430. Zou, L.L., J.L. Ma, T. Wang, T.B. Yang, and C.B. Liu, *Cell-penetrating peptide-mediated therapeutic molecule delivery into the central nervous system.* Current Neuropharmacology, 2013. **11**(2): p. 197-208.
431. Khafagy el, S. and M. Morishita, *Oral biodrug delivery using cell-penetrating peptide.* Adv Drug Deliv Rev, 2012. **64**(6): p. 531-9.
432. Margus, H., K. Padari, and M. Pooga, *Cell-penetrating peptides as versatile vehicles for oligonucleotide delivery.* Mol Ther, 2012. **20**(3): p. 525-33.
433. Zhang, Q., J. Tang, L. Fu, et al., *A pH-responsive alpha-helical cell penetrating peptide-mediated liposomal delivery system.* Biomaterials, 2013. **34**(32): p. 7980-93.
434. Gao, H., S. Zhang, S. Cao, et al., *Angiopep-2 and Activatable Cell-Penetrating Peptide Dual-Functionalized Nanoparticles for Systemic Glioma-Targeting Delivery.* Molecular Pharmaceutics, 2014. **11**(8): p. 2755-2763.
435. Liu, Q., Y.-D. Dong, T.L. Hanley, and B.J. Boyd, *Sensitivity of Nanostructure in Charged Cubosomes to Phase Changes Triggered by Ionic Species in Solution.* Langmuir, 2013. **29**(46): p. 14265-14273.
436. Lombardo, D., M.A. Kiselev, Magaz, et al., *Amphiphiles Self-Assembly: Basic Concepts and Future Perspectives of Supramolecular Approaches.* Advances in Condensed Matter Physics, 2015. **2015**: p. 22.
437. Teng, H., H. Zhang, J. Wang, K. Zhang, and Y. Chen, *Synthesis of lamellar mesoporous silica materials using LCs as templates.* Journal of Dispersion Science and Technology, 2017. **38**(12): p. 1744-1748.
438. Pitchaimani, A., T.D.T. Nguyen, M. Koirala, Y. Zhang, and S. Aryal, *Impact of cell adhesion and migration on nanoparticle uptake and cellular toxicity.* Toxicology in Vitro, 2017. **43**(Supplement C): p. 29-39.
439. Marques, E.F., *Size and stability of catanionic vesicles: effects of formation path, sonication, and aging.* Langmuir, 2000. **16**(11): p. 4798-4807.

440. Karukstis, K.K., S.A. McCormack, T.M. McQueen, and K.F. Goto, *Fluorescence Delineation of the Surfactant Microstructures in the CTAB-SOS-H 2O Catanionic System.* Langmuir, 2004. **20**(1): p. 64-72.
441. Yuan, S., L. Ma, X. Zhang, and L. Zheng, *Molecular dynamics studies on monolayer of cetyltrimethylammonium bromide surfactant formed at the air/water interface.* Colloids and Surfaces A: Physicochemical and Engineering Aspects, 2006. **289**(1–3): p. 1-9.
442. Mao, M., J. Huang, B. Zhu, H. Yin, and H. Fu, *The structural transition of catanionic vesicles induced by toluene.* Langmuir, 2002. **18**(8): p. 3380-3382.
443. Allen, J.M., J. Xu, M. Blahove, et al., *Synthesis of less toxic gold nanorods by using dodecylethyldimethylammonium bromide as an alternative growth-directing surfactant.* Journal of Colloid and Interface Science, 2017. **505**(Supplement C): p. 1172-1176.
444. Tang, F. and J.A. Hughes, *Synthesis of a single-tailed cationic lipid and investigation of its transfection.* Journal of Controlled Release, 1999. **62**(3): p. 345-358.
445. Lv, H., S. Zhang, B. Wang, S. Cui, and J. Yan, *Toxicity of cationic lipids and cationic polymers in gene delivery.* Journal of Controlled Release, 2006. **114**(1): p. 100-109.
446. Dziuba, D., P. Jurkiewicz, M. Cebecauer, M. Hof, and M. Hocek, *A Rotational BODIPY Nucleotide: An Environment-Sensitive Fluorescence-Lifetime Probe for DNA Interactions and Applications in Live-Cell Microscopy.* Angewandte Chemie International Edition, 2016. **55**(1): p. 174-178.
447. Colombo, S., D. Cun, K. Remaut, et al., *Mechanistic profiling of the siRNA delivery dynamics of lipid–polymer hybrid nanoparticles.* Journal of Controlled Release, 2015. **201**: p. 22-31.
448. Meisel, J.W. and G.W. Gokel, *A Simplified Direct Lipid Mixing Lipoplex Preparation: Comparison of Liposomal-, Dimethylsulfoxide-, and Ethanol-Based Methods.* Scientific Reports, 2016. **6**: p. 27662.
449. Xia, Y., J. Tian, and X. Chen, *Effect of surface properties on liposomal siRNA delivery.* Biomaterials, 2016. **79**: p. 56-68.
450. Leventis, R. and J.R. Silvius, *Interactions of mammalian cells with lipid dispersions containing novel metabolizable cationic amphiphiles.* BBA - Biomembranes, 1990. **1023**(1): p. 124-132.
451. Tabatt, K., M. Sameti, C. Olbrich, R.H. Müller, and C.-M. Lehr, *Effect of cationic lipid and matrix lipid composition on solid lipid nanoparticle-mediated gene transfer.* European Journal of Pharmaceutics and Biopharmaceutics, 2004. **57**(2): p. 155-162.
452. Gjetting, T., N.S. Arildsen, C.L. Christensen, et al., *In vitro and in vivo effects of polyethylene glycol (PEG)-modified lipid in DOTAP/cholesterol-mediated gene transfection.* Nanomedicine, 2010. **5**: p. 371-83.
453. Tabatt, K., C. Kneuer, M. Sameti, et al., *Transfection with different colloidal systems: comparison of solid lipid nanoparticles and liposomes.* Journal of Controlled Release, 2004. **97**(2): p. 321-332.
454. Felgner, P.L., T.R. Gadek, M. Holm, et al., *Lipofection: a highly efficient, lipid-mediated DNA-transfection procedure.* Proceedings of the National Academy of Sciences, 1987. **84**(21): p. 7413-7417.
455. Bennett, C.F., M.-Y. Chiang, H. Chan, and S. Grimm, *Use of Cationic Lipids to Enhance the Biological Activity of Antisense Oligonucleotides.* Journal of Liposome Research, 1993. **3**(1): p. 85-102.

456. Puri, A., S. Zampino, M. Viard, and B.A. Shapiro, *Oxime Ether Lipids as Transfection Agents: Assembly and Complexation with siRNA*, in *RNA Nanostructures : Methods and Protocols*, E. Bindewald and B.A. Shapiro, Editors. 2017, Springer New York: New York, NY. p. 241-253.
457. Jubeli, E., W.P.D. Goldring, and M.D. Pungente, *Cationic Lipid-Based Nucleic Acid Vectors*, in *Non-Viral Gene Delivery Vectors: Methods and Protocols*, G. Candiani, Editor. 2016, Springer New York: New York, NY. p. 19-32.
458. Ren, T., Y. Song, G. Zhang, and D. Liu, *Structural basis of DOTMA for its high intravenous transfection activity in mouse.* Gene therapy, 2000. **7**(9): p. 764.
459. Ghosh, Y.K., S.S. Visweswariah, and S. Bhattacharya, *Nature of linkage between the cationic headgroup and cholesteryl skeleton controls gene transfection efficiency.* FEBS Letters, 2000. **473**(3): p. 341-344.
460. Song, Y.K., F. Liu, S. Chu, and D. Liu, *Characterization of Cationic Liposome-Mediated Gene Transfer In Vivo by Intravenous Administration.* Human Gene Therapy, 1997. **8**(13): p. 1585-1594.
461. Perez-Soler, R. and A.R. Khokhar, *Lipophilic Cisplatin Analogues Entrapped in Liposomes: Role of Intraliposomal Drug Activation in Biological Activity.* Cancer Research, 1992. **52**(22): p. 6341-6347.
462. Goodman, C.M., C.D. McCusker, T. Yilmaz, and V.M. Rotello, *Toxicity of Gold Nanoparticles Functionalized with Cationic and Anionic Side Chains.* Bioconjugate Chemistry, 2004. **15**(4): p. 897-900.
463. Wilhelm, C., C. Billotey, J. Roger, et al., *Intracellular uptake of anionic superparamagnetic nanoparticles as a function of their surface coating.* Biomaterials, 2003. **24**(6): p. 1001-1011.
464. Petaccia, M., L. Giansanti, F. Leonelli, et al., *Synthesis, characterization and inclusion into liposomes of a new cationic pyrenyl amphiphile.* Chemistry and Physics of Lipids, 2016. **200**: p. 83-93.
465. Janich, C., A. Hädicke, U. Bakowsky, G. Brezesinski, and C. Wölk, *Interaction of DNA with Cationic Lipid Mixtures—Investigation at Langmuir Lipid Monolayers.* Langmuir, 2017. **33**(39): p. 10172-10183.
466. Casadó, A., M.C. Giuffrida, M.L. Sagristá, et al., *Langmuir monolayers and Differential Scanning Calorimetry for the study of the interactions between camptothecin drugs and biomembrane models.* Biochimica et Biophysica Acta (BBA) - Biomembranes, 2016. **1858**(2): p. 422-433.
467. Gew, L.T. and M. Misran, *Interaction between C18 fatty acids and DOPE PEG2000 in Langmuir monolayers: effect of degree of unsaturation.* Journal of Biological Physics, 2017. **43**(3): p. 397-414.
468. Bhattarai, R., T. Sutradhar, B. Roy, et al., *Double-Tailed Cystine Derivatives as Novel Substitutes of Phospholipids with Special Reference to Liposomes.* The Journal of Physical Chemistry B, 2016. **120**(41): p. 10744-10756.
469. Langmuir, I., *THE CONSTITUTION AND FUNDAMENTAL PROPERTIES OF SOLIDS AND LIQUIDS. II. LIQUIDS.1.* Journal of the American Chemical Society, 1917. **39**(9): p. 1848-1906.
470. Langmuir, I., *The mechanism of the surface phenomena of flotation.* Transactions of the Faraday Society, 1920. **15**(June): p. 62-74.
471. Moghaddam, B., M.H. Ali, J. Wilkhu, et al., *The application of monolayer studies in the understanding of liposomal formulations.* International Journal of Pharmaceutics, 2011. **417**(1–2): p. 235-244.
472. Gálvez Ruiz, M.J. and M.A. Cabrerizo Vilchez, *A study of the miscibility of bile components in mixed monolayers at the air-liquid interface I. Cholesterol,*

lecithin, and lithocholic acid. Colloid and Polymer Science, 1991. **269**(1): p. 77-84.
473. Seoane, R., J. Miñones, O. Conde, et al., *Thermodynamic and Brewster Angle Microscopy Studies of Fatty Acid/Cholesterol Mixtures at the Air/Water Interface.* The Journal of Physical Chemistry B, 2000. **104**(32): p. 7735-7744.
474. Costin, I.S. and G.T. Barnes, *Two-component monolayers. II. Surface pressure—area relations for the octadecanol—docosyl sulphate system.* Journal of Colloid and Interface Science, 1975. **51**(1): p. 106-121.
475. Rattanapak, T., K. Young, T. Rades, and S. Hook, *Comparative study of liposomes, transfersomes, ethosomes and cubosomes for transcutaneous immunisation: characterisation and in vitro skin penetration.* Journal of Pharmacy and Pharmacology, 2012. **64**(11): p. 1560-1569.
476. Ma, G. and H.C. Allen, *DPPC Langmuir Monolayer at the Air−Water Interface: Probing the Tail and Head Groups by Vibrational Sum Frequency Generation Spectroscopy.* Langmuir, 2006. **22**(12): p. 5341-5349.
477. Dynarowicz-Łątka, P., A. Dhanabalan, and O.N. Oliveira Jr, *Modern physicochemical research on Langmuir monolayers.* Advances in Colloid and Interface Science, 2001. **91**(2): p. 221-293.
478. Chapman, D., N.F. Owens, M.C. Phillips, and D.A. Walker, *Mixed monolayers of phospholipids and cholesterol.* Biochimica et Biophysica Acta (BBA) - Biomembranes, 1969. **183**(3): p. 458-465.
479. Muir, B.W., G. Zhen, P. Gunatillake, and P.G. Hartley, *Salt Induced Lamellar to Bicontinuous Cubic Phase Transitions in Cationic Nanoparticles.* The Journal of Physical Chemistry B, 2012. **116**(11): p. 3551-3556.
480. Talmon, Y., J.L. Burns, M.H. Chestnut, and D.P. Siegel, *Time-resolved cryotransmission electron microscopy.* Journal of Electron Microscopy Technique, 1990. **14**(1): p. 6-12.
481. de Campo, L., A. Yaghmur, L. Sagalowicz, et al., *Reversible Phase Transitions in Emulsified Nanostructured Lipid Systems.* Langmuir, 2004. **20**(13): p. 5254-5261.
482. Bouwstra, J.A., G.S. Gooris, W. Bras, and H. Talsma, *Small angle X-ray scattering: possibilities and limitations in characterization of vesicles.* Chemistry and Physics of Lipids, 1993. **64**(1): p. 83-98.
483. Kiselev, M.A., P. Lesieur, A.M. Kisselev, et al., *Sucrose solutions as prospective medium to study the vesicle structure: SAXS and SANS study.* Journal of Alloys and Compounds, 2001. **328**(1): p. 71-76.
484. Wasungu, L., M.C.A. Stuart, M. Scarzello, J.B.F.N. Engberts, and D. Hoekstra, *Lipoplexes formed from sugar-based gemini surfactants undergo a lamellar-to-micellar phase transition at acidic pH. Evidence for a non-inverted membrane-destabilizing hexagonal phase of lipoplexes.* Biochimica et Biophysica Acta (BBA) - Biomembranes, 2006. **1758**(10): p. 1677-1684.
485. Genç, R., M. Ortiz, and C.K. O′Sullivan, *Curvature-Tuned Preparation of Nanoliposomes.* Langmuir, 2009. **25**(21): p. 12604-12613.
486. Fong, C., T. Le, and C.J. Drummond, *Lyotropic liquid crystal engineering-ordered nanostructured small molecule amphiphile self-assembly materials by design.* Chemical Society Reviews, 2012. **41**(3): p. 1297-1322.
487. Meikle, T.G., A. Zabara, L.J. Waddington, et al., *Incorporation of antimicrobial peptides in nanostructured lipid membrane mimetic bilayer cubosomes.* Colloids and Surfaces B: Biointerfaces, 2017. **152**(Supplement C): p. 143-151.

488. Boge, L., A. Umerska, N. Matougui, et al., *Cubosomes post-loaded with antimicrobial peptides: characterization, bactericidal effect and proteolytic stability.* International Journal of Pharmaceutics, 2017. **526**(1): p. 400-412.
489. Azmi, I.D.M., P.P. Wibroe, L.-P. Wu, et al., *A structurally diverse library of safe-by-design citrem-phospholipid lamellar and non-lamellar liquid crystalline nano-assemblies.* Journal of Controlled Release, 2016. **239**(Supplement C): p. 1-9.
490. Zhang, Y. and W.M. Pardridge, *Blood–brain barrier targeting of BDNF improves motor function in rats with middle cerebral artery occlusion.* Brain Research, 2006. **1111**(1): p. 227-229.
491. Soenen, S.J.H., A.R. Brisson, and M. De Cuyper, *Addressing the problem of cationic lipid-mediated toxicity: The magnetoliposome model.* Biomaterials, 2009. **30**(22): p. 3691-3701.
492. Lappalainen, K., I. Jääskeläinen, K. Syrjänen, A. Urtti, and S. Syrjänen, *Comparison of Cell Proliferation and Toxicity Assays Using Two Cationic Liposomes.* Pharmaceutical Research, 1994. **11**(8): p. 1127-1131.
493. Thanou, M., B.I. Florea, M. Geldof, H.E. Junginger, and G. Borchard, *Quaternized chitosan oligomers as novel gene delivery vectors in epithelial cell lines.* Biomaterials, 2002. **23**(1): p. 153-159.
494. Tandrup Schmidt, S., C. Foged, K. Smith Korsholm, T. Rades, and D. Christensen, *Liposome-Based Adjuvants for Subunit Vaccines: Formulation Strategies for Subunit Antigens and Immunostimulators.* Pharmaceutics, 2016. **8**(1): p. 7.
495. Baczynska, D., K. Widerak, M. Ugorski, and M. Langner, *Surface Charge and the Association of Liposomes with Colon Carcinoma Cells*, in *Zeitschrift für Naturforschung C*. 2001. p. 872.
496. Wiethoff, C.M., M.L. Gill, G.S. Koe, J.G. Koe, and C.R. Middaugh, *The Structural Organization of Cationic Lipid-DNA Complexes.* Journal of Biological Chemistry, 2002. **277**(47): p. 44980-44987.
497. Campbell, R.B., S.V. Balasubramanian, and R.M. Straubinger, *Phospholipid-cationic lipid interactions: influences on membrane and vesicle properties.* Biochimica et Biophysica Acta (BBA) - Biomembranes, 2001. **1512**(1): p. 27-39.
498. Mao, S., O. Germershaus, D. Fischer, et al., *Uptake and Transport of PEG-Graft-Trimethyl-Chitosan Copolymer–Insulin Nanocomplexes by Epithelial Cells.* Pharmaceutical Research, 2005. **22**(12): p. 2058-2068.
499. He, C., Y. Hu, L. Yin, C. Tang, and C. Yin, *Effects of particle size and surface charge on cellular uptake and biodistribution of polymeric nanoparticles.* Biomaterials, 2010. **31**(13): p. 3657-3666.
500. Farquhar, M.G., *Recovery of surface membrane in anterior pituitary cells. Variations in traffic detected with anionic and cationic ferritin.* The Journal of Cell Biology, 1978. **77**(3): p. R35-R42.
501. Doherty, G.J. and H.T. McMahon, *Mechanisms of Endocytosis.* Annual Review of Biochemistry, 2009. **78**(1): p. 857-902.
502. Tsuji, A., *Small Molecular Drug Transfer across the Blood-Brain Barrier via Carrier-Mediated Transport Systems.* NeuroRX, 2005. **2**(1): p. 54-62.
503. Ma, K., D. Fu, D. Yu, et al., *Targeted delivery of in situ PCR-amplified Sleeping Beauty transposon genes to cancer cells with lipid-based nanoparticle-like protocells.* Biomaterials, 2017. **121**: p. 55-63.

504. Wang, J., E. Ayano, Y. Maitani, and H. Kanazawa, *Enhanced cellular uptake and gene silencing activity of siRNA using temperature-responsive polymer-modified liposome.* International Journal of Pharmaceutics, 2017. **523**(1): p. 217-228.
505. Yin, H., R.L. Kanasty, A.A. Eltoukhy, et al., *Non-viral vectors for gene-based therapy.* Nature Reviews Genetics, 2014. **15**: p. 541.
506. Bailus, B.J., B. Pyles, M.M. McAlister, et al., *Protein Delivery of an Artificial Transcription Factor Restores Widespread Ube3a Expression in an Angelman Syndrome Mouse Brain.* Molecular Therapy, 2016. **24**(3): p. 548-555.
507. Schenk, G.J. and H.E. de Vries, *Altered blood–brain barrier transport in neuro-inflammatory disorders.* Drug Discovery Today: Technologies, 2016. **20**(Supplement C): p. 5-11.
508. Peetla, C. and V. Labhasetwar, *Effect of Molecular Structure of Cationic Surfactants on Biophysical Interactions of Surfactant-Modified Nanoparticles with a Model Membrane and Cellular Uptake.* Langmuir, 2009. **25**(4): p. 2369-2377.
509. Kim, T.W., H. Chung, I.C. Kwon, H.C. Sung, and S.Y. Jeong, *Optimization of Lipid Composition in Cationic Emulsion as In Vitro and In Vivo Transfection Agents.* Pharmaceutical Research, 2001. **18**(1): p. 54-60.
510. Zhi, D., S. Zhang, B. Wang, et al., *Transfection Efficiency of Cationic Lipids with Different Hydrophobic Domains in Gene Delivery.* Bioconjugate Chemistry, 2010. **21**(4): p. 563-577.
511. Spitsbergen, J.M. and M.L. Kent, *The state of the art of the zebrafish model for toxicology and toxicologic pathology research--advantages and current limitations.* Toxicol Pathol, 2003. **31 Suppl**: p. 62-87.
512. Langheinrich, U., *Zebrafish: A new model on the pharmaceutical catwalk.* BioEssays, 2003. **25**(9): p. 904-912.
513. Teraoka, H., W. Dong, and T. Hiraga, *Zebrafish as a novel experimental model for developmental toxicology.* Congenital Anomalies, 2003. **43**(2): p. 123-132.
514. Kalueff, A.V., A.M. Stewart, and R. Gerlai, *Zebrafish as an emerging model for studying complex brain disorders.* Trends in Pharmacological Sciences, 2014. **35**(2): p. 63-75.
515. McGrath, P. and C.Q. Li, *Zebrafish: a predictive model for assessing drug-induced toxicity.* Drug Discov Today, 2008. **13**(9-10): p. 394-401.
516. Kalueff, A.V., D.J. Echevarria, and A.M. Stewart, *Gaining translational momentum: More zebrafish models for neuroscience research.* Progress in Neuro-Psychopharmacology and Biological Psychiatry, 2014. **55**: p. 1-6.
517. Kari, G., U. Rodeck, and A.P. Dicker, *Zebrafish: An Emerging Model System for Human Disease and Drug Discovery.* Clinical Pharmacology & Therapeutics, 2007. **82**(1): p. 70-80.
518. Augustine-Rauch, K., C.X. Zhang, and J.M. Panzica-Kelly, *In vitro developmental toxicology assays: A review of the state of the science of rodent and zebrafish whole embryo culture and embryonic stem cell assays.* Birth Defects Research Part C: Embryo Today: Reviews, 2010. **90**(2): p. 87-98.
519. Bowman, T.V. and L.I. Zon, *Swimming into the Future of Drug Discovery: In Vivo Chemical Screens in Zebrafish.* ACS Chemical Biology, 2010. **5**(2): p. 159-161.
520. Rubinstein, A.L., *Zebrafish assays for drug toxicity screening.* Expert Opinion on Drug Metabolism & Toxicology, 2006. **2**(2): p. 231-240.
521. Goldsmith, P., *Zebrafish as a pharmacological tool: the how, why and when.* Current Opinion in Pharmacology, 2004. **4**(5): p. 504-512.

522. McGrath, P. and W.L. Seng, *Use of zebrafish apoptosis assays for preclinical drug discovery.* Expert Opinion on Drug Discovery, 2013. **8**(10): p. 1191-1202.
523. Sukardi, H., H.T. Chng, E.C.Y. Chan, Z. Gong, and S.H. Lam, *Zebrafish for drug toxicity screening: bridging the in vitro cell-based models and in vivo mammalian models.* Expert Opinion on Drug Metabolism & Toxicology, 2011. **7**(5): p. 579-589.
524. de Esch, C., R. Slieker, A. Wolterbeek, R. Woutersen, and D. de Groot, *Zebrafish as potential model for developmental neurotoxicity testing: A mini review.* Neurotoxicology and Teratology, 2012. **34**(6): p. 545-553.
525. Laggner, C., D. Kokel, V. Setola, et al., *Chemical informatics and target identification in a zebrafish phenotypic screen.* Nat Chem Biol, 2012. **8**(2): p. 144-146.
526. MacRae, C.A. and R.T. Peterson, *Zebrafish-Based Small Molecule Discovery.* Chemistry & Biology, 2003. **10**(10): p. 901-908.
527. Lieschke, G.J. and P.D. Currie, *Animal models of human disease: zebrafish swim into view.* Nat Rev Genet, 2007. **8**(5): p. 353-367.
528. Zon, L. and R. Peterson, *In vivo drug discovery in the zebrafish.* Nat Rev Drug Discov, 2005. **4**(1): p. 35 - 44.
529. Spence, R., G. Gerlach, C. Lawrence, and C. Smith, *The behaviour and ecology of the zebrafish, Danio rerio.* Biological Reviews, 2008. **83**(1): p. 13-34.
530. Butt, A.M., H.C. Jones, and N.J. Abbott, *Electrical resistance across the blood–brain barrier in anaesthetized rats: a developmental study.* J Physiol, 1990. **429**.
531. MacRae, C.A. and R.T. Peterson, *Zebrafish as tools for drug discovery.* Nature Reviews Drug Discovery, 2015. **14**: p. 721.
532. Lawson, N.D. and B.M. Weinstein, *In Vivo Imaging of Embryonic Vascular Development Using Transgenic Zebrafish.* Developmental Biology, 2002. **248**(2): p. 307-318.
533. Nishimura, Y., S. Murakami, Y. Ashikawa, et al., *Zebrafish as a systems toxicology model for developmental neurotoxicity testing.* Congenital Anomalies, 2015. **55**(1): p. 1-16.
534. Stewart, A.M., O. Braubach, J. Spitsbergen, R. Gerlai, and A.V. Kalueff, *Zebrafish models for translational neuroscience research: from tank to bedside.* Trends in Neurosciences, 2014. **37**(5): p. 264-278.
535. Tropepe, V. and H. Sive, *Can zebrafish be used as a model to study the neurodevelopmental causes of autism?* Genes Brain Behav, 2003. **2**(5): p. 268 - 281.
536. Dean, M. and T. Annilo, *Evolution of the ATP-binding cassette (ABC) transporter superfamily in vertebrates.* Annu. Rev. Genomics Hum. Genet., 2005. **6**: p. 123-142.
537. Fleming, A., H. Diekmann, and P. Goldsmith, *Functional Characterisation of the Maturation of the Blood-Brain Barrier in Larval Zebrafish.* PLOS ONE, 2013. **8**(10): p. e77548.
538. Jeong, J., H. Kwon, J. Ahn, et al., *Functional and developmental analysis of the blood-brain barrier in zebrafish.* Brain Res Bull, 2008. **75**(5): p. 619 - 628.
539. Xie, J., E. Farage, M. Sugimoto, and B. Anand-Apte, *A novel transgenic zebrafish model for blood-brain and blood-retinal barrier development.* BMC Dev Biol, 2010. **10**: p. 76.
540. Hjorth, J. and B. Key, *Development of axon pathways in the zebrafish central nervous system.* International Journal of Developmental Biology, 2004. **46**(4): p. 609-619.

541. Hanneman, E. and M. Westerfield, *Early expression of acetylcholinesterase activity in functionally distinct neurons of the zebrafish.* The Journal of Comparative Neurology, 1989. **284**(3): p. 350-361.
542. Wilson, S.W., L.S. Ross, T. Parrett, and S.S. Easter, *The development of a simple scaffold of axon tracts in the brain of the embryonic zebrafish, Brachydanio rerio.* Development, 1990. **108**(1): p. 121-145.
543. Eisen, J.S., *Developmental neurobiology of the zebrafish.* J Neurosci, 1991. **11**(2): p. 311-317.
544. Kawai, H., N. Arata, and H. Nakayasu, *Three-dimensional distribution of astrocytes in zebrafish spinal cord.* Glia, 2001. **36**(3): p. 406-413.
545. Kimmel, C.B., R.M. Warga, and T.F. Schilling, *Origin and organization of the zebrafish fate map.* Development, 1990. **108**(4): p. 581-594.
546. Brösamle, C. and M.E. Halpern, *Characterization of myelination in the developing zebrafish.* Glia, 2002. **39**(1): p. 47-57.
547. Watanabe, K., Y. Nishimura, T. Nomoto, et al., *In vivo assessment of the permeability of the blood-brain barrier and blood-retinal barrier to fluorescent indoline derivatives in zebrafish.* BMC Neuroscience, 2012. **13**(1): p. 101.
548. Parng, C., C. Ton, Y.-X. Lin, N.M. Roy, and P. McGrath, *A zebrafish assay for identifying neuroprotectants in vivo.* Neurotoxicology and Teratology, 2006. **28**(4): p. 509-516.
549. Yang, T., P. Martin, B. Fogarty, et al., *Exosome Delivered Anticancer Drugs Across the Blood-Brain Barrier for Brain Cancer Therapy in Danio Rerio.* Pharmaceutical Research, 2015. **32**(6): p. 2003-2014.
550. Li, S., Z. Peng, J. Dallman, et al., *Crossing the blood–brain–barrier with transferrin conjugated carbon dots: A zebrafish model study.* Colloids and Surfaces B: Biointerfaces, 2016. **145**: p. 251-256.
551. Rubin, L. and J. Staddon, *The cell biology of the blood-brain barrier.* Annual review of neuroscience, 1999. **22**(1): p. 11-28.
552. Parkins, K.M., A.M. Hamilton, A.V. Makela, et al., *A multimodality imaging model to track viable breast cancer cells from single arrest to metastasis in the mouse brain.* Scientific Reports, 2016. **6**: p. 35889.
553. Thorek, D.L.J., D. Ulmert, N.-F.M. Diop, et al., *Non-invasive mapping of deep-tissue lymph nodes in live animals using a multimodal PET/MRI nanoparticle.* Nature Communications, 2014. **5**: p. 3097.
554. de Boer, P., J.P. Hoogenboom, and B.N.G. Giepmans, *Correlated light and electron microscopy: ultrastructure lights up!* Nature Methods, 2015. **12**: p. 503.
555. Paddock, S.W. and K.W. Eliceiri, *Laser Scanning Confocal Microscopy: History, Applications, and Related Optical Sectioning Techniques*, in *Confocal Microscopy: Methods and Protocols*, S.W. Paddock, Editor. 2014, Springer New York: New York, NY. p. 9-47.
556. Lichtman, J.W. and J.-A. Conchello, *Fluorescence microscopy.* Nature Methods, 2005. **2**: p. 910.
557. White, J.G., W.B. Amos, and M. Fordham, *An evaluation of confocal versus conventional imaging of biological structures by fluorescence light microscopy.* The Journal of Cell Biology, 1987. **105**(1): p. 41-48.
558. Swedlow, J.R., K. Hu, P.D. Andrews, D.S. Roos, and J.M. Murray, *Measuring tubulin content in Toxoplasma gondii: A comparison of laser-scanning confocal and wide-field fluorescence microscopy.* Proceedings of the National Academy of Sciences, 2002. **99**(4): p. 2014-2019.

559. Verveer, P.J., J. Swoger, F. Pampaloni, et al., *High-resolution three-dimensional imaging of large specimens with light sheet–based microscopy.* Nature Methods, 2007. **4**: p. 311.
560. Carrington, W.A., K.E. Fogarty, L. Lifschitz, and F.S. Fay, *Three-dimensional Imaging on Confocal and Wide-field Microscopes*, in *Handbook of Biological Confocal Microscopy*, J.B. Pawley, Editor. 1990, Springer US: Boston, MA. p. 151-161.
561. Husebye, H. and S.L. Doyle, *Using Confocal Microscopy to Investigate Intracellular Trafficking of Toll-Like Receptors*, in *Toll-Like Receptors: Practice and Methods*, C.E. McCoy, Editor. 2016, Springer New York: New York, NY. p. 65-77.
562. Soeller, C., Y. Hou, I.D. Jayasinghe, D. Baddeley, and D. Crossman, *Correlative Single-Molecule Localization Microscopy and Confocal Microscopy*, in *Super-Resolution Microscopy: Methods and Protocols*, H. Erfle, Editor. 2017, Springer New York: New York, NY. p. 205-217.
563. Carlsson, K., P.E. Danielsson, R. Lenz, et al., *Three-dimensional microscopy using a confocal laser scanning microscope.* Optics Letters, 1985. **10**(2): p. 53-55.
564. Amos, W.B. and J.G. White, *How the Confocal Laser Scanning Microscope entered Biological Research.* Biology of the Cell, 2003. **95**(6): p. 335-342.
565. French, A.P., S. Mills, R. Swarup, M.J. Bennett, and T.P. Pridmore, *Colocalization of fluorescent markers in confocal microscope images of plant cells.* Nature Protocols, 2008. **3**: p. 619.
566. Hoebe, R., C. Van Oven, T. Gadella Jr, et al., *Controlled light-exposure microscopy reduces photobleaching and phototoxicity in fluorescence live-cell imaging.* Nature biotechnology, 2007. **25**(2): p. 249.
567. Kitamura, A. and M. Kinjo, *Determination of diffusion coefficients in live cells using fluorescence recovery after photobleaching with wide-field fluorescence microscopy.* Biophysics and Physicobiology, 2018. **15**: p. 1-7.
568. Kubitscheck, U., *Fluorescence microscopy: from principles to biological applications*. 2017: John Wiley & Sons.
569. Song, L., E. Hennink, I.T. Young, and H.J. Tanke, *Photobleaching kinetics of fluorescein in quantitative fluorescence microscopy.* Biophysical journal, 1995. **68**(6): p. 2588.
570. Wang, J., M. Yang, L. Yang, et al., *A Confocal Endoscope for Cellular Imaging.* Engineering, 2015. **1**(3): p. 351-360.
571. Aizawa, H., I.H. Bianco, T. Hamaoka, et al., *Laterotopic Representation of Left-Right Information onto the Dorso-Ventral Axis of a Zebrafish Midbrain Target Nucleus.* Current Biology, 2005. **15**(3): p. 238-243.
572. Brand, M., C.P. Heisenberg, Y.J. Jiang, et al., *Mutations in zebrafish genes affecting the formation of the boundary between midbrain and hindbrain.* Development, 1996. **123**(1): p. 179-190.
573. Holder, N. and J. Hill, *Retinoic acid modifies development of the midbrain-hindbrain border and affects cranial ganglion formation in zebrafish embryos.* Development, 1991. **113**(4): p. 1159-1170.
574. Lee, J., P. Fei, R.R. Packard, et al., *4-Dimensional light-sheet microscopy to elucidate shear stress modulation of cardiac trabeculation.* J Clin Invest, 2016. **126**(5): p. 1679-90.
575. Waters, J.C., *Accuracy and precision in quantitative fluorescence microscopy.* The Journal of Cell Biology, 2009. **185**(7): p. 1135-1148.

576. Cromey, D.W., *Avoiding Twisted Pixels: Ethical Guidelines for the Appropriate Use and Manipulation of Scientific Digital Images.* Science and engineering ethics, 2010. **16**(4): p. 639-667.
577. Visscher, K., G. Brakenhoff, and T. Visser, *Fluorescence saturation in confocal microscopy.* Journal of Microscopy, 1994. **175**(2): p. 162-165.
578. McCloy, R.A., S. Rogers, C.E. Caldon, et al., *Partial inhibition of Cdk1 in G2 phase overrides the SAC and decouples mitotic events.* Cell Cycle, 2014. **13**(9): p. 1400-1412.
579. Burgess, A., S. Vigneron, E. Brioudes, et al., *Loss of human Greatwall results in G2 arrest and multiple mitotic defects due to deregulation of the cyclin B-Cdc2/PP2A balance.* Proceedings of the National Academy of Sciences, 2010. **107**(28): p. 12564-12569.
580. Prewitt, J. and M.L. Mendelsohn, *The analysis of cell images.* Annals of the New York Academy of Sciences, 1966. **128**(1): p. 1035-1053.
581. Tapia, J.C., N. Kasthuri, K. Hayworth, et al., *High contrast en bloc staining of neuronal tissue for field emission scanning electron microscopy.* Nature protocols, 2012. **7**(2): p. 193-206.
582. Nixon, S.J., R.I. Webb, M. Floetenmeyer, et al., *A Single Method for Cryofixation and Correlative Light, Electron Microscopy and Tomography of Zebrafish Embryos.* Traffic, 2009. **10**(2): p. 131-136.
583. Hasadsri, L., J. Kreuter, H. Hattori, T. Iwasaki, and J.M. George, *Functional Protein Delivery into Neurons Using Polymeric Nanoparticles.* Journal of Biological Chemistry, 2009. **284**(11): p. 6972-6981.
584. Zhang, X., M. Zhang, D. Li, et al., *Highly photostable, reversibly photoswitchable fluorescent protein with high contrast ratio for live-cell superresolution microscopy.* Proceedings of the National Academy of Sciences, 2016. **113**(37): p. 10364-10369.
585. Liu, Y., Y. Ma, J. Xu, et al., *Apolipoproteins adsorption and brain-targeting evaluation of baicalin nanocrystals modified by combination of Tween80 and TPGS.* Colloids and Surfaces B: Biointerfaces, 2017. **160**: p. 619-627.
586. Voigt, N., P. Henrich-Noack, S. Kockentiedt, et al., *Surfactants, not size or zeta-potential influence blood–brain barrier passage of polymeric nanoparticles.* European Journal of Pharmaceutics and Biopharmaceutics, 2014. **87**(1): p. 19-29.
587. Sandez-Macho, I., M. Casas, E.V. Lage, et al., *Interaction of poloxamine block copolymers with lipid membranes: Role of copolymer structure and membrane cholesterol content.* Colloids and Surfaces B: Biointerfaces, 2015. **133**: p. 270-277.
588. Goliaei, A., E.Y. Lau, U. Adhikari, E. Schwegler, and M.L. Berkowitz, *Behavior of P85 and P188 Poloxamer Molecules: Computer Simulations Using United-Atom Force-Field.* The Journal of Physical Chemistry B, 2016. **120**(33): p. 8631-8641.
589. Alexandridis, P. and T. Alan Hatton, *Poly(ethylene oxide)□poly(propylene oxide)□poly(ethylene oxide) block copolymer surfactants in aqueous solutions and at interfaces: thermodynamics, structure, dynamics, and modeling.* Colloids and Surfaces A: Physicochemical and Engineering Aspects, 1995. **96**(1): p. 1-46.
590. Pelaz, B., P. del Pino, P. Maffre, et al., *Surface Functionalization of Nanoparticles with Polyethylene Glycol: Effects on Protein Adsorption and Cellular Uptake.* ACS Nano, 2015. **9**(7): p. 6996-7008.
591. Aggarwal, P., J.B. Hall, C.B. McLeland, M.A. Dobrovolskaia, and S.E. McNeil, *Nanoparticle interaction with plasma proteins as it relates to particle*

biodistribution, biocompatibility and therapeutic efficacy. Advanced Drug Delivery Reviews, 2009. **61**(6): p. 428-437.
592. Amani, A., P. York, H. de Waard, and J. Anwar, *Molecular dynamics simulation of a polysorbate 80 micelle in water*. Soft Matter, 2011. **7**(6): p. 2900-2908.
593. Sperling, R.A., P. Rivera Gil, F. Zhang, M. Zanella, and W.J. Parak, *Biological applications of gold nanoparticles.* Chemical Society Reviews, 2008. **37**(9): p. 1896-1908.
594. Rasch, M.R., E. Rossinyol, J.L. Hueso, et al., *Hydrophobic Gold Nanoparticle Self-Assembly with Phosphatidylcholine Lipid: Membrane-Loaded and Janus Vesicles.* Nano Letters, 2010. **10**(9): p. 3733-3739.
595. Guo, Y., E. Terazzi, R. Seemann, J.B. Fleury, and V.A. Baulin, *Direct proof of spontaneous translocation of lipid-covered hydrophobic nanoparticles through a phospholipid bilayer.* Science Advances, 2016. **2**(11).
596. Mhashal, A.R. and S. Roy, *Effect of Gold Nanoparticle on Structure and Fluidity of Lipid Membrane.* PLOS ONE, 2014. **9**(12): p. e114152.
597. Shah, F.A., B.R. Johansson, P. Thomsen, and A. Palmquist, *Ultrastructural evaluation of shrinkage artefacts induced by fixatives and embedding resins on osteocyte processes and pericellular space dimensions.* Journal of Biomedical Materials Research Part A, 2015. **103**(4): p. 1565-1576.
598. Chen, S., A.E. Goode, J.N. Skepper, et al., *Avoiding artefacts during electron microscopy of silver nanomaterials exposed to biological environments.* Journal of Microscopy, 2016. **261**(2): p. 157-166.
599. Sonzini, S., S.T. Jones, Z. Walsh, and O.A. Scherman, *Simple fluorinated moiety insertion on Abeta 16-23 peptide for stain-free TEM imaging.* Analyst, 2015. **140**(8): p. 2735-40.
600. Korn, E.D. and R.A. Weisman, *I. loss of lipids during preparation of amoebae for electron microscopy.* Biochimica et Biophysica Acta (BBA) - Lipids and Lipid Metabolism, 1966. **116**(2): p. 309-316.
601. Bangham, A.D. and R.W. Horne, *Negative staining of phospholipids and their structural modification by surface-active agents as observed in the electron microscope.* Journal of Molecular Biology, 1964. **8**(5): p. 660-IN10.
602. Lutz, J. and E. Pernicka, *ENERGY DISPERSIVE X-RAY FLUORESCENCE ANALYSIS OF ANCIENT COPPER ALLOYS: EMPIRICAL VALUES FOR PRECISION AND ACCURACY.* Archaeometry, 1996. **38**(2): p. 313-323.
603. Söderholm, K.-J., M. Zigan, M. Ragan, W. Fischlschweiger, and M. Bergman, *Hydrolytic Degradation of Dental Composites.* Journal of Dental Research, 1984. **63**(10): p. 1248-1254.
604. Newbury, D.E. and N.W.M. Ritchie, *Performing elemental microanalysis with high accuracy and high precision by scanning electron microscopy/silicon drift detector energy-dispersive X-ray spectrometry (SEM/SDD-EDS).* Journal of Materials Science, 2015. **50**(2): p. 493-518.
605. Mikula, S. and W. Denk, *High-resolution whole-brain staining for electron microscopic circuit reconstruction.* Nature Methods, 2015. **12**: p. 541.
606. Fawcett, D.W., *Observations on the Cytology and Electron Microscopy of Hepatic Cells1, 2.* JNCI: Journal of the National Cancer Institute, 1955. **15**(Supplement_5): p. 1475-1503.
607. Shi, D., G.J. Mi, S. Bhattacharya, S. Nayar, and T.J. Webster, *Optimizing superparamagnetic iron oxide nanoparticles as drug carriers using an in vitro blood-brain barrier model.* International Journal of Nanomedicine, 2016. **11**: p. 9.

608. Schmitz, F., P. Pierozan, H. Biasibetti-Brendler, et al., *Methylphenidate disrupts cytoskeletal homeostasis and reduces membrane-associated lipid content in juvenile rat hippocampus.* Metabolic Brain Disease, 2017.
609. Hamilton, J.A., C.J. Hillard, A.A. Spector, and P.A. Watkins, *Brain uptake and utilization of fatty acids, lipids and lipoproteins: application to neurological disorders.* J Mol Neurosci, 2007. **33**(1): p. 2-11.
610. Morawski, M., T. Reinert, W. Meyer-Klaucke, et al., *Ion exchanger in the brain: Quantitative analysis of perineuronally fixed anionic binding sites suggests diffusion barriers with ion sorting properties.* Scientific Reports, 2015. **5**: p. 16471.
611. Zhu, M., G. Nie, H. Meng, et al., *Physicochemical Properties Determine Nanomaterial Cellular Uptake, Transport, and Fate.* Accounts of Chemical Research, 2013. **46**(3): p. 622-631.
612. Lockman, P.R., J.M. Koziara, R.J. Mumper, and D. Allen, *Nanoparticle surface charges alter blood-brain barrier integrity and permeability.* Journal of Drug Targeting, 2004. **12**(9-10): p. 635-641.
613. Kim, J.A., A. Salvati, C. Aberg, and K.A. Dawson, *Suppression of nanoparticle cytotoxicity approaching in vivo serum concentrations: limitations of in vitro testing for nanosafety.* Nanoscale, 2014. **6**(23): p. 14180-4.
614. Schleich, N., F. Danhier, and V. Préat, *Iron oxide-loaded nanotheranostics: Major obstacles to in vivo studies and clinical translation.* Journal of Controlled Release, 2015. **198**: p. 35-54.
615. Braakhuis, H.M., S.K. Kloet, S. Kezic, et al., *Progress and future of in vitro models to study translocation of nanoparticles.* Archives of Toxicology, 2015. **89**(9): p. 1469-1495.
616. Saeidnia, S., A. Manayi, and M. Abdollahi, *From in vitro Experiments to in vivo and Clinical Studies; Pros and Cons.* Curr Drug Discov Technol, 2015. **12**(4): p. 218-24.
617. Fede, C., I. Fortunati, V. Weber, et al., *Evaluation of gold nanoparticles toxicity towards human endothelial cells under static and flow conditions.* Microvascular Research, 2015. **97**: p. 147-155.
618. Grabinski, C., M. Sharma, E. Maurer, et al., *The effect of shear flow on nanoparticle agglomeration and deposition in in vitro dynamic flow models.* Nanotoxicology, 2016. **10**(1): p. 74-83.
619. Pozzi, D., G. Caracciolo, A.L. Capriotti, et al., *Surface chemistry and serum type both determine the nanoparticle–protein corona.* Journal of Proteomics, 2015. **119**: p. 209-217.
620. Canesi, L., C. Ciacci, R. Fabbri, et al., *Interactions of cationic polystyrene nanoparticles with marine bivalve hemocytes in a physiological environment: Role of soluble hemolymph proteins.* Environmental Research, 2016. **150**: p. 73-81.
621. Taguchi, K., M. Hashimoto, S. Ogaki, et al., *Effect of Repeated Injections of Adenosine Diphosphate-Encapsulated Liposomes Coated with a Fibrinogen γ-Chain Dodecapeptide Developed as a Synthetic Platelet Substitute on Accelerated Blood Clearance in a Healthy and an Anticancer Drug-Induced Thrombocytopenia Rat Model.* Journal of Pharmaceutical Sciences, 2015. **104**(9): p. 3084-3091.
622. Sheng, L., L. Wang, M.Y. Su, et al., *Mechanism of TiO2 nanoparticle-induced neurotoxicity in zebrafish (Danio rerio).* Environmental Toxicology, 2016. **31**(2): p. 163-175.

623. Kettler, K., K. Veltman, D. van de Meent, A. van Wezel, and A.J. Hendriks, *Cellular uptake of nanoparticles as determined by particle properties, experimental conditions, and cell type.* Environmental Toxicology and Chemistry, 2014. **33**(3): p. 481-492.
624. Mirshafiee, V., R. Kim, S. Park, M. Mahmoudi, and M.L. Kraft, *Impact of protein pre-coating on the protein corona composition and nanoparticle cellular uptake.* Biomaterials, 2016. **75**: p. 295-304.
625. Jiang, Y., S. Huo, T. Mizuhara, et al., *The Interplay of Size and Surface Functionality on the Cellular Uptake of Sub-10 nm Gold Nanoparticles.* ACS Nano, 2015. **9**(10): p. 9986-93.
626. Kasibhatla, S., G.P. Amarante-Mendes, D. Finucane, et al., *Acridine orange/ethidium bromide (AO/EB) staining to detect apoptosis.* Cold Spring Harbor Protocols, 2006. **2006**(3): p. pdb. prot4493.
627. Traganos, F. and Z. Darzynkiewicz, *Lysosomal proton pump activity: supravital cell staining with acridine orange differentiates leukocyte subpopulations*, in *Methods in cell biology*. 1994, Elsevier. p. 185-194.
628. Ferlini, C. and G. Scambia, *Assay for apoptosis using the mitochondrial probes, Rhodamine123 and 10-N-nonyl acridine orange.* Nature protocols, 2007. **2**(12): p. 3111.
629. Feurstein, D., K. Holst, A. Fischer, and D.R. Dietrich, *Oatp-associated uptake and toxicity of microcystins in primary murine whole brain cells.* Toxicology and Applied Pharmacology, 2009. **234**(2): p. 247-255.
630. Costa, P.M., M. Bourgognon, J.T.W. Wang, and K.T. Al-Jamal, *Functionalised carbon nanotubes: From intracellular uptake and cell-related toxicity to systemic brain delivery.* Journal of Controlled Release, 2016. **241**: p. 200-219.
631. Severino, P., M. Szymanski, M. Favaro, et al., *Development and characterization of a cationic lipid nanocarrier as non-viral vector for gene therapy.* European Journal of Pharmaceutical Sciences, 2015. **66**: p. 78-82.
632. Knudsen, K.B., H. Northeved, P.K. Ek, et al., *In vivo toxicity of cationic micelles and liposomes.* Nanomedicine: Nanotechnology, Biology and Medicine, 2015. **11**(2): p. 467-477.
633. Pinnaduwage, P., L. Schmitt, and L. Huang, *Use of a quaternary ammonium detergent in liposome mediated DNA transfection of mouse L-cells.* Biochimica et Biophysica Acta (BBA) - Biomembranes, 1989. **985**(1): p. 33-37.
634. Seo, J.Y., R. Praveenkumar, B. Kim, et al., *Downstream integration of microalgae harvesting and cell disruption by means of cationic surfactant-decorated Fe3O4 nanoparticles.* Green Chemistry, 2016. **18**(14): p. 3981-3989.
635. Wang, S., W. Lu, O. Tovmachenko, et al., *Challenge in understanding size and shape dependent toxicity of gold nanomaterials in human skin keratinocytes.* Chemical Physics Letters, 2008. **463**(1): p. 145-149.
636. Wang, G., J.J. Wang, F. Li, and S.S.T. To, *Development and Evaluation of a Novel Drug Delivery: Pluronics/SDS Mixed Micelle Loaded with Myricetin in Vitro and in Vivo.* Journal of Pharmaceutical Sciences, 2016. **105**(4): p. 1535-1543.
637. Alkilany, A.M. and C.J. Murphy, *Toxicity and cellular uptake of gold nanoparticles: what we have learned so far?* Journal of Nanoparticle Research, 2010. **12**(7): p. 2313-2333.
638. Zhang, F., P. Durham, C.M. Sayes, B.L.T. Lau, and E.D. Bruce, *Particle uptake efficiency is significantly affected by type of capping agent and cell line.* Journal of Applied Toxicology, 2015. **35**(10): p. 1114-1121.

639. Cho, W.-S., M. Cho, J. Jeong, et al., *Acute toxicity and pharmacokinetics of 13 nm-sized PEG-coated gold nanoparticles.* Toxicology and Applied Pharmacology, 2009. **236**(1): p. 16-24.
640. Gnach, A., T. Lipinski, A. Bednarkiewicz, J. Rybka, and J.A. Capobianco, *Upconverting nanoparticles: assessing the toxicity.* Chemical Society Reviews, 2015. **44**(6): p. 1561-1584.
641. Chompoosor, A., K. Saha, P.S. Ghosh, et al., *The Role of Surface Functionality on Acute Cytotoxicity, ROS Generation and DNA Damage by Cationic Gold Nanoparticles.* Small, 2010. **6**(20): p. 2246-2249.
642. Lin, T.T., P.F. Zhao, Y.F. Jiang, et al., *Blood-Brain-Barrier-Penetrating Albumin Nanoparticles for Biomimetic Drug Delivery via Albumin-Binding Protein Pathways for Antiglioma Therapy.* Acs Nano, 2016. **10**(11): p. 9999-10012.
643. Tosi, G., T. Musumeci, B. Ruozi, et al., *The "fate" of polymeric and lipid nanoparticles for brain delivery and targeting: Strategies and mechanism of blood-brain barrier crossing and trafficking into the central nervous system.* Journal of Drug Delivery Science and Technology, 2016. **32**: p. 66-76.
644. Chandran, I.S. and P.M. Prasanna, *Polysorbate80 coated liposomes for loperamide delivery to brain for its antinociceptive activity through central opiate receptors.* International Journal of Pharmaceutical Sciences Review and Research, 2016. **40**(1): p. 286-291.
645. Liu, C., Y. Sun, D. Wang, et al., *Performance and mechanism of low-frequency ultrasound to regenerate the biological activated carbon.* Ultrasonics Sonochemistry, 2017. **34**(Supplement C): p. 142-153.
646. Song, H., H.Q. Geng, J. Ruan, et al., *Development of polysorbate 80/phospholipid mixed micellar formation for docetaxel and assessment of its in vivo distribution in animal models.* Nanoscale Res Lett, 2011. **6**.
647. S. Duttagupta, A., H. M. Chaudhary, K. R. Jadhav, and V. J. Kadam, *Cubosomes: Innovative Nanostructures for Drug Delivery.* Current Drug Delivery, 2016. **13**(4): p. 482-493.
648. Peng, X., Y. Zhou, K. Han, et al., *Characterization of cubosomes as a targeted and sustained transdermal delivery system for capsaicin.* Drug Design, Development and Therapy, 2015. **9**: p. 4209-4218.
649. Ramge, P., R.E. Unger, J.B. Oltrogge, et al., *Polysorbate-80 coating enhances uptake of polybutylcyanoacrylate (PBCA)-nanoparticles by human and bovine primary brain capillary endothelial cells.* European Journal of Neuroscience, 2000. **12**(6): p. 1931-1940.
650. Peura, L., K. Malmioja, K. Huttunen, et al., *Design, Synthesis and Brain Uptake of LAT1-Targeted Amino Acid Prodrugs of Dopamine.* Pharmaceutical Research, 2013. **30**(10): p. 2523-2537.
651. Wang, Z., D. Xie, H. Liu, Z. Bao, and Y. Wang, *Toxicity assessment of precise engineered gold nanoparticles with different shapes in zebrafish embryos.* RSC Advances, 2016. **6**(39): p. 33009-33013.
652. Jo, D.H., J.H. Kim, T.G. Lee, and J.H. Kim, *Size, surface charge, and shape determine therapeutic effects of nanoparticles on brain and retinal diseases.* Nanomedicine: Nanotechnology, Biology, and Medicine, 2015. **11**(7): p. 1603-1611.
653. Vaidyanathan, S., J. Chen, B.G. Orr, and M.M. Banaszak Holl, *Cationic Polymer Intercalation into the Lipid Membrane Enables Intact Polyplex DNA Escape from Endosomes for Gene Delivery.* Molecular pharmaceutics, 2016. **13**(6): p. 1967-1978.

654. Elnaggar, Y.S.R., S.M. Etman, D.A. Abdelmonsif, and O.Y. Abdallah, *Novel piperine-loaded Tween-integrated monoolein cubosomes as brain-targeted oral nanomedicine in Alzheimer's disease: pharmaceutical, biological, and toxicological studies.* International Journal of Nanomedicine, 2015. **10**: p. 5459-5473.
655. Pinzón-Daza, M.L., R. Garzón, P.O. Couraud, et al., *The association of statins plus LDL receptor-targeted liposome-encapsulated doxorubicin increases in vitro drug delivery across blood–brain barrier cells.* British Journal of Pharmacology, 2012. **167**(7): p. 1431-1447.
656. Scott, C.J., W.M. Marouf, D.J. Quinn, et al., *Immunocolloidal Targeting of the Endocytotic Siglec-7 Receptor Using Peripheral Attachment of Siglec-7 Antibodies to Poly(Lactide-co-Glycolide) Nanoparticles.* Pharmaceutical Research, 2008. **25**(1): p. 135-146.
657. Lee, S.-Y., J.Y. Tyler, S. Kim, K. Park, and J.-X. Cheng, *FRET Imaging Reveals Different Cellular Entry Routes of Self-Assembled and Disulfide Bonded Polymeric Micelles.* Molecular Pharmaceutics, 2013. **10**(9): p. 3497-3506.
658. Gordon, S., K. Young, R. Wilson, et al., *Chitosan hydrogels containing liposomes and cubosomes as particulate sustained release vaccine delivery systems.* Journal of Liposome Research, 2012. **22**(3): p. 193-204.
659. Corbo, C., R. Molinaro, A. Parodi, et al., *The impact of nanoparticle protein corona on cytotoxicity, immunotoxicity and target drug delivery.* Nanomedicine, 2016. **11**(1): p. 81-100.
660. Fleischer, C.C. and C.K. Payne, *Nanoparticle–Cell Interactions: Molecular Structure of the Protein Corona and Cellular Outcomes.* Accounts of Chemical Research, 2014. **47**(8): p. 2651-2659.
661. Pinazo, A., V. Petrizelli, M. Bustelo, et al., *New cationic vesicles prepared with double chain surfactants from arginine: Role of the hydrophobic group on the antimicrobial activity and cytotoxicity.* Colloids and Surfaces B: Biointerfaces, 2016. **141**: p. 19-27.
662. Brown, M. and J. Goldstein, *Lipoprotein receptors in the liver. Control signals for plasma cholesterol traffic.* The Journal of clinical investigation, 1983. **72**(3): p. 743-747.
663. Blanco, E., H. Shen, and M. Ferrari, *Principles of nanoparticle design for overcoming biological barriers to drug delivery.* Nature Biotechnology, 2015. **33**: p. 941.
664. Zhang, F., Y.A. Lin, S. Kannan, and R.M. Kannan, *Targeting specific cells in the brain with nanomedicines for CNS therapies.* Journal of Controlled Release, 2016. **240**: p. 212-226.
665. Muller, F., A. Salonen, M. Dulle, and O. Glatter. *Salt-Induced Behavior of Internally Self-Assembled Nanodrops: Understanding Stabilization by Charged Colloids*. 2011. Berlin, Heidelberg: Springer Berlin Heidelberg.
666. Leesajakul, W., M. Nakano, A. Taniguchi, and T. Handa, *Interaction of cubosomes with plasma components resulting in the destabilization of cubosomes in plasma.* Colloids and Surfaces B: Biointerfaces, 2004. **34**(4): p. 253-258.
667. Nielsen, L.H., T. Rades, B. Boyd, and A. Boisen, *Microcontainers as an oral delivery system for spray dried cubosomes containing ovalbumin.* European Journal of Pharmaceutics and Biopharmaceutics, 2017. **118**: p. 13-20.